Sideways Launching of Ships using Fluid-Structure Interaction

Vom Promotionsausschuss der
Technischen Universität Hamburg
zur Erlangung des akademischen Grades
Doktor-Ingenieur (Dr.-Ing.)
genehmigte Dissertation

von
Albert Ulbertus

aus
Emden

2024

1. Gutachter: Prof. Dsc. (Tech.) Sören Ehlers

2. Gutachter: Prof. Dr.-Ing. Moustafa Abdel-Maksoud

Vorsitz der Prüfungskommission: Prof. Dr.-Ing. Friedrich Wirz

Tag der mündlichen Prüfung: 05. April 2024

DOI: 10.15480/882.9564

ORCID: 0000-0002-3311-8289

Acknowledgements

First of all, I would like to express my sincere gratitude to my doctorate supervisor Prof. Dsc. (Tech.) Sören Ehlers for his advice and continuous support throughout my doctoral study. This is all the more true as I did my doctoral study externally. I am very grateful that Prof. Dsc. (Tech.) Sören Ehlers gave me his trust and the opportunity to do my doctorate at the TUHH. At the same time I would like to thank all staff members of the Institute for Ship Structural Design and Analysis, who had warmly welcomed me as one of their own. Additionally, I would like to thank Prof. Dr.-Ing. Moustafa Abdel-Maksoud for reviewing my work and Prof. Dr.-Ing. Friedrich Wirz for taking on the chair of the examination committee.

Furthermore, I like to thank all colleagues, who supported my doctoral study. In particular, I would like extend my sincere gratitude to my colleague and friend Dr.-Ing. Martin Schöttelndreyer for his support and the numerous professional discussions. His support has played a considerable part in making this work possible.

Finally, my appreciation goes out to my family and friends for their encouragement and support through my studies all these years.

Albert Ulbertus Hamburg, 14th April, 2024

Abstract

Within this work the sideways launching process of ships is investigated based on different approaches. Many different ship types were successfully launched in the past using a sideways launching process as the method of choice. Although different shipyards have a lot of experience, publicly available literature regarding insights about the mechanics of sideways launchings is scarce. This is especially true for loads resulting on the ship hull at the moment of impact with the water surface. No knowledge regarding load mechanism acting upon a hull structure as well as the subsequent hull structural loads during a sideways launching process can be found in literature. The same is true for the influence of different parameters relevant for a safe sideways launching process.

Nowadays, available computational resources enable an increased usage of multi-physics simulation approaches. In such simulations two or more different physical domains are combined and solved simultaneously. In naval architecture simulation techniques considering fluid-structure interaction (FSI) are especially of significance. Within this work a simulation-based approach using FSI based on an Arbitrary-Lagrangian-Eulerian (ALE) approach for the assessment of sideways launching of ships is proposed. After an adequate setup and verification of the proposed ALE approach based upon model tests, the sideways launching process of a special purpose vessel is investigated. This investigation includes the ship motion as well as the resulting hull structural loads.

The results obtained with the ALE approach are compared to common approaches. This includes rule-based approaches, analytical formulations, model tests as well as simulation-based approaches without FSI. Benefits and drawbacks of each of the different approaches are discussed. Based on the ALE approach two different load mechanism acting upon the hull structure during a sideways launching process can be observed: loads due to impact with the water surface and loads due to the deceleration of the hull structure. The first load mechanism (impact with water surface) and the corresponding hull structural loads can be compared to slamming events (asymmetrical slamming event with oblique speed). The second load mechanism (deceleration of hull structure) results in high shear stresses inside transversal members of the hull structure.

Compared to the aforementioned common approaches, the proposed ALE approach allows for the most detailed assessment of the sideways launching process. Not only can the ship motion and resulting hull structural loads be assessed simultaneously using just one simulation model, but also could the second load mechanism (deceleration of hull structure) only be observed based on the simulation-based approach using FSI. Simulations without FSI based on a load model derived from model tests are not able to account for this load mechanism.

Furthermore, by using an optimized setup for the ALE approach the necessary computational effort can be reduced to a level just slightly higher compared to simulations without FSI. This allows the use of the proposed ALE approach within the context of optimizations (e.g. weight reduction of hull structure) or parametric studies. The conducted study includes the coefficient of friction between palls and slipway, height of the palls, water level inside the launch basin as well as loading condition of the investigated special purpose vessel. The influence of these parameters on the ship motion as well as the resulting hull structural loads is investigated and discussed.

Contents

List of Abbreviations v

List of Symbols vii

1. Introduction 1
1.1. Investigated case study . . . 4

2. State of the art 7
2.1. Sideways launching process . . . 7
2.2. Launching of free-fall lifeboats . . . 8
2.3. Slamming phenomena . . . 10
2.3.1. Analytical models . . . 10
2.3.2. Experiments . . . 12
2.3.3. Simulation-based approaches . . . 13
2.4. Scope of work . . . 14
2.4.1. Research questions and hypothesis . . . 14
2.4.2. Structure of this work . . . 16

3. Theoretical framework 17
3.1. Arbitrary-Lagrangian-Eulerian approach . . . 17
3.2. Fluid-structure interaction algorithm . . . 19
3.3. Material models . . . 21
3.3.1. Steel . . . 21
3.3.2. Media surrounding ship hull . . . 24

4. Conventional approaches 27
4.1. Rule-based approach . . . 27
4.2. Analytical approach . . . 28
4.2.1. Ship motion based on ordinary differential equations of motion . . . 29
4.2.2. Impact loads on ship hull due to slamming . . . 35
4.2.3. Numerical implementation . . . 35
4.2.4. Results . . . 38
4.2.5. Benefits and Limitations . . . 39
4.3. Experimental approach . . . 41
4.3.1. Setup of model tests . . . 41
4.3.2. Results . . . 47
4.3.3. Benefits and limitations . . . 56

5. Simulation-based approach without fluid-structure interaction 59
5.1. Overview of highly loaded areas . . . 59
5.2. Modelling of hull structure . . . 59
5.3. Load models . . . 63
5.3.1. Rule-based approach . . . 63
5.3.2. Experimental approach . . . 65
5.3.3. Computational fluid dynamics . . . 67

5.4. Results . . . 68
5.4.1. Ship motion . . . 68
5.4.2. Hull structural loads . . . 68
5.5. Benefits and limitations . . . 72

6. Simulation-based approach using fluid-structure interaction **75**
6.1. Setup of Arbitrary-Lagrangian-Eulerian approach . . . 75
6.2. Parametric study of settings used for fluid-structure interaction . . . 77
6.2.1. Motion of box structure . . . 78
6.2.2. Hull structural loads inside box structure . . . 79
6.3. Verification of Arbitrary-Lagrangian-Eulerian approach . . . 80
6.4. Optimization of computational effort . . . 85
6.5. Results . . . 90
6.5.1. Ship motion . . . 90
6.5.2. Hull structural loads . . . 92
6.6. Benefits and limitations . . . 99

7. Discussion of results **101**
7.1. Newfound insights regarding the mechanics of sideways launching . . . 101
7.2. Comparison and evaluation of different approaches . . . 102
7.3. Consequences regarding the design of the special purpose vessel . . . 104

8. Conclusion **105**

Bibliography **109**

A. Appendix **119**
A.1. Different phases of sideways launching process . . . 119
A.2. Regulations of classification societies: launching and bottom slamming . . . 122
A.3. Results of analytical approach . . . 125
A.4. Results of experimental approach . . . 126
A.5. Modelling of hull structure of the special purpose vessel . . . 131
A.6. User defined load model in LS-DYNA - rule-based approach . . . 136
A.7. User defined load model in LS-DYNA - experimental approach . . . 137
A.8. Parametric study of settings used for fluid-structure interaction . . . 138
A.9. Verification of Arbitrary-Lagrangian-Eulerian approach . . . 148
A.10.Settings used for Arbitrary-Lagrangian-Eulerian approach . . . 152
A.11.Ship motion obtained with Arbitrary-Lagrangian-Eulerian approach . . . 155
A.12.Resulting hull structural loads . . . 163

List of Abbreviations

ABS American Bureau of Shipping

ALE Arbitrary-Lagrangian-Eulerian

BC boundary conditions

BV Bureau Veritas

CAD computer-aided design

CCS China Classification Society

CFD computational fluid dynamics

CII Carbon Intensity Indicator

COB center of bouyancy

COG center of gravity

DNV Det Norske Veritas

DOF degree of freedom

EEDI Energy Efficiency Design Index

EOS equation of state

FEM finite element method

FFLB free-fall lifeboat

FFT fast Fourier transform

FSI fluid-structure interaction

GWM generalized Wagner model

IMO International Maritime Organization

IACS International Association of Classification Societies

KR Korean Register of Shipping

LR Lloyd's Register

MLM modified Longvinovich model

MPP massively parallel processing

NFRPC natural fiber reinforced composites

NK Nippon Kaiji Kyōkai

ODE ordinary differential equation

OLM original Longvinovich model

PS portside

RCB recursive coordinate bisection

RFR Required Freight Rate

RINA Registro Italiano Navale

SMP symmetric multi-processing

SPV special purpose vessel

STB starboard

VBA Visual Basic for Application

List of Symbols

Latin Symbols

Symbol	description
A	area
A_0	initial cross-sectional area of specimen at uniaxial tensile test
A_{frame}	area of ship frame
A_s	area of structure containing slave nodes in FSI algorithm
A_{xy}	waterline area of ship (xy-plane) in analytical approach (phase 3 — 4)
A_{xz}	projected centerline area of ship (xz-plane) below waterline in analytical approach (phase 3 — 4)
a_{panel}	distance between stiffeners of vibrating plate panel
B_{frame}	breadth of ship frame
B_{wl}	breadth of ship at design waterline
b_i	specific body force vector in ALE formulation
b_{panel}	length of vibrating plate panel
C_i	material coefficients in general polynomial EOS
C_{CS}	material coefficient in Cowper-Symonds equation
COG_i	position of COG in i-direction
CV_i	coefficient of variation of measurement series i in model tests
c_0	velocity of sound at reference state of thermodynamic EOS
$c_{w\,ij}$	dimensionless resistance coefficient in hydrodyanmic force valid for ij-plane in analytical approach (phase 3 — 4)
D_{main}	height of main deck of ship above baseline
D_{pen}	damping ratio of spring-damper-system in FSI algorithm
DR	mesh density ratio between ALE and Lagrangian elements in ALE approach
d_{pen}	damping coefficient of spring-damper-system in FSI algorithm
$dy_{COG_{tot}\,0}$	arm of lever of weight force in y-direction in analytical approach (phase 0)
$dy_{crane\,0}$	arm of lever of crane force in y-direction in analytical approach (phase 0)
$dz_{COG_{tot}\,0}$	arm of lever of weight force in z-direction in analytical approach (phase 0)
$dz_{crane\,0}$	arm of lever of crane force in z-direction in analytical approach (phase 0)
E	energy in ALE formulation / thermodynamic EOS
E_0	energy at reference state of thermodynamic EOS
E_H	energy at Rankine-Hugoniot state of thermodynamic EOS
E_i	internal energy per unit reference volume in thermodynamic EOS
E_Y	Young's modulus
F_{crane}	force induced by crane in analytical approach (phase 0)
F_d	downhill force in analytical approach (phase 1 — 3)
F_f	frictional force in analytical approach (phase 1 — 3)
$F_{hyd\,stat}$	hydrostatic force in analytical approach (phase 3 — 4)
$F_{hyd\,dyn\,i}$	hydrodynamic force in i-direction in analytical approach (phase 3 — 4)
F_i	force in i-direction
F_n	normal force in analytical approach (phase 1 — 3)

Symbol	description
F_{pen}	coupling force in FSI algorithm
$F_{pen\,f}$	coupling force on fluid in FSI algorithm
$F_{pen\,s}$	coupling force on structure in FSI algorithm
F_{pier}	reaction force of slipway in analytical approach (phase 1 — 3)
F_w	weight force in analytical approach
f	frequency
f_{cutoff}	cutoff frequency of lowpass filter
f_{eigen}	eigenfrequency of a dynamic system
$f_{encounter}$	encounter frequency
$\overline{GM}_0$	metacentric height of ship
g	gravitational acceleration of earth
h_{drop}	height of drop around edge of pier during sideways launching
h_p	height of palls used for sideways launching
$h_{SR\,i}$	width of integration interval in Simpson's rule of integration
h_{wl}	height of water level in launch basin
$i,\ j$	running indices / placeholder
I_{ij}	moment of inertia
$I^*_{xx\,ra}$	moment of inertia of rocker arms around x-axis referred to rotational axis of rocker arms in analytical approach (phase 0)
$I^*_{xx\,tot}$	moment of inertia of ship + palls around x-axis referred to rotational axis of rocker arms in analytical approach (phase 0)
$I^\dagger_{xx\,tot}$	moment of inertia of ship + palls around x-axis referred to edge of pier in analytical approach (phase 2 — 3)
$I_{xx\,tot}$	moment of inertia of ship + palls around x-axis referred to COG of ship + palls in analytical approach (phase 4)
i_{ij}	radius of gyration
J	impulse
$J_{i\,50ms}$	impulse in 50ms time period after peak pressure at pressure transducer i in model tests
$J_{i\,50ms\,ALE}$	value for $J_{i\,50ms}$ obtained with ALE approach
$J_{i\,50ms\,mean}$	mean value of $J_{i\,50ms}$ for measurement series in model tests
K	bulk modulus
K_f	bulk modulus of fluid
K_{hard}	strength coefficient in power law
k_{ij}	form coefficients for calculation of added masses using Lewis-frames
k_{mt}	decay constant in load model based on model tests
k_{pen}	spring stiffness of spring-damper-system in FSI algorithm
k_{sl}	hull form shape coefficient in rule-based load model
k_v	correction factor for speed at impact in load model based on model tests
k_β	correction factor for deadrise angle in load model based on model tests
L	length
L_0	initial length of specimen at uniaxial tensile test
L_{ALE}	element size of ALE elements in ALE approach
$L_{ALE\,refine}$	element size of ALE elements in area of refinement in ALE approach
$L_{Lagrangian}$	element size of Lagrangian elements in simulation-based approaches

Symbol	description
L_{pp}	length between perpendiculars of ship
LC	loading condition of ship
ΔL	elongation / change of length of specimen at uniaxial tensile test
M_{crane}	moment induced by crane in analytical approach (phase 0)
M_i	moment around i-axis
$M_{upright}$	moment responsible for uprighting of ship + palls in analytical approach (phase 3 — 4)
M_{tip}	moment responsible for tipping of ship + palls around edge of pier in analytical approach (phase 2 —3)
M_{weight}	moment induced by weight of ship + palls in analytical approach (phase 0)
m	mass
m_f	mass of fluid of spring-damper-system in FSI algorithm
m_s	mass of structure of spring-damper-system in FSI algorithm
m_{tot}	mass of ship + palls in analytical approach
n	natural number
n_{hard}	hardening coefficient in power law
n_{panel}	number of plate fields of vibrating plate panel
p	pressure
p_0	pressure at reference state of thermodynamic EOS
p_{bi}	design pressure due to bottom slamming in rule-based load model
p_{dyn}	(hydro-)dynamic pressure
p_{fac}	user-defined scaling factor for stiffness in FSI algorithm
p_H	pressure at Rankine-Hugoniot state of thermodynamic EOS
$p_{i\ max}$	peak pressure of pressure transducer i in model tests
$p_{i\ max\ mean}$	mean value of $p_{i\ max}$ for measurement series in model tests
p_{mt}	pressure-time-function in load model based on model tests
$p_{mt\ max}$	peak pressure in load model based on model tests
p_{rb}	pressure-time-function in rule-based load model
q_{CS}	material coefficient in Cowper-Symonds equation
R_m	tensile strength
S_i	static moment around i-axis
$S_{MG\,i}$	material coefficients in Mie-Grüneisen EOS
S_n	sum of a function using Simpson's rule of integration
SD_i	standard deviation of measurement series i in model tests
T	temperature
T_0	temperature at reference state of thermodynamic EOS
T_{design}	draught of ship at design loading condition
T_{frame}	depth / draught of ship frame
t	time
t_i	time at ith time step
t_{impact}	time at impact with water surface
$t_{p_{i\ max}}$	time of peak pressure of pressure transducer i in model tests
t_r	time of rise / drop of pressure-time-function in rule-based load model
$t_{r\ mt}$	time of decay of pressure-time-function in load model based on model tests
t_{shell}	plate thickness of plate panel

Symbol	description
Δt	time step size
Δt_e	characteristic time step size of explicit time integration scheme
Δt_{RK}	time step size of Runge-Kutta method in analytical approach
V	volume
V_0	volume at reference state of thermodynamic EOS
V_f	volume of fluid containing master elements in FSI algorithm
V_{rel}	relative volume in thermodynamic EOS
v_{conv}	convective velocity in ALE formulation
v_i	speed in i-direction
$v_{i\ impact}$	speed in i-direction at impact with water surface
v_{ij}	speed in ij-plane
$v_{ij\ impact}$	speed in ij-plane at impact with water surface
v_{mat}	velocity of material in ALE formulation
v_{mesh}	velocity of mesh in ALE formulation
v_{slam}	speed perpendicular to water surface at impact with water surface
$v_{sway\ impact}$	speed of sway motion of ship at impact with water surface
$\bar{X}_i$	mean value of measurement series i in model tests
$x,\ y,\ z$	Cartesian coordinates / global coordinate system
$x_s,\ y_s,\ z_s$	local coordinate system of ship used in analytical approach
x_i	Eulerian coordinates in ALE formulation
x_{pen}	penetration in FSI algorithm
$\dot{x}_{pen}$	speed of penetration in FSI algorithm
$y_{A_{frame}}$	y-coordinate of centroid of A_{frame} in analytical approach
$y_{A_{xy}}$	y-coordinate of centroid of A_{xy} in analytical approach (phase 3 — 4)
y_{COB}	y-coordinate of COB of ship in analytical approach (phase 3 — 4)
y_{COG}	y-coordinate of COG of ship
$y_{COG\ impact}$	y-coordinate of COG of ship at impact with water surface
$y_{COG_{tot}}$	y-coordinate of COG of ship + palls in analytical approach
y_{pier}	y-coordinate of edge of pier in analytical approach
$z_{A_{frame}}$	z-coordinate of centroid of A_{frame} in analytical approach
$z_{A_{xz}}$	z-coordinate of centroid of A_{xz} in analytical approach (phase 3 — 4)
z_{COG}	z-coordinate of COG of ship
$z_{COG\ impact}$	z-coordinate of COG of ship at impact with water surface
$z_{COG_{tot}}$	z-coordinate of COG of ship + palls in analytical approach
z_{pier}	z-coordinate of edge of pier in analytical approach
z_{wl}	z-coordinate of water level in launch basin in analytical approach

Greek Symbols

Symbol	description
β_{frame}	plumpness of ship frame
β_{impact}	deadrise angle

Symbol	description
Δ	displacement of ship
Δ_{design}	displacement of ship for design loading condition
δ	out-of-plane bending deformation of plate panel
ε	strain
ε_{break}	strain of specimen at break at uniaxial tensile test
ε_{eng}	engineering strain
ε_{true}	true strain
ε_{ue}	strain of specimen at uniform elongation at uniaxial tensile test
$\dot{\varepsilon}$	strain rate
Γ_{MG}	Grüneisen gamma (material coefficient) in Mie-Grüneisen EOS
κ	heat capacity ratio of a gas
λ_{ij}	added mass of ship in i-direction due to acceleration in j-direction
λ_{panel}	added mass of vibrating plate panel
λ_{sm}	scale of ship model in model tests
μ_{EOS}	ratio of compressibility in thermodynamic EOS
μ_{panel}	form coefficient for calculation of added mass of vibrating plate panel
μ_{sw}	coefficient of sliding friction between slipway and palls
ν	Poisson's ratio
φ	roll angle / angle around x-axis of ship
φ_{impact}	roll angle / angle around x-axis of ship at impact with water surface
φ_{max}	maximal roll angle on STB during sideways launching process
$\lvert\varphi_{min}\rvert$	maximal roll angle on PS during sideways launching process
φ_{sw}	inclination of slipway of sideways launching system
ρ	density
ρ_0	density at reference state of material model / thermodynamic EOS
ρ_w	density of water
$\rho_{w\ fs}$	density of water in full scale version of model tests
$\rho_{w\ ms}$	density of water in model scale version of model tests
$\sigma_{amplitude}$	amplitude of stresses resulting with FFT
σ_{eng}	engineering stress
σ_{eqv}	equivalent stress (von Mises)
σ_i	normal / membrane stress in i-direction
σ_{ij}	Cauchy stress tensor
σ_{perm}	permissible normal / membrane stress
σ_{true}	true stress
σ_Y	yield strength at quasi-static loading
σ_{YD}	yield strength at dynamic loading
τ_{ij}	shear stress in ij-plane
τ_{perm}	permissible shear stress
ω_i	angular velocity around i-axis
$\omega_{i\ impact}$	angular velocity around i-axis at impact with water surface
ω_{pen}	angular frequency of spring-damper-system in FSI algorithm

Mathematical Symbols

Symbol	description
∇	buoyancy of ship
$\mathcal{O}(\,)$	Big O / Bachmann–Landau notation

1. Introduction

The ship design process can be understood as an optimization problem with several, often conflicting constraints. Such constraints result from different requirements regarding the intended ship design [77]. Driven by regulatory bodies as the International Maritime Organization (IMO) economical aspects like the Required Freight Rate (RFR) for instance, are no longer the primary goal of a ship design. In recent years environmental aspects became more and more relevant. Regulations like the Energy Efficiency Design Index (EEDI) or more recently the introduction of the Carbon Intensity Indicator (CII) in 2023 measure and regulate how efficiently a ship can transport goods or passengers in relation to its CO_2 emissions.

Besides a switch towards alternative fuels for commercial ships, the use of appropriate simulation-based approaches to optimize economical as well as ecological aspects of a ship design is a key factor for dealing with these stricter requirements and regulations. Especially in the past two decades increasing computational resources allowed for a leap in available simulation methods, complexity as well as size of models. In naval architecture this enabled an increased level of optimization of a ship design based on numerical simulations. A common example is the optimization the shape of a ship hull. By now it is state of the art to use a parametric description of the ship hull within an optimization framework. Combining this framework with corresponding computational fluid dynamics (CFD) simulations the resistance and delivered power at the propulsion system can be reduced, thus improving RFR, EEDI as well as CII. Examples for such approaches can be found in literature, e.g. in the work by Zaraphonitis *et al.* [119].

Another approach is the optimization of the hull structure of a ship. By carrying out according finite element method (FEM) simulations the weight of the hull structure can be reduced compared to the mere application of rules and regulations of classification societies. For this purpose the most common load cases are considered (e.g. local strength of structural components, longitudinal strength, assessment of fatigue strength, structural dynamics like forced vibrations among others) and used as the basis for such optimizations. Reducing the weight of the hull structure results in an increased payload to displacement ratio, thus improving the RFR, EEDI and CII as well. Examples for such approaches can be found in literature, too. A good overview is provided by Rigo *et al.* [87].

For effectively optimizing the hull structure of a ship regarding its weight, the principles of lightweight design are crucial. For an effective lightweight design a detailed and accurate understanding of loads acting upon a structure is essential. Without this knowledge a structure will contain unnecessary conservatism and safety margins ultimately destroying the potential of any lightweight design or optimization approach [67]. If the full potential of a lightweight design is utilized, the structure is loaded near its load carrying capacity. In general, a lightweight design of a structure is done according to its standard operating loads [67].

However, this means that an optimized structure can be more prone to failure against loads outside of these standard operating loads, even if these load cases only occur once in the lifetime of such a structure. Common practices including the corresponding load cases can become suddenly risky or even outright dangerous. This is especially true for practices and load cases, that heavily rely upon experience of the involved engineers and technicians. Great care has to be taken, that such an optimized structure is able to withstand these

load cases without damages. But it is also important, that the potential weight savings due to the optimizations are not nullified by necessary reinforcements of a structure against such load cases. Therefore, it can be necessary to revaluate common practices, even if they were successfully used for decades, with modern knowledge and approaches to account for optimizations and as a consequence thereof reduced safety margins.

In the case of naval architecture an example for a common practice, which heavily relies on the experience of the personnel of a shipyard, is the launching of a ship. Depending on the launching system installed at a shipyard high loads can be induced into the hull structure, that just occur once at the beginning of the ship's lifetime. This is true for an end launching as well as a sideways launching process. An general overview of different launching methods is provided by Leavitt [56]. While the calculation of loads resulting during an end launching process of a of ship is documented well in literature (e.g. in [56]), the corresponding knowledge is not available for the sideways launching process as discussed in more detail later within this work.

This lack in knowledge is to some extent surprising, as the sideways launching process is still nowadays a commonly used approach in naval architecture. In the past century a variety of different ship types were launched using this method. One example for the use of sideways launchings up to this day is the shipyard *Ferus-Smit* located in Leer, Germany. In recent years many different ships were successfully launched using a sideways launching process at *Ferus-Smit*. Examples are general cargo ships of the *Arklow*-series [109], [110] and *Symphony*-series [46] or tanker ships of the *Thun*-series [47], [66]. An photograph of the sideways launching process of the *Thun Equality* is shown in Figure 1.1. This photograph gives a good impression of the different, complex physical phenomena relevant during a sideways launching process:

- non-linear response of the ship: complete range of stability is relevant
- six degree of freedom (DOF) motion with according equation of motions including added masses and hydrodynamic damping
- free water surface with spray root, water pile up and waves forming around the ship hull
- dynamic loads at the impact of the ship hull with the water surface comparable to slamming events
- effects of hydro-elasticity during the the impact of the ship hull with the water surface
- dynamically loaded hull structure with high stresses at certain areas, which can result in non-linear behavior (buckling, plastic deformation or in worst case failure of parts of the hull structure)

An in-depth description of the sideways launching process itself is given in [56]. In general, the physical problem and phenomena can be split into two different problems: the ship motion and the loads resulting on the hull structure during the impact with the water surface. For assessing the ship motion during the sideways launching process, the process can be split into four different phases [56]:

- phase 1 — sliding of ship down the slipway

Figure 1.1.: sideways launching process of *Thun Equality* [66]

- phase 2 — tipping of ship around edge of pier
- phase 3 — tipping of ship around edge of pier plus immersion of the ship
- phase 4 — dropping and raise of ship (free ship motion)

An visualization of the different phases is given in Appendix A.1. Naturally, the loads resulting on the hull structure during the sideways launching process are highly depending on the trajectory of the ship. These two aspects including the corresponding physical phenomena are to be assessed accordingly by an approach or method of choice. This can be either done subsequently (estimation of ship motion and trajectory → assessment of loads resulting on ship hull) with approaches commonly used during the ship design process. Possible are analytical or experimental approaches as well as simulation-based approaches without fluid-structure interaction (FSI). Alternatively, the ship motion as well as resulting loads on the ship hull can be assessed simultaneously with a simulation-based approach using FSI as proposed within this work.

An inadequate assessment of the above mentioned aspects can have devastating consequences. Capsizing or damages to the hull structure are possible, if certain aspects are assessed incorrectly during the ship design phase. A recent example is the sideways launching of the *USS Cleveland* in April 2023, where damages to the hull structure due to a collision with a tugboat occurred [70].

From the point of view of the ship design process, a sideways launching process is a comprehensive task as well. Many branches of naval architecture are to be assessed in close conjunction with each other. Different design parameters and decisions can have

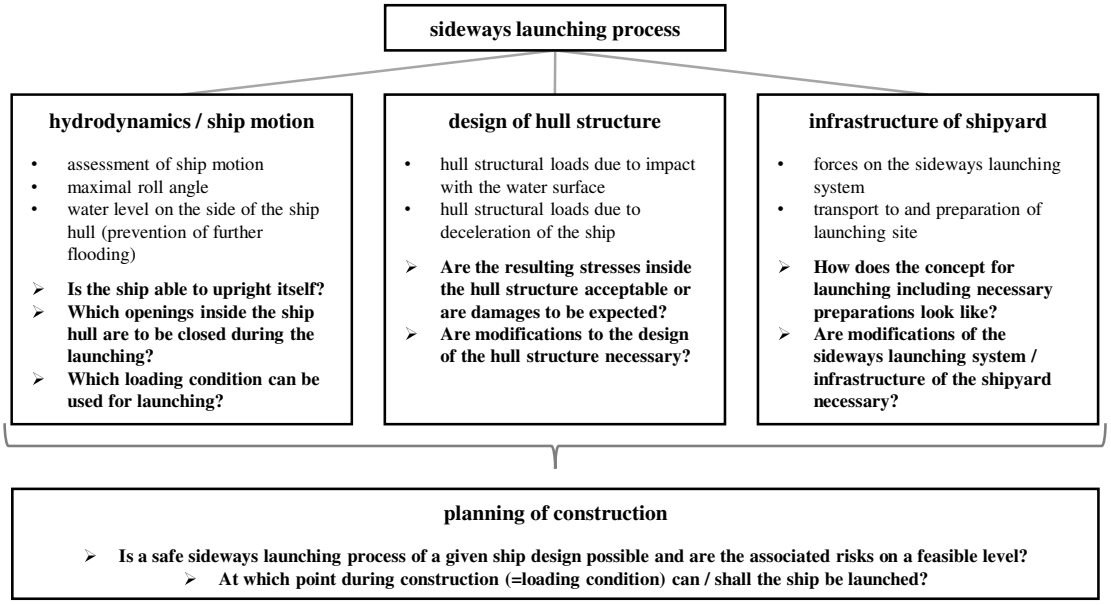

Figure 1.2.: different aspects of a sideways launching process

a significant influence on the sideways launching process and vice versa. This includes hydrodynamics / ship motion, design of the hull structure, infrastructure at the shipyard and planning process of the construction. These aspects and different tasks are visualized in Figure 1.2. These questions have to be answered as early and holistically as possible during the design phase, in order to minimize costs and risks associated with a sideways launching process.

1.1. Investigated case study

Within this work the sideways launching process for a special purpose vessel (SPV) is investigated in detail. The problem became relevant during the basic design phase of the SPV, as a potential construction shipyard has an according sideways launching system installed at site. This system as well as the setup of the sideways launching process for the SPV is visualized in Figure 1.3.

The system as shown in Figure 1.3 is slightly different compared to the description in [56]. The ship and palls are placed on rocker arms and are not inclined at the beginning of the sideways launching process. To start the sideways launching process, the rocker arms are lifted by a crane, aligning the ship and palls with the inclination of the slipway. This phase is introduced as phase 0 — rotation of ship within this work. After lifting the rocker arms, the SPV starts with the sliding motion (start of phase 1).

All above mentioned aspects regarding the ship motion and loads resulting on the ship hull are to be assessed for the SPV. In comparison to ships typically launched sideways, the SPV has distinct features making an accurate assessment of the sideways launching process inevitable. The hull form of the SPV does not have vertical side walls. The frame contour above the water line is inclined towards the centre line. This can result in a high maximal roll angle during the sideways launching process. The upper parts of the hull,

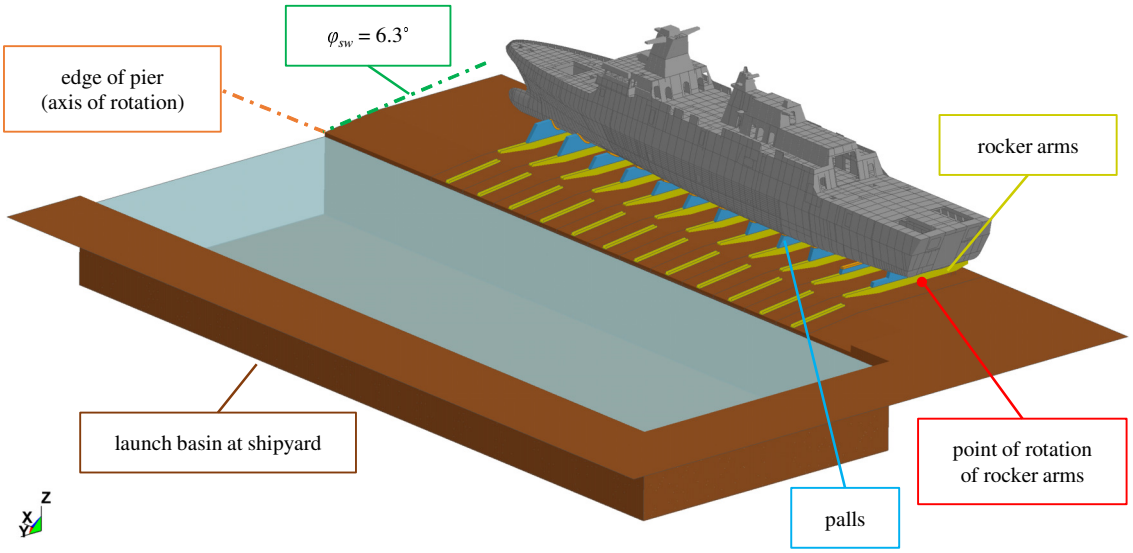

Figure 1.3.: investigated case study: sideways launching process of a SPV

which will generate the necessary moment to upright the SPV, will immerse late into the water. Therefore, the ship motion and range of stability of the SPV are to be checked carefully.

As the SPV is a fast ship, the hull structure of the SPV is highly optimized regarding its weight. The complete hull structure is designed with high tensile steel, to reduce necessary plate thicknesses and sizes of stiffeners. Numerical methods like FEM were used to further reduce the weight of the hull structure with regards to static and dynamic loading (e.g. local loads, longitudinal strength or vibrational aspects). In comparison to commercial ships of similar size — e.g. general cargo, tanker, bulker or container ships — plate thicknesses used for the shell plating are thinner between a factor of two up to three. As the hull structure of the SPV is highly optimized regarding its weight, the potential safety margin during a sideways launching process is small in comparison. This is especially true, as the loads resulting from a sideways launching process are not a load case considered during the initial design or subsequent optimization of the hull structure of the SPV.

To avoid any damages to the hull structure, a detailed understanding of the load mechanisms acting upon the hull structure as well as an accurate assessment of the resulting hull structural loads is necessary. In addition, such a detailed understanding of the resulting hull structural loads is necessary in accordance with the principles of lightweight design.

2. State of the art

In this chapter the current state of the art / available literature regarding the sideways launching process is discussed. As from a physical point of view the launching of a free-fall lifeboat (FFLB) is to a certain degree comparable to a sideways launching process, the current state of the art regarding the launching of FFLBs is reviewed as well. As these two methods of launching are closely related to slamming events ($\rightarrow$ impact with water surface), a brief overview of literature regarding slamming phenomena relevant for this work is given.

Based on the reviewed state of the art research questions to be answered within this work are formulated. These are joined by the corresponding research hypothesis. Lastly, based on the research hypothesis an overview of the structure of this work is provided.

2.1. Sideways launching process

Publicly available literature regarding sideways launching processes is scarce. A comprehensive overview of the sideways launching process is provided in Leavitt [56]. This includes the preparation, execution and subsequent evaluation.

Different approaches to solve the corresponding ordinary differential equation (ODE) of motion for the different phases of the sideways launching process as illustrated in Appendix A.1 can be found in literature. In general, these approaches consider three DOF including the translation in y-direction (horizontal movement) and z-direction (vertical movement) as well as the rotation about the x-axis (roll angle). In [56] closed analytical solutions of the ODE of motion are provided. These allow for the assessment of certain aspects of the ship motion, e.g. the speed of a ship at the end of the slipway or the maximal roll angle. In the work by Ye [115] numerical solutions of these ODE of motion as well as an implementation of appropriate numerical solution schemes is proposed. In the work by Ramzi and Pacuraru [81] a similar approach as in [115] is presented. However, the approach in [81] is limited to the ODE of motion for phase 1 — sliding up to the end of phase 3 — tipping and immersion (compare Figures provided in Appendix A.1). The free ship motion in phase 4 is not considered in [81].

In [56], [115] the hydrodyanmic forces acting upon the ship hull during the sideways launching process are calculated based on analytical equations including the according assumptions. In more advanced approaches these hydrodyanmic forces are calculated using hydrodyanmic codes, which are coupled with the solution of the according ODE of motion. This allows for a more detailed and accurate assessment of the hydrodyanmic forces acting upon the ship hull during the sideways launching process. One example for such an approach is given in the work by Hak [38]. In [38] the hydrodynamic forces are calculated using the hydrodyanmic code COMFLO. A similar approach is proposed in the work by Krawskowski [54], who used the hydrodyanmic code COMET for this purpose. In both cases the hydrodyanmic forces obtained with the hydrodyanmic codes are coupled with self developed routines for solving the corresponding ODE of motion. Although the results obtained in [38], [54] are qualitatively comparable to their respective references (model tests / test cases), discrepancies regarding the trajectory as well as roll angle could be observed. These are contributed to either the implementation of the self-developed routines itself [38], [54] or wrong / too simple assumptions during the calculation like missing reflections of waves inside the launch basin [54].

A simulation-based approach without FSI is given in the work by Fitriadhy and Malek [34]. In [34] the sideways launching process of a tanker was successfully simulated using the commercial CFD software Flow-3D. A parametric study was carried out investigating the influence of the inclination of the slipway as well as the distance between the ship and the launch basin in horizontal direction. For the case study investigated within this work these parameters are not of interest, as these are fixed by the design of the sideways launching system to be used for the launch of the SPV. No verification of the conducted CFD simulations is provided in [34].

Within the discussed literature regarding the sideways launching process only the trajectory / ship motion is investigated. The loads resulting during the impact of the ship hull with the water surface are not addressed by any of the given references.

2.2. Launching of free-fall lifeboats

As available literature regarding the sideways launching process of ships is so scarce, a closer look at comparable physical processes / methods of launching is taken. Closely related to sideways launching of ships is the launching of a FFLB. From a physical point of view the launching of a FFLB is to a certain degree comparable to a sideways launching process. In both cases, the ship / the FFLB is subjected to a free-fall motion before impacting with the water surface. The same physical phenomena are relevant for both a sideways launching process as well as the launching of a FFLB.

The launch of a FFLB can be split in too similar phases as shown in Appendix A.1: sliding down a ramp, rotating around the edge of the ramp water, free-fall and lastly the impact with the water surface and immersion. Approaches and methods used to assess the physical phenomena during the launch of a FFLB can be used or adapted for the sideways launching process of the SPV.

In the last three decades a lot of research was published regarding the design of FFLBs. A good overview of relevant literature regarding the launch of FFLB and the corresponding loads is given by Ringsberg *et al.* [88]. The classification society Det Norske Veritas (DNV) does provide a complete standard for the design of FFLBs [29]. As with the sideways launching process, the launch of a FFLB is split into two aspects within [29]: estimating the motion / trajectory of the FFLB and subsequently assessing the loads resulting on the FFLB based on the estimated trajectory. For assessing the trajectory different approaches can be used according to [29] (Section 4.5.3.14):

- simplified method by solving the corresponding ODE of motion, preferably for all six DOF (= analytical approach; comparable approach as given in [56], [115])
- numerical methods such as CFD (= simulation-based approach without FSI; comparable approach as given in [34])
- model tests (= experimental approach)

Details and guidance notes for each method are provided within [29]. For the design of the hull structure, slamming pressure on the hull from water entry as well as inertia forces on the FFLB due to deceleration are to be considered [29] (Section 4.5.5.2). As with the assessment of the trajectory, the same three methods can be used: analytical models for slamming, numerical methods like CFD-simulations or model tests.

As stated in in [29] (Section 4.5.6.2), determining the slamming loads on a lifeboat during impact is considered complex and difficult to describe using simple expressions. CFD simulations are to be validated by model or full-scale tests. For using model tests to derive the slamming loads, a sufficient number of suitable pressure sensors during model tests are necessary.

For all approaches mentioned in [29] examples can be found in literature. One of the first models to assess the forces during the water entry phase of the FFLB including corresponding slamming loads was proposed by Boef [12], [13]. An analytical approach for assessing the trajectory of the FFLB during its free-fall is given by DNV in [29]. The corresponding ODE of motion consider three DOF, including the translation in x-and z-direction as well as rotation around y-axis (pitch of FFLB). Qiu *et al.* [79] proposed a model for assessing the trajectory of the FFLB through water, which includes the loads at the impact with the water surface. In addition, the model in [79] accounts for the motion of the ship (= launching platform) and the elevation of the water surface due to waves / different sea states. Recently Qiu *et al.* [80] extended the model to six DOF considering the asymmetric impact forces during the water entry of the FFLB.

One example for the use of numerical methods is the work by Tredge *et al.* [95]. In [95] the launch of a FFLB is investigated with the commercial CFD code Star CCM+. Based on the conducted CFD simulations the trajectory, resulting accelerations ($\rightarrow$ important for occupant safety) as well as slamming loads were assessed. The numerical results in [95] show good agreement with full-scale tests.

Different methods for assessing the structural response of a FFLB during the water entry phase are discussed in [88]. This includes a comparison of linear-elastic and non-linear beam models with FEM simulations as well as transient with quasi-static load modelling approaches. A comparison of the different approaches based on experimental results measured during a model test of a FFLB in scale 1:9 are provided in [88].

An example for a more holistic simulation-based approach without FSI is presented by Califano and Brinchmann [20]. In [20] CFD and FEM simulations are combined, in order to assess the loads resulting during the impact with the water surface of a FFLB. For this purpose the trajectory, accelerations as well as pressure on the hull of the FFLB were calculated using CFD simulations in Star CCM+. The resulting pressure was mapped for defined time steps onto the mesh of the FEM model of the FFLB inside the FEM software Abaqus. Quasi-static FEM simulations were carried out considering the pressure on the hull as well as the resulting inertia loads. Therefore, the approach proposed by Califano and Brinchmann [20] is a one-way coupling from CFD to FEM without actual FSI. Effects of hydro-elasticity are not considered using this approach.

Bae *et al.* [10] proposed a simulation-based approach with FSI to assess the trajectory during the launching of FFLB. This approach is based on the Arbitrary-Lagrangian-Eulerian (ALE) approach inside the FEM software LS-DYNA. Using the ALE approach the water entry of a FFLB based on model tests in scale 1:5 was successfully simulated in [10]. Focus in [10] was the accelerations resulting during the impact of the FFLB with the water surface, as these are relevant for occupational safety. While the peak accelerations showed reasonable agreement to the experimental data of the model test, the acceleration-time-signal showed some discrepancy. As stated in in [10], the differences could be the result from the complexity of the FSI algorithm used for the ALE approach inside LS-DYNA.

Based on the results in [10], Bae and Zakki [9] did a closer investigation regarding different ALE element formulations (single-material vs. multi-material ALE elements) for the use

case of the water entry of a FFLB. Although the multi-material ALE element formulation did yield results slightly closer to experimental data, there were still uncertainties regarding different settings of the FSI algorithm [9]. A parametric study of different parameters relevant for the FSI algorithm used for the ALE approach is suggested in [9]. Besides the uncertainties regarding setting of the FSI algorithm, a major drawback of the model setup as proposed in [10] is the use of a rigid shell element formulation for the model of the FFLB. No assessment of the hull structural loads resulting during the launch of the FFLB is possible using that modelling approach.

Despite this lack of in-depth knowledge regarding FSI settings, the applicability and benefits of the ALE approach for the design of a FFLB could be shown using the model setup as proposed in [10]. Zakki *et al.* [117] investigated the influence of different launching parameters (angle of skid, sliding distance and fall height) on the resulting motion pattern / trajectory during the water entry phase of a FFLB. Limits for a safe motion pattern according to rules and regulations provided by DNV [29] were derived based on the simulations with the ALE approach. Zakki *et al.* [118] developed a new V-shaped hull form for a new FFLB based on the ALE approach. Accelerations could be actively resulting during the water entry phase of the newly developed FFLB, thus increasing the occupational safety [118]. However, in [117], [118] it is stated, that simulations using the ALE approach should be verified using experimental data / model tests due to the complexity of the underlying FSI algorithm.

2.3. Slamming phenomena

The impact with the water surface during both methods of launching — sideways launching of ships and launching of FFLBs — is comparable to slamming events. Slamming phenomena and the resulting impact loads on ships and marine structures are a subject of research since at least 100 years. With increasing computational resources and methods the research is still ongoing. A recent overview of the current state of research including analytical formulations of impact problems, relevant slamming experiments and simulation-based approaches is given by Abrate [1] as well as Wang and Guedes Soares [104].

2.3.1. Analytical models

Over the past century different analytical formulations were developed, which are able to predict the pressure on a structure as it impacts with the water surface and immerses into the water. The first theories based on potential flow assumptions were derived nearly 100 years ago. In 1929 Kármán [45] assessed impact forces on sea plane floats during a water landing by using momentum theory. In 1932 Wagner [103] proposed his theory for 2D rigid wedge-shaped bodies with small deadrise angles β_{impact}.

Especially the Wagner model was widely used and further enhanced in the past. By introducing additional terms into the velocity potential distribution in the contact domain [104], more general forms of the model of Wagner were derived. These models show good agreements with experimental results. Noteworthy are the following three models:

- original Longvinovich model (OLM) proposed by Logvinovich [63] in 1972
- generalized Wagner model (GWM) proposed by Zhao *et al.* [120] in 1996

- modified Longvinovich model (MLM) proposed by Korobkin and Malenica [51] in 2005

A brief overview of the different models is provided in [18]. An in-depth comparison including the mathematical modelling of these models is given in [52]. Like most slamming experiments found in literature, these models are valid for symmetric, two-dimensional configurations at one DOF. Such a configuration is shown for an exemplary wedge in Figure 2.1. Such models cannot be applied or adapted directly for the sideways launching of ships, as the sideways launching process is a highly asymmetric slamming event. This can be seen in the photograph in Figure 1.1.

Judge *et al.* [44] carried out slamming experiments for an asymmetric wedge configuration with horizontal as well vertical speed at impact with the water surface (two DOF). The different configurations investigated in [44] are illustrated in Figure 2.2. These are very similar to the one observed during the impact of the SPV with the water surface during the sideways launching process, as a comparison of Figure A.3 with Figure 2.2 shows. A numerical model is proposed in [44], too. This model involves the discretization of the surfaces of the wedge and an iterative solution scheme. The method in [44] is based upon two-dimensional vortex distributions to model the boundary-value problem given by the asymmetric impact of the wedge. Good agreement between experimental data and the proposed model were found for small degrees of asymmetry and small ratios of horizontal to vertical velocity at impact [44]. This configuration is a so-called type A flow, where no separation of the flow and no ventilation occurs. This configuration is shown in Figure 2.2a. The agreement found in [44] is true for the position of the the spray root on both sides of the wedge as well as the resulting wetted surface forming during the immersion of the wedge.

However, differences between experimental data and the proposed model in [44] are bigger for configurations with higher degree of asymmetry (high ratio of horizontal to vertical velocity at impact) and small deadrise angles. This is a so-called type B flow with flow separation and ventilation, as illustrated in Figure 2.2b. As the model tests and the simulation-based approach using FSI show, the type B flow with flow separation and ventilation is present during the sideways launching process of the SPV. Due to the shape of the hull of the SPV in combination with geometry of the slipway, a high degree of asymmetry is given ($v_{y\ impact}/v_{z\ impact} > 2$ and $\beta_{impact} \approx 0$).

In addition, there are further limitations of the model proposed by in [44] relevant for the sideways launching process. The model in [44] considers only two DOF (horizontal and vertical translation). No rotation of the wedge is considered (= roll motion of SPV during sideways launching process). Furthermore, the effect of hydro-elasticity is not accounted for in [44], which plays an important role for the resulting peak pressure at small deadrise angles [18].

A mathematical model considering three DOF including the rotation during the impact of an asymmetric, rigid wedge configuration is proposed by Xu *et al.* [114]. The model is based on the MLM. The conditions of the wedge (initial velocities and trajectory) investigated in [114] are comparable to the one of the SPV during the sideways launching process. A general model is proposed by Moore *et al.* [69]. In [69] a model for three-dimensional oblique water-entry problems based on the GWM is proposed.

As the model is described for generalized three-dimensional problems at oblique angles, the resulting model is very complex. The focus in the work done in [69], [114] lies on the mathematical modelling rather than on physical phenomena / applicability of the proposed models. A thorough verification based on appropriate experimental data — e.g. like provided in [44] — is missing for both models proposed in [69], [114].

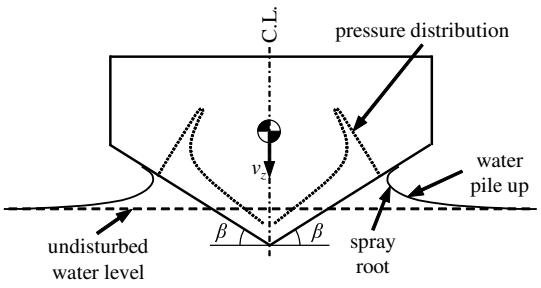

Figure 2.1.: symmetrical slamming event

2.3.2. Experiments

In the past decades a broad variety of different slamming experiments were conducted. Besides [1], [104] an overview of different slamming experiments is given in the work by Lewis *et al.* [58]. In the following, a brief overview of slamming experiments relevant and referred to within this work is given.

Lewis *et al.* [58] investigated the general uncertainties regarding pressure measurements during slamming events based on a symmetric wedge with an deadrise angle of 25°. A sophisticated test setup designed for best possible repeatability was used in [58]. The goal of [58] was to provide a test setup producing high quality data for the validation / verification of numerical methods for slamming applications.

Tödter *et al.* [94] conducted slamming experiments with a flat bottom structure ($\beta_{impact} = 0°$). The investigations were carried out for a rigid as well as flexible bottom structure, where the effects of hydro-elasticity played an important role. 30 runs of each test case were conducted, allowing for a good assessment of the uncertainties involved with a flat bottom structure. Using high speed cameras, the complex flow conditions right after the impact are visualized. A cushion of air was trapped between the water surface and the flat bottom structure, which is subjected to oscillations and thus influenced the resulting pressure. The oscillations were more pronounced for the flexible bottom structure [94]. The investigated conditions in [94] are comparable to the conditions given during model tests of the sideways launching process ($\beta_{impact} \approx 0°$ and $v_{slam} \approx 1$m/s in model scale).

Judge *et al.* [44] investigated the behavior and flow conditions around an asymmetric wedge with horizontal and vertical speed at impact. Such a configuration is similar to the one observed during the the sideways launching process of the SPV (compare Figure A.3 with Figure 2.2). For small deadrise angles and / or a higher level of asymmetry, flow separation and ventilation did occur during experiments conducted in [44]. At the side of the wedge opposite to the water surface, ventilation could be observed. This ventilation lead to complex flow conditions around the investigated wedge, as the water is moved around the wedge towards the area of ventilation [44].

The experiments conducted by Javaherian *et al.* [43] were used for verification purposes of the simulation-based approach using FSI proposed within the context of this work. In contrast to many other slamming experiments, a wedge with flexible bottom plating constructed with aluminium was used in [43]. The flexible bottom plating does resemble a typical hull structure of a ship (plate-stiffener construction) more realistically than a rigid wedge. This allowed for the consideration of the effects of hydro-elasticity. During slamming experiments conducted in [43] the following data were measured:

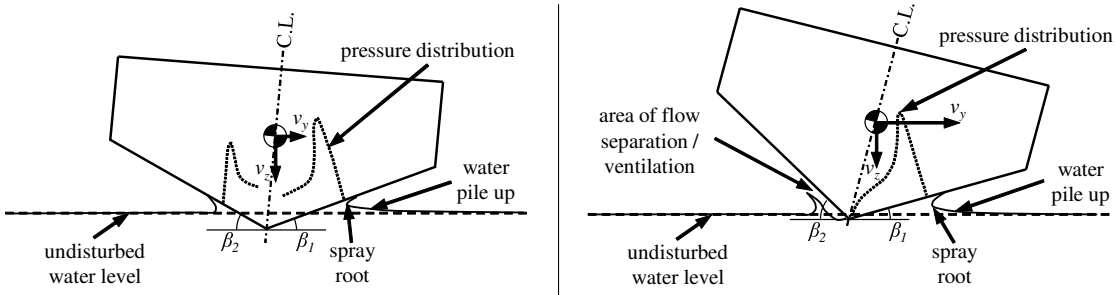

(a) type A flow — low level of asymmetry

(b) type B flow — high level of asymmetry

Figure 2.2.: asymmetrical slamming event according to [44]

- mean vertical velocity of the wedge
- deformation of the bottom plating
- pressure-time-signals resulting on the bottom plating at different positions

These data were used for verifying the simulation-based approach using FSI proposed within the context of this work.

Lastly, the experimental work done by Chuang [23] is worth mentioning. In [23] a systematic study on the influence of different parameters on the resulting peak pressure at the impact with the water surface was carried out. This included rigid wedges with different deadrise angles (flat bottom up to 45°) as well as different drop heights / speeds at impact. Different sets of curves are provided in [23] allowing for an estimation / approximation of the expected peak pressure for different slamming configurations.

2.3.3. Simulation-based approaches

Due to the increasing availability of computational resources — especially in the last two decades — a broad variety of different simulation-based approaches for assessing slamming phenomena / water entry problems can be found in literature. These approaches range from CFD simulations, which assess the motion as well as the pressure resulting on different bodies during a slamming event, to simulation-based approaches using FSI. An overview of different approaches is provided in [1] as well as in [104].

Most of the research regarding slamming phenomena was focused on symmetrical slamming events as shown in Figure 2.1. Naturally, this results in higher knowledge regarding different numerical methods in favour of such symmetrical slamming events. Besides [44], the work by Xu *et al.* [113] is one of the first investigations regarding numerical methods with a focus on asymmetrical slamming events. Only in recent years a shift of interest towards the investigation of asymmetrical slamming events can be observed.

One example is the work conducted by Wang and Guedes Soares [105]. The approach and configuration used in [105] is comparable to the proposed simulation-based approach using FSI within this work. In [105] parametric studies regarding the loads resulting on a rigid wedge impacting the water surface at oblique angles combined with a roll angle were conducted using an ALE approach. In the work by Izadi *et al.* [42] the effects of hydroelasticity were considered, while investigating the water entry problem of an asymmetric

wedge with an oblique speed in a similar way as [105] . More recently these numerical methods were adapted / extended from simpler 2D wedges towards the investigation of asymmetric slamming events of ship hull structures. Examples are the work by Xie *et al.* [112] or Lu *et al.* [64]. Besides the work presented in [9], [10], [117], [118], these investigations are a good starting point for the simulation-based approach using FSI proposed within this work.

2.4. Scope of work

Based on the reviewed state of the art, different research questions do arise. These are formulated within this section and are joined by the corresponding research hypothesis.

2.4.1. Research questions and hypothesis

As slamming phenomena were researched quite intensively over the past century, a lot of literature including standards, rules and regulations, best practices regarding the assessment of slamming are available, e.g. [3], [18], [25]. The same is true for the launching of FFLB. Starting in the 1990s a lot of research regarding the launch of FFLB was conducted, which ultimately resulted in its own standard for the design of FFLB [29]. For both types of problems different approaches are available in literature, that allow for an assessment of the trajectory as well as of the resulting loads on a structure (either a wedge, ship hull or FFLB). As for both type of problems the hull structural loads resulting during the impact with the water surface are to be accounted for during the design of the hull structure, the according loads and load mechanism are well studied.

In contrast to this, available literature regarding the sideways launching process of ships is scarce, as this type of launching is often conducted by shipyards based upon experience. Especially methods or models for assessing the loads resulting on the ship hull during a sideways launching process are missing. As weight optimization of hull structures becomes more and more relevant for present and future ship designs, conducting a sideways launching process of such a weight optimized ship design without a profound knowledge of the resulting loads on the ship hull does involve a certain level of risks. This results in the first question to be investigated within this work:

> How do the loads on a ship hull during the different phases of a sideways launching process look like as a function of time?

As the loads resulting on the ship hull are only one part of the equation, the hull structural loads resulting during a sideways launching process are to be known as well. Therefore, the following questions have to be asked:

> Which hull structural loads can be observed during a sideways launching process at different parts of the hull structure? What are the main load mechanisms acting upon the hull structure?

As no information regarding these questions is available in literature, systematic studies regarding relevant parameters during a sideways launching process cannot be found either. This is true for the ship motion as well the loads resulting on the ship hull / resulting hull structural loads. As for planning and conducting a sideways process knowledge of these parameters is important, the following questions are to be investigated as well:

> Which parameters of a sideways launching process are the most relevant ones regarding the ship motion as well as the resulting loads on the hull structure / hull structural loads? How big is the influence of each parameters on the different aspects of a sideways launching process?

Lastly, the focus of research regarding simulation-based approaches for the use case of water entry problems was mainly on symmetric slamming events in the past. Especially simulation-based approaches using FSI were mostly applied to symmetric slamming events or limited to smaller models in the case of asymmetric slamming events (e.g. simulation of slamming experiments; often of 2D wedges). Investigations of asymmetric slamming events using models of a ship's hull structure are up to this day still at early stages of research. This results in the following question from an methodical point of view:

> How does a setup of a sufficient and reliable simulation-based approach look like, which is able to account for the relevant physical effects of asymmetrical slamming events as present during a sideways launching process?

Especially in the case of a simulation-based approach using FSI a good knowledge of relevant parameters and settings for the FSI algorithm of choice [9] as well as a thorough verification are necessary [117], [118]. This is especially true as these parameters and settings vary from use case to use case [59].

For answering these research questions different approaches can be used. Besides conventional approaches like the use of rules and regulations of classification societies, analytical models or conducting model tests, a common choice are simulation-based approaches. Nowadays, available computational resources are enabling an increased usage of multi-physics simulation approaches. In such simulation approaches two or more different physical domains and / or simulation approaches are combined and solved simultaneously.

In naval architecture simulation techniques considering FSI are especially of significance, because with fluid dynamics and structural mechanics two important disciplines of the ship design can be assessed simultaneously. Such simulation-based approaches using FSI allow for a very detailed understanding and assessment of loads resulting on a ship hull, as the interaction between the media surrounding a ship hull and the ship's hull structure is accounted for. This is especially of interest for dynamic loading of the hull structure, e.g. loads due to the impact with water surface like slamming or a sideways launching process. Only with such an detailed understanding, a hull structure can be designed and optimized to a full extent without unnecessary safety margins.

Altogether, these aspects lead up to the following research hypothesis:

> A simulation-based approach using FSI is the best-suited choice for assessing water entry problems / slamming phenomena like a sideways launching process of a ship, as these are the only approaches able to consider all relevant physical aspects and phenomena accordingly allowing for a holistic assessment and optimization of a ship design.

2.4.2. Structure of this work

The study of the formulated research questions is based on the sideways launching process of the SPV, as presented in section 1.1. For investigating the above postulated research hypothesis, different approaches commonly used within naval architecture are applied to the sideways launching process of the SPV:

- conventional approaches without the use of simulations including:
  - rule-based approach
  - analytical approach
  - experimental approach
- simulation-based approach without FSI

After investigating these approaches, a simulation-based approach using FSI based on an ALE approach is proposed. A parametric study of relevant settings of the FSI algorithm is carried out and a verification based on model tests of the sideways launching process of the SPV is conducted. In addition, different measures to reduce the computational effort of the chosen ALE approach are discussed.

As all the different approaches are applied to the same problem (sideways launching process of the SPV), a direct comparison of the results obtained with the simulation-based approach using FSI with the established approaches is possible. Benefits and drawbacks of the proposed simulation-based approach using FSI are discussed. Based on the results obtained from the different approaches the research questions are outlined. Lastly, the postulated research hypothesis is evaluated by the comparison of the different approaches.

3. Theoretical framework

Within this chapter the theoretical framework necessary for the proposed simulation-based approach using FSI is given. This includes the theory of the ALE approach and FSI algorithm. In addition, the material models used for the hull structure of the SPV and the media surrounding the ship hull (air and water) are presented.

3.1. Arbitrary-Lagrangian-Eulerian approach

As already described in the introduction, a sideways launching process is a dynamic process. Due to the interaction with the free water surface spray roots, water pile up and waves around the ship hull can be observed. A simulation must be able to capture these effects sufficiently. Within the proposed simulation-based approach using FSI the problem is broken down into two parts: the hull structure of the SPV and the media surrounding the ship hull consisting of air and water. The hull structure of the SPV is described with a common Lagrangian element formulation. The media surrounding the ship hull are modelled using an ALE approach. The implementation within the commercial FEM software LS-DYNA is used for this purpose.

The following explanation of the ALE approach are a brief introduction to this topic. An in-depth description of the concept of ALE approaches, aspects regarding the numerical implementation as well as further references can be found in literature, e.g. in the work by Donea *et al.* [30]. The implementation of an ALE formulation for FSI problems is discussed in detail by Souli *et al.* [92]. Aspects regarding the implementation inside LS-DYNA are given in the *LS-DYNA® Theory Manual* [59].

In Lagrangian algorithms, which are mainly used for structural mechanics, the nodes of the computational mesh are following the displacement of the associated material during the calculation. Such algorithms are good for tracking interfaces between different materials (e.g. contact surfaces), but are generally less robust in regards to high distortion. Eulerian algorithms are commonly used for fluid dynamics. In the Eulerian approach the mesh is fixed and the fluid is moving with respect to the grid. Large movements or distortion (e.g. vortices) can be calculated well. But interface or free surfaces can only be handled sufficiently with a high mesh resolution at these area and by introducing additional algorithms to track such surfaces. An visualization of both Lagrangian and Eulerian element formulations is given in Figure 3.1.

ALE methods are combining the Lagrangian and Eulerian approach and are able to overcome the disadvantages of both approaches to a certain extent. Using an ALE formulation the nodes can move with a continuum (Lagrangian), be fixed in space (Eulerian) or move in an arbitrarily way to enable continuous rezoning capability [30]. For this purpose a third arbitrary referential coordinate is introduced in addition to the Lagrangian and Eulerian coordinates [92]. This third reference frame is introduced into the ALE formulation by the initial mesh of the ALE elements. As the nodes can move arbitrary with respect to their referential coordinates, material can move trough the elements of this referential system. This is illustrated in Figure 3.1. Therefore, the conversation laws are to be considered and solved. The conversation laws (mass, momentum and energy) in the ALE formulation can

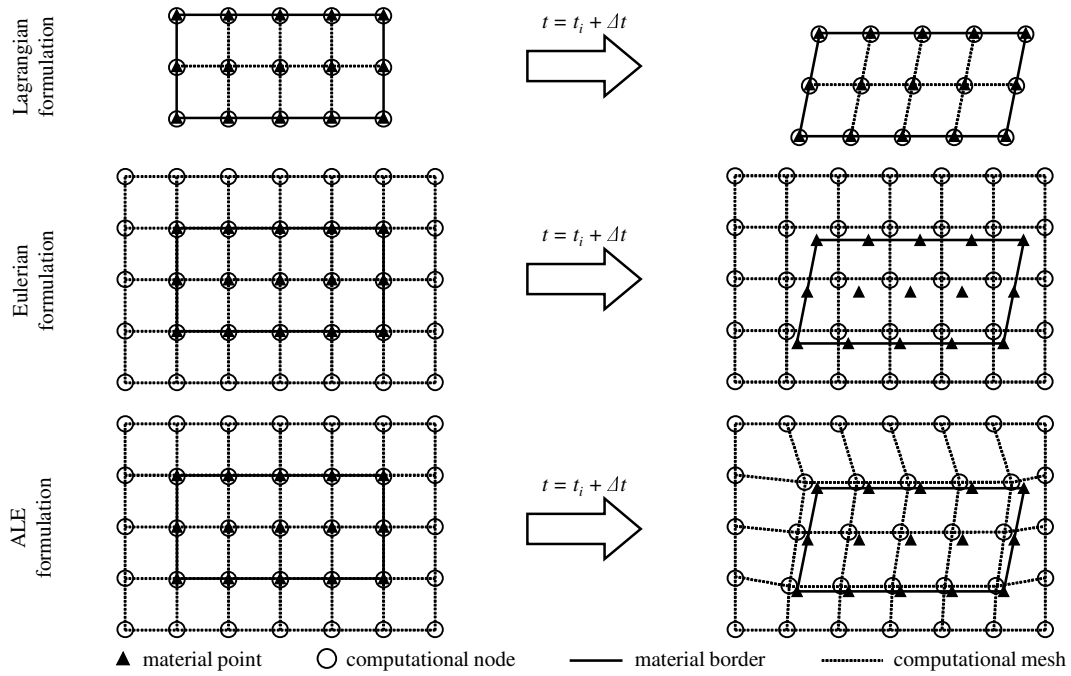

Figure 3.1.: different element formulations in comparison

be written as follows [92]:

$$\frac{\partial \rho}{\partial t} = -\rho \frac{\partial v_{mat}}{\partial x_i} - v_{conv\,i} \frac{\partial \rho}{\partial x_i} \tag{3.1}$$

$$\frac{\partial v_{mat}}{\partial t} = -\left(\sigma_{ij} + \rho b_i\right) - \rho v_{conv\,i} \frac{\partial v_{mat\,i}}{\partial x_j} \tag{3.2}$$

$$\frac{\partial E}{\partial t} = -\left(\sigma_{ij} v_{mat\,ij} + \rho b_i v_{mat\,j}\right) - \rho v_{conv\,i} \frac{\partial E}{\partial x_j} \tag{3.3}$$

In equation 3.1 to 3.3 the term ρ is the density of the material, x_i the Eulerian coordinates and $v_{conv\,i}$ the convective velocities. The convective velocity is defined as the difference of the velocity of the material v_{mat} and the velocity of the mesh v_{mesh}, so that $v_{conv} = v_{mat} - v_{mesh}$. The expression σ_{ij} is the Cauchy stress tensor, while b_i is the specific body force vector. Lastly, E is the energy. Note that the Eulerian equations of conservation laws can be obtained, by assuming $v_{conv} = v_{mat}$ [30], [92]. By doing so the velocity of the referential system v_{mesh} is equal to zero.

In order to solve the conversation laws in the ALE formulation as given in equation 3.1 to 3.3, two calculation steps are used during a time step of the simulation [30], [92]. The first step is a classical Lagrangian step. The second step, which is also referred to as an advection step [59], performs a rezone of the computational mesh. Different algorithms and methods can be used for the rezoning of the mesh depending on the physical problem to be solved. In LS-DYNA this rezone is done incremental. The nodes of the mesh are only moved a small fraction of the element size of surrounding elements. This is shown in Figure 3.1. In LS-DYNA different algorithms are implemented for the moving the computational mesh relative to the material [59], [92]: an equipotential method developed by Winslow [108], simple averaging of surrounding nodes or a volume weighting algorithm. In addition,

during the advection step the transport of mass, internal energy and momentum across element boundaries is calculated [30], [92]. For this purpose different advection algorithms are implemented in LS-DYNA. The influence of different advection algorithms for the case study of the sideways launching process is assessed at a later stage. The donor cell with half index shift and Van Leer with half index shift are investigated. A detailed description of these algorithms is given in [59].

Due to this freedom of moving the computational mesh, an ALE approach allows for greater distortions than a classic Lagrangian algorithm while simultaneously providing a higher resolution than that of an Eulerian algorithm [30]. ALE formulations are especially useful for tracking moving boundaries or free surfaces, e.g. in the context of FSI problems [92]. Therefore, the ALE-approach is a well-suited choice for the simulation-based approach using FSI for the investigated case study of the sideways launching process. The drawback is higher computational costs for each time step due to the advection step (rezoning of computational mesh and calculation of advection terms). The computational cost of an advection step is typically two to five times the cost of the Lagrangian time step [59]. The computational costs of the ALE approach for the simulation-based approach using FSI are investigated and discussed for the sideways launching process in detail at a later point of this work.

3.2. Fluid-structure interaction algorithm

Within the proposed simulation-based approach using FSI the hull structure of the SPV and the media surrounding the ship hull are modelled completely independent from each other. While the hull structure is modelled using a Lagrangian element formulation, an ALE formulation is used for air and water. The connection between these two parts is done by a FSI algorithm. For this purpose a FSI algorithm based on the penalty method is utilized. The work of Wriggers [111] is a good source for general information regarding contact problems and algorithms like the penalty method.

The FSI algorithm applied within the simulation-based approach using FSI is presented in the work by Aquelet *et al.* [7]. The FSI algorithm in [7] is similar to the penalty method commonly used for contact problems using a Lagrangian element formulation. An visualization of the FSI algorithm proposed in [7] is given in Figure 3.2. The nodes of the ALE elements (fluid) are the master side, while the nodes of the structure (Lagrangian formulation) are the slave side within this FSI algorithm proposed in [7]. The FSI algorithm checks, if the slave side is penetrating into the master side. If penetration is detected, a spring-damper-system is introduced (see Figure 3.2). The coupling forces F_{pen} of the FSI algorithm are calculated similar to a penalty method contact algorithms as a function of the occurring penetration x_{pen} [7]:

$$F_{pen} = k_{pen} \cdot x_{pen} + d_{pen} \cdot \dot{x}_{pen} \tag{3.4}$$

The term k_{pen} in equation 3.4 is the spring stiffness of the spring-damper-system of the FSI algorithm, while d_{pen} is the damping coefficient. The spring stiffness of the FSI algorithm is based on the following equation [7]:

$$k_{pen} = p_{fac} \cdot \frac{K_f \cdot A_s}{V_f} \tag{3.5}$$

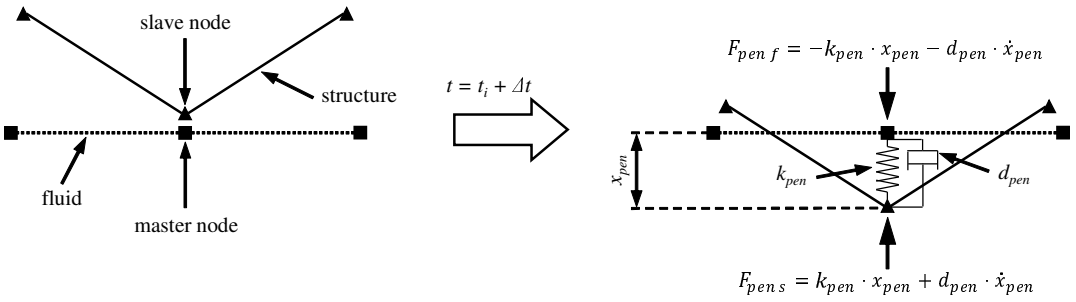

Figure 3.2.: FSI algorithm based on penalty method

In equation 3.5 K_f is the bulk modulus of the fluid, V_f the volume of the fluid element containing the master node and A_s the average area of the structure elements connected to the slave node. The expression p_{fac} is a user-defined scaling factor for the stiffness, which is between 0 and 1. Besides a constant factor for p_{fac}, it is also possible to define this factor as function of the penetration x_{pen} [59].

As water is nearly incompressible due to its high bulk modulus, the stiffness k_{pen} is very high as well. This can result in high frequency oscillations within the FSI algorithm, which could potentially lead to numerical instabilities [7]. To avoid such instabilities a damping force is introduced into the FSI algorithm. This damping force helps to gain a smoother and more stable response [7]. The damping coefficient d_{pen} is calculated based on a specified damping ratio D_{pen} using the ODE of motion of the spring-damper-system:

$$d_{pen} = \frac{2 \cdot D_{pen} \cdot k_{pen}}{\omega_{pen}} = \frac{2 \cdot D_{pen} \cdot k_{pen}}{\sqrt{k_{pen} \cdot \frac{m_s + m_f}{m_s \cdot m_f}}} \tag{3.6}$$

The terms m_s and m_f in equation 3.6 are the nodal masses of the structure and fluid. The damping ratio D_{pen} is user specified. A damping ratio close to an optimal damping ($D_{pen} = 1$) is recommended for the best effect of the damping [7]. However, especially for high damping ratios it is to be checked carefully, if the numerical damping within the FSI algorithm alters the physical behavior of the investigated problem [7].

As with penalty based contact algorithms, the FSI algorithm utilized within the simulation-based approach using FSI is complex. A lot of user input based on experience is necessary. The scale factor p_{fac} for the stiffness and the damping ratio D_{pen} are highly depending on the investigated problem [59]. The influence of the settings of the FSI algorithm are to be checked carefully. The sweet spot between a sufficient coupling (no leakage / penetration of the fluid through the structure) without introducing undesired numerical effects (oscillations / instabilities, unrealistically high coupling forces among others) is to be found for different type of applications of the FSI algorithm [7]. For this purpose parametric studies as well as verifications based on experiments / model tests are suggested by [7], [9], [10], [117], [118]. Both a parametric study as well as a verification based on model tests of the sideways launching process of the SPV including sufficient settings for the ALE approach and FSI algorithm are provided within this work.

3.3. Material models

Within this section the material models used for the hull structure of the SPV as well as the media surrounding the ship hull (air and water) within the simulation-based approaches are presented.

3.3.1. Steel

The hull structure of the investigated SPV is designed with the high-tensile steel alloy 1.0584 (VL D-36). At the impact of the hull structure with the water surface during the sideways launching process, plastic deformations could potentially occur in a very short time period. This is especially true, as the peak pressure observed during the impact with the water surface lasts only a few milliseconds. Therefore, the material model used within the simulation-based approaches must enable an adequate assessment of plastic deformation and hardening. In addition, strain rate effects are to be considered.

To account for these two phenomena, according material models for VL D-36 inside the simulation-based approaches are necessary. As steel alloys can be considered isotropic, the necessary material models can be derived based on the results obtained from uniaxial tensile tests. Results of such tensile tests of VL D-36 in the form of engineering stress-strain curves are given in Figure 3.3a. The data presented in Figure 3.3a are the result of the work by Kubiczek *et al.* [55]. These results are used as the basis for the material models for VL D-36 in the simulation-based approaches within this work. General properties used for the material model of VL D-36 are provided in Table 3.1.

A general overview of the material behavior of steel alloys within the context of the design of ship structures can be found in literature, e.g. in the work by Paik [75]. The behavior of an steel alloy during an uniaxial tensile test can be split into different phases. After elastic deformation up to yield strength σ_Y, plastic deformation can be observed. Up to tensile strength R_m at uniform elongation ε_{ue} no necking occurs. After uniform elongation is passed, necking of the specimen can be observed. Lastly, the test specimen fails at elongation of break ε_{break}.

The elastic part of the deformation is described by Hooks law based on the Young's modulus E_Y and yield strength σ_Y. For considering the plastic deformation inside FEM simulations corresponding material curves covering the strain range of interest are necessary. For LS-DYNA true stress-strain curves are needed as an input for suitable material models [59]. In general, uniaxial tensile tests do provide the engineering stress-strain curves. These are obtained using the following two relations:

$$\varepsilon_{eng} = \frac{L - L_0}{L_0} = \frac{\Delta L}{L_0} \tag{3.7}$$

$$\sigma_{eng} = \frac{F}{A_0} \tag{3.8}$$

The engineering strain ε_{eng} is defined as the ratio of the elongation of the test specimen ΔL and its initial length L_0, while the engineering stress σ_{eng} is defined as the ratio between the force F acting upon the test specimen and its initial cross-sectional area A_0. In contrast to engineering stress-strain curves, the strain and stresses for the true stress-strain curves are calculated based on the current values. The true strain ε_{true} for an uniaxial tensile test

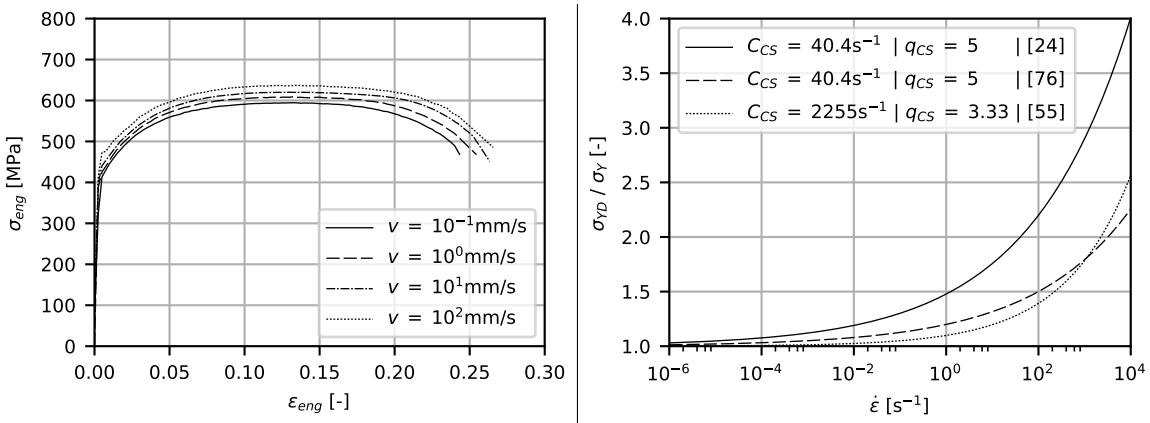

(a) engineering stress-strain curves

(b) influence of strain rate

Figure 3.3.: material model for VL D-36 based on [55]

is defined as the integral of the elongation:

$$\varepsilon_{true} = \int_{L_0}^{L} \frac{dL}{L} = ln\left(\frac{L}{L_0}\right) = ln\left(1 + \varepsilon_{eng}\right) \tag{3.9}$$

The true stress σ_{true} is calculated as the ratio of the current force F acting upon a test specimen to the current cross-sectional area A as follows:

$$\sigma_{true} = \frac{F}{A} \tag{3.10}$$

The current cross section data can be obtained by assuming that the volume of the test specimen stays constant. This assumption yields the following relationship:

$$\sigma_{true} = \frac{F \cdot (1 + \varepsilon_{eng})}{A_0} = \sigma_{eng} \cdot (1 + \varepsilon_{eng}) \tag{3.11}$$

With equation 3.9 and 3.11 the true stress-strain curve can be calculated directly based on the engineering stress-curves obtained from uniaxial tensile tests. However, equation 3.9 and 3.11 are only valid as long as the assumption of a constant volume of the test specimen is true. After the start of necking at the uniform elongation, a constant volume of the test specimen is no longer given.

For assessing the material behavior after the uniform elongation different approaches are possible. A common approach for steel alloys is the use of a power law as proposed by Hollomon [41]:

$$\sigma_{true} = K_{hard} \cdot {\varepsilon_{true}}^{n_{hard}} \tag{3.12}$$

The expression K_{hard} and n_{hard} in equation 3.12 are the strength and hardening coefficient, respectively. These are depending on the steel alloy of interest. For VL D-36 $K_{hard} = 864.8$MPa and $n_{hard} = 0.125$ can be used [55]. The power law proposed in [41] was successfully used to determine the necessary material curves for the simulation of ship structures in the context of ship collisions in the past. Examples are the work by Peschmann [78] or Ehlers *et al.* [31]. However, as the power law in equation 3.12 is only a fit of the

Table 3.1.: material parameters used for VL D-36

parameter	unit	value
ρ_0	$[\mathrm{kg/m^3}]$	7,850
E_Y	[GPa]	206
ν	[-]	0.30
$\sigma_Y{}^*$	[MPa]	355
C_{CS}	$[\mathrm{s^{-1}}]$	2,225
q_{CS}	[-]	3.33

*: set to minimal yield strength for VL D-36 during simulations

material curve, deviations between experimental data and simulations using the power law can occur. As shown in [55], by using a material curve based on the power law the results of the tensile tests are underestimated. But assuming that a power law fit does always lead to conservative results is not true. As shown by Ehlers and Varsta [32] an overestimation of experimental results could be observed as well.

Therefore, a better approach is to determine the true stress-strain curves directly based on the on the uniaxial tensile tests. In [32] a concept based on an optical measurement system called *Aramis* is presented. A stochastic greyscale pattern is applied to the surface of the test specimen, which is tracked by a camera system during the uniaxial tensile tests. This system allows for very precise measurement of the 3D deformation of the test specimen. As the current cross section A is measured using this approach, the true stresses can be calculated directly using equation 3.10. As shown in [32], simulation results based on the true stress-strain curves obtained with *Aramis* system show very good agreement with the conducted uniaxial tensile tests.

Another approach to determine true stress-strain curves is given in [55]. Tensile tests were carried out for VL D-36 for four different test speeds v / strain rates $\dot{\varepsilon}$. The true stress-strain curves were derived by an optimization routine in combination with a FEM model of the uniaxial tensile tests in LS-DYNA using the optimization tool LS-OPT. The true stress-strain curves used in the FEM model were fitted by LS-OPT, so that the results of the FEM simulations matched the experimental data from the uniaxial tensile tests. More details are provided in [55] as well as in the work by Schöttelndreyer [89].

As the engineering stress-strain curves in Figure 3.3a show, the material behavior of VL D-36 is influenced by the strain rate. With an increasing strain rate the yield strength, tensile strength as well as elongation of break are increased. One common approach to account for the strain rate effects is the Cowper-Symonds equation [24]. The Cowper-Symonds equation describes the ratio of the dynamic yield strength σ_{YD} to the yield strength under quasi-static loading σ_Y as a function of the strain rate $\dot{\varepsilon}$:

$$\frac{\sigma_{YD}}{\sigma_Y} = 1 + \left(\frac{\dot{\varepsilon}}{C_{CS}}\right)^{\frac{1}{q_{CS}}} \tag{3.13}$$

The coefficients C_{CS} as well as q_{CS} in equation 3.13 are material parameters unique for each steel alloy. An visualization of the Cowper-Symonds equation 3.13 for different steel alloys is provided in Figure 3.3b. Common coefficients for the Cowper-Symonds equation 3.13 are given (mild steel obtained by Cowper and Symonds [24] and high tensile steel

derived by Paik and Chung [76]). In addition, the coefficients obtained in [55] for VL D-36 are provided in Figure 3.3b.

As shown in [55] a more accurate approach than the Cowper-Symonds equation 3.13 is the use of different true stress-strain curves obtained for different strain rates. By doing so a material surface is spanned as a function of the current strain rate. Especially the behavior beyond the uniform elongation up to the failure of the test specimen is covered more accurately using this approach [55].

For the investigated case study of the sideways launching process a failure of the ship's hull structure is not of interest. Therefore, no according failure criteria are considered within the simulation-based approaches. Regarding the use of different failure criteria suitable for ship structures, the work of Ehlers and Varsta [32] as well as Schöttelndreyer [89] provide a good overview. In [32], [89] the applicability of different failure criteria within the context of ship collisions is investigated.

3.3.2. Media surrounding ship hull

Within the ALE approach, fluids and gasses can be described using thermodynamic equation of state (EOS). In general, an EOS is linking state variables such as the pressure p, the volume V or the temperature T. This allows for describing thermodynamic processes of media surrounding the ship hull.

Air

It is possible to describe gasses by using a general polynomial approach for the EOS [59]:

$$p = C_0 + C_1 \cdot \mu_{EOS} + C_2 \cdot \mu_{EOS}^2 + C_3 \cdot \mu_{EOS}^3 + \left(C_4 + C_5 \cdot \mu_{EOS} + C_6 \cdot \mu_{EOS}^2\right) \cdot E_i \quad (3.14)$$

In equation 3.14 the parameters C_1 to C_6 are material parameters depending on the gas and thermodynamic process, whereas E_i is the internal energy per unit reference volume. The expression μ_{EOS} in equation 3.14 is the compression, which is defined as follows [59]:

$$\mu_{EOS} = \frac{\rho}{\rho_0} - 1 = \frac{1}{V_{rel}} - 1 \quad (3.15)$$

In equation 3.15 the term ρ is the current density, while ρ_0 is a reference density. The expression V_{rel} is the relative volume. An ideal gas can be modelled by setting the constants C_1 to C_6 in equation 3.14 as follows [59]:

$$C_0 = C_1 = C_2 = C_3 = C_6 = 0 \quad (3.16)$$

$$C_4 = C_5 = \kappa - 1 \quad (3.17)$$

The value κ in equation 3.17 is the heat capacity ratio of the corresponding gas, which is defined as the ratio of the specific heat capacity at constant pressure to the specific heat capacity at constant temperature. By introducing equation 3.16 and 3.17 into equation 3.14, the behavior of the air is modelled according to the ideal gas law. This EOS is also known as the gamma-law EOS [59]:

$$p = (1 + \mu_{EOS}) \cdot (\kappa - 1) \cdot E_i \quad (3.18)$$

Table 3.2.: material parameters used for air

parameter	unit	value
ρ_0	$[\mathrm{kg/m^3}]$	1.20
κ	[-]	1.40

Using this EOS it is possible, to describe isentropic processes. Compression and expansion processes inside the gas can be covered. This allows for assessing the free water surface during the sideways launching process. In addition, consideration of the effects of hydroelasticity for small deadrise angles during the impact with the water surface is possible, as the compressibility of air plays an important role for this physical phenomena (entrapment of an air cushion between ship hull and water surface at impact).

For EOS 3.18 only two material parameters are necessary: the density at a reference state ρ_0 and the heat capacity ratio κ. Values for air are provided in Table 3.2 for standard atmospheric pressure $p_0 = 101,325\mathrm{Pa}$ and ambient temperature $T_0 = 20°\mathrm{C}$.

Water

For water the use of different EOS is possible [40]. Analogously to air a general polynomial approach for the EOS as given in equation 3.14 can be used. Another approach is the Mie-Grüneisen EOS. The Mie-Grüneisen EOS was originally derived for calculating shock waves in solids at high pressures and is used often for the assessment of seismological phenomena [40]. By using suitable parameters for the Mie-Grüneisen EOS it is also possible to describe fluids like water under impact loads, as water is nearly incompressible due to its high bulk modulus. Examples for this use case can be found in literature. Within the work published by Steinberg [93], Shin *et al.* [91] and Hamashima *et al.* [39] the Mie-Grüneisen EOS was successfully used to model water within the context of underwater explosions.

The water within the proposed simulation-based approach using FSI is modelled with the Mie-Grüneisen EOS. The general form of the Mie-Grüneisen EOS is given by the following equation [40]:

$$p = p_H - \frac{\Gamma_{MG}}{V} \cdot (E_i - E_H) \tag{3.19}$$

In equation 3.19 the term Γ_{MG} is the Grüneisen gamma, which is a material coefficient. The expression p_H and E_H are the pressure and energy at the Rankine-Hugoniot state. The Rankine-Hugoniot state describes the behavior / state of a shock wave travelling through a medium [40]. By introducing the Rankine-Hugoniot state into the general Mie-Grüneisen EOS 3.19 and linearising the system, the following EOS can be obtained for describing the pressure [59]:

$$p = \frac{\rho_0 \cdot c_0^2 \; \mu_{EOS} \cdot \left[1 + \left(1 - \frac{\Gamma_{MG}}{2}\right) \cdot \mu_{EOS}\right]}{\left[1 - (S_{MG\,1} - 1) \cdot \mu_{EOS} - S_{MG\,2} \cdot \frac{\mu_{EOS}^2}{\mu_{EOS}+1} - S_{MG\,3} \cdot \frac{\mu_{EOS}^3}{(\mu_{EOS}+1)^2}\right]^2} + \Gamma_{MG} \cdot E_i \tag{3.20}$$

The expression c_0 in equation 3.20 is the velocity of sound at a reference state, while $S_{MG\,1}$ to $S_{MG\,3}$ are material coefficients describing the Rankine-Hugoniot condition inside the material. With EOS 3.20 compression waves inside a solid or fluid can be assessed.

Table 3.3.: material parameters used for water

parameter	unit	value
ρ_0	[kg/m^3]	1,010
c_0	[m/s]	1,485
$S_{MG\,1}$	[-]	1.79
$S_{MG\,2}$	[-]	0.00
$S_{MG\,3}$	[-]	0.00
Γ_{MG}	[-]	1.65

To account for expansion and tension waves inside a material, a second EOS has to be introduced. For this purpose, the following EOS can be used [59]:

$$p = \rho_0 \cdot c_0^2 \cdot \mu_{EOS} + \Gamma_{MG} \cdot E_i \tag{3.21}$$

Using EOS 3.20 and EOS 3.21, water can be modelled as a compressible media. This material model allows for assessing water under shock and impact loads, like slamming or a sideways launching process. The material coefficients used for the Mie-Grüneisen EOS for water are provided in Table 3.3. These values are obtained from [39] and adapted to the conditions given inside launch basin of the investigated case study.

4. Conventional approaches

Within this chapter the sideways launching process of the SPV is investigated with conventional approaches, that are not based on simulations. This includes a rule-based, an analytical as well as an experimental approach based on model tests. The applicability, obtained results, benefits and limitations of each of this three approaches for the use case of a sideways launching process are discussed.

4.1. Rule-based approach

One common approach for the design of a ship's hull structure is a rule-based approach. Different classification societies provide rules and regulations for different ship types, which are to be met by a ship's hull structure to gain certain class notations. These rules and regulations provide assistance and approaches for deriving design loads for different parts of the hull structure, that cover different load cases. The most common rule-based approach regarding the design of a hull structure is calculating design loads valid for different structural components (e.g. shell, bottom structure, decks, bulkheads, superstructure...) due to local or global load cases. With such a design load the resulting stresses inside a structural member can be calculated and compared to the permissible stresses as defined by the specific rule / regulation. As this approach does not need complex calculations or simulations, this approach is often used during the early design phases of a ship.

Therefore, rules and regulations of common classifications societies, which are members of International Association of Classification Societies (IACS), are checked regarding any consideration of the launching process of a ship. Applicable rules and regulations for the SPV are checked for the following members of IACS (in alphabetical order):

- American Bureau of Shipping (ABS)
- Bureau Veritas (BV)
- China Classification Society (CCS)
- Det Norske Veritas (DNV)
- Korean Register of Shipping (KR)
- Lloyd's Register (LR)
- Nippon Kaiji Kyōkai (NK)
- Registro Italiano Navale (RINA)

In total, 20 different rules and regulations applicable or relevant for the SPV are checked. An overview is provided in Appendix A.2. Only in *Rules and Regulations for the Classification of Naval Ships* [61], the launching process of a ship is mentioned. Loads resulting during launching are to be considered (see quote in Appendix A.2). However, no approach for assessing these loads is provided in [61].

As discussed within the state of the art in chapter 2 of this work, the loads resulting at the impact with water surface during the sideways launching process are comparable

to loads observed during slamming events. The rules and regulations are checked regarding approaches for considering and estimating slamming loads as well. Especially bottom slamming / impact loads are of interest due to the geometric configuration given at the sideways launching process. Nearly all rules and regulations checked provide load models to account for bottom slamming / impact loads (compare Appendix A.2).

In order to adapt a load model for bottom slamming / impact loads for the sideways launching process, it should contain the conditions at the moment of impact with the water surface. The easiest way to adapt a model for the sideways launching process is based upon the velocity of the ship hull relative to the water surface v_{slam} as well as the deadrise angle β_{impact} (angle between water surface and ship hull at the moment of impact). This is the case for the design loads as given in [4], [5], [49], [61], [71]. Purely empirical load models, where the design loads are calculated based solely upon different correction factors using the ship main dimensions, ship form, ship speed among others cannot be adapted. No information / correlation regarding the conditions at the moment of impact with the water surface can be derived from such an approach. Such empirical approaches are given in [17], [19], [27], [28], [62], [86].

In almost all cases only (quasi-)static loads are provided by the checked rules and regulations of classification societies. However, for a local analysis of parts of a hull structure quasi-static approaches are problematic, as hydro-elasticity plays an important role [18]. As high impact pressures might occur, a direct application on the structure within a quasi-static approach could induce severe structural failure [18]. To overcome this issue to some extent, a dynamic load model is preferable compared to a quasi-static one. Only LR provides a dynamic load model in the event of bottom slamming in [61]. The impact loads in the form of a design pressure on the bottom plating is defined as a function of the velocity and deadrise angle, which can be idealized using a triangular pulse load [61]. A load model for the sideways launching process of the SPV based on [61] is proposed for the simulation-based approach without FSI later on in this work.

Besides rules and regulations, BV [18] DNV [25] as well as ABS [3] do provide further, more in-depth knowledge regarding slamming loads in the form of guidelines or recommended practices. In [18], [25] common analytical theories for assessing the resulting loads at the impact of a wedge with the the water surface are presented. In [3] it is discussed how to assess slamming phenomena using defined conditions for a ship (speed, loading condition, heading) combined with environmental conditions (wave environments) to calculate the ship motion relative to the water surface. Based on the relative motion the slamming pressure is to be derived using appropriate theories and then converted to a design slamming pressure used for the strength assessment of a hull structure.

4.2. Analytical approach

In the past decades computational resources were not as widely available as today. For assessing a sideways launching process analytical approaches were used like the one provided in [56] or [115]. In the following, the problem is split into two parts for the analytical approach:

- ship motion
- loads resulting on the ship hull

Based on the corresponding ODE of motion an analytical approach is proposed, which is able to predict the motion of the SPV during the sideways launching process. For the loads resulting on the ship hull at the moment of impact with the water surface common analytical approaches for the assessment of slamming phenomena are investigated regarding their applicability for the sideways launching process.

4.2.1. Ship motion based on ordinary differential equations of motion

For each of the different phases of the sideways launching process as given in Appendix A.1 the corresponding ODE of motion are derived. Regarding the ship motion the following parameters are especially of interest during the sideways launching process:

- maximal roll angle
- trajectory of the ship
- point of deepest immersion

To cover these parameters, the ODE of the ship motion can be reduced to three DOF instead of complete six DOF [56], [115]. Therefore, only the translation in y-direction (horizontal movement), z-direction (vertical movement) and rotation about the x-axis (roll angle) are considered for deriving the according ODE during the analytical approach by using the following relations:

$$v_x = \omega_y = \omega_z = 0 \tag{4.1}$$

For the DOF of interest, the following system of ODE is valid:

$$\begin{cases} m_{tot} \cdot \left(\frac{\partial v_y}{\partial t} - v_z \cdot \omega_x \right) = F_y \\ m_{tot} \cdot \left(\frac{\partial v_z}{\partial t} + v_y \cdot \omega_x \right) = F_z \\ I_{xx\ tot} \cdot \frac{\partial \omega_x}{\partial t} = M_x \end{cases} \tag{4.2}$$

Within the analytical approach the ship and palls are idealized as one single rigid body. For the mass, position of the center of gravity (COG) as well as moment of inertia in the equations below the sum of the ship and palls is used, which are denoted by the subscript *tot* (=total). For better readability, only "ship" is used instead of "ship and palls" within this section.

In equation 4.2 the parameter m_{tot} is the mass of the ship, whereas $I_{xx\ tot}$ is the moment of inertia around the corresponding x-axis of the ship. The expression v_i are the translational velocities in the corresponding direction, while ω_i are the angular velocities around the given axis of the ship. On the right hand side of equation 4.2 are the external forces F_i and moments M_i acting upon the ship. Equation 4.2 is given for a ship-fixed coordinate system with the origin at the principle axis of the ship. Thus the off-diagonal elements of the inertia matrix are zero ($I_{xy} = I_{xz} = I_{yz} = 0$) as well as the static moments ($S_x = S_y = S_z = 0$), which simplifies the underlying ODE.

The ODE system as given in equation 4.2 does only consider inertia forces resulting from the ship itself. The influence of the water surrounding the ship hull is not included. In naval architecture the concept of added masses is a common approach for considering the

inertia effects of water. Details regarding the concept of added masses can be found in literature. The work of Korotkin [53] can be seen as one of the standard works regarding the topic of added masses of ship structures.

Using this approach the inertia effects are considered as virtual or added masses λ_{ij} and are added to the corresponding ODE of the ship motion. If all six DOF are considered, a ship does have 36 different added masses: λ_{11} up to λ_{66}. If the assumption of infinite fluid symmetry conditions are met, the following condition is true [53]:

$$\lambda_{ij} = \lambda_{ji} \tag{4.3}$$

This reduces the terms of added masses from 36 to 21 independent terms. The investigated ship hull is symmetrical regarding the xz-plane. Due to this, the following added masses are equal to zero [53]:

$$\lambda_{23} = \lambda_{24} = \lambda_{34} = 0 \tag{4.4}$$

By introducing the added masses into the system of ODE as given in equation 4.2, the following system of ODE for the ship motion inside water can be obtained:

$$\begin{cases} (m_{tot} + \lambda_{22}) \cdot \frac{\partial v_y}{\partial t} - (m + \lambda_{33}) \cdot v_z \cdot \omega_x = F_y \\ (m_{tot} + \lambda_{33}) \cdot \frac{\partial v_z}{\partial t} + (m + \lambda_{22}) \cdot v_y \cdot \omega_x = F_z \\ (I_{xx\,tot} + \lambda_{44}) \cdot \frac{\partial \omega_x}{\partial t} + (\lambda_{33} - \lambda_{22}) \cdot v_y \cdot v_z = M_x \end{cases} \tag{4.5}$$

This system of ODE can be used to asses the ship motion in phase 4 — dropping and raise, while the ship is able to move freely in the water. For all the previous phases the boundary conditions (BC) imposed by the geometry / kinematics of the sideways launching system are to be taken into account in ODE 4.2 and 4.5.

Phase 0 — rotation

This phase is visualized in Figure A.1 and A.2. In this phase the rocker arms are lifted by a crane with a designated force F_{crane} counteracting the weight forces of the ship. The rocker arms and ship will rotate about the designated rotational axis of the rocker arms (compare Figure A.1; rotation axis denoted with $*$). The following moments act around the rotational axis of the rocker arms during phase 0:

$$M_{crane}(\varphi) = F_{crane} \cdot [dy_{crane\,0} \cdot cos(\varphi) - dz_{crane\,0} \cdot sin(\varphi)] \tag{4.6}$$

$$M_{weight}(\varphi) = -m_{tot} \cdot g \cdot [dy_{COG_{tot}\,0} \cdot cos(\varphi) - dz_{COG_{tot}\,0} \cdot sin(\varphi)] \tag{4.7}$$

An overview of different forces resulting in the moments as given in equation 4.6 and 4.7 is provided in Figure A.1. The corresponding arms of lever can be obtained from Figure A.1 as well. The COG of the rocker arms lies very close to their rotational axis. Therefore, forces and moments induced by the rocker arms are neglected.

Based on the two external moments the following ODE of motion can be derived for phase 0:

$$\frac{\partial \omega_x}{\partial t} = \frac{1}{(I^*_{xx\,tot} + I^*_{xx\,ra})} \cdot [M_{crane} + M_{weight}] \tag{4.8}$$

The moments of inertia of the ship $I^*_{xx\,tot}$ as well as the rocker arms $I^*_{xx\,ra}$ in equation 4.8 are defined with the rotational axis of the rocker arms as the point of reference. These are constant during phase 0. The roll angle of the ship is equal to the rotation of the rocker arms during phase 0 due the kinematics of the sideways launching system. The coordinates of the COG of the ship in the global coordinate system can be calculated using trigonometry.

The end of phase 0 is reached, if the rotation around the x-axis φ is equal to the inclination of the slipway φ_{sw}. At this angle the rocker arms are flat on the ground as illustrated in Figure A.2.

Phase 1 — sliding

This phase is visualized in Figure A.2 and A.3. In this phase the ship slides down the slipway. The physics of the problem is identical to an inclined plane including friction. Therefore, the weight force can be split into the following three different parts:

- downhill force F_d
- normal force F_n
- frictional force F_f

The resulting downhill force F_d acting upon the ship can be calculated based on the weight force by using trigonometry:

$$F_d = m_{tot} \cdot g \cdot sin\left(-\varphi_{sw}\right) \tag{4.9}$$

The same approach is true for the normal force F_n, which is acting upon the slipway:

$$F_n = m_{tot} \cdot g \cdot cos\left(\varphi_{sw}\right) \tag{4.10}$$

Based on the normal force F_n, the frictional force F_f acting against the downhill force during the sliding process can be calculated as follows:

$$F_f = F_n \cdot \mu_{sw} \tag{4.11}$$

The expression μ_{sw} in equation 4.11 is the coefficient of sliding friction between the palls and slipway. Values for μ_{sw} for different launching systems and conditions are given in [56]. Depending on the launching system, type of grease, resulting grease pressure and temperature μ_{sw} the range lies typically between 0.015 and 0.030 [56].

The two forces resulting in the sliding motion of the ship in this phase are the downhill force F_d and the frictional force F_f. As illustrated in Figure A.3, the normal F_n is counteracted by the reaction force inside the slipway F_{pier}:

$$F_{pier} = -F_n \tag{4.12}$$

During this phase the ship do only move in the yz-plane and do not rotate around the x-axis. This results in y and z as the two active DOF during this phase. Using trigonometric relationships, the following system of ODE can be derived for phase 1:

$$\begin{cases} \frac{\partial v_y}{\partial t} = \frac{1}{m_{tot}} \cdot \left(F_d - F_f\right) \cdot cos\left(\varphi_{sw}\right) \\ \\ \frac{\partial v_z}{\partial t} = -\frac{1}{m_{tot}} \cdot \left(F_d - F_f\right) \cdot sin\left(-\varphi_{sw}\right) \end{cases} \tag{4.13}$$

The end of phase 1 is reached, if the COG of the ship is aligned with the edge of the pier ($y_{COG_{tot}} \geq 0$) as shown in Figure A.3.

Phase 2 — tipping

This phase is visualized in Figure A.3 and A.4. In this phase the COG of the ship is beyond the edge of the pier, so that it starts to tip. The centre of the rotation is the edge of the pier as marked with † in Figure A.3. The motion during this phase consists of two parts: a sliding movement and a forced rotation around the edge of the pier as a fixed axis of rotation. Both motions are acting simultaneously and can be superimposed.

For the sliding motion of the ship the same forces as in phase 1 are valid. In contrast to phase 1 the inclined plane is not fixed in space. The ship starts to rotate around the edge of the pier. This edge is designed with a small radius at its edge. The center of this radius is the center of the forced rotation of the ship. The normal force of the ship will always act perpendicular to the inclined plane towards the center of the forced rotation. Therefore, the normal force F_n, the downhill force F_d and frictional force F_f will rotate together with the ship. This is illustrated in Figure A.4. The corresponding equations as given in phase 1 are now a function of the current rotation φ around the x-axis:

$$F_d(\varphi) = m_{tot} \cdot g \cdot sin(-\varphi) \tag{4.14}$$

$$F_n(\varphi) = m_{tot} \cdot g \cdot cos(\varphi) \tag{4.15}$$

$$F_f(\varphi) = F_n \cdot \mu_{sw} \tag{4.16}$$

With an increasing rotation around the x-axis of the ship, the forces resulting for the sliding movement will start to point more and more in the z-direction accelerating the rotation around the edge of the pier. This results in a tipping motion around the edge of the pier. The moment resulting in the tipping motion M_{tip} is defined by the following forces (compare Figure A.3 and A.4):

- y-component of the difference of downhill and frictional force $F_d - F_f$
- z-component of the difference of downhill and frictional force $F_d - F_f$
- z-component of the normal force F_n

The tipping moment M_{tip} can be calculated as follows:

$$\begin{aligned} M_{tip}(y_{COG_{tot}},\ z_{COG_{tot}},\ \varphi) = \quad & -(F_d - F_f) \cdot cos(\varphi) \cdot [z_{COG_{tot}} - z_{pier}] \\ & -(F_d - F_f) \cdot sin(-\varphi) \cdot [y_{COG_{tot}} - y_{pier}] \\ & +F_n \cdot cos(\varphi) \cdot [y_{COG_{tot}} - y_{pier}] \end{aligned} \tag{4.17}$$

The corresponding arms of lever for each component are given in Figure A.3 and A.4. During this phase all three DOF are active and have to be considered for the system of ODE. Based on the kinematics of this phase, the following system of ODE can be derived for phase 2:

$$\begin{cases} \frac{\partial v_y}{\partial t} = \frac{1}{m_{tot}} \cdot (F_d - F_f) \cdot cos(\varphi) \\ \frac{\partial v_z}{\partial t} = -\frac{1}{m_{tot}} \cdot (F_d - F_f) \cdot sin(-\varphi) \\ \frac{\partial \omega_x}{\partial t} = \frac{1}{I^{\dagger}_{xx\ tot}} \cdot M_{tip} \end{cases} \tag{4.18}$$

The moments of inertia of the ship $I^{\dagger}_{xx\ tot}$ in equation 4.18 are defined with the edge of the pier as the point of reference, which is variable during phase 2. It is a function of the distance between the edge of the pier as the axis of rotation and the current position of the COG of the ship.

The end of phase 2 is reached, when the ship has the first contact with water surface as illustrated in Figure A.4.

Phase 3 — tipping and immersion

This phase is visualized in Figure A.4 and A.5. In this phase the palls are still in contact with the pier, while the ship start to immerse in the water. Because of the contact of the palls to the pier, the forces and moments of phase 2 are still valid.

Due to the contact of the ship with the water surface, additional hydrostatic and hydrodynamic forces are acting upon the ship body. The hydrostatic force $F_{hyd\ stat}$ is based on the buoyancy ∇ of the ship:

$$F_{hyd\ stat}\left(y_{COG_{tot}},\ z_{COG_{tot}},\ \varphi\right) = \rho_w \cdot g \cdot \nabla \tag{4.19}$$

This hydrostatic force as stated in 4.19 is a function of the actual buoyancy of the ship and therefore depending on the actual position of the ship relative to the water surface. In addition, hydrodynamic forces act upon the ship. In accordance with [56] these hydrodynamic forces are idealized as resistance forces. This results in the following hydrodynamic force $F_{hyd\ dyn\ y}$ acting upon the ship hull in the y-direction:

$$F_{hyd\ dyn\ y}\left(y_{COG_{tot}},\ z_{COG_{tot}},\ \varphi,\ v_y\right) = \frac{\rho_w}{2} \cdot c_{w\ xz} \cdot A_{xz} \cdot v_y^2 \cdot \frac{v_y}{|v_y|} \tag{4.20}$$

In equation 4.20 the term A_{xz} is the projected area of the centerline of the ship below the waterline (area in global xy-plane). The term $c_{w\ xz}$ is a dimensionless coefficient of resistance valid for the centerline area of the ship.

The same approach is used for the hydrodynamic force in the z-direction $F_{hyd\ dyn\ z}$:

$$F_{hyd\ dyn\ z}\left(y_{COG_{tot}},\ z_{COG_{tot}},\ \varphi,\ v_z\right) = \frac{\rho_w}{2} \cdot c_{w\ xy} \cdot A_{xy} \cdot v_z^2 \cdot \frac{v_z}{|v_z|} \tag{4.21}$$

The expression A_{xy} is the waterline area of the ship (area in global xy-plane), whereas $c_{w\ xy}$ is again a dimensionless coefficient of resistance valid for the waterline area of the ship. In accordance with [56] a coefficient of 1.00 is used for both $c_{w\ xz}$ and $c_{w\ xy}$. The expression $v_i/|v_i|$ are added in equation 4.20 and 4.21 to account for the direction in which the hydrodynamic force components are acting.

Based on the hydrostatic and hydrodynamic forces, an additional moment is acting upon the ship. This moment $M_{upright}$ will counteract the tipping moment M_{tip}. The following force components are to be considered for $M_{upright}$:

- z-component of hydrostatic force $F_{hyd\ stat}$
- y-component of hydrodyanmic force $F_{hyd\ dyn\ y}$
- z-component of hydrodyanmic force $F_{hyd\ dyn\ z}$

An overview of this forces and their arms of lever can be obtained from Figure A.5 as well as Figure A.6. The hydrostatic force is acting upon the center of bouyancy (COB) of the ship as marked with ⋄ in Figure A.5. It is assumed that the hydrodynamic components of the forces will attack at the centroid of the centerline or waterline area, respectively, marked with □ in Figure A.6.

Based on the hydrostatic and hydrodynamic force components with their corresponding arms of lever, the following moment $M_{upright}$ can be derived:

$$\begin{aligned} M_{upright}\left(y_{COG_{tot}},\ z_{COG_{tot}},\ \varphi\right) = \quad & F_{hyd\ stat} \cdot \left[y_{COB} - y_{COG_{tot}}\right] \\ & -F_{hyd\ dyn\ z} \cdot \left[y_{A_{xy}} - y_{COG_{tot}}\right] \\ & +F_{hyd\ dyn\ y} \cdot \left[z_{A_{xz}} - z_{COG_{tot}}\right] \end{aligned} \tag{4.22}$$

The system of ODE for phase 3 can be derived by expanding the system of ODE used for phase 2 as given in equation 4.18 with the hydrostatic and hydrodyanmic force components, the moment $M_{upright}$ as well the corresponding added masses λ_{ii}. This results in the following system of ODE for phase 3:

$$\begin{cases} \frac{\partial v_y}{\partial t} = \frac{1}{(m_{tot}+\lambda_{22})} \cdot \left[\left(F_d - F_f\right) \cdot cos\left(\varphi\right) - F_{hyd\ dyn\ y}\right] \\ \frac{\partial v_z}{\partial t} = \frac{1}{(m_{tot}+\lambda_{33})} \cdot \left[-\left(F_d - F_f\right) \cdot sin\left(-\varphi\right) + F_{hyd\ stat} - F_{hyd\ dyn\ z}\right] \\ \frac{\partial \omega_x}{\partial t} = \frac{1}{\left(I^{\dagger}_{xx\ tot}+\lambda_{44}\right)} \cdot \left[M_{tip} + M_{upright}\right] \end{cases} \tag{4.23}$$

During phase 3 and 4 it is assumed, that the palls are hydrodynamic transparent structures. No hydrostatic and hydrodynamic force components are considered for the palls.

The end of phase 3 is reached as soon as the palls loose contact to the edge of the pier.

Phase 4 — dropping and raise (free ship motion)

During the last phase the ship is able to move freely, as Figure A.6 is illustrating. A contact of the palls to the pier is not given anymore. Therefore, only the hydrostatic and hydrodyanmic force of the ship are acting upon the ship as external forces. These forces are given in 4.19 to 4.21. The resulting moment $M_{upright}$ as given in equation 4.22 is still valid, too. In addition, the weight force of the ship is acting in the z-direction.

Because the ship is moving freely, the system of ODE for the ship motion considering the inertia effects of the surrounding water as stated in equation 4.5 is valid. Considering the above mentioned external forces and moments, the following system of ODE can be derived for phase 4:

$$\begin{cases} \frac{\partial v_y}{\partial t} = \frac{1}{(m_{tot}+\lambda_{22})} \cdot \left[\left(m_{tot} + \lambda_{33}\right) \cdot v_z \cdot \omega_x - F_{hyd\ dyn\ y}\right] \\ \frac{\partial v_z}{\partial t} = \frac{1}{(m_{tot}+\lambda_{33})} \cdot \left[-\left(m_{tot} + \lambda_{22}\right) \cdot v_y \cdot \omega_x - m_{tot} \cdot g + F_{hyd\ stat} - F_{hyd\ dyn\ z}\right] \\ \frac{\partial \omega_x}{\partial t} = \frac{1}{(I_{xx\ tot}+\lambda_{44})} \cdot \left[-\left(\lambda_{33} - \lambda_{22}\right) \cdot v_y \cdot v_z + M_{upright}\right] \end{cases} \tag{4.24}$$

The calculation of phase 4 is ended, as soon as the ship is in the upright position ($\varphi \geq 0$).

4.2.2. Impact loads on ship hull due to slamming

A configuration comparable to the sideways launching process of the SPV was investigated experimentally in [44], where also an analytical model to assess the resulting loads at impact with the water surface is proposed. Due to limitations of the model proposed in [44] (hydro-elasticity not accounted for and differences between experimental data and proposed model for configurations with higher degree of asymmetry and small deadrise angles) and the high effort necessary for implementation (complex systems of equation, discretization of structure and iterative solution scheme necessary), the use of this model is not further considered for assessing the loads resulting on the hull of the SPV. Other applicable models like [69], [114] lack thorough verification based on experimental results.

Because of this no further investigation of modelling the slamming loads based on analytical approaches is conducted. The cost benefit ratio (effort for implementation of an appropriate model compared to the limitations of even the more sophisticated models) within the context of the ship design process does not justify the use of such an approach. An implementation and adaptation for a sideways launching process of a ship during the ongoing ship design process, where design decisions (sideways launching process safe for SPV $\rightarrow$ yes or no?) are to be made on a sound basis, are not feasible.

4.2.3. Numerical implementation

To evaluate the ship motion, the systems of ODE for the different phases of the sideways launching process are to be solved. Not all phases of the analytical approach can be solved in an analytical closed-form. Beginning with phase 3 — tipping and immersion, a closed analytical solution will not be possible. The systems of ODE are a function of the current floating position of the ship, which changes over time. This is true for the buoyancy ∇, the position of the COB, the projected area of the centerline of the ship below the waterline A_{xz} as well as the waterline area A_{xy} or the added masses λ_{ii}. Therefore, the systems of ODE are solved with numerical methods. The implementation of the analytical approach for the ship motion is done in the programming language Visual Basic for Application (VBA).

Solving of ODE

For solving the systems of ODE the four-stage Runge-Kutta method is chosen. Details regarding this method can be found in literature. Within this work the implementation is done according to the work by Griffiths and Higham [36]. Although the four-stage Runge-Kutta method is more complex to implement and does need more computational resources per time step compared to an Euler integration scheme [36], it is chosen because of its high accuracy. The error is $\mathcal{O}\left(t_{RK}^4\right)$ [36]. During the analytical approach a constant time step size of $\Delta t_{RK} = 0.001$s is used. This small time step is chosen due to the large movement and rapid changes in the floating position of the ship during phase 3 and 4.

Numerical integration schemes

In order to solve the system of ODE using the stage-for Runge-Kutta method, the buoyancy ∇, position of the COB, projected area of the centerline of the ship below the waterline A_{xz}, waterline area A_{xy} as well as added masses λ_{ii} are to be determined for each time step. For this purpose the assumptions of strip theory are used. A brief introduction to

the topic of strip theory and underlying numerical methods is provided in literature. One example is the work by Moctar *et al.* [68].

Using the strip method, the ship is divided into several transverse ship sections / frame contours. External forces or moments acting upon the hull and added masses are computed for each of these transverse sections separately and independent from each other. Afterwards, the data obtained for each frame contour are integrated along the x-axis of the ship. One drawback of this approach is the assumption of a flow of the water around the ship hull, which is confined to the yz-plane. 3D effects around the ship hull are neglected [68].

For the numerical integration the frame contours of the ship hull investigated are idealized as polygons. Each frame contour is described by a given set of n points in the yz-plane by the coordinates y_i and z_i. The point n and $n+1$ of the frame contour are then connected by straight lines forming the polygon. Exemplary frame contours of the investigated ship hull are shown in Figure 4.1. To account for the details of each frame contour, the points are spaced equally with a distance of 100mm along each frame contour. Depending on the size of the frame contour, this spacing results in 360 up to 530 points for each frame contour. By using polygons the area of each frame A_{frame} can be calculated with the following integration scheme as given by Bourke [15]:

$$A_{frame} = \frac{1}{2} \cdot \sum_{i=0}^{n-1} \left(y_i \cdot z_{i+1} - y_{i+1} \cdot z_i \right) \tag{4.25}$$

Equation 4.25 is valid for a closed polygon, which does not intersect itself. The centroid of each frame contour can be calculated by the following equations [15]:

$$y_{A_{frame}} = \frac{1}{6 \cdot A_{frame}} \cdot \sum_{i=0}^{n-1} \left(y_i + y_{i+1} \right) \cdot \left(y_i \cdot z_{i+1} - y_{i+1} \cdot z_i \right) \tag{4.26}$$

$$z_{A_{frame}} = \frac{1}{6 \cdot A_{frame}} \cdot \sum_{i=0}^{n-1} \left(z_i + z_{i+1} \right) \cdot \left(y_i \cdot z_{i+1} - y_{i+1} \cdot z_i \right) \tag{4.27}$$

The projected area of the centerline of the ship below the waterline A_{xz} as well as the waterline area A_{xy} are calculated using the same integration scheme.

For the integration across all frame contours along the x-axis of the ship, Simpson's rule of integration is used. The Simpson's rule of integration can be formulated as follows [33]:

$$S_n(f) = \sum_{i=1}^{n/2} \frac{h_{SR\,i}}{3} \cdot \left[f\left(x_{2i-2}\right) + 4 \cdot f\left(x_{2i-1}\right) + f\left(x_{2i}\right) \right] \tag{4.28}$$

In equation 4.28 the sum S_n of the function f is approximated by n integration intervals with a width of $h_{SR\,i}$. For Simpson's rule of integration an even number of integration intervals n / odd number of interpolation points i is needed [33]. The investigated SPV is divided into 59 frame contours evenly spaced among its length.

Within the analytical approach Simpson's integration rule is used to calculate the buoyancy ∇, the corresponding position of the COB as well as the added masses λ_{220}, λ_{33} and λ_{44} for the complete ship. Due to it's high accuracy (error of $\mathcal{O}\left(h_{SR}^4\right)$ [33]) Simpson's integration rule is commonly used in naval architecture to calculate stability data of a ship [82].

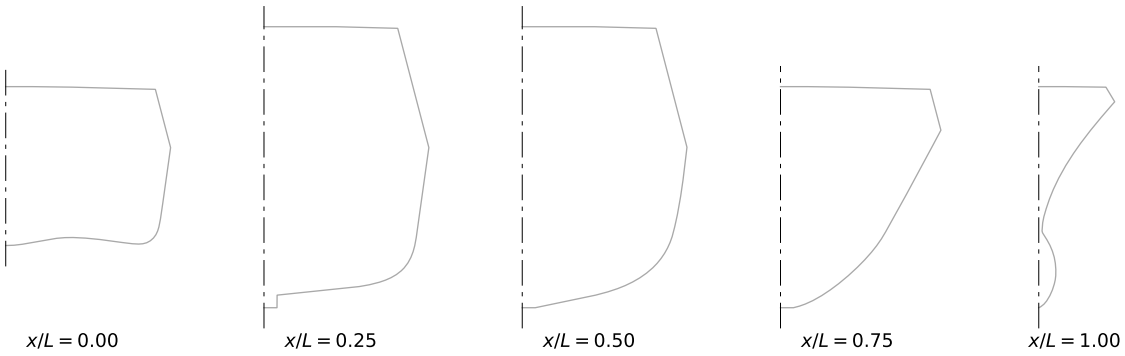

Figure 4.1.: exemplary frame contours used within analytical approach

Added masses

For the calculation of added masses around the ship hull, the concept of Lewis-frames is used for the analytical approach. Lewis [57] used the method of conformal mapping to calculate the added mass of duplicated ship frame contours. Lewis was able to calculate the flow around ship like contours in the complex plane and map the results back to a circle, for which an analytical solution for the added mass can be obtained. With this approach the added masses around a ship-like contour can be calculated if adequate mapping functions are chosen. Details regarding this approach can be found in literature, such as [53], [57]. Note that this approach is valid for a two-dimensional contour in an ideal incompressible and unlimited flow in a two-dimensional plane [53], [57]. The following equations are valid for the added mass λ_{ij} of a duplicated frame contour [53]:

$$\lambda_{220} = \frac{2 \cdot \rho_w \cdot B_{frame}^2}{\pi} \cdot k_{220} \tag{4.29}$$

$$\lambda_{33} = \frac{\pi \cdot \rho_w \cdot T_{frame}^2}{8} \cdot k_{33} \tag{4.30}$$

$$\lambda_{44} = \frac{\pi \cdot \rho_w \cdot T_{frame}^4}{256} \cdot k_{44} \tag{4.31}$$

In equation 4.29 to 4.31 the term B_{frame} is the breadth of the frame contour, whereas T_{frame} is the depth of each frame contour. The coefficients k_{220}, k_{33} as well as k_{44} are a function of the contour of the ship frame. These coefficients are depending on the aspect ratio B_{frame} / $(2 \cdot T_{frame})$ and the plumpness of the ship frame defined as $\beta_{frame} = A_{frame}$ / $(B_{frame} \cdot T_{frame})$ [53]. Note that equation 4.29 does take the presence of a free water surface into account. Values for k_{220}, k_{33} as well as k_{44} for a wide variety of frame contours can be found in [53].

Equation 4.29 to 4.31 are valid for symmetrical frame contours and not applicable to inclined ship frames. Therefore, a different approach is chosen. The added masses are calculated using Lewis-frames for different draughts of the SPV ($0 \cdot T_{design}$ to $2.5 \cdot T_{design}$). For each frame the necessary input data B_{frame}, T_{frame}, A_{frame}, the aspect ratio and the plumpness are calculated. Based on these values, the coefficients k_{220}, k_{33} as well as k_{44} are approximated based on the data provided in [53]. In the next step, the added masses λ_{220}, λ_{33} and λ_{44} are calculated for each ship frame based on equation 4.29 to 4.31. The

total added masses for the ship are calculated using Simpson's rule of integration (equation 4.28). Using this approach the added masses are obtained as functions of the buoyancy of the SPV. The current added masses at each time step during phase 3 and 4 are then approximated as a function of the current buoyancy of the SPV.

It shall be noted this approach is only an estimation of the added masses of the SPV, because the roll angle during the sideways launching process is not considered. The added masses based on equation 4.29 to 4.31 are valid for duplicated frame contours, where symmetry of the ship hull regarding the xz-plane is given. This not true for an inclined ship, so that discrepancies with the actual added masses are to be expected.

4.2.4. Results

For an evaluation of the results of the analytical approach the roll angle as well as the trajectory of the COG are compared to the results obtained by the model tests conducted within the experimental approach. The results for the design point are used for this purpose (see Table 4.2 for details). As Figure 4.3 shows, the behaviour up to the end of phase 2 are virtually identical. This shows, that the proposed ODE are capturing the physical behavior behind the sideways launching process accordingly and are solved correctly by the presented numerical implementation. However, beginning with the start of phase 4 the results obtained with the analytical approach differ compared to the experimental approach. Whereas the maximal roll angle does fit well (compare Figure 4.3a), the trajectory of the COG as obtained by the analytical approach is off (compare Figure 4.3b). The path travelled in the y-direction is significantly longer compared to the model tests.

The obvious explanation is the influence of the free water surface. The ship and water surface do interact with each other. Waves and spray form besides the ship hull right after the impact with surface. The water rises up the ship hull (formation of a spray root). This interaction results in different hydrodynamic conditions as assumed within the analytical approach. Especially the following aspects are influenced by the free water surface / spray root forming during the sideways launching process:

- The projected area of the centerline A_{xz} is bigger
- The centroid of A_{xz} is higher than assumed
- The waterline area of the ship A_{xy} is bigger
- The projected draught of the ship hull is bigger, which results in a change of the buoyancy ∇ and added masses λ_{ii}

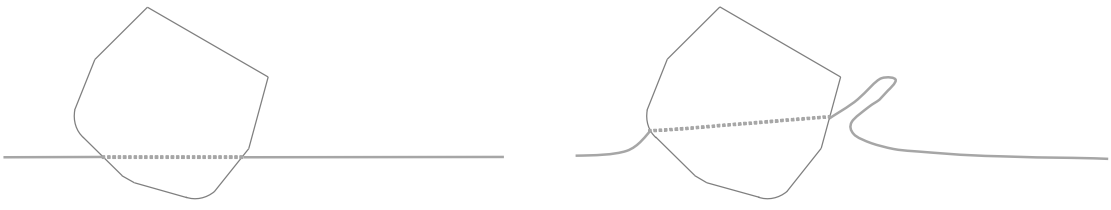

(a) assumption for analytical approach (b) behavior observed during model tests

Figure 4.2.: interaction of ship hull with water surface

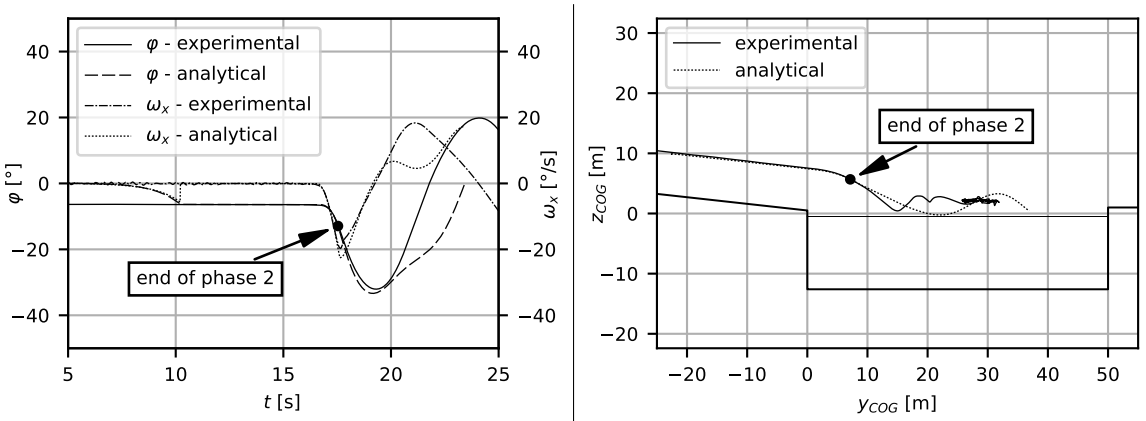

(a) roll angle and velocity

(b) trajectory of COG

Figure 4.3.: results of analytical approach

All these aspects can not be captured explicitly by the proposed systems of ODE of the analytical approach. The systems of ODE as given in section 4.2.1 do not consider any change of the waterline. The height of the waterline is constant at z_{wl} during all phases of the analytical approach. This is visualized in Figure 4.2.

Minor tweaks to the system of ODE can be done to account for these effects. An overview of the proposed modifications are given in Appendix A.3. These modifications are found iteratively based on the results for the design point of the model tests. As Figure 4.4 shows, introducing the modifications as proposed in Table A.1 into the according system of ODE does yield in results closer to experimental approach. The roll angle and velocity are almost identical, whereas the trajectory of the COG shows a much better agreement with the behaviour during the model tests.

However, it shall be noted that by introducing these modifications to the system of ODE, the consideration of the free water surface and the interaction with the ship hull inside the analytical approach are fitted especially to the conditions as present during the design point of the model tests. In addition, the presented modifications can only be derived if results for a ship with a given loading condition are known — e.g. based on model tests. For verifying these modifications, the different test setups as investigated during model tests are assessed using the analytical approach with the proposed modifications to the systems of ODE considered. The maximal roll angles are compared, which are given in Appendix A.3. The differences between the analytical approach and model tests are quite significant. A factor between 0.62 up to 1.42 for the maximal roll angle between the analytical approach and model tests can be observed (compare Figure A.7).

4.2.5. Benefits and Limitations

The analytical approach is a very useful tool in the context of the ship design process. The setup of the corresponding ODE of motion and numerical integration schemes is straight forward and can be done without too much effort. This is especially true, if only phase 0 up to the end of phase 2 are considered, as for these ODE of motion no implementation of strip theory is necessary. The computational time up to the end of phase 2 is less than one minute.

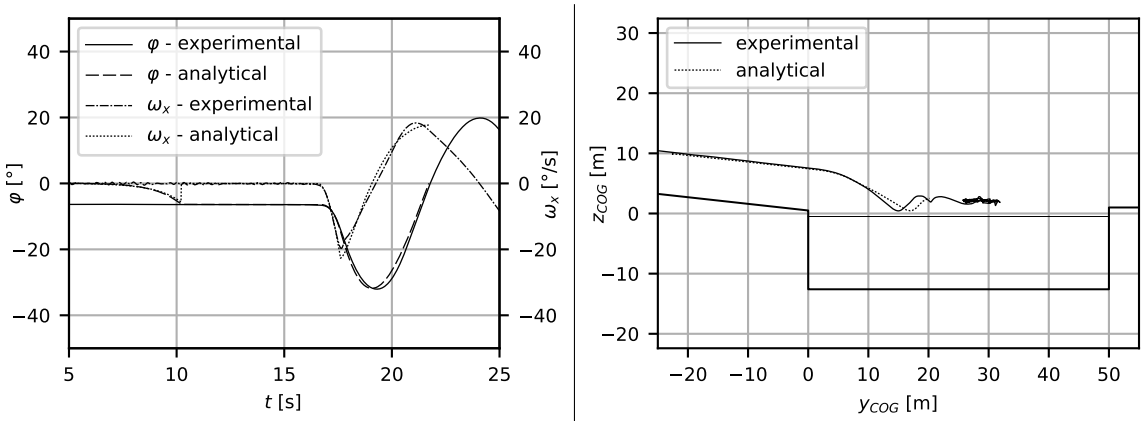

(a) roll angle and velocity

(b) trajectory of COG

Figure 4.4.: results of analytical approach — modified settings

For the ship design process as well as other approaches (experimental or simulation-based), the results at the end of phase 2 are of particular interest. The influence of relevant parameters during the sideways launching process like the loading condition of the SPV, the height of the palls, the water level inside the launch basin (tidal range) or the coefficient of friction between the palls and the slipway on the configuration given at the moment of impact with the water surface can be investigated. This is especially of interest, as the deadrise angle and speed of the ship hull at the impact have an significant influence on the resulting loads on the hull of the SPV. In addition, the results at the end of phase 2 are used for the derivation of the text matrix for the experimental approach as well as the initial conditions for further investigations using both simulations-based approaches (without FSI and with FSI). This includes the position of the SPV relative to the water surface as well as the speed right before the impact with the water surface.

However, the analytical approach has clear limitations. The approach based on the ODE of motion is only a reliable tool for the prediction of the behaviour during the sideways launching process up to the point of the first contact of the ship hull with the water surface (end of phase 2). The free ship motion can not be assessed accurately with the proposed analytical approach by solving the system of ODE using strip theory. The influence of the free water surface and resulting interaction with the ship hull is not accounted for with the proposed approach (see Figure 4.2). This results in a wrong estimation of the hydrodyanmic forces acting upon the ship hull. In addition, due to the use of the strip theory the proposed analytical approach is not able to predict local loads on the ship hull.

One possibility to improve the current analytical approach could be combining the corresponding ODE of motion of the sideways launching process as given in section 4.2.1 with the model proposed in [44] (see section 2.3 for details regarding [44]). The model in [44] could be used to assess the impact loads upon the ship hull starting at the first contact with the water surface (start of phase 3) and use the resulting forces within the corresponding systems of ODE in phase 3 and 4 of the analytical approach. Such an approach would comparable to [38], [54]. However, the implementation of the model proposed in [44] is complex, because a discretization of the ship hull and implementation of an iterative solution scheme is necessary. As the focus of this work is on a simulation-based approach using FSI, such a combination of these two models is potentially the work for future research.

4.3. Experimental approach

In 2020 model tests of the sideways launching process of the SPV were conducted at a ship model basin. During these model tests the ship motion and pressure at different locations on the ship hull were measured. The goal of the model tests was gaining a understanding for feasible limits to ensure a safe sideways launching process. In addition, the data obtained from the model tests was used as the basis for the verification of the proposed simulation-based approach using FSI.

Different parameters of the sideways launching process were varied during model tests. This included the loading condition of the ship, the height of the water level inside the launch basin (tidal range), the height of the palls used during launching and the coefficient of friction between the palls and the slipway. A parametric study was conducted, where the influence of these parameters on the resulting ship motion as well as resulting pressure on the ship hull was investigated. If not stated otherwise, all results from the experimental approach are presented for the full scale version of the SPV.

4.3.1. Setup of model tests

The model tests of the sideways launching process were conducted to account as closely to the conditions of the potential construction shipyard of the SPV as possible. The test setup at the ship model considered the slipway and did enable a free six DOF motion of the ship model. The model tests were carried out based on Froude similarity. An overview of the different data measured during the model tests as well as the applied scaling laws is provided in Table A.2 in Appendix A.4.

Ship model

A ship model in the scale of $\lambda_{sm} = 32$ was used for the model tests. A photograph of the model is shown in Figure 4.5. The model contained the complete watertight volume of the ship as given during the sideways launching process. Therefore, the complete shell of the

Figure 4.5.: ship model used for model tests

ship hull, three decks including their bulwarks, necessary transversal walls (like the back wall of hangar or front wall of the deckhouse) were modelled. These parts were all built using natural fiber reinforced composites (NFRPC). The average thickness of the shell was approx. 4mm, whereas the decks and transversal walls were built using an average thickness of 5mm. Additional support frames built with wood were added the ship model below the transversal walls to add rigidity (compare Figure 6.3).

Besides the hull structure, the superstructure of the ship (yardarm and mast modules) was considered during model tests. In addition, relevant appendages were considered. This included a pair of rudders, fin stabilizers and bilge keels as well as two propulsion shafts with bossing, V-brackets, hub of propellers and dummy propeller blades. The superstructure and appendages were built with ABS plastic using 3D-printing technology. The different appendages can be seen in Figure 4.5.

Loading conditions

Four different loading conditions were investigated during the model tests:

- LC01: LC02 with tanks in bottom structure filled to lower COG of ship
- LC02: weight distribution as designated for sideways launching process (tanks empty)
- LC03: COG_z 5% higher than LC02
- LC04: COG_z 10% higher than LC02

Note, that LC01 is used as the design point during the parametric study conducted with the model tests (compare Table 4.2). An overview of the most important parameters of the loading conditions is given in Table 4.1. All values provided in Table 4.1 are normalized. The reference frame for each value for the radii of gyration i_{ii} is the corresponding COG. All values are provided for a dry ship without added masses. The loading conditions were realized by trimming weights inside the ship model, whose positions were set accordingly to match the specified loading conditions. For LC01 additional weights were added, to account for the increase of weight due to the contents inside the tanks of the bottom structure.

These loading conditions were investigated to assess a variety of different weight distributions feasible for the sideways launching process. One one hand the influence of actively

Table 4.1.: loading conditions used for model tests

parameter	unit	LC01	LC02	LC03	LC04
Δ	[t]	$0.926 \cdot \Delta_{design}$	$0.837 \cdot \Delta_{design}$	$0.837 \cdot \Delta_{design}$	$0.837 \cdot \Delta_{design}$
COG_x^*	[m]	$0.465 \cdot L_{pp}$	$0.458 \cdot L_{pp}$	$0.465 \cdot L_{pp}$	$0.465 \cdot L_{pp}$
COG_y	[m]	$0.000 \cdot B_{wl}$	$0.000 \cdot B_{wl}$	$0.000 \cdot B_{wl}$	$0.000 \cdot B_{wl}$
COG_z	[m]	$0.466 \cdot D_{main}$	$0.507 \cdot D_{main}$	$0.533 \cdot D_{main}$	$0.560 \cdot D_{main}$
$\overline{GM}_0$	[m]	$0.630 \cdot T_{design}$	$0.580 \cdot T_{design}$	$0.490 \cdot T_{design}$	$0.398 \cdot T_{design}$
i_{xx}	[m]	$0.412 \cdot B_{wl}$	$0.417 \cdot B_{wl}$	$0.406 \cdot B_{wl}$	$0.408 \cdot B_{wl}$
i_{yy}	[m]	$0.250 \cdot L_{pp}$	$0.258 \cdot L_{pp}$	$0.257 \cdot L_{pp}$	$0.257 \cdot L_{pp}$
i_{zz}	[m]	$0.248 \cdot L_{pp}$	$0.257 \cdot L_{pp}$	$0.257 \cdot L_{pp}$	$0.257 \cdot L_{pp}$

*: referred to aft perpendicular

lowering the position of the COG by filling tanks in the bottom structure could be assessed. On the other hand upper limits regarding a feasible or safe position of the COG could be investigated. A shift of the COG during the detailed design phase of the ship is still possible due to different reasons. Examples are more detailed weight calculations or changes of the level of equipment as specified for the sideways launching process.

Launch basin, slipway and palls

The launch basin and slipway were built with wooden plates and aluminium supports in accordance to the conditions at the shipyard. An illustration of the launch basin and the slipway is given in Figure 4.6. The slipway of the model was equipped with two low-friction roller conveyors to simulate the sliding process of the ship. Two palls were mounted to the ship model, that allowed for rolling down the roller conveyors. These palls were built with wood and fixed to the ship model. Using these roller conveyors, the friction between the palls and the slipway was not modelled directly. The friction was considered by controlling the sliding speed during model tests. This was done by a winch system located at the top of the slipway, which is marked in Figure 4.6. This winch system was connected with strings to the palls of the ship model. At the beginning of the sideways launching process the winch was accelerated to the defined sliding speed and the rate of rotation was fixed. Shortly before the ship model started to rotate around the edge of the pier, the connection between the palls and winch system was released by a little ramp located on the slipway. This release mechanism is marked in Figure 4.6.

In addition, the water level within the basin could be raised or lowered by pumps allowing for the investigation of the influence of the water level inside the launch basin (tidal range).

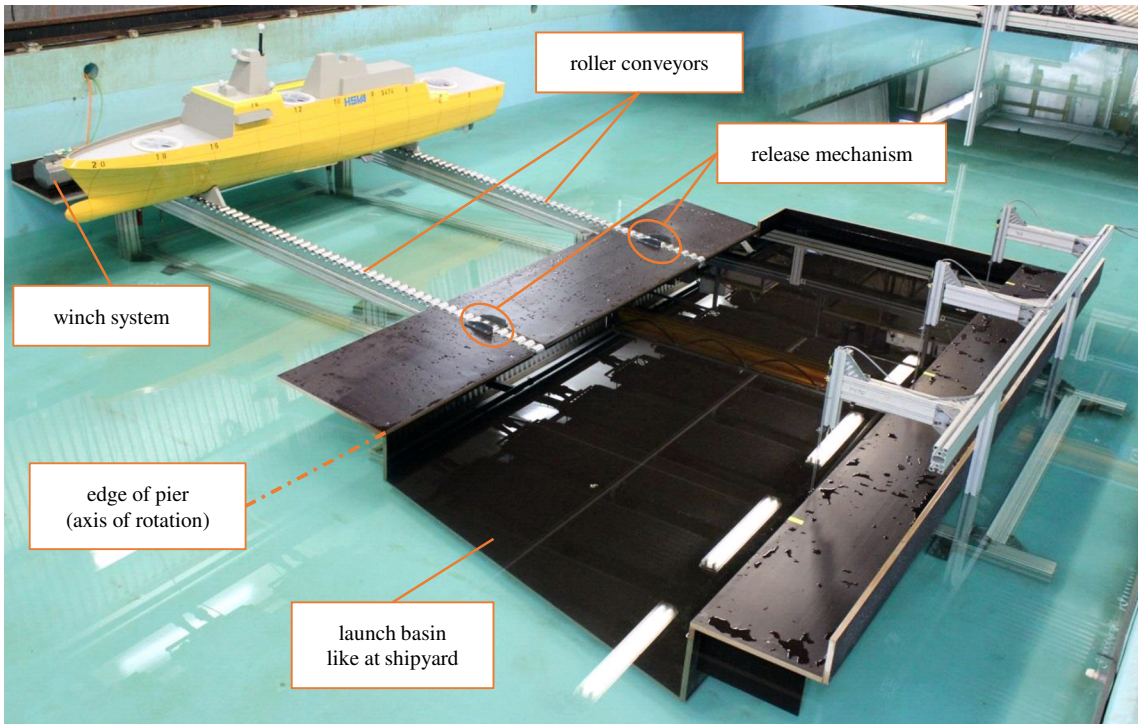

Figure 4.6.: test setup used for model tests

Test matrix

Different conditions for the sideways launching process were investigated. Especially parameters, that can change during the ship design process, and relevant external parameters were varied. This included the following aspects:

- change of loading conditions, especially a change of the COG / $\overline{GM}_0$
- height of palls h_p
- water level h_{wl} (influence of tidal range)
- coefficient of friction μ_{sw} between palls and slipway

The test matrix as given in Table 4.2 gives an overview of all conducted model tests. The specified speed v_{yz} in Table 4.2 is defined as the sliding speed at the end of the slipway, right before the ship start ro rotate around the edge of the pier. This point is identical the end of phase 1 of the analytical approach as shown in Figure A.3 (see 4.2.1 for details). The speeds v_{yz} for the different test setups specified in Table 4.2 are calculated using the analytical approach. The water level h_{wl} is measured from the edge of the pier to the water surface (negative value = water level below edge of pier), whereas the height of the palls h_p is specified as the distance between the slipway and the flat keel of the SPV.

Within this frame of the parametric study only one parameter at a time was changed between the different test setups. By doing so, the influence of each of the four parameter could be investigated systemically. All investigations are started from the design point. In addition, different "worst case" scenarios were investigated. In contrast to the parametric study, for each "worst case" scenario several parameters were changed simultaneously. The intention of the "worst case" scenarios was getting a better understanding of feasible limits for the sideways launching process.

A visualization of the different conditions is presented in Figure 4.7. Those two graphs visualize the different conditions at the moment of impact of the ship hull with the water surface. The data presented in both figures are obtained by the analytical approach. In Figure 4.7a the conditions at the moment of impact are given for the COG of the SPV. The x-axis plots the translational velocity of the ship in the yz-plane ($v_{yz\ impact}$), while the y-axis represents the rotational velocity about the x-axis of the ship at the moment of impact ($\omega_x\ impact$). Initially while preparing the models test, it was assumed that a higher translational velocity $v_{yz\ impact}$ would be more critical regarding the hull structure (higher kinetic energy), while a higher rotational speed ($\omega_x\ impact$) will be more critical regarding the stability of the ship (higher rotational energy). As Figure 4.7a indicates, the "worst case" scenarios are all in the lower right corner. This results in more critical conditions for the sideways launching process. This is true for the stability of the SPV as well as the loads on the hull structure.

In Figure 4.7b a closer look is taken upon the conditions given at the ship hull at the moment of impact of the SPV with the water surface. The x-axis represents the velocity v_{slam} perpendicular to the water surface, while the y-axis represents the angle β_{impact} between the ship hull and the water surface at the moment of impact. In accordance with slamming experiments, an increased v_{slam} should correspond to higher loads on the ship hull. The angle at impact β_{impact} did not change significantly for the different test setups. An average of about -1.1° could be observed. As Figure 4.7b shows, the "worst

Table 4.2.: test matrix used for model tests

design point for parametric study:

case	LC_0	$\mu_{sw\,0}$ [-]	$h_{wl\,0}$ [m]	$h_{p\,0}$ [m]	$v_{yz\,0}$ [m/s]	remark
—	LC01	0.03	-0.50	1.00	5.90	= LC_01

variation of loading condition / COG:

case	LC	μ_{sw} [-]	h_{wl} [m]	h_p [m]	v_{yz} [m/s]	remark
LC_01*	LC01	$\mu_{sw\,0}$	$h_{wl\,0}$	$h_{p\,0}$	5.90	design point
LC_02*	LC02	$\mu_{sw\,0}$	$h_{wl\,0}$	$h_{p\,0}$	5.90	
LC_03	LC03	$\mu_{sw\,0}$	$h_{wl\,0}$	$h_{p\,0}$	5.90	
LC_04	LC04	$\mu_{sw\,0}$	$h_{wl\,0}$	$h_{p\,0}$	5.90	

*: conducted 4x for replicating pressure measurement

variation of height of palls:

case	LC	μ_{sw} [-]	h_{wl} [m]	h_p [m]	v_{yz} [m/s]	remark
HP_01	LC01	$\mu_{sw\,0}$	$h_{wl\,0}$	$h_{p\,0}$	5.90	= LC_01
HP_02	LC01	$\mu_{sw\,0}$	$h_{wl\,0}$	$h_{p\,0} + 0.50$	5.90	

variation of water level:

case	LC	μ_{sw} [-]	h_{wl} [m]	h_p [m]	v_{yz} [m/s]	remark
WL_01	LC01	$\mu_{sw\,0}$	$h_{wl\,0}$	$h_{p\,0}$	5.90	= LC_01
WL_02	LC01	$\mu_{sw\,0}$	$h_{wl\,0} - 0.50$	$h_{p\,0}$	5.90	
WL_03	LC01	$\mu_{sw\,0}$	$h_{wl\,0} - 1.00$	$h_{p\,0}$	5.90	
WL_04	LC01	$\mu_{sw\,0}$	$h_{wl\,0} - 0.66$	$h_{p\,0}$	5.90	wrong h_{wl}

variation of coefficient of friction:

case	LC	μ_{sw} [-]	h_{wl} [m]	h_p [m]	v_{yz} [m/s]	remark
FC_01	LC01	$0.25 \cdot \mu_{sw\,0}$	$h_{wl\,0}$	$h_{p\,0}$	6.66	
FC_02	LC01	$0.50 \cdot \mu_{sw\,0}$	$h_{wl\,0}$	$h_{p\,0}$	6.42	
FC_03	LC01	$0.75 \cdot \mu_{sw\,0}$	$h_{wl\,0}$	$h_{p\,0}$	6.17	
FC_04	LC01	$\mu_{sw\,0}$	$h_{wl\,0}$	$h_{p\,0}$	5.90	= LC_01
FC_05	LC01	$1.25 \cdot \mu_{sw\,0}$	$h_{wl\,0}$	$h_{p\,0}$	5.63	
FC_06	LC01	$1.50 \cdot \mu_{sw\,0}$	$h_{wl\,0}$	$h_{p\,0}$	5.35	
FC_07	LC01	$2.00 \cdot \mu_{sw\,0}$	$h_{wl\,0}$	$h_{p\,0}$	4.72	

investigation of "worst case" scenarios:

case	LC	μ_{sw} [-]	h_{wl} [m]	h_p [m]	v_{yz} [m/s]	remark
WC_01	LC01	$0.25 \cdot \mu_{sw\,0}$	$h_{wl\,0} - 0.50$	$h_{p\,0} + 0.50$	6.65	
WC_02	LC02	$0.25 \cdot \mu_{sw\,0}$	$h_{wl\,0} - 0.50$	$h_{p\,0} + 0.50$	6.65	
WC_03	LC03	$0.25 \cdot \mu_{sw\,0}$	$h_{wl\,0} - 0.50$	$h_{p\,0} + 0.50$	6.65	
WC_04	LC04	$0.25 \cdot \mu_{sw\,0}$	$h_{wl\,0} - 0.50$	$h_{p\,0} + 0.50$	6.64	
WC_05	LC01	$0.25 \cdot \mu_{sw\,0}$	$h_{wl\,0} - 0.66$	$h_{p\,0} + 0.50$	6.65	wrong h_{wl}

Σ 19 different test setups and 26 measurement series

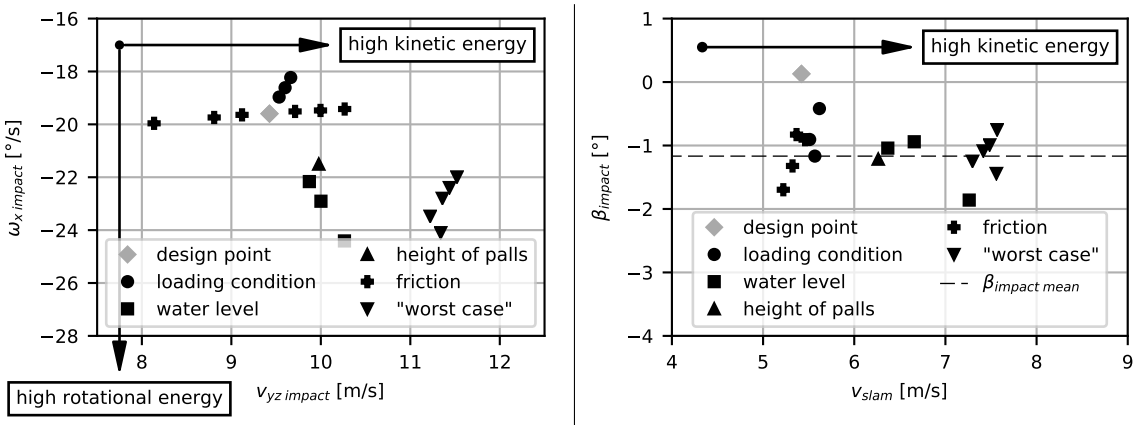

(a) COG (b) ship hull

Figure 4.7.: test matrix used for model tests — conditions at impact with water surface

case" scenarios are all in the right hand side as well, which should correspond to higher loads on the ship hull during these test setups.

In total 19 different test setups were investigated with a total of 26 measurement series. The two test setups LC_01 and LC_02 were conducted four times each. This was done to evaluate the sensitivity of the pressure measurement due to it's dynamic nature. The two test setups WL_04 and WC_05 were not specified before conducting the model tests. These test setups were investigated due to a wrong water level within the test basin of the ship model test facility during model tests (see remark in Table 4.2).

Measurement equipment

During model tests different results were measured. An overview of the measured variables including the used measurement devices is provided in Table A.2 in Apendix A.4.

The ship motion was measured using an optical tracking system called *Qualisys*. The ship motion was measured for all six DOF. For this purpose the ship model was equipped with markers at different positions, which were captured by the optical tacking system. The position of these markers is shown in Figure 4.8. In addition, an inertial measurement unit inside the ship model was used to capture the accelerations during the sideways launching process. As with the optical tracking system, the inertial measurement unit did capture the accelerations for all six DOF.

The resulting pressure-time-signals at four different points on the ship hull were investigated using pressure transducers. The arrangement of pressure transducers is shown in Figure 4.8. The pressure transducers were arranged around the area, where the ship hull did have the first contact with the water surface. The pressure transducers were offset in longitudinal as well as horizontal direction. These positions were determined beforehand using the analytical approach. This allowed to capture the presumably highest peak pressures at the impact of the ship hull with the water surface. The pressure-time-signals were measured using miniature pressure transducers *XTM-190*-series from *Kulite*. The measurement area of the pressure transducers were circular in shape with a diameter of 3.8mm corresponding to 0.122m in full scale. The pressure transducers used a sampling frequency of 4,800Hz corresponding to 848.5Hz in full scale. Pressure transducers with a high sampling

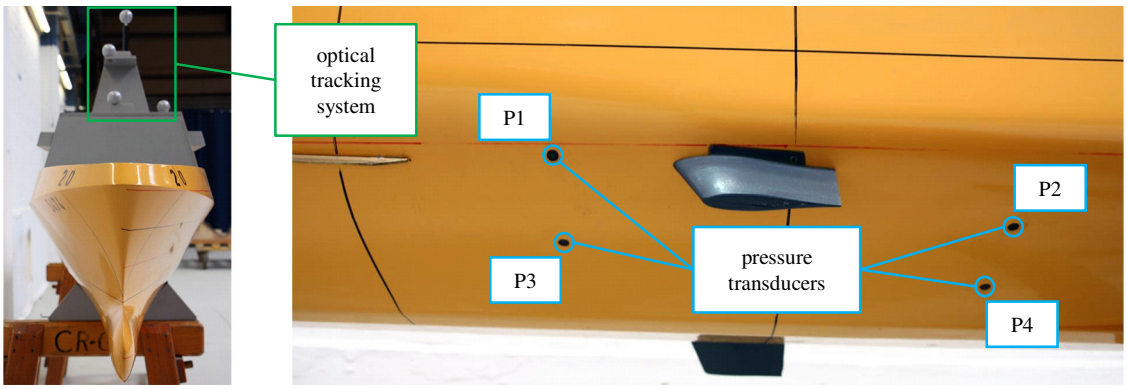

front view of model

view below bottom shell of model (PS | about amidships)

Figure 4.8.: measurement devices used during model tests

frequency were chosen to capture the highly dynamic peak pressures sufficiently. The measured pressure-time-signals consisted of the hydrodyanmic as well as hydrostatic pressure. The pressure-time-signals were calibrated on the standard atmosphere p_0 of 101,325Pa.

4.3.2. Results

In general, the test setup was able to successfully reproduce the behaviour of a ship during the sideways launching process. Using the eject mechanism at the end of the slipway, the ship was able to rotate freely around the edge of the pier and started to incline before the impact with the water surface. An impression of the model tests is presented in Appendix A.4 as a series of pictures. For further assessment, the results of the model tests are split into two parts: the ship motion and the resulting loads on the ship hull.

Ship motion

The model tests allow for a detailed assessment of the ship motion, as the ship motion was measured for a long time period. For the design point LC_01 the measured ship motion is plotted in Figure 4.9. As the test setups LC_01 and LC_02 were measured four times each, the sensitivity of the measurement of the ship motion could be evaluated. Table A.3 demonstrates, that the test setup was able to replicate the ship motion very reliable. For the maximal roll angle $|\varphi_{min}|$ a coefficient of variation CV below 1% was given.

During the parametric study the SPV was able to upright itself. No capsizing could be observed for any case. For the design point of the model tests (LC_01) a maximal roll angle of 32.1° was given, while for the loading condition as designated for the sideways launching process (LC_02) a maximum roll angle of 39.3° was reached. The biggest maximum roll angle of 74.6° was observed during WC_04. In cases with high maximal roll angles (especially LC_04 and WC_04) the main deck comes into contact with water and is partially flooded. This observation is important for the prevention of further flooding due to openings in the main deck or ventilation ducts, overflow pipes among others located in that area.

In all cases, sufficient clearance between the SPV (including palls and appendices) and the launch basin (both sides and bottom) could be observed. The SPV did more or less

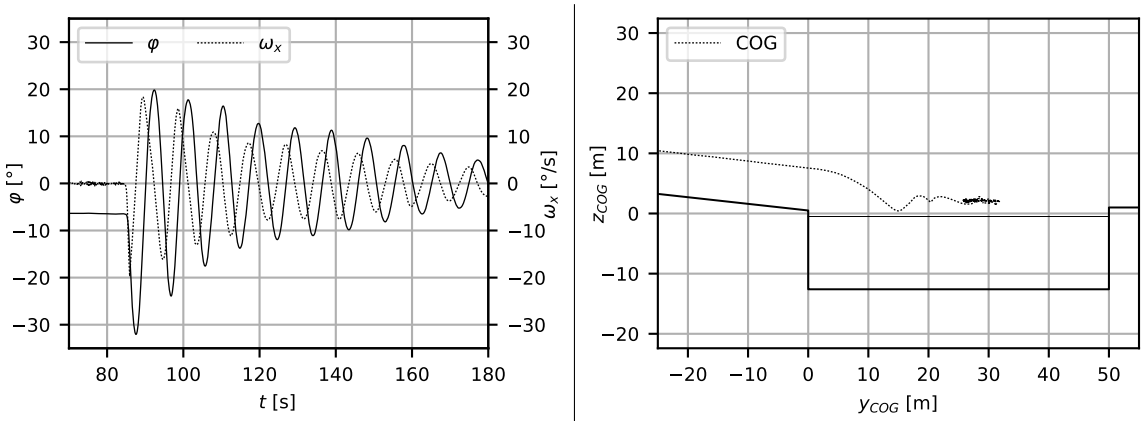

(a) roll angle and velocity

(b) trajectory of COG

Figure 4.9.: results of model tests — ship motion @ LC_01 (run No. 2)

center itself within the launch basin without applying external forces (e.g. use of trosses). This behavior can be seen in Figure 4.9b, as well.

The interaction between the ship hull and water surface was clearly visible during model tests. The water rose up significantly the portside (PS) of the ship's hull, reaching much higher levels than water surface at rest. This behavior is similar to slamming experiments like [44]. In addition, significant waves and spray were forming reaching several meters in height. The waves rose easily above the opposite side of the pier of the launch basin. The pictures in Appendix A.4 give a good impression of these observations.

The influence of the different parameters varied during model tests on the ship motion in the form of the maximal roll angle $|\varphi_{min}|$ is visualized in Figure 4.10. Besides the loading condition, the influence of the remaining parameters on the maximal roll angle can be nearly approximated using linear relationships.

In Figure 4.10a the influence of the coefficient of friction μ_{sw} is shown. With an increasing coefficient of friction and decreasing ship speed at the edge of the pier, the maximal roll angle did increase. This behaviour is to be expected, as the SPV had more time to rotate around the edge of the pier and built rotational energy, before the impact with the water surface. The influence on the maximal roll angle is only minor. An increase of μ_{sw} by a factor of two, did result in an increase of approx. 2.5° of the maximal roll angle during model tests. A decrease of μ_{sw} by a factor of two, did result in a decrease of approx. 0.9° of the maximal roll angle.

In contrast to the maximal roll angle, the trajectory of the COG is strongly influenced by the coefficient of friction. For test setup FC_07 (slowest ship speed) the COG travelled a distance of 29.6m in y-direction in reference to the edge of the pier, while during FC_01 (fastest ship speed) this distance was about 38.0m. The difference of 9.4m is equal to an increase of approx. 31.8%. With an increasing ship speed v_{yz} the translational energy was higher, resulting in a greater distance needed to decelerate the SPV.

In Figure 4.10b and 4.10d the influence of the height of palls h_p and water level h_{wl} inside the launch basin on the maximal roll angle during model tests is plotted. Both phenomena are based on the same physical effect: an increase of the height of palls like a decrease of the water level did result in a higher drop height of the SPV around the edge of the pier. The SPV had more time to tip around the edge of the pier and to build more rotational

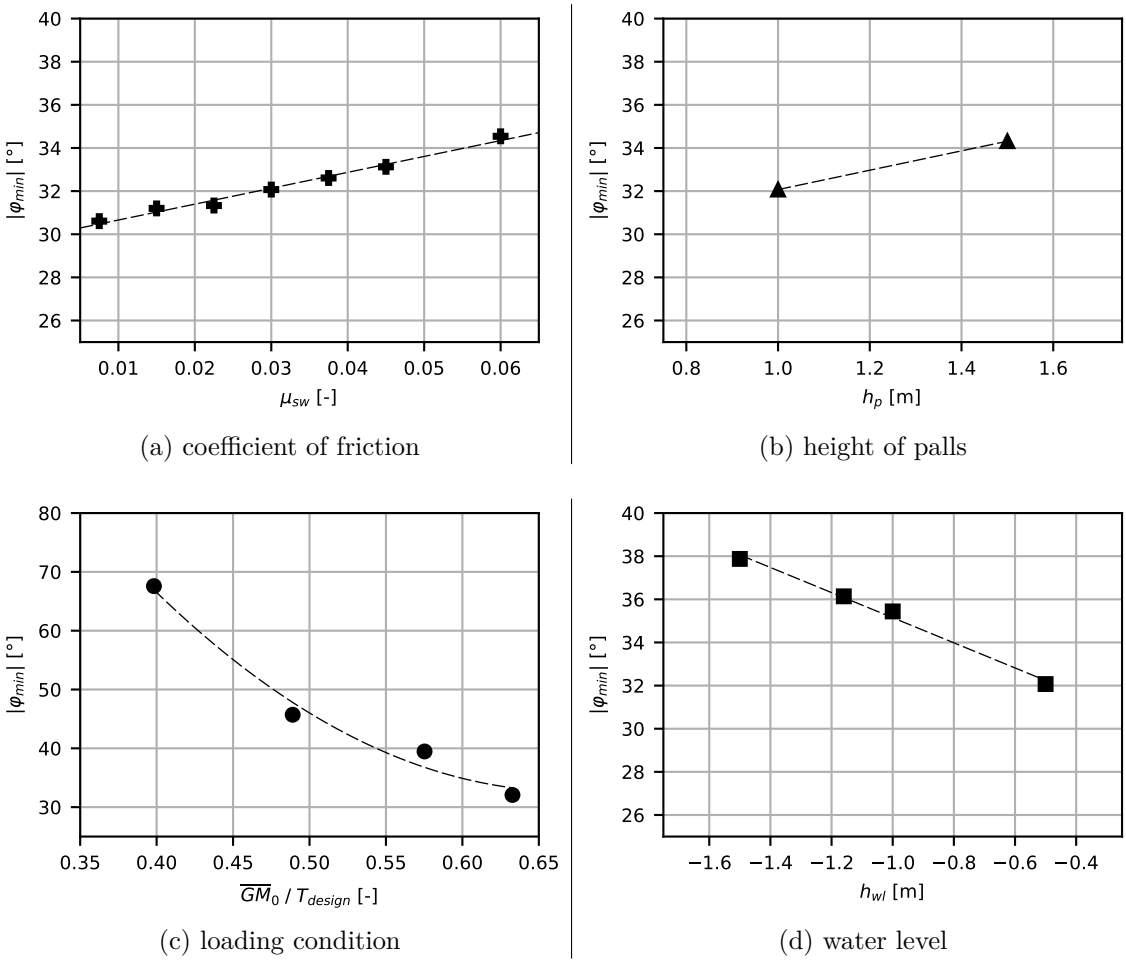

(a) coefficient of friction

(b) height of palls

(c) loading condition

(d) water level

Figure 4.10.: results of model tests — parametric study of maximal roll angle

energy before the impact with the water surface. As with the influence of the coefficient of friction, the influence of height of the drop is only of minor significance for the resulting maximal roll angle during model tests. An increase of 0.50m will result in an increase of 2.2° of the maximal roll angle, while a decrease of 0.50m will result in an increase of 3.3°.

Interestingly, the influence of the water level is slightly bigger than the height of the palls. By increasing the height of the palls, the moments of inertia around the pier $I^{\dagger}_{xx\,tot}$ in the system of ODE as given in equation 4.18 is increased noticeable due to the parallel axes theorem / Steiner's theorem. This resulted in a slower rotation around the pier, so that less rotational energy is built up during the tipping phase compared to a decrease of the water level.

As to be expected, the loading condition of the SPV had the most significant influence on the maximal roll angle during model tests. The influence of the loading condition is plotted in Figure 4.10c as a function of the metacentric height $\overline{GM}_0$. A small change of the metacentric height, e.g. from loading condition LC_01 to LC_02 (compare Table 4.1), did increase the maximal roll angle by 7.1°. This change was bigger as with all other parameters (coefficient of friction, height of palls or water level). If the COG_z is raised by additional 10% (LC_04 compared to LC_02), the maximal roll angle nearly doubled. In the case of

LC_04 a maximal roll angle of 67.6° was observed, which is equal to an increase of 35.5° (+111%) compared to LC_01.

Although the influence by shifting COG_z regarding the ship motion was significant, this behaviour was to be expected. For this purpose the illustration as given in Figure A.6 is quite useful. If COG_z is shifted upwards, the distance between the point of origin of the hydrostatic and hydrodyanmic forces and the COG of the ship is drastically reduced. This will results in a smaller arm of lever for the moment $M_{upright}$ (see equation 4.22). This results ultimately in smaller moment $M_{upright}$, which will upright the ship inside the launch basin. Therefore, the ship will need more time to counteract the given rotational energy and momentum resulting in a higher maximal roll angle $|\varphi_{min}|$. The physics are similar as with the cross curves of stability of a ship. An increase of COG_z will ultimately decrease the arm of lever and range of stability of a ship. Details regarding the stability of a ship in general as well as the more explanations of the underlying physics can be found in literature, e.g. in [82].

In contrast to the coefficient of friction, height of palls or water level, the influence of $\overline{GM}_0$ on the maximal roll angle $|\varphi_{min}|$ was non-linear. The non-linear behaviour was given due to the hull form of the SPV. As Figure 4.1 shows, the hull form does have a knuckle line above the design waterline. Above this knuckle line the frame contours point inwards. If the roll angle during sideways launching gets high enough, the knuckle line comes into contact with the water. Due to the inwards frame contours, the point of origin of the hydrostatic forces does only shift slowly outwards creating a sufficient arm of lever. A much higher roll angle will be needed, to create a sufficient $M_{upright}$. This effect is obvious, while comparing the maximal roll angle of LC_04 and LC_03 to LC_02. While an increase of COG_z of 5% in the case of LC_03 will increase the maximal roll angle by 6.5° (+16.6%) in relation to LC_02, the shift of COG_z of 10% in the case of LC_04 results in increase of 28.4° (+72.4%) in relation to LC_02.

As a result, an exact and detailed weight calculation and estimation of the COG is crucial during the design phase. Small changes of COG_z can drastically alter the maximal roll angle reached during the sideways launching process. A higher maximal roll than estimated, can lead to unplanned flooding of decks or further flooding via openings (ventilation ducts, overflow pipes among others) if not anticipated. All other parameters (ship speed / coefficient of friction, height of palls, water level) are only of minor importance in comparison to the loading condition.

Loads on ship hull

Exemplary pressure-time-signals measured during model tests are shown in Figure 4.11. The data shown in Figure 4.11 is calibrated to the standard atmospheric pressure p_0. For the pressure transducers, that came into contact early during the sideways launching process, high and harsh peak pressures could be observed. For the pressure-time-signals as shown in Figure 4.11 this was true for P2 and P4. Those peak pressures were only of very short duration and could only be observed for one or two measurement intervals. For pressure transducers, which were later in contact with the water surface like P1, the pressure-time-signals were not as harsh and the peak is smoother and longer.

As shown in Table 4.2, the two test setups LC_01 and LC_02 were measured four times each to account for uncertainties and fluctuations during measurement of the pressure-time-signals. An overview of the peak pressure $p_{i\,max}$ measured for these to two test setups is

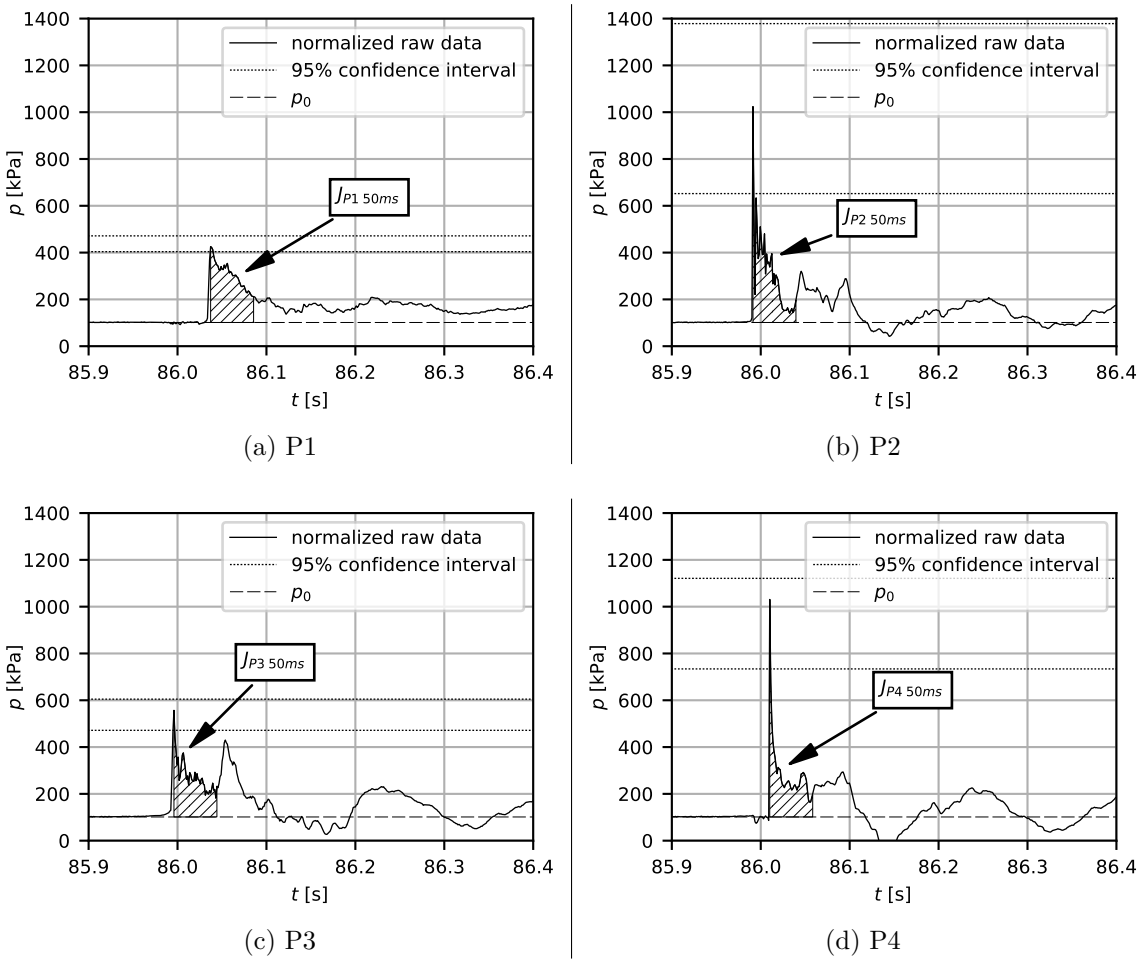

(a) P1 (b) P2

(c) P3 (d) P4

Figure 4.11.: results of model tests — pressure-time-signals @ LC_01 (run No. 2)

given in Table 4.3 for all conducted runs. To account for effects of the water surface like surface tension during model tests, two runs of each test setup have been conducted at choppy conditions while the other two runs have been conducted at calm water conditions (glass-smooth). However, as Table 4.3 suggests, no systematic influence of the water surface on the maximal pressure is noticeable.

In addition, Table 4.3 provides the mean value $\bar{X}$, the standard deviation SD as well as the coefficient of variation CV of the peak pressures $p_{i\,max}$. This data is visualized in 4.12a. This bar chart shows the mean values of the peak pressures $p_{i\,max\,mean}$ including the standard deviation as error bars.

As Figure 4.12a illustrates, the fluctuations were noticeably higher for pressure transducers, that showed sharp peak pressures during impact. This was especially true for pressure transducer P2 for both test setups LC_01 and LC_02. During LC_01 the coefficient of variation was 22.5%, while during LC_02 it was 17.2%. These fluctuations are inherent to slamming problems. As Figure 4.11b shows, the peak of pressure was extremely sharp and could only observed at one sampling frame during measurement. This was still true, although the chosen pressure transducers used a high sampling frequency of 4,800Hz. Thus small variations during measurements (e.g. slight variation of the initial conditions or tim-

Table 4.3.: results of model tests — peak pressure at different pressure transducers

LC_01:

transducer	$p_{i\,max}$ in [kPa] @ run				$\bar{X}_i$	SD_i	CV_i
	No. 1	No. 2	No. 3	No. 4	in [kPa]	in [kPa]	in [%]
P1	432	425	419	474	438	21	4.85
P2	1,221	1,024	935	881	1,015	228	22.50
P3	520	557	594	482	538	42	7.79
P4	977	1,031	982	720	927	122	13.12
calm water	✓	✓	X	X	-	-	-

LC_02:

transducer	$p_{i\,max}$ in [kPa] @ run				$\bar{X}_i$	SD_i	CV_i
	No. 1	No. 2	No. 3	No. 4	in [kPa]	in [kPa]	in [%]
P1	472	467	484	477	475	6	1.26
P2	1,092	1,184	1,093	908	1,069	184	17.22
P3	521	482	704	708	604	103	17.10
P4	747	744	760	838	772	39	4.99
calm water	✓	X	✓	X	-	-	-

Table 4.4.: results of model tests — impulse at different pressure transducers

LC_01:

transducer	$J_{i\,50ms}$ in [kPa·s] @ run				$\bar{X}_i$	SD_i	CV_i
	No. 1	No. 2	No. 3	No. 4	in [kPa·s]	in [kPa·s]	in [%]
P1	9.73	9.91	9.27	9.51	9.61	0.23	2.48
P2	9.84	9.82	10.09	10.84	10.15	0.65	6.40
P3	8.29	8.42	9.01	9.35	8.77	0.43	4.92
P4	8.90	8.86	8.43	8.58	8.69	0.20	2.26
calm water	✓	✓	X	X	-	-	-

LC_02:

transducer	$J_{i\,50ms}$ in [kPa·s] @ run				$\bar{X}_i$	SD_i	CV_i
	No. 1	No. 2	No. 3	No. 4	in [kPa·s]	in [kPa·s]	in [%]
P1	9.75	9.87	9.87	9.74	9.81	0.06	0.63
P2	9.99	9.96	10.03	9.20	9.79	0.45	4.57
P3	8.98	8.69	8.98	8.84	8.87	0.12	1.35
P4	9.51	9.46	9.02	9.25	9.31	0.20	2.10
calm water	✓	X	✓	X	-	-	-

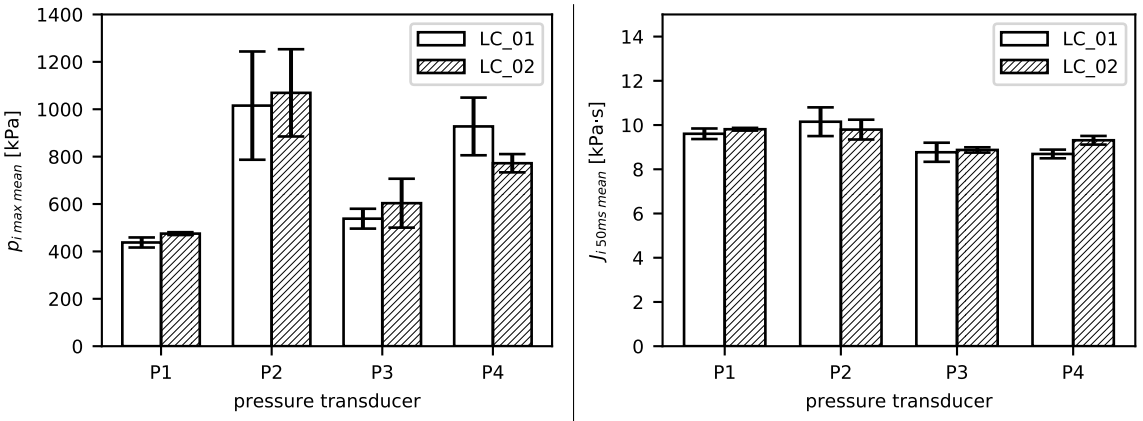

(a) peak pressure

(b) impulse

Figure 4.12.: results of model tests — peak pressure and impulse

ing during measurement) did result in different peak pressures. Based on data provided in [23], a difference of the deadrise angle of 1° (flat bottom vs. deadrise angle of 1°) does result in a difference of the peak pressure of roughly 10% for the impact speeds observed during the model tests of the sideways launching process.

Investigations regarding uncertainties related to the measurement of the resulting peak pressure during slamming experiments can be found in literature. In [58] the systematic error were determined with 1.1% based on a sophisticated test setup designed for best possible repeatability. In [94] it is shown, that uncertainties during slamming experiments with flat bottom structures are significantly higher. Between 6.5% for a rigid and 7.4% for a flexible bottom structure were observed. In [44] it is discussed, that the level of uncertainty rises even further by a factor between two and three for slamming experiments with a high level of asymmetry (high ratio between horizontal and vertical speed like given during the sideways launching process).

Considering these investigations, the fluctuations of the peak pressure observed during model tests are within an expected and feasible range. However, due to the high coefficient of variation of the peak pressure, a parametric study based on these values is not reliable. This is especially true, because during the parametric study only one run of each test setup was conducted.

Therefore, a different approach based on the impulse is used to compare different test setups. In general the impulse J is defined as follows:

$$J = \int F dt \tag{4.32}$$

The force F in equation 4.32 can be substituted with $p \cdot A$, so that the impulse can be calculated using the measured pressure-time-signal as a basis. For comparing the results of the parametric study the pressure-time-signal is integrated per unit area over a time period of 50ms after the peak pressure peak $p_{i\,max}$ occurs. The value for $J_{i\,50ms}$ is calculated using the following equation based on a trapezoidal integration scheme:

$$J_{i\,50ms} = \int_{t_{p_{i\,max}}}^{t_{p_{i\,max}}+50ms} (p_i - p_0)\, dt \tag{4.33}$$

The atmospheric pressure p_0 is subtracted in equation 4.33 as it is constant during all measurements. The resulting impulses are marked in Figure 4.11 as the hatched areas below the pressure-time-signals. As this Figure shows, the impulse $J_{i\,50ms}$ covers the range, where the peak pressures already decayed.

Guedes Soares [37] proposed, that the slamming force acting upon a ship hull is the sum of two different components. The first component is the impact with the water surface, which is described by the harsh peak pressure. As observed during model tests of the sideways launching process, this peak pressure only lasts for a few milliseconds [37]. The second component of the slamming force is defined by the rate of change of the hydrodynamic momentum as the hull enters into the water [37]. Based on calculations carried out for different ship sections, Fonseca *et al.* [35] were able to show that the second component of the slamming force (change of hydrodyanmic momentum) is larger than the first one (peak pressure) for ship sections with a small deadrise angle. Hence the impulse $J_{i\,50ms}$ can be used as an good representation of the loads transferred on the ship hull right after impact with the water surface, as both components of the slamming forces are considered adequately.

As with the peak pressure, the mean value $\bar{X}$, the standard deviation SD as well as the coefficient of variation CV were calculated to assess the fluctuation of the impulse $J_{i\,50ms}$. These values are given in Table 4.4. A visualization of the mean value $J_{i\,50ms\,mean}$ and corresponding standard deviation can be found in Figure 4.12b. The impulse is a lot less sensitive to fluctuations. The coefficient of variation of the impulse is significant lower than of the peak pressure. For P2 the coefficient of variation is reduced from 22.5% to 6.4% for LC_01 and from 17.2% to 4.6% in case of LC_02. This corresponds to a reduction by a factor of approx. 3.5.

Hence, the impulse is more robust to assess the loads on the ship's hull structure after the impact with the water surface and is used to compare the different test setups of the parametric study. Pressure transducer P2 is used as the basis of the parametric study, as P2 is the pressure transducer with the highest impulse in case of LC_01 and LC_02 (compare Figure 4.12b).

In Figure 4.13a the influence of the coefficient of friction μ_{sw} on the resulting impulse is plotted. The influence can be approximated using a linear regression. As expected a lower coefficient of friction and thus higher ship speed does result in a higher impulse. If $\mu_{sw} = 0.25 \cdot \mu_{sw\,0}$, which corresponds to an increase of the translational speed of the ship at impact $v_{yz\,impact}$ of about 8.9% (compare Figure 4.7a), an increase of about 12.9% of $J_{P2\,50\,ms}$ can be observed. If the ship speed $v_{yz\,impact}$ is decreased by 13.7% ($\mu_{sw} = 2.00 \cdot \mu_{sw\,0}$), the impulse $J_{P2\,50\,ms}$ is decreased by 11.7%. The influence of the coefficient of friction on the impulse is moderate. As discussed later on, the rotation around the edge of the pier is more relevant for the resulting loads on the ship hull of the SPV. The tipping of the SPV around the edge of the pier is only slightly influenced by the coefficient of friction. The speed at impact on the ship hull v_{slam} remains nearly constant for all investigated coefficients of friction (compare Figure 4.7b).

The same is true for the influence of the loading condition on the impulse, as Figure 4.13c shows. Like the coefficient of friction, the speed at impact on the ship hull v_{slam} remained nearly constant for all investigated loading conditions (compare Figure 4.7b). Due to a constant v_{slam} only slight variations of the impulse could be observed during model tests.

A more significant influence on the impulse is given by altering the water level h_{wl} or the height of the palls h_p during model tests. This influence is illustrated in Figure 4.13d

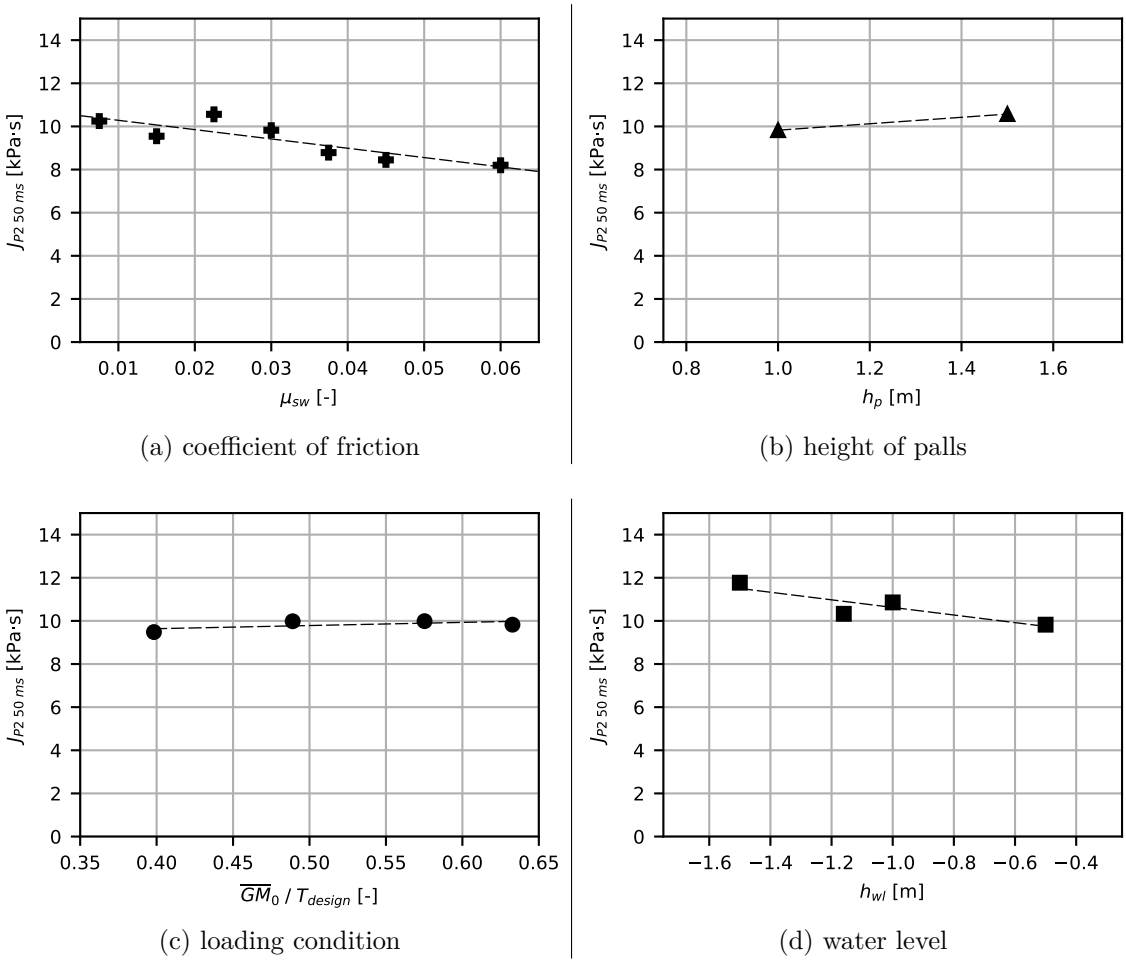

(a) coefficient of friction

(b) height of palls

(c) loading condition

(d) water level

Figure 4.13.: results of model tests — parametric study of impulse (shown for P2)

and 4.13b, respectively. Both parameters are based on the same physical phenomena: the height of the drop during phase 2 — tipping is increased resulting in higher rotational speed at the moment at impact (compare Figure 4.7a). Due to the hull shape of the SPV (sloped bottom), the higher rotational speed did correspond to a higher speed at impact of the ship hull v_{slam}. This effect can be seen in Figure 4.7b.

An increase of the drop height of 0.50m corresponds roughly in an increase of 9.0% of the resulting impulse $J_{P2\,50\,ms}$. As the influence of the drop height can be approximated linearly (see Figure 4.13d), the impulse $J_{P2\,50\,ms}$ is increased 18.1% if the drop height is raised by 1.00m. For comparison: if $\mu_{sw} = 0.25 \cdot \mu_{sw\,0}$, which is quite an significant change of the coefficient of friction for a full-scale sideways launching process (compare [56]), the resulting impulse $J_{P2\,50\,ms}$ is increased by about 12.9%. This level of increase is already achieved by a change of 0.70m of the drop height — either by a change of the height of palls or the water level (tidal effects).

As the investigation of the different parameters varied during model tests emphasizes, the speed at impact on the ship hull v_{slam} has the main influence of the impulse. This relationship between v_{slam} and the impulse $J_{i\,50ms}$ is visualized in Figure 4.14 for all four pressure transducers. Note, that impulse as plotted in Figure 4.14 is corrected for the

angle between the ship hull and the water surface β_{impact} as given in Figure 4.7b. For this purpose the correction factor $[1 - tan\,(2 \cdot \beta_{impact})]^{-1}$ as suggested by Lloyd's Register [61] for bottom slamming is used.

For all four pressure transducers the impulses resulting from a change of the coefficient of friction as well as loading condition fluctuates around the design point. If the drop height was changed by altering the water level or height of palls, a shift of v_{slam} accompanied by an increase of the impulse is clearly visible Figure 4.14. The same is true for the worst case scenarios, were both water level or height of palls were changed simultaneously. For all four pressure transducers the resulting impulse can be approximated using a linear regression. This is in contrast to empirical equations given in rules and regulations of classification societies for the resulting pressure on the bottom in case of slamming, where the resulting loads are described often as a quadratic function of v_{slam}.

However, the slope of the linear regression is not constant for all four pressure transducers. While a slope of 1.12kPa·s^2/m can be observed for P4, a slope of 2.13kPa·s^2/m is given for P1. The differences of the slope for the different pressure transducers can be explained by the fact, that for each different test setup (especially true while changing the drop height) a different part of the ship hull did come into contact with the water surface first. This is also the reason for the small fluctuations of β_{impact} in Figure 4.7b. Due to the form of the ship hull, P1 will come into contact earlier with the water surface with an increasing drop height than e.g. P4. Therefore, a higher increase of the impulse for P1 can be observed.

From a ship design point of view, a precise estimation of the drop height during the sideways launching process is very important, in order to assess the resulting loads on the ship hull accurately. The height of palls h_p are to be minimized, while allowing for sufficient clearance during the sideways launching process as well as for installation of systems during the construction phase (e.g. propulsion shaft and propellers, rudders among others). The water level h_{wl} should be as high as possible. The tidal range at the launch basin is to be used efficiently if applicable, e.g. launching at high tide or even spring tide.

It shall be noted, that the observations regarding the loads on the ships hull are specific for the given shape of the hull of the SPV, which has a sloped bottom, in combination with the geometry of the investigated slipway. This combination did result in a deadrise angle of nearly 0° for every test setup investigated during the model tests. For different ship forms (e.g. plump hull forms like bulker or tankers with no sloped bottom) or a change of the geometry of the slipway, these observations will be different. In such cases the conditions at the impact are different (v_{slam} as well as β_{impact}), so that the influence of the individual parameters (coefficient of friction, loading condition, water level and height of palls) may shift significantly.

4.3.3. Benefits and limitations

The experimental approach based on model tests of the sideways launching process of the SPV does provide a lot of benefits regarding the ship design process. A lot of different setups and configurations were investigated during model tests. The experimental approach is an excellent method for conducting parametric studies for this use case. The influence of different loading conditions of the SPV, height of palls, water level (influence of tidal range) and the coefficient of friction between the palls and the slipway were investigated with the experimental approach.

With a time frame of two days for 26 measurement series of the sideways launching

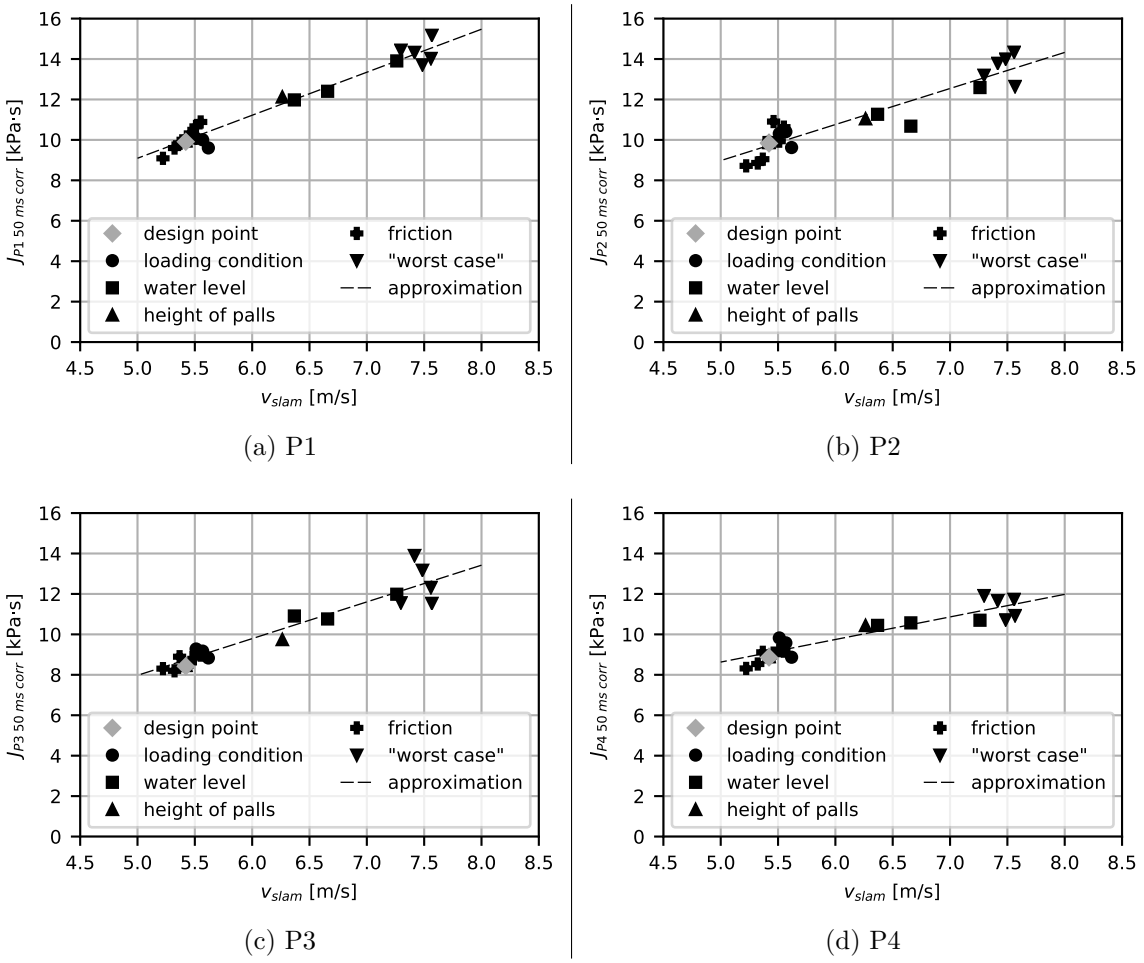

(a) P1 (b) P2

(c) P3 (d) P4

Figure 4.14.: results of model tests — influence of velocity of ship hull on impulse

process, the experimental approach is a really fast way to assess a wide design space. This approach is extremely useful to get an understanding of physical aspects of the problem itself as well as the influence of different parameters on the behavior of the SPV during the sideways launching process. Relevant parameters can be identified well based on the model tests. Regarding the ship motion the vertical position of the COG has the most significant influence on the resulting maximal roll angle, which is one of the most important aspects of the ship motion (compare questions in Figure 1.2). This is visualized in Figure 4.10c. Evaluating the pressure-time-signals based on the impulse resulting during a 50ms time period right after impact, the speed of the ship hull at impact normal to the water surface v_{slam} is the most important parameter. The relationship between v_{slam} and the resulting loads is given in Figure 4.14. The speed v_{slam} is mainly influenced by the height of the palls and the water level inside the launch basin.

Using the experimental approach important design parameters regarding the sideways launching process can not only be qualified, but quantified as well. In order to minimize the maximal roll resulting during the sideways launching process (more safety against capsizing; less openings in direct contact with water), the COG of the SPV should be as low as possible. An exact and detailed weight calculation and estimation of COG_z is crucial during the

design as well as construction phase. Small changes of COG_z can significantly increase the maximal roll angle during the sideways launching process (compare Figure 4.10c; non-linear relationship). To decrease the resulting hull structural loads during the sideways launching process, the height of the drop around the edge of the pier is to be minimized. That means, the height of the palls should be as low as possible while allowing for sufficient clearance between the ship hull and pier during the sideways launching process. In addition, the water level inside the launch basin should be as high as possible. The tidal range should be used to actively reduce the loads resulting on the hull of the SPV (launch at high tide or even spring tide). The correlation between the height of the drop around the pier and the resulting hull structural loads can be made using the relationships provided in Figure 4.14.

Besides a good general understanding of the different parameters important for the sideways launching process, the results obtained from the experimental approach are an excellent basis for verification purposes. The proposed simulation-based approach using FSI based on the ALE approach is thoroughly verified using the data measured and obtained during the the model tests.

There are drawbacks and limitations regarding the use of the experimental approach as well. First, the experimental approach is expensive. For successfully conducting the model tests, a lot of effort for preparation was necessary (developing an adequate test setup, derivation of test matrix, construction of ship model and test setup among others). As the model tests cannot be conducted at the shipyard itself, but rather at a ship model basin, the planning has to be done in advance. Changes to the ship design or the sideways launching process, which are to be checked additionally after the initial model tests, cannot be assessed ad hoc. Further investigations and model tests are depending on the time slots available at the ship model basin.

In addition, the experimental approach is only feasible starting at a certain of the ship design process, mainly during the basic design phase. Although important parameters of the ship design like the loading condition could be quickly varied during the model tests, the shape of the hull has to be close the final design. Alterations of the ship hull (e.g. main dimensioning, changes to the lines plan) cannot be realized without much effort. Eventually a complete new ship model would be necessary, if the changes of ship hull form are too drastic.

Lastly, the loads measured during the model tests in the form of pressure-time-signals do not allow for a direct assessment of the resulting hull structural loads of the SPV. Additional simulations are to be carried out. However, the data obtained from the experimental approach can be used within the context of the simulation-based approach without FSI. Within this work a load model based on the results obtained from the model tests is proposed, which allows for the assessment of the hull structural loads resulting right after the impact with the water surface using simulations without FSI. The obtained results are discussed and compared to the results based on the simulation-based approach using FSI later on in this work.

5. Simulation-based approach without fluid-structure interaction

Besides rule-based, analytical or experimental approaches, simulation-based approaches are common during the ship design process. Within this section the most common simulation-based approach used for the design of a ship's hull structure based on FEM is investigated. These simulations are not utilizing any form of FSI. Therefore, external load models accounting for the loads resulting on the hull of the SPV during the sideways launching process have to be derived and applied to a FEM model of the hull structure. After presenting the according FEM models of the hull structure of the SPV, different approaches for load modelling are proposed. Lastly, the results obtained with the simulation-based approach without FSI in the form of the resulting hull structural loads at highly loaded areas of the hull structure of the SPV are discussed.

5.1. Overview of highly loaded areas

Based on simulations without FSI as well as with FSI different areas of the hull structure of the SPV could be identified, which are highly loaded during the sideways launching process. This includes parts of the shell plating, web frames of the shell, floor plating (especially around manholes / inspection holes) as well as plating of transversal bulkheads. The highly loaded areas are limited to PS around amidships ($0.35 < x/L < 0.65$).

For each of these for highly loaded areas the resulting hull structural loads for one representative shell element are evaluated and assessed. The location of the corresponding elements and their element coordinate system are illustrated in Figure 5.1. All resulting hull structural loads are normalized with their corresponding permitted limit values σ_{perm} or τ_{perm}. Besides the resulting stresses the bending deformation of one highly loaded shell panels is assessed. A complete overview of the hull structural loads for the chosen elements of the hull structure is provided in Appendix A.12.

5.2. Modelling of hull structure

For the investigation of the resulting hull structural loads during the sideways launching process, the following FEM models of the hull structure of the SPV were used:

- global FEM model
- detailed FEM model of highly loaded areas
- combined FEM model (combination of global and detailed FEM model)

A description of each FEM model is provided below. A comparison of the general properties and size of each FEM model is given in Table 5.1. All values in Table 5.1 are rounded to the nearest hundred.

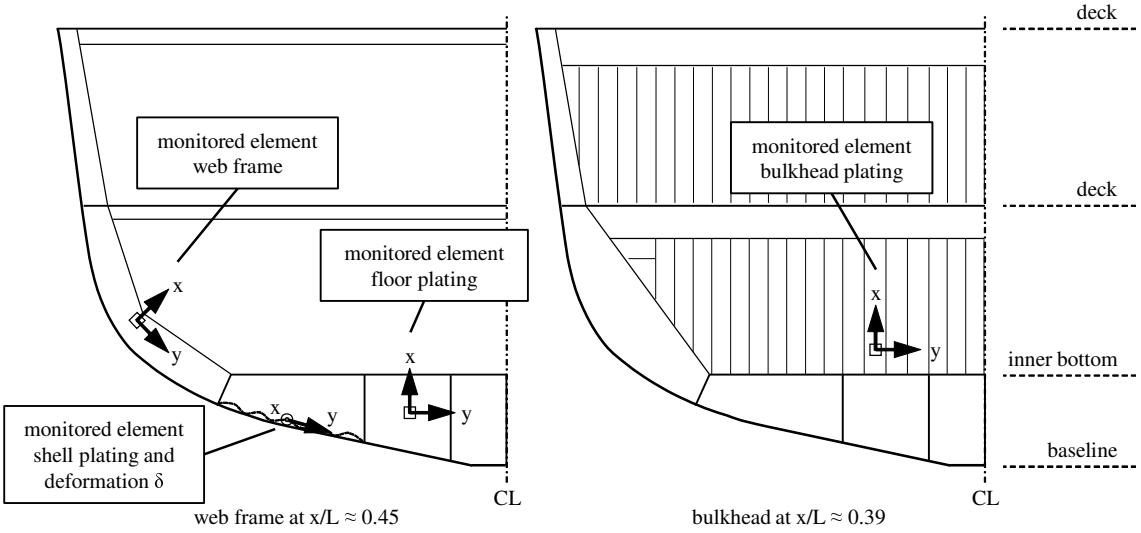

Figure 5.1.: highly loaded areas of the hull structure of the SPV

Table 5.1.: properties of different FEM models of the SPV

parameter	unit	global	detailed	combined
shell elements	[-]	197,600	2,236,800	2,452,100
beam elements	[-]	110,900	155,900	248,000
nodes	[-]	203,900	1,914,300	2,386,500

Modelling approach

The different FEM models of the SPV are based on a 3D computer-aided design (CAD) model of the hull structure inside the CAD software AVEVA Marine. An interface called *AVEVA Hull Finite Element Modeler* in AVEVA Marine is used to idealize and prepare the CAD model for FEM simulations. The functionality of this interface is described by Bohm *et al.* [14]. Besides [14], the use of this interface within early phases of the ship design process is discussed by Bayatfar *et al.* [11] or Ulbertus and Schöttelndreyer [98]. Final pre-processing and meshing is conducted within the software Altair HyperMesh.

The different FEM models are modelled in accordance to guidelines and recommendations as provided in *Class Guideline: Finite element analysis (DNV-CG-0127)* [26] by DNV. Hence, only differences of the corresponding FEM models compared to [26] are described below. The different element types used for the FEM models of the hull structure inside LS-DYNA are provided in Appendix A.5.

Global FEM model

A global FEM model of the hull structure of the SPV was set up, that considers all primary members of the hull structure (shell, bottom structure, decks, bulkheads, walls, web frames, superstructure among others). In contrast to conventional global FEM models of commercial ships, the level of detail of the global FEM model of the SPV is equal to the recommendations for partial ship structural analysis according to [26]. An average element

between size 400x400mm and 300x300mm is used. This element size is a good comprise between assessing the structural dynamic behavior of the hull structure on a global level and the local behavior of structural components like decks or walls.

Figure A.10 provides a view inside the global FEM model. Plates / panels are modelled using shell elements (compare grey elements in A.10). The same is true for the web of frames and girders. Stiffeners, flanges and pillars are modelled using beam elements with according offsets to account for the corresponding moment of inertia (compare blue elements in A.10). Openings smaller than the average element size are considered by reducing the plate thicknesses in the area of openings according to [26].

Detailed FEM model of highly loaded area

Different parts of the hull structure are highly loaded during the sideways launching process. As the model tests showed, the resulting loads at impact are comparable to slamming events. These impact loads are especially critical for the shell of the hull structure and its supporting structural members (web frames, bottom structure and bulkheads). To assess the resulting hull structural loads accordingly, a detailed FEM model of these areas was set up. The extent of the detailed FEM model is visualized in Figure 5.2. A look inside the detailed FEM model is given in Figure A.11.

The detailed FEM model is modelled in accordance to the requirements for local structure strength analysis as defined in [26]. A fine mesh size of 50x50mm is used. All structural members are modelled as shell elements. Only the bulbs of the bulbous profiles are modelled with beam elements (compare Figure A.11).

The chosen mesh size enables a detailed analysis of plating subjected to lateral loads and the resulting bending deformation. This is especially important for the shell plating of the hull structure subjected to the high impact loads. In addition, plates and stiffeners subjected to compression and shear loads are able to buckle during the dynamic simulations (e.g. floor plating or bulkheads). Another aspect is the consideration of the stiffness as given by the connection of stiffeners to transverse structural members. This is accounted for by using solely shell elements within the detailed FEM model (compare Figure A.11). The stiffness of such connections is especially relevant for the longitudinal stiffeners of the shell plating.

Combined FEM model

In the combined FEM model the detailed FEM model of the highly loaded areas is integrated into the global FEM model of the hull structure. This combination is illustrated in Figure 5.2. Within the combined FEM model the stiffness as well as the mass and inertia of the complete hull structure is considered during simulations. As discussed later, this is important for the proposed simulation-based approach using FSI.

For combining both FEM models, the area of the global FEM model adjacent to the detailed FEM model is gradually refined to fit the mesh of the detailed FEM model. The area of transition is shown in Figure A.12. The models are connected by merging the coinciding nodes at the cutting edges. The longitudinal stiffeners of the global FEM model (beam elements) are connected to the longitudinal stiffeners of the detailed FEM model (shell elements) by overlapping the beam elements with the shell elements. This enables a transfer of bending moments of the stiffeners.

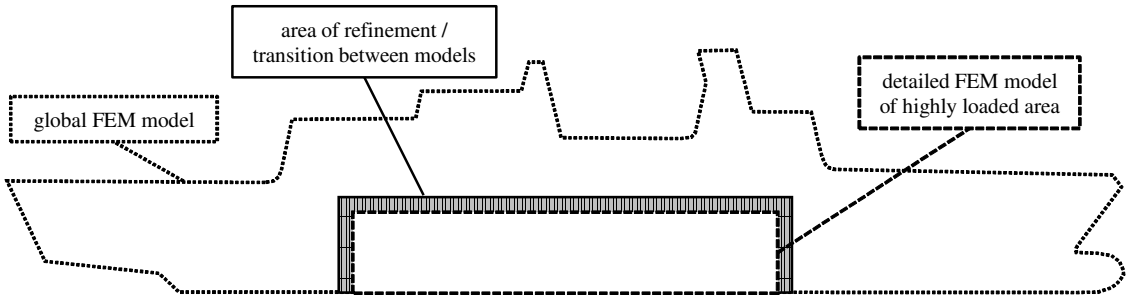

Figure 5.2.: overview of combined FEM model of the SPV

Boundary conditions

The BC used for the hull structure of the SPV are given in Appendix A.5. Within the simulation-based approach without FSI the BC for the global and combined FEM model as given in Figure A.13 are used, while for the detailed FEM model BC_01 and BC_02 as shown in Figure A.14 and A.15 are used.

Weight distribution

Masses modelled inside the FEM models of the SPV are split into different parts. As the hull structure is modelled using shell and beam elements, its mass is considered accordingly. Bigger components and systems installed during the sideways launching process of the SPV are modelled explicitly with `*CONSTRAINED_NODAL_RIGID_BODY_INERTIA` in LS-DYNA. Examples are the main engines, gear box, gensets or propeller. Paint, insulation or flooring material, which will vibrate together with the hull structure, are considered as homogenous surface masses. For decks an additional mass of 40kg/m^2 is used, whereas for walls and bulkheads 25kg/m^2 is considered. Lastly the difference between the modelled mass and the mass given by a loading condition of the SPV is considered. This difference is distributed on stiffer nodes of the hulls structure like crossing points of walls and decks, so that the local structural dynamic behavior of the hull structure is not altered.

By modelling the masses in the described way, the loading condition (weight, position of COG as well as moments of inertia) are considered accordingly inside the different FEM models. The modelling of mass is done sequentially for each web frame of the SPV with the use of according macros. An in-depth description of this modelling approach is provided in the work by Burchard [16].

Two different loading conditions are investigated within the simulation-based approaches: LC LAUNCH and LC LSW. The loading condition LC LAUNCH resembles the weight distribution of the SPV as planned during the sideways launching process, while LC LSW is the weight distribution of the fully equipped ship (light ship weight). An overview of both loading conditions is given in Appendix A.5. Figure A.9 shows the distribution of the weight along the x-axis of the SPV.

Added masses

For the simulations without FSI the added mass around the hull structure of the SPV are to be considered separately. In [53] approaches for considering added masses around

vibrating hull structures are provided. In the event of the sideways launching process, a lateral bending deformation of the different plate fields of the shell plating is to be expected. This mode of deformation is comparable to the vibration of multi-span plates as given in [53], where the plate fields oscillate between the stiffeners of the shell while the longitudinal stiffeners remain rigid. The added mass λ_{plate} for that mode of deformation can be calculated based on the following equation [53]:

$$\lambda_{plate} = \rho_w \cdot a_{panel} \cdot \mu_{panel} \left(\frac{a_{panel}}{b_{panel}} \ , \ n_{panel} \right) \tag{5.1}$$

In equation 5.1 a_{panel} is the distance between the stiffeners, while b_{panel} is the length of the panel. The coefficient μ_{plate} is function of the aspect ratio of the panel (a_{panel} / b_{panel}) and number of plate fields n_{plate}. Values for μ_{panel} can be found in [53] for different BC (symmetric vs antisymmetric eigenmode; freely supported vs clamped edges). For the SPV μ_{plate} is determined for freely supported edges and an antisymmetric form of oscillations, as the symmetric form of oscillations is only possible for plates with an aspect ratio a_{plate} / $l_{plate} \geq 2.5$ [53].

For a typical panel of the shell plating located at the inclined bottom structure of the SPV, an added mass of $\lambda_{plate} = 168\text{kg/m}^2$ is obtained using equation 5.1. The ratio of the added mass to the weight of the shell plating is about 3.3 for a typical panel. The added masses within the simulation-based approach without FSI are considered as non-structural mass per unit area within the definition of the different sections of the shell elements inside LS-DYNA.

5.3. Load models

Two different load models to account for the loads resulting on the hull of the SPV during the sideways launching process are proposed. One load model is based on rules and regulations by classification societies, while the other is based on the results obtained from the experimental approach. Lastly, the option of a load model based on CFD simulations is discussed.

5.3.1. Rule-based approach

As discussed in section 4.1, different rules and regulations of classification societies provide equations for assessing loads acting upon a ship's hull structure during slamming events. In [61] an approach for impact loads on bottom plating in case of slamming events is given, which allows for a dynamic load model (compare Appendix A.2). The pressure p_{bi} in [kN/m^2] can be calculated as follows [61]:

$$p_{bi} = 0.5 \cdot k_{sl} \cdot v_{slam}^2 \tag{5.2}$$

The factor k_{sl} in equation 5.2 is a hull form shape coefficient [61]:

$$k_{sl} = \begin{cases} 28 \cdot [1 - tan\,(2 \cdot \beta_{impact})] & , \ \beta_{impact} < 10° \\ \\ \frac{\pi}{tan(\beta_{impact})} & , \ \beta_{impact} \geq 10° \end{cases} \tag{5.3}$$

According to [61] it can be assumed, that the pressure-time signal of such an slamming event can be represented by a triangular pulse load. The time period for the rise and fall of the impulse t_r can be calculated according to the following equation [61]:

$$t_r = \frac{1}{4 \cdot \sqrt{p_{bi}}} \tag{5.4}$$

Based on this approach provided in [61] the following rule-based load model is proposed, which describes the pressure p_{rb} on the shell plating of the hull structure of the SPV during the sideways launching process as the following function of time:

$$p_{rb} = \begin{cases} 0 & , \ t < t_{impact} \\ p_{bi} \cdot \frac{t - t_{impact}}{t_r} & , \ t_{impact} \leq t < (t_{impact} + t_r) \\ p_{bi} - (p_{bi} - p_{dyn}) \cdot \frac{t - (t_{impact} + t_r)}{t_r} & , \ (t_{impact} + t_r) \leq t < (t_{impact} + 2 \cdot t_r) \\ p_{dyn} & , \ t \geq (t_{impact} + 2 \cdot t_r) \end{cases} \tag{5.5}$$

A visualization of this rule-based load model is given in Figure 5.3. In equation 5.5 the pressure p_{rb} is split into four parts. If no contact with the water surface is given ($t < t_{impact}$), the resulting loads are zero. As soon as the shell plating is in contact with the water surface, the pressure rises linear to p_{bi} within the time period of t_r. After the peak is reached at $t = t_{impact} + t_r$, the pressure drops linear within the time period t_r to the hydrodynamic pressure p_{dyn} acting upon shell plating. As only a very short time period is assessed using this load model, the resulting hydrostatic pressure is neglected, as $p_{dyn} >> p_{stat}$ at the moment of impact. The hydrodyanmic pressure p_{dyn} is calculated as follows:

$$p_{dyn} = \frac{\rho_w}{2} \cdot v_{slam}^2 \tag{5.6}$$

A comparison of this rule-based load model with a pressure-time-signal obtained from model tests is given in Figure 5.3b. The rule-based load model does result in lower loads compared to model tests. The impulse $J_{50\,ms}$ transferred in 50ms into the ship's hull structure is roughly 54% of the impulse as measured during model tests at pressure transducer P2 (pressure transducer with first contact to the water surface). The impulse of the rule-based load model is 5.51kPa·s (see Figure 5.3a), whereas the mean impulse at P2 for case LC_01 is 10.15kPa·s (compare Table 4.4).

For calculating the pressure p_{rb} according to equation 5.5 the following input data is necessary: t_{impact}, v_{slam} and β_{impact}. These three parameters are calculated using the analytical approach. Due to the shape of the hull of the SPV (no parallel midship section), these information are needed for each shell element of the shell plating separately, as different parts of the hull structure will get in contact with the water surface at a different time.

For the implementation of the rule-based load model in LS-DYNA different approaches are possible [59]. One way is developing a function / model inside the loading subroutine via `*USER_LOADING` and compiling a new version of LS-DYNA using a Fortran compiler. A brief introduction of how to set up a subroutine via `*USER_LOADING` is given by Adoum and Lapoujade [2]. This approach is quite complex as for implementing `*USER_LOADING` a

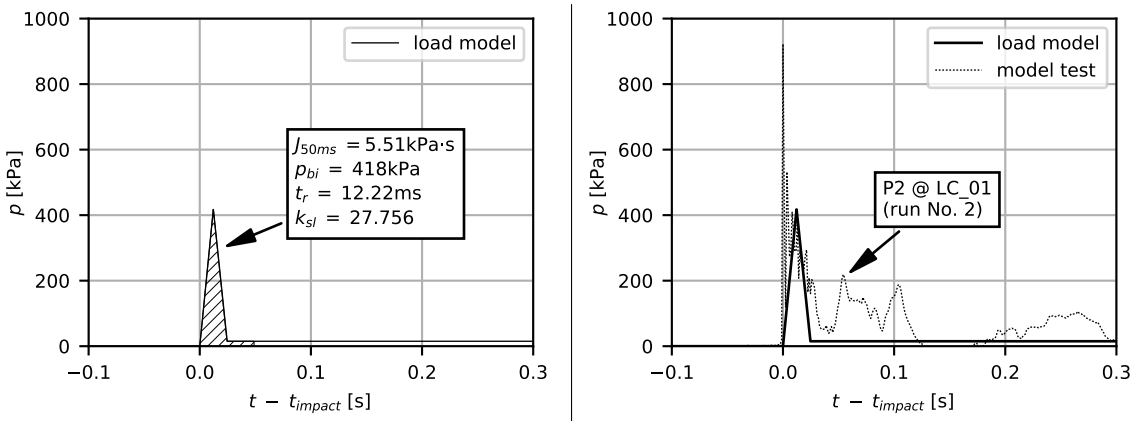

(a) exemplary pressure-time-signal

(b) comparison with model tests

Figure 5.3.: rule-based load model

deep understanding of the internal variables of LS-DYNA and compiling of a new version of LS-DYNA are necessary. Therefore, this approach will not be used, as the load model will be tied to a specific executable and version of LS-DYNA. Changes made to the load model within `*USER_LOADING` will make re-compiling of the solver necessary. Therefore, the alternative way of `*DEFINE_FUNCTION` together with `*LOAD_SEGMENT_SET` is used to implement the rule-base load model as defined in equation 5.5.

This is realized by splitting the shell plating of the ship's hull structure into different segments. Each segments consists of the shell elements between longitudinal stiffeners / girders located on the shell. For each of these segments a separate function is defined using `*DEFINE_FUNCTION`. For each segment t_{impact}, v_{slam} and β_{impact} are calculated for the moment where $z_i \leq z_{wl}$ is given at the centre of each segment. These values are then used as the basis, to set up the load models as described by equation 5.5. This procedure is done for the shell plating (PS) of the SPV from centreline to one deck above the inner bottom at the highly loaded area between $0.35 < x/L < 0.65$. This results in approx. 670 different functions to be set up for the simulation-based approach without FSI. This implementation yields in a high preprocessing effort, as for different conditions of the sideways launching process all functions are to be set up again / updated.

An exemplary implementation of this load model for an segment of the shell can be found in Appendix A.6. The definition of the function in `*DEFINE_FUNCTION` is based on the programming language C++. A combination of VBA and Python macros is used to set up the functions based on the results of the analytical approach.

5.3.2. Experimental approach

Another approach is the development of a load model based on the results of the experimental approach as presented in section 4.3.2. The development of a load model based on model tests / experiments is a possible approach according to classification societies [3], [29]. The requirements are, that a sufficient amount of data is collected during experiments. Different conditions and configurations are to be checked and pressure-time-signals are to be measured at different locations on the model. These requirements are fulfilled for the experimental approach as presented in section 4.3.

For the use of a load model derived from the experimental approach within the context of the ship design process, an universal and adaptable load model is preferable. Therefore, a generalization of the measured pressure-time signals is conducted. The pressure-time-signals observed during model tests showed a harsh peak pressure followed by a quick decay towards the dynamic pressure. The same behavior can be observed in other slamming experiments as well, e.g in [43], [58], [94].

Such a behavior can be approximated by the use of an exponential function. The following load model is proposed, to assess the pressure p_{mt} resulting on the hull of the SPV based on the results of the model tests:

$$p_{mt} = \begin{cases} 0 & , \; t < t_{impact} \\ k_v \cdot k_\beta \cdot p_{mt\,max} \cdot e^{-k_{mt} \cdot (t - t_{impact})} & , \; t_{impact} \leq t < (t_{impact} + t_{r\,mt}) \\ p_{dyn} & , \; t \geq (t_{impact} + t_{r\,mt}) \end{cases} \tag{5.7}$$

A visualization of this load model is provided in Figure 5.4. In equation 5.7 the pressure p_{mt} resulting on the ship hull is described in three stages. In the first stage, no contact with the water is given ($p_{mt} = 0$). After the impact of the ship hull with the water surface at $t = t_{impact}$ the pressure rises instantly to the maximal peak pressure $p_{mt\,max}$. The peak pressure is obtained from model tests as given in Table 4.3 corrected by p_0. Afterwards, a decay of the pressure is described by the exponential function, where the decaying behavior is defined by the decay constant k_{mt}. The time of the decay to the dynamic pressure p_{dyn} (third phase) is defined by the expression $t_{r\,mt}$. Values for k_{mt} and $t_{r\,mt}$ in equation 5.7 can be derived by using the following conditions and solving the corresponding system of equations for those two parameters:

- the impulse resulting on the ship hull $J_{i\,50ms}$ as used for the assessment of the model tests in section 4.3.2 is equal for the load model and model tests
- continuity between phase two and three of the proposed load model as given by $p_{mt} = p_{dyn}$ at $t = t_{impact} + t_{r\,mt}$

In Figure 5.4a values for equation 5.7 obtained for pressure transducer P2 at test setup LC_01 are provided. These values are used, as P2 does result in the highest impulse for the design point of the model tests (compare Table 4.4). A comparison of the proposed load model with measured pressure-time-signal is given in Figure 5.4b. The proposed load model is able to fit the measured data well.

As discussed in section 4.3.2, the resulting impulse $J_{i\,50ms}$ is a function of the speed at the ship hull at the moment of impact v_{slam}. As illustrated in Figure 4.14, the impulse can be described as a function of v_{slam} by the means of a linear approximation. To account for this effect inside the proposed load model, the factor k_v is introduced in equation 5.7. Based on the slope of the linear approximation as observed for pressure transducer P2 as given in Figure 4.14b, the factor k_v can be calculated as follows:

$$k_v = 1 + 0.1784 \cdot (v_{slam} - 5.42) \tag{5.8}$$

Equation 5.8 scales the resulting pressure p_{mt} according to the slope as approximated in Figure 4.14b. Values for v_{slam} are to be input in [m/s] in equation 5.8.

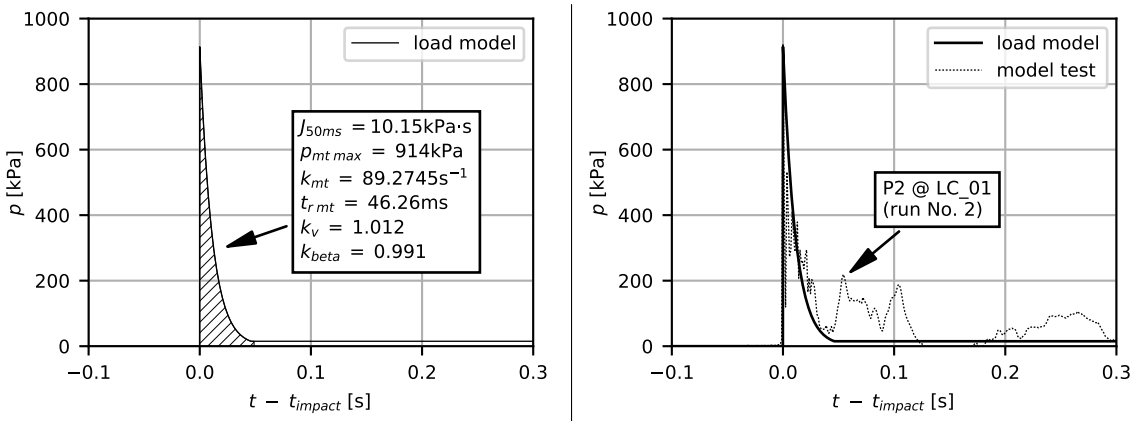

(a) exemplary pressure-time-signal

(b) comparison with model tests

Figure 5.4.: load model based on experimental approach

In addition to the speed at impact, the deadrise angle β_{impact} does have a significant influence on the resulting loads during a slamming event [23]. As Figure 4.7b shows, the deadrise angle was approx. zero during all model tests. Due to this, no correction of the load model based on the conducted model tests is possible. Therefore, the influence of the deadrise angle is accounted for by the approach as provided in [61]. Based on equation 5.3 the factor k_β can be formulated as follows:

$$k_\beta = \begin{cases} 1 - tan\left(2 \cdot \beta_{impact}\right) & for\ \beta_{impact} < 10° \\ \\ \frac{\pi}{28 \cdot tan(\beta_{impact})} & for\ \beta_{impact} \geq 10° \end{cases} \tag{5.9}$$

Equation 5.9 results in the same scaling of pressure as function of the deadrise angle as used for the rule-based load model in section 5.3.1.

The implementation of the load model based on the experimental approach is done in LS-DYNA analogously to the rule-based load model (see section 5.3.1). An exemplary implementation of this load model can be found in Appendix A.7.

5.3.3. Computational fluid dynamics

A third option for the simulations without FSI is a load model based on CFD simulations. Such an approach is pretty common in naval architecture for determining loads during slamming events [1], [104]. It is further referenced in rules and regulations, e.g. in [3], [18], [25]. As already discussed in section 2.2, the sideways launching process of a ship is from a physical point of view pretty similar to the launch of a FFLB. One example for a simulation-based approach without FSI is proposed in [20], where CFD and FEM simulations were combined in order to assess the hull structural loads resulting inside a FFLB during its launch and water entry phase. This approach is a one-way coupling from CFD to FEM without actual FSI, meaning that the resulting pressure of the CFD simulations is mapped for defined time steps onto the mesh of the FEM model of the FFLB. As one-way coupling together with quasi-static FEM simulations was used, no effects of hydro-elasticity were considered during simulations in [20].

As discussed in [18], quasi-static approaches for water entry problems are problematic. Especially in cases where effects of hydro-elasticity are of importance — which is true for the sideways launching process of the SPV — ($\beta_{impact} \approx 0°$), loads can be severely overestimated [18]. Therefore, an approach similar as proposed in [20] is not further investigated for the sideways launching process of the SPV, as no clear benefits compared to the load model based on the experimental approach or the simulation-based approach with FSI as proposed within this work are given.

5.4. Results

Within the following section, the results of the simulation-based approach without FSI are discussed. The resulting hull structural loads inside the SPV are assessed and the underlying load mechanism is investigated. Additionally, the influence of the different load models as well as FEM models of the SPV are discussed.

5.4.1. Ship motion

The load models proposed for the simulation-based approach without FSI do not allow for an assessment of the ship motion during the sideways launching process. For assessing the ship motion, other approaches have to be used additionally. Possible are an experimental approach as presented in section 4.3 or the use of CFD simulations.

5.4.2. Hull structural loads

Resulting load mechanism

The dominant load mechanism observed with the simulation-based approach without FSI are hull structural loads resulting from the impact with the water surface. The principle of this load mechanism is illustrated in Figure 5.5. The loads resulting from this load mechanism are acting upon the shell of the hull structure and are transferred into its supporting structure (web frames and bottom structure). The resulting hull structural loads for highly loaded areas are shown and explained in Figure 5.6.

As the model tests showed, a deadrise angle of nearly 0° between could be observed for all test setups (compare Figure 4.7b). This configuration leads to very high peak pressures right after impact with the water surface. Lateral bending deformation of the shell plating with high bending stresses inside the shell plating can be observed, as shown in Figure 5.6a. At very highly loaded areas (first contact with the water surface with highest speed at impact), parts of the shell plating undergo minor plastic bending deformation (compare Figure 5.6b). For the sideways launching process of the SPV such a plastic bending deformation of the shell plating is unacceptable.

Besides the shell plating, the structural members supporting the shell are highly loaded. Inside the floor plating moderate compression stresses right after impact with the water surface are observed, as presented in Figure 5.6d. Only in areas with manholes / inspection holes higher, localized stress concentrations can be observed due to notch effects. The web frames supporting the shell are higher loaded. Inside the corner of the web frames high compression stresses are present, as shown in Figure 5.6c. The plating of the web

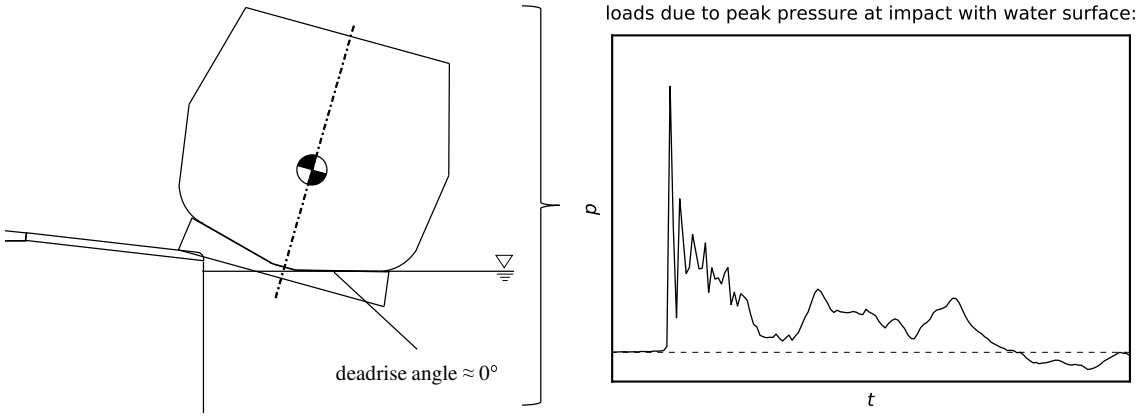

Figure 5.5.: load mechanism 1 — impact with water surface

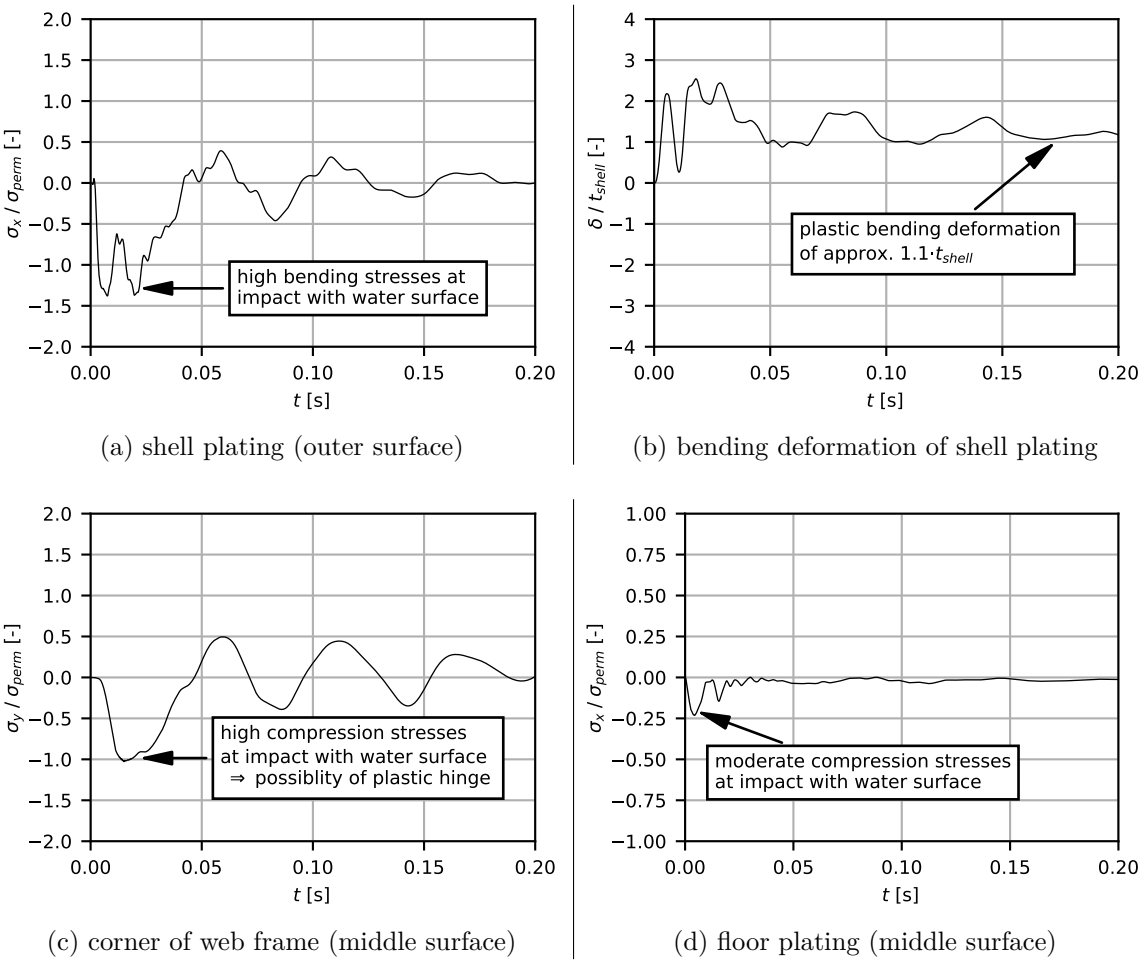

(a) shell plating (outer surface)

(b) bending deformation of shell plating

(c) corner of web frame (middle surface)

(d) floor plating (middle surface)

Figure 5.6.: resulting hull structural loads — load mechanism 01 (load model based on model tests + combined FEM model of SPV + LC LAUNCH)

frames could buckle under these compression loads, resulting in a loss of the stability of the corresponding web frame and the formation of a plastic hinge.

These high hull structural loads resulting from this load mechanism are limited to the area of first contact of the hull of the SPV. Potential damages or failure of the hull structure would be limited locally to individual structural components. Potential failure modes are permanent plastic deformation of the shell plating due to lateral bending and / or buckling of structural members supporting the shell such as the bottom structure and web frames due to the resulting compression loads.

The loads during the impact of the SPV with the water surface are mainly influenced by the speed of the hull at the moment of impact v_{slam}, as the model tests showed (compare Figure 4.14). The main parameter influencing the resulting impulse on the ship hull is the height of the drop around the edge of the pier. A change of the drop height can either be achieved by altering the height of the palls or a lower water level inside the launch basin (low tide). As a consequence regarding the sideways launching process of the SPV, the height of the drop around the edge of the pier should be as low as possible to actively reduce the hull structural loads resulting from this load mechanism. The height of the palls should be as low as possible while allowing for a sufficient clearance between the edge of the pier and the SPV. The tidal range should be used to the full extent (high tide; preferably spring tide). The influence of the drop height is investigated later in this work based on the proposed simulation-based approach using FSI.

Influence of load models

Simulations without FSI are carried out with the both the rule-based load model as well as the load model derived from the experimental approach. The influence and differences of the two load models on the hull structural loads are investigated using the combined FEM model of the SPV. A comparison between the two load models of the resulting hull structural loads for the highly loaded areas is provided in Figure A.36.

Besides the shape of the pressure-time-signal (triangular vs. exponential function), the main difference between the rule-based load model and load model based on the experimental approach, is the impulse transferred into the ship hull after the impact with the water surface. Comparing Figure 5.3a and Figure 5.4a, the impulse $J_{i\,50ms}$ is 84% higher based on the experimental approach. This is almost a factor of two between both load models.

These lower loads in the rule-based load model are reflected in the resulting hull structural loads as Figure 5.7 shows. The bending stresses resulting inside the shell plating are about four times lower for the rule-based load model compared to the experimental approach, as Figure 5.7a shows. The same factor can be observed for the corner of the web frame (compare Figure 5.7b). Using the rule-based load model no plastic bending deformation of the shell plating as shown in Figure 5.6b can be observed. No part of the hull structure is highly or even critically loaded while using the rule-based load model.

The factor of nearly two for the impulse does not translate proportionately into the resulting hull structural loads. One explanation for this difference is the different form of the pressure-time signals. The pressure-time signal derived from the experimental approach shows a much steeper form compared to the model as given by rules of LR [61] (compare Figure 5.3a and 5.4a). The harsher pressure-time signal does result in more severe hull structural loads.

If the design of the hull structure of the SPV against the hull structural loads resulting

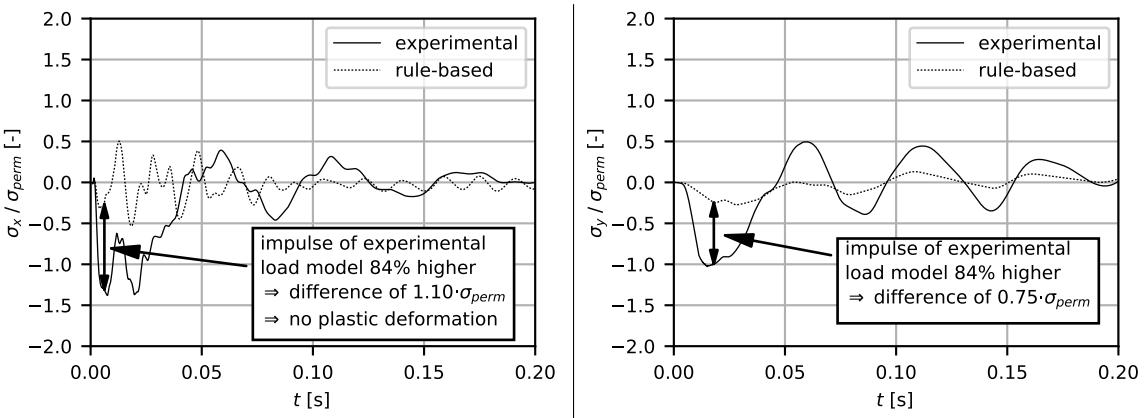

(a) shell plating (outer surface)

(b) corner of web frame (middle surface)

Figure 5.7.: resulting hull structural loads — influence of different load models (combined FEM model of SPV + LC LAUNCH)

from the sideways launching process were based solely on simulations without FSI, the application of the rule-based load model is not recommended. There is the possibility of severely underestimating the hull structural loads including subsequent damages of the hull structure of the SPV during the sideways launching process.

Influence of FEM models of hull structure

The influence of the FEM models of the SPV on the hull structural loads within the context of the simulation-based approach without FSI is investigated using the load model based on the experimental approach. A comparison of the resulting hull structural loads for the highly loaded areas is provided in Figure A.37. An overview of the different BC used for the FEM models of the SPV is given in Appendix A.5.

The global FEM model of the SPV is not able to account geometrically for the bending deformation of the shell plating, as only one shell element is used over the width of an average panel of the shell plating. Therefore, the resulting stresses in x-direction are underestimated by roughly a factor of three compared to the detailed or combined FEM model. This difference is visualized in Figure 5.8a. The same behavior can be observed for the supporting members of the shell. While the resulting loads inside the floor plating are quite comparable (see Figure A.37d), for the web frame as well as the bulkhead a factor of approx. two between the global and detailed FEM model of the hull structure can be observed. This difference is shown for the web frame in Figure 5.8b.

There are two reasons for this difference. One one hand, the global FEM model is not able to account sufficiently for the stress concentrations around hot spots like corners of the web frames (notch effect). The detailed FEM model can cover these effects due to the finer mesh size. On the other hand, the shell plating plus supporting members (floor plating and web frames) of the global FEM model are stiffer compared to the detailed FEM model of the highly loaded area. As the shell of the hull structure is able to undergo a bigger bending deformation in the detailed FEM model, a shift of the the hull structural loads can be observed. Inside the global FEM model the loads are distributed more evenly among all supporting members of the shell, while in the detailed FEM model a transfer of the

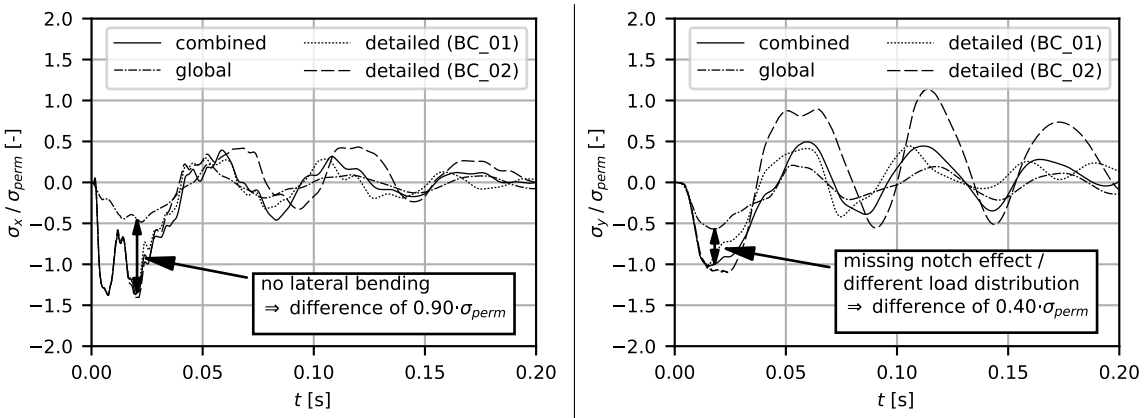

(a) shell plating (outer surface)

(b) corner of web frame (middle surface)

Figure 5.8.: resulting hull structural loads — influence of different FEM models of SPV (load model based on model tests + LC LAUNCH)

resulting loads towards the bulkheads can be observed. Due to the higher stiffness of the bulkheads compared to rest of supporting members of shell, the bulkheads are subjected to higher loads inside the detailed FEM model.

As the hull structural loads resulting during the sideways launching are underestimated by a factor between two and three compared to the detailed FEM model, the global FEM model is not a suitable choice for the hull structural design in the event of the sideways launching process. As the resulting stresses are underestimated, damages to the hull structure during the sideways launching process could potentially occur if only a global FEM model is used.

The detailed FEM model as well as the combined FEM model of the hull structure show pretty similar results, especially at the moment of impact with the water surface. Both models are a valid choice for the simulation-based approach without FSI, as both models are able to capture and assess relevant details and components of the hull structure. As Figure A.37 shows, the influence of the different BC on the resulting hull structural loads using the detailed FEM model is negligible.

5.5. Benefits and limitations

Benefits of the simulation-based approach without FSI are the lower modelling as well as computational effort compared to the proposed simulation-based approach using FSI. The resulting hull structural loads obtained with a detailed FEM model of the highly loaded areas of the hull structure are very similar compared to the combined FEM model of the SPV, which considers the complete hull structure (compare Figure 5.2). Therefore, the model inside the simulation-based approach without FSI can be limited to the area of interest saving necessary modelling effort. In addition, the computational effort is lower compared to the simulations using the ALE approach by at least a factor of two. The necessary computational effort of both simulation-based approaches is discussed in more detail later within this work.

One of the major difficulties of the simulation-based approach without FSI is assessing the resulting loads on the ship hull as present during the sideways launching process. An

adequate load model has to be derived. Two load models are proposed: a rule-based load model and a load model based on an experimental approach (model tests). As a comparison of the resulting hull structural loads show, the results of these two load models differ significantly. The impulse transferred into the hull structure of the SPV is 84% higher using the load model based on the experimental approach. This difference results in approx. four times higher hull structural loads inside the shell plating and its supporting structure like the web frames (compare Figure 5.7). If solely the rule-based load model were used during the design of the SPV, local damages or failure of the hull structure as explained in section 5.4.2 could occur during the sideways launching process.

It has to be noted that the proposed load model based on the experimental approach is only valid for the investigated SPV. Due to the combination given by the shape of the hull (inclination of bottom structure) and the geometry of the slipway, the deadrise angle during the sideways launching is approx. zero for all investigated configurations. This is visualized in Figure A.4. For other ship types with flat bottom structures, the bilge will be most likely the point of first contact with the water surface resulting in vastly different deadrise angles at the moment of impact. As the peak pressure resulting on a structure decreases significantly if the deadrise angle of the structure is increased [23], applying the proposed load model based on the experimental results to different geometric configuration or other ship types will presumably result in too high loads.

One major drawback of the simulation-based approach without FSI compared to the prosed simulation-based approach using FSI is the fact, that the proposed load models do not allow for an assessment of the resulting ship motion during a sideways launching process. For this purpose different approaches are to be used in addition to the simulation-based approach without FSI, like the experimental approach or CFD simulations. Furthermore, there are physical effects, which are not accounted for by the simulation-based approach without FSI. Like the analytical approach proposed in section 4.2, the simulation-based approach without FSI is not able to account for the elevation of the water surface and its interaction with the ship hull during the immersion of the SPV.

As the deadrise angle between the hull of the SPV and the water surface during the sideways launching is approx. zero for all investigated configurations, the interaction between the ship's hull structure and the water surface plays an important role regarding the peak pressure observed at the moment of impact. The peak pressure at impact is reduced by up to 30% for an elastic bottom structure compared to a rigid one [94]. Therefore, the load model obtained from the experimental approach is too conservative, as the stiffness of the ship model used during model tests is significant higher ($\approx$ rigid bottom structure) and not in scale with the hull structure of the SPV (= elastic bottom structure). Effects of hydro-elasticity are not accounted for.

6. Simulation-based approach using fluid-structure interaction

After investigating the use of simulations without FSI for the sideways launching process of the SPV, a simulation-based approach using FSI based on an ALE approach is proposed within this section. After explaining the general setup of the ALE approach, a parametric study of relevant setting of the FSI algorithm for the use case of the sideways launching process is conducted. Using these results, a verification of the ALE approach based on the model tests of the sideways launching process of the SPV is conducted. In addition, the necessary computational effort for the ALE approach is discussed and compared to simulations without FSI. Different approaches for optimizing the performance of the ALE approach are investigated. Lastly, the results obtained with the simulation-based approach using FSI (ship motion and hull structural loads) are discussed. This includes a parametric study regarding the resulting hull structural loads.

6.1. Setup of Arbitrary-Lagrangian-Eulerian approach

The model of the sideways launching process is set up using three different, independent parts: a FEM model of the hull structure of the SPV, the launch basin at the shipyard and the surrounding fluids (air and water) using an ALE element formulation. An illustration of the setup of the simulation-based approach using FSI is given in Figure 6.1. General properties of the FEM of the ALE domain are provided in Table 6.1. All values in Table 6.1 are rounded to the nearest hundred.

The coupling of the ALE elements with the FEM model of the SPV and launch basin is done by `*CONSTRAINED_LAGRANGE_IN_SOLID` in LS-DYNA. This function activates the FSI algorithm based on the penalty method. The theoretical framework behind this approach is explained in section 3.2. By using this penalty method, the FSI between the hull of the SPV and surrounding fluids is accounted for. This approach allows to describe the hull structure of the SPV with a classic Lagrangian element formulation.

Therefore, the same models of the SPV as for the simulation-based approach without FSI can be used, which are described in section 5.2. No modifications of these models are needed. This enables a modular modelling approach with very quick swapping of the FEM model of a ship's hull structure. A more detailed description of this modular modelling approach is given in [98]. This is very handy especially during the early design phase. The FEM model can be updated and swapped easily to account for alterations or an increasing level of detail of the hull structure as the design phase progresses.

The surrounding media of the ship hull (air and water) are modelled using 3D ALE elements together with the corresponding EOS as described in section 3.3. Cubical 3D elements with eight nodes and an aspect ratio of 1 are used for the ALE domain, which results in simple and fast generation of the mesh of the ALE domain. An one point ALE multi-material element formulation (`ELFORM`=11 in LS-DYNA) is utilized for the ALE domain. The multi-material element formulation allows mixing different fluids inside ALE elements. With this element formulation the free water surface including waves and spray are accounted for. As explained in section 3.1, the mesh of the ALE domain is only used as a reference frame for the start of the simulation. The different media inside the ALE

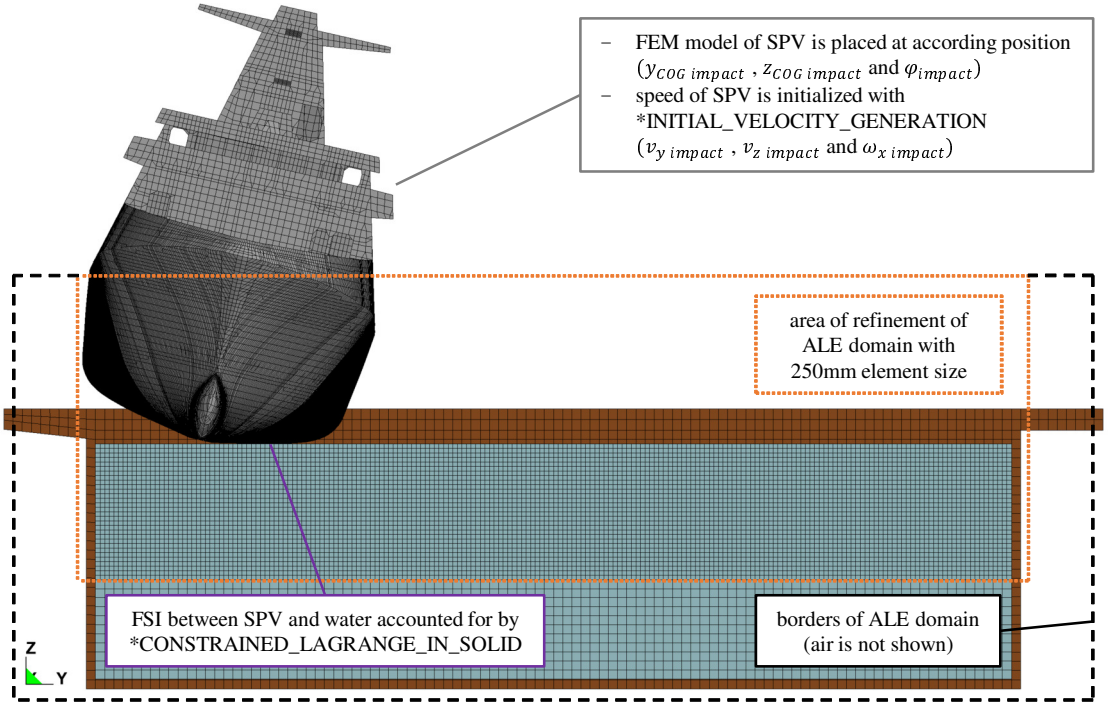

Figure 6.1.: setup of ALE approach for the sideways launching process of the SPV

Table 6.1.: properties of FEM model used for ALE domain

parameter	unit	value
solid elements (pier)	[-]	55,200
ALE elements (total)	[-]	7,302,000
ALE elements (area of refinement)	[-]	6,597,400
nodes	[-]	7,570,000

domain are initialized in LS-DYNA as so-called multi-material groups. The water inside the launch basin is initialized using `*INITIAL_VOLUME_FRACTION_GEOMETRY` inside LS-DYNA. Using this function, the different multi-material groups inside the ALE domain are initialized according to given geometric specifications independently from the initial mesh of the ALE domain. This functionality allows for very fast setup of different conditions. E.g the water level inside the launch basin can be changed by defining it as a parameter inside `*INITIAL_VOLUME_FRACTION_GEOMETRY`.

Based on the results as provided in [99], an element length of $L_{ALE} = 500\text{mm}$ is used for the ALE elements during simulations. In order to assess the interaction of the ship hull with the water in more detail, the area the ship will immerses into the water is refined locally. Within this area of refinement the element size of the ALE domain is halved to $L_{ALE\,refine} = 250\text{mm}$, as shown in Figure 6.1. Due to the size of the launch basin at the shipyard, the ALE-domain is large. Around 7.3 million 3D ALE elements are used for modelling the water and air inside the launch basin (see Table 6.1).

The launch basin is considered inside the FEM model, as Figure 6.1 shows. It is considered solely to account for the interaction between the water surface and the launch basin

(e.g. reflection of waves inside the launch basin). The launch basin is modelled based on the conditions at the potential construction shipyard of the SPV using 3D solid elements (Lagrangian element formulation; linear elastic material model).

The simulation-based approach using FSI starts just before the first contact of the ship's hull with the water surface to save computational time. The starting point is shown in 6.1. The initial conditions are calculated using the analytical approach as proposed in section 4.2.1. The conditions at the end of phase 2 — tipping are used as initial conditions for the simulation-based approach using FSI. This includes the position of the SPV relative to water surface ($y_{COG\ impact}$, $z_{COG\ impact}$ and φ_{impact}) as well as the velocity ($v_{y\ impact}$, $v_{z\ impact}$ and $\omega_{x\ impact}$). The velocities are initialized using `*INITIAL_VELOCITY_GENERATION` in LS-DYNA. Besides the inertia loads of the ship, only gravitational loads are acting within the simulation-based approach using FSI.

6.2. Parametric study of settings used for fluid-structure interaction

As suggested in [9], [10], a parametric study regarding different settings and parameters was carried out due to the complexity of the ALE approach and the FSI algorithm based on the penalty method. The goal was to investigate, which parameters are relevant regarding the results of the sideways launching process (ship motion and hull structural loads). Each parameter was varied one at time starting from a baseline. The settings for the baseline were derived based on experience with the simulation of underwater explosion for the design of naval vessels as presented in [98]. A more in-depth description of the conducted parametric study is given in [99]. Only the most relevant aspects and results are considered within this section. An overview of all investigated parameters is provided in Appendix A.8. All results obtained from this parametric study are given in Appendix A.8 as well.

Due to the size of the ALE domain and complexity of the simulation model of the SPV, the parametric study was carried using a smaller FEM model resembling the conditions given at a sideways launching process. This FEM model is shown in Figure 6.2 and consists of a simple rectangular box structure comparable to a pontoon, a small fluid domain and a launch basin. The dimensions and initial conditions used for the box structure are given in Figure 6.2. The setup of this model is exactly as described in section 6.1.

Similar parametric studies regarding the setup of the ALE approach and relevant settings of the FSI algorithm can be found in literature. One example is the work by Wang *et al.* [107], who carried out such a parametric study for the water entry problem of a sphere. As found in [107], the density ratio DR between ALE and Lagrangian elements is the most relevant parameter. The density ratio DR is defined as follows:

$$DR = \frac{L_{ALE}}{L_{Lagrange}} \tag{6.1}$$

In equation L_{ALE} and $L_{Lagrange}$ are the sizes of the ALE and Lagrangian elements. In [107] $DR \approx 0.5$ is suggested, while in [59] $DR \approx 1.0$ is recommended for a sufficient coupling based on the penalty method. The setup of the ALE domain together with the global FEM model of the SPV result in $0.6 \leq DR \leq 0.7$ for the proposed simulation-based approach using FSI. A similar value is used as the baseline for the conducted parametric study ($DR = 0.625$, see Figure 6.2).

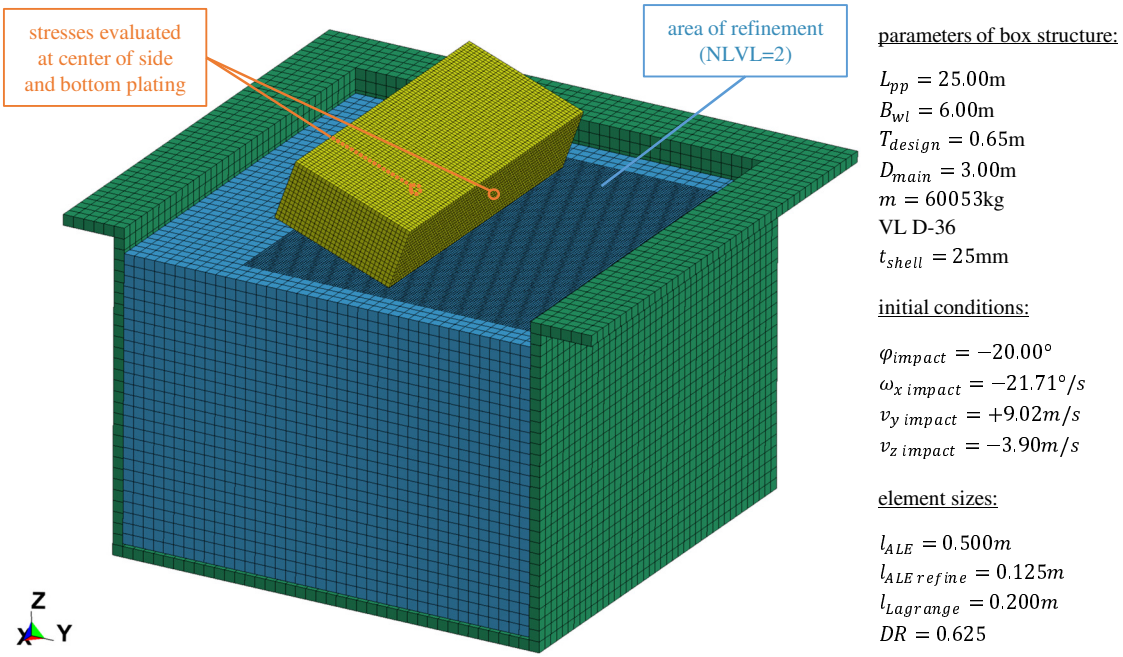

Figure 6.2.: FEM model used for parametric study of FSI settings

6.2.1. Motion of box structure

Different aspects of the ship motion are of interest during the sideways launching. Only the two most important aspects of the box structures motion are discussed within this section: the trajectory of the box structure and the maximum roll angle.

The different FSI settings influence the motion of the box structure in two different ways. On one hand, the fluid can be made stiffer. This can be obtained if a coarser element size of the ALE elements (`NLVL`=1 | $DR = 1.25$) is used. The box structure is decelerated more quickly and does not travel as far in the transverse direction (see Figure A.24e). This deceleration increases the maximum roll angle due to higher resistance of the fluid (see Figure A.22e). The box structure gets "stuck" inside the fluid.

On the other hand, the fluid can be made less stiff resulting in a more dynamic behavior of the box structure. This can be done by setting the coupling direction inside the FSI algorithm to `DIREC`=2 (compression only). The box structure is not decelerated as fast and will immerse deeper (see Figure A.25a). The roll angle is higher, too. But in contrast to the stiffer fluid, the box structure will upright itself more dynamically (compare Figure A.22a). This more dynamic behavior is apparent, if a closer look is taken on ω_x at t ($\varphi = 0$) in Figure A.21. The roll velocity is almost 50% higher compared to the baseline and all other simulations of this parametric study.

Besides the mesh size of the ALE elements and direction of coupling, other parameters do not significantly influence the motion of the box structure. This is especially true for the maximum roll angle, as Figure A.18 shows. The motion of the box structure is quite robust in regards to the setup of ALE approach and settings of the FSI algorithm.

6.2.2. Hull structural loads inside box structure

Besides the motion of the box structure, the influence of the investigated parameters on the resulting hull structural loads inside the box structure are investigated. For this purpose the resulting equivalent von-Mises stresses of chosen shell elements located at the centre of the bottom and side plating are assessed (compare Figure 6.2).

Figure A.26 and A.27 show, that the direction of coupling `DIREC` as well the mesh size of the ALE elements (`NLVL` | change of DR) are the most relevant parameters for the resulting hull structural loads inside the box structure. A coupling direction of `DIREC`=2 (compression only) does result in slightly higher stress levels, while simultaneously showing a smoother stress-time-signal with less fluctuations.

As Figure A.26e as well as A.27e illustrate, the mesh size of the ALE elements is extremely important if stresses inside a structure are of interest. Using `NLVL`=1 ($DR = 1.250$ | coarser ALE mesh than baseline) the fluctuations of the stresses are very high. In fact, the fluctuations are so high, that no reasonable evaluation of stresses inside the box structure is possible. When using `NLVL`=3 ($DR = 0.313$ | finer ALE mesh than baseline), the stresses are smoother and seem to be filtered.

If the frequencies of fluctuations are compared, they appear to be in correlation with the encounter frequency between the Lagrangian elements of the box structure and ALE elements of the fluid. This could indicate that the fluctuations as seen in Figure A.26 and A.27 could be induced numerically by the FSI algorithm, while the Lagrangian elements travelling through the ALE elements. For the first part of the simulation the encounter frequency $f_{encounter}$ between the Lagrangian elements and ALE elements can be roughly estimated using the following equation:

$$f_{encounter} \approx v_y \cdot \frac{cos\,(\varphi)}{L_{ALE}} \tag{6.2}$$

A plot of $f_{encounter}$ can be found in the Appendix in Figure A.28a to A.30a. By using fast Fourier transform (FFT) the stress-time-signals are transferred into the frequency domain. The results of the FFT are given in Figure A.28a to A.30b. If a closer look is taken on the baseline (see Figure A.29b), the encounter frequency can be identified as peaks inside the frequency domain based on the FFT. This backs up, that the fluctuations of the stresses are induced numerically by the FSI algorithm.

In the case of `NLVL`=1 the encounter frequency is nearly halved compared to the baseline. The frequency sweep is slower, so that each encounter frequency is acting upon the box structure for a longer time period. Additionally, for the case of the box structure an eigenmodes around 11Hz, 17Hz and 20Hz can be observed based on the peaks in the FFT (compare Figure A.29b). The encounter frequency in the case of `NLVL`=1 is within the range of these eigenmodes, so that resonance occurs. The numerical fluctuations induced by the FSI algorithm excite these eigenmodes, which are an explanation for the severe fluctuation of the resulting stresses as observed in Figure A.26e. In contrast to `NLVL`=1, the encounter frequency is nearly doubled while using `NLVL`=3 compared to the baseline. The frequency sweep is way faster, meaning that each encounter frequency is only acting for a very short time period on the box structure. Possible eigenmodes are excited for a much shorter time period reducing stress fluctuations quite drastically. In addition, the encounter frequency lies above the observed eigenfrequencies.

To avoid resonance / high fluctuations of the stresses inside Lagrangian elements, a check whether $f_{encouter} \approx f_{eigen}$ of the Lagrangian structure is advisable. The mesh size of the

ALE domain should be checked and account for this phenomena. A smaller element size for the ALE elements will result in a faster frequency sweep of the encounter frequency. This results in less fluctuations minimizing the risk of resonance inside the Lagrangian elements. Using a higher damping in the FSI algorithm (`DAMP` in `*CONSTRAINED_LAGRANGE_IN_SOLID`), reduces these fluctuations only slightly (compare Figure A.26c). The use of `DIREC`=2 (compression only) does result in lower fluctuations compared to `DIREC`=1 (tension and compression), as Figure A.26a shows.

All other parameter do not majorly influence the stresses observed inside the plating of the box structure. Only the fluctuations are altered slightly by the different parameters. The stress levels on a global scale are not altered significantly.

6.3. Verification of Arbitrary-Lagrangian-Eulerian approach

Before applying the proposed simulation-based approach using FSI on the sideways launching process of the SPV, a thorough verification of the utilized ALE approach and FSI algorithm for this use case is necessary. Therefore, a verification of the ALE approach is done based on the model tests as conducted in section 4.3. Two aspects are important: the ship motion and the loads resulting on the ship hull. Especially the loads at the impact with the water surface are to be checked.

During the verification process the results and knowledge obtained by the parametric study as given in section 6.2 are used to find settings adequate for the use case of a sideways launching process. This includes settings regarding the general setup of the ALE approach as well as the different aspects of the FSI algorithm. All relevant settings for the proposed simulation-based approach using FSI are provided in Appendix A.10.

Slamming experiments

Before conducting a verification of the ALE approach based on the complex model tests of the sideways launching process (three DOF, high level of asymmetry, $\beta_{impact} \approx 0$, influence of hydro-elasticity), a verification based on simpler slamming experiments (one DOF, symmetric, $\beta_{impact} \neq 0$, no effects of hydro-elasticity) is advisable. Such verifications can be found in literature. One of the earliest examples for such a verification is [7]. More recent examples for the use of an ALE approach for slamming and water entry problems can be found in [96], [97], [106], [107], [116].

The settings for the proposed simulation-based approach using FSI as given in Appendix A.10 were verified using slamming experiments as well. For this purpose the slamming experiments conducted in [43] were used. As shown in [99], the kinematics of the wedge (displacement and velocity), the loads resulting on the bottom plating of the wedge (pressure-time-signals) as well as the effects of hydro-elasticity (deformation of bottom plating) could be assessed very well with the settings as provided in Appendix A.10.

FEM model of experimental approach

A verification of the ALE approach was conducted based on the model tests of the sideways launching process, which is also presented in [99]. The test setups LC_01 and LC_02 according to Table 4.2 were used for verification purposes, as for these test setups several

measurement series (4x each) are available. The results within this section are limited to LC_01 (design point).

A FEM model was set up as closely as possible to the conditions of the model tests. The same setup for the ALE approach as proposed in section 6.1 was used. The according initial conditions (position relative to the water surface and speed of ship model) were obtained from the results of the model tests. The ALE domain was scaled down by the model scale ($\lambda_{sm} = 32$). This results in element size of 7.8mm in the area of refinement for the ALE elements. The FEM model of the SPV was set up to in accordance with the ship model as used during the model tests. A depiction of this FEM model is shown in Figure 6.3. General properties of this FEM model can be found in Table A.7. The element size is in scale with the global FEM model of the SPV resulting in average element size of approx. 12.5mm. Masses relevant during model tests (e.g. measurement equipment and trimming weights) were considered according to weight calculation sheets provided by the ship model basin. Using `*CONSTRAINED_NODAL_RIGID_BODY_INERTIA`, these masses were connected to the shell elements of the ship model as illustrated in Figure 6.3. Great care was taken to model the weight distribution in the FEM model as closely to the model tests as possible.

As the deadrise angle was nearly zero during model tests, effects of hydro-elasticity are of importance for the resulting peak pressure on the hull of the SPV [18], [94]. Therefore, the elasticity of the hull of the ship model was considered during the verification to obtain reasonable results. As mentioned in section 4.3.1, the hull of the ship model was built using NFRPC. As the ship model was built in single production, no information regarding the thicknesses and orientation of different NFRPC layers are available, which could be considered accordingly inside the FEM model. Hence, a linear, isotropic material model was used for the NFRPC. This corresponds to a quasi-isotropic laminate lay-up [90]. Average values for hand lay-up for the material model of the NFRPC were used inside the FEM model. The material properties used for the FEM model are given in Table A.6.

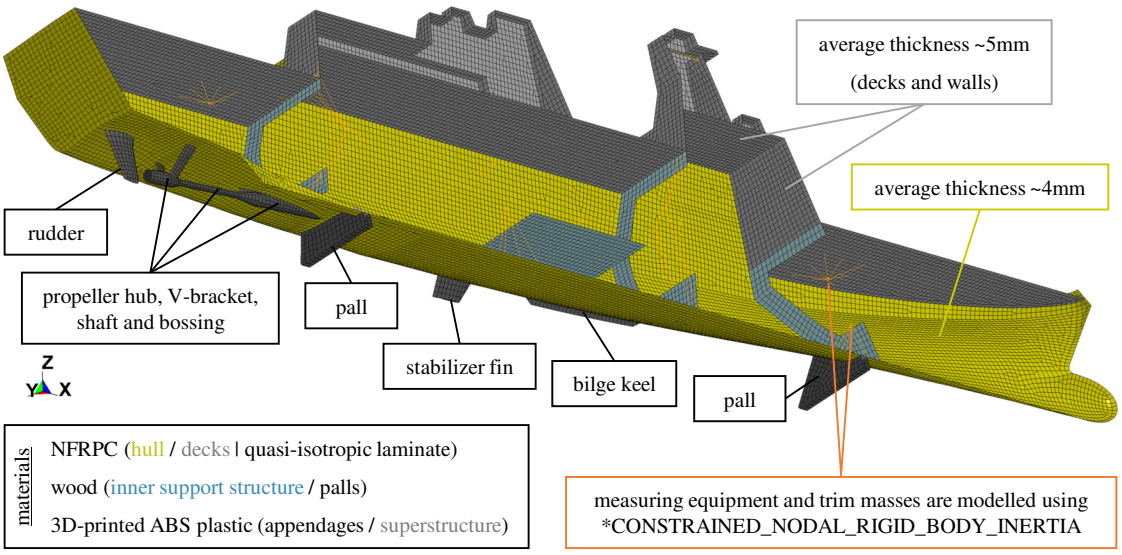

Figure 6.3.: verification of ALE approach — FEM model of ship model

Ship motion

For the verification of the ALE approach the ship motion is compared to the results of the model tests. For this purpose the roll angle as well as the trajectory at the COG are used. In Figure 6.4 the ship motion obtained with the ALE approach is compared to the results of the model tests. Note, that these results are given in model scale, as the FEM model of the experimental approach was set up in model scale. In addition, a detailed comparison of the results obtained with the ALE approach and model tests is given in Appendix A.9. The simulation results are compared with images captured during model tests at the ship model basin.

The roll angle resulting with the ALE approach shows very good agreement with the model tests. The maximal roll angle is virtually identical, as Figure 6.4a shows. Using the ALE-approach $|\varphi_{min}| = 31.3°$ compared to 32.2° observed during model tests for LC_01. The difference is about -2.8%, which is just slightly higher as the coefficient of variation observed during the measurement of the maximal roll angle (see Table A.3). Therefore, one of the most critical parameters of the sideways launching process regarding the ship motion can be assessed adequately with the proposed simulation-based approach using FSI. Similar observations can be made for the dynamic behavior of the roll motion of the SPV. The roll angle as well as roll velocity resulting with the ALE approach are very close the results of the model tests.

Only slight deviations of these two signals compared to the model tests can be observed. These deviations can be explained by the model scale. During model tests a lot of very fine spray at the ship hull was given. As soon as these effects are apparent (see second to fourth picture of Figure A.32), slight divergence between the ALE approach and model tests can be observed. This point is marked in Figure 6.4a. The chosen element size for the ALE domain is not fine enough to account for these effects.

In addition, slight deviations of the resulting roll period of the SPV are given. The results obtained with the ALE approach show a slightly higher roll period compared to model tests. On explanation for this phenomena are the added masses. As shown in [99], the added masses resulting with the ALE approach are overestimated by approx. 10%. Slightly higher added masses result in a more inert motion of the ship, as the ODE of motion 4.5 suggests.

As illustrated in Figure 6.4b, the trajectory of the COG resulting with the ALE approach shows good agreement with the model tests as well. The point of deepest immersion (clearance between ship and bottom of launch basin) is almost identical. The only difference is that the SPV is decelerated more quickly while using the ALE approach. Based on the parametric study of the different FSI settings as conducted in section 6.2, this behavior indicates that the mesh size of the ALE elements is slightly too big (compare Figure A.24e as well as A.25e). Using an finer element size for the ALE domain would result in a slower deceleration of the SPV. The density ratio DR between the ALE and Lagrangian elements is with $0.6 \leq DR \leq 0.7$ slightly higher than the suggestion in [107] ($DR = 0.50$). However, an element size of 7.8mm (250mm in full scale) for the ALE domain is a good compromise between accuracy and computational effort, as discussed later on within this chapter.

In total, the ship motion during the sideways launching process can be assessed very well with the proposed simulation-based approach using FSI. Especially the maximal roll angle resulting with the ALE approach is virtually identical to the results obtained during model tests. The dynamic behavior of the SPV can be assessed well using the ALE approach,

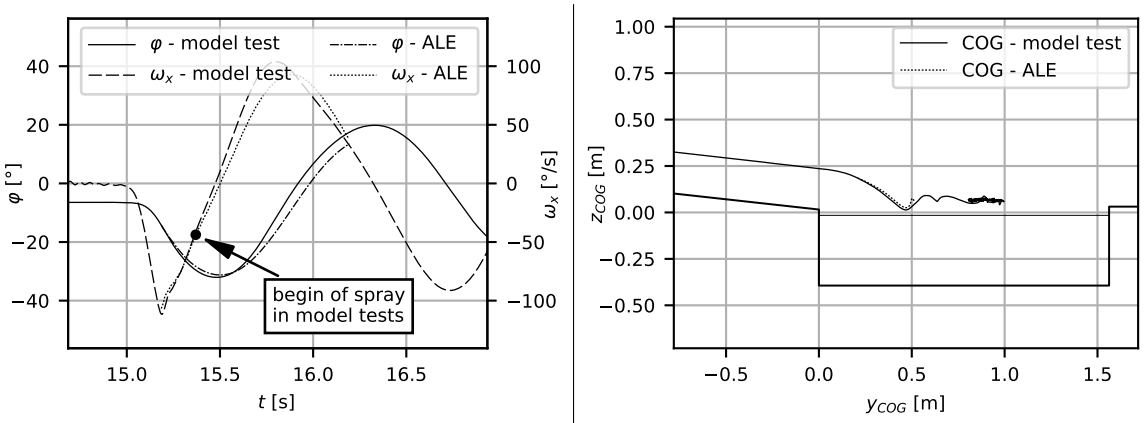

(a) roll angle and velocity

(b) trajectory of COG

Figure 6.4.: verification of ALE approach — ship motion @ LC_01 (model scale)

too. Only minor deviations can be observed. The ship motion is slightly more inert with the ALE approach. From a design point of view these differences are negligible for the assessment of the sideways launching process of the SPV.

Pressure on ship hull

Besides the motion, the pressure-time-signals obtained with the ALE approach are compared with model tests. A comparison for all four pressure transducers is given in Figure 6.5. Note, that these results are given in model scale. The pressure-time-signals shown for the ALE approach are lowpass-filtered using a cutoff frequency $f_{cutoff} = 250$Hz.

The pressure-time-signals resulting with the ALE approach show adequate agreement with the model tests. The peak pressure at impact with the water surface can be assessed with the ALE approach - especially for P2 to P4. The results for P1 are bit attenuated compared to model tests (see Figure 6.5a). As P1 came into contact with the water later than the other pressure transducers, the peak pressure is dominated by the spray root forming at the ship hull [43], [44], [102]. As already discussed, the mesh size used for the ALE domain is not fine enough to account for the spray forming in model scale sufficiently.

A big challenge while evaluating the pressure-time-signals resulting with the ALE approach are high frequency fluctuations. There are four main reasons for these fluctuations. As described in section 3.3.2, water is modelled using the Mie-Grüneisen-EOS. Using this EOS water is modelled as a compressible medium. Due the high bulk modulus of water small changes of the density will result in high fluctuations of the pressure. Secondly, a FSI algorithm based on the penalty method is used for the simulation-based approach using FSI (see section 3.2). This method induces high frequency oscillations by the transfer of forces into the water as discussed in detail in [7]. Although these fluctuations can be reduced by using a higher value for the damping inside the FSI algorithm, the fluctuations could not be avoided completely. Thirdly, the pressure transducers used during model tests have a specified area of measurement ($\rightarrow$ spatial filtering), whereas the monitoring of the pressure-time-signals within the ALE approach is limited to a point without any expansion. Lastly, due to the very small ALE domain in model scale, pressure fluctuations travelling in the form of pressure / shock waves inside the water basin are reflected very quickly back to the

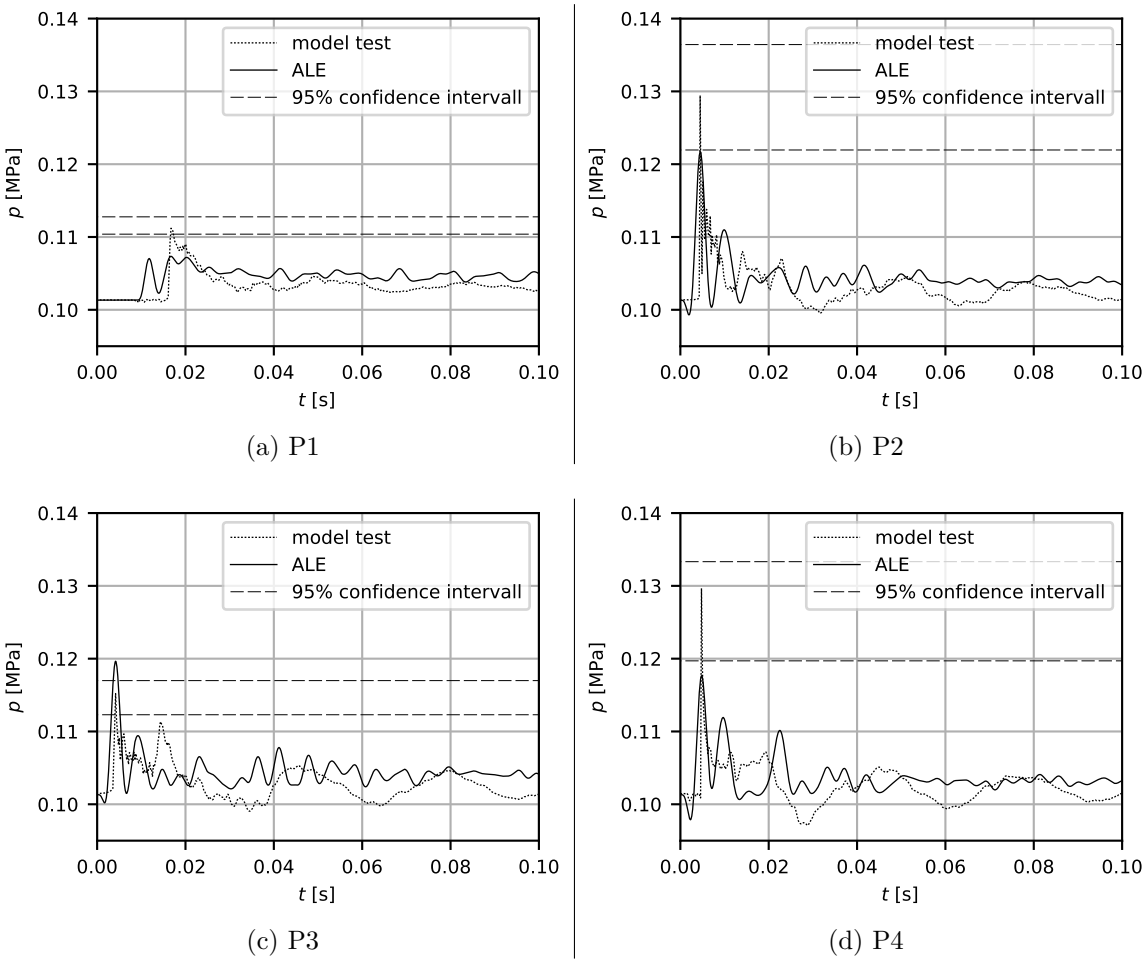

(a) P1 (b) P2

(c) P3 (d) P4

Figure 6.5.: verification of ALE approach — pressure-time-signals @ LC_01 (model scale)

pressure transducers. Based on the given geometry of the launch basin in model scale and the speed of sound of water, a shock wave travelling from the water surface to the bottom of the launch basin back to the water surface needs about 0.50ms.

These reasons explain why the pressure-time-signals based on the ALE approach contains a lot of high frequency fluctuations and are more noisy compared to the signals obtained with the pressure transducers used during model tests (compare Figure A.31d). Therefore, the use of a lowpass filter is necessary to obtain pressure-time-signals suited for comparison with the results of the model tests. Choosing an adequate cutoff frequency is always a compromise (high $f_{cutoff} \rightarrow$ noisy signal vs. low $f_{cutoff} \rightarrow$ attenuation of peak pressure). The influence of the chosen cutoff frequency is investigated in Figure A.31. A cutoff frequency of 250Hz is a good compromise.

As discussed in section 4.3.2, the assessment of the pressure peak is not a meaningful way to asses the loads resulting on the ship hull. The peak pressure observed during model tests of the sideways launching process were subjected to a certain degree of fluctuation. In case of the ALE approach the deviation of the peak pressure is further determined by the chosen cutoff frequency for the lowpass filter. For this reason the evaluation of the loads resulting on the ship hull is based on the impulse analogously to the results of the model tests (see

Table 6.2.: verification of ALE approach — impulse at different pressure transducers (full scale)

transducer	$J_{i\,50ms}$ in [kPa·s] model test	ALE approach	difference in [%]
P1	9.61	8.11	-15.61
P2	10.15	10.51	+3.55
P3	8.77	9.34	+6.54
P4	8.69	9.82	+13.00

section 4.3.2 for details). As the model used for the verification of the ALE approach is in model scale, the impulse is evaluated based on the resulting pressure-time-signals in model scale and afterwards transferred to full scale. The following equation is used for this purpose:

$$J_{i\,50ms\;ALE} = \left[\int_{t_{p_i\,max}}^{t_{p_i\,max}+50ms\cdot\lambda_{sm}^{-0.5}} (p_i - p_0)\; dt \right] \cdot \lambda_{sm}^{3.5} \tag{6.3}$$

The impulses resulting with equation 6.3 are given in Table 6.2. The impulses obtained with the ALE approach are in good accordance with the results obtained using model tests. The deviation of the impulse between the ALE approach and model tests is slightly higher as the uncertainties observed during model tests (compare Table 4.4). Besides deviation of the peak pressure due to filter settings, another aspect are the initial conditions used for the FEM model of the verification. Slight deviations between model tests and the FEM model can significantly alter the results obtained with the ALE approach. As mentioned above: Based on data provided in [23], a difference of the deadrise angle of 1° does result in a difference of the peak pressure of roughly 10% for the impact speeds observed during the model tests.

All in all, the proposed simulation-based approach using FSI is able to assess the loads resulting on the ship hull sufficiently on an integral level. The ship motion obtained with the ALE approach is almost identical to the results of the model tests. If the pressure resulting with the ALE approach and transferred via the FSI algorithm onto the hull of the SPV were just slightly off, the ship motion would be altered significantly over the time period simulated for the verification.

6.4. Optimization of computational effort

One of the drawbacks of the ALE approach is the increased computational effort and thus necessary simulation time compared to the simulation-based approach without FSI. However, some settings of the ALE approach as well as FSI algorithm can be optimized for decreasing the computational effort. An overview of the investigated aspects is provided in Figure 6.6. The influence of each of these different aspects on the computational effort is discussed in the following section. All investigations within this section are based upon the combined FEM model of the SPV. All values are provided for simulations using 16 cores on an Intel Xeon Gold 6154 processor @3.70GHz (boost speed) and LS-DYNA release R13.1.

By considering all measures as given in Figure 6.6, a speedup of 3.4 is achieved for the

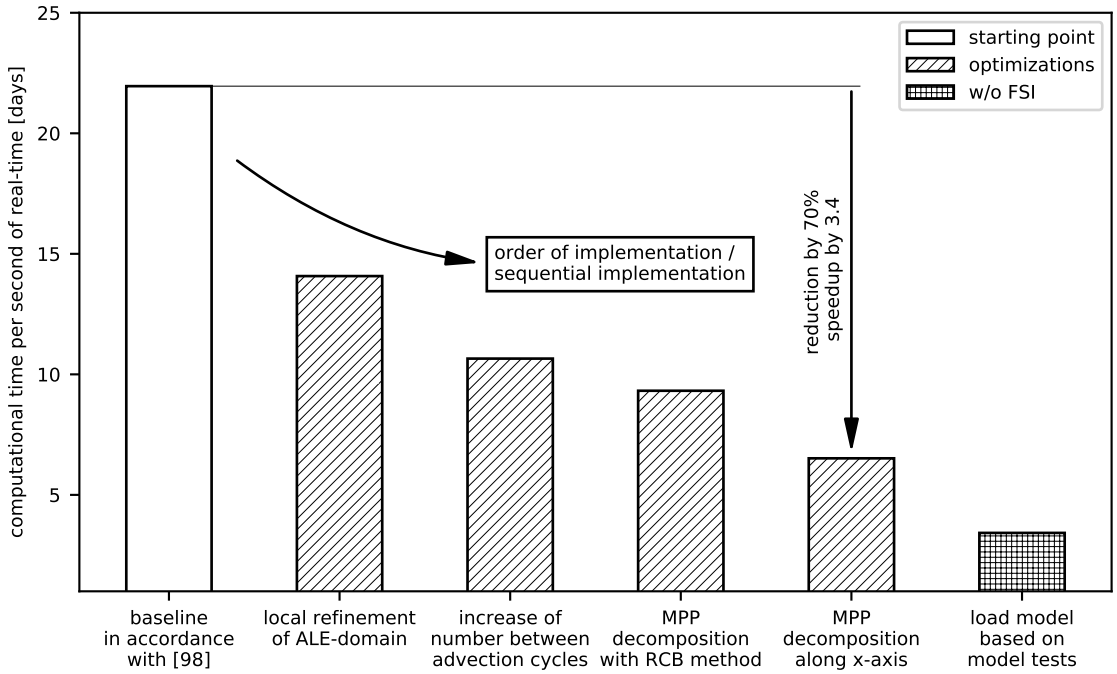

Figure 6.6.: influence of different settings on computational effort of ALE approach

simulation-based approach using FSI compared to the baseline as given in [98]. About 6.5 days are needed to simulate one second of real time of the sideways launching process. For comparison, this is about 1.9 of the computational effort for the simulations without FSI (compare Figure 6.6). For the assessment of the different aspects of the sideways launching process of the SPV the following computational times are necessary:

- 3 days: assessment of hull structural loads (about 400ms simulation time necessary)
- 16 days: maximal roll angle on PS
- 52 days: maximal roll angle on starboard (STB)
- 68 days: one full roll period of the SPV

The assessment of the ship motion is despite all optimizations still expensive regarding the computational effort. For assessing the maximum roll angle during the sideways launching process about 16 days of computational time is necessary. In contrast to the ship motion, the resulting hull structural loads can be assessed rather quickly within three days. As discussed later, this allowed for an optimization of necessary reinforcements of the hull structure of the SPV regarding their weight using the ALE approach.

Homogenous mesh of hull structure

One of the biggest room for adjustment of computational effort is given by the mesh used for the FEM model of the SPV. As in both simulation-based approaches an explicit time integration scheme is used, the time step is determined by the mesh of the FEM model. Each element has a characteristic time step Δt_e. If this time step is exceeded, the explicit

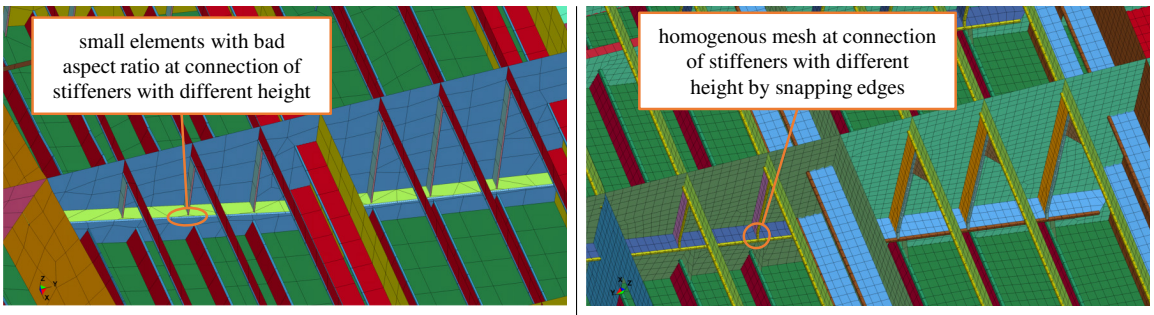

(a) inhomogeneous mesh ($\Delta t_e = 4.56 \cdot 10^{-7}$s) (b) homogeneous mesh ($\Delta t_e = 2.33 \cdot 10^{-6}$s)

Figure 6.7.: influence of mesh on characteristic time step Δt_e

time integration scheme can become unstable. The calculation of the characteristic time step Δt_e in LS-DYNA for different element types is given in [59].

The characteristic time step is defined by the element size used within the FEM model. A finer mesh size (smaller elements) does result in a smaller characteristic time step. In addition, elements with an aspect ratio not equal to one do have a smaller characteristic time step. This effect becomes more severe the worse the aspect ratio of an element is [59]. Especially the second aspect is important to keep in mind while modelling the hull structure within FEM model to be used with an explicit time integration scheme.

As the hull structure of the SPV is irregular (especially at the bottom structure and shell), a completely homogenous mesh is not possible. However, by taken care during pre-processing and meshing of the hull structure, elements with a really bad aspect ratio can be avoided. In Figure 6.7 two meshes used for the connection of two stiffeners with different heights are shown. The more homogeneous mesh as shown in Figure 6.7b increases the characteristic time step by nearly a factor of five compared to Figure 6.7a. This translates directly into a decrease of the computational effort of approx. 80%, as fewer calculation steps are to be carried for a given time period. This decrease of computational effort is valid for both simulation-based approaches.

Local refinement of ALE domain

The local refinement functionality inside LS-DYNA allows for splitting the initial ALE elements in a specified area by a factor of 2 (`NLVL`=1 in `*CONTROL_REFINE_ALE`), of 4 (`NLVL`=2) and so forth. The theoretical framework and numerical implementation inside LS-DYNA are described in the work by Aquelet [8]. By using a local refinement of the ALE domain as shown in Figure 6.1, the area of interest of can be meshed using a sufficient element size without meshing the whole ALE domain with a finer element size. The density ratio DR between ALE and Lagrangian elements within the refined area is ≈ 0.71 (250mm/≈350mm based on global FEM model of the SPV).

For the domain as shown in Figure 6.1, local refinement is used for the area of interaction with the hull of the SPV (spray root and waves forming) as well as the water surface inside the launch basin (reflection of waves). Therefore, the local refinement is used for a big part of the ALE domain (compare Figure 6.1). In total, about 7.3 million ALE elements are used, from which 6.6 million elements are located in the area of refinement. If the complete ALE domain was meshed without the local refinement with consistent element

size of 250mm, about 12.6 million ALE elements would be necessary. By using the the local refinement function the number of ALE elements is reduced by roughly 5.3 million or 42%. The reduction of ALE elements does decrease the computational effort by an almost similar margin of 36%, as Figure 6.6 shows.

The local refinement function is useful to reduce the necessary computational effort. However, it is not able to reduce the element size of the ALE domain at will. In [107] $DR \approx 0.50$ is recommended for water entry problems. Reducing DR from ≈ 0.71 to ≈ 0.50, would result in an increase of the number of ALE elements by a factor of 2.9. This would yield in 21.3 million ALE elements, meaning that $DR \approx 0.50$ is not feasible due to the very high computational effort needed. But as shown in section 6.3 within the verification of the ALE approach, $DR \approx 0.71$ allows for a sufficient assessment of the relevant physical phenomena of the sideways launching process.

FSI settings

Another way for reducing the computational effort of the simulations with the ALE approach is optimizing the FSI settings. As explained in section 3.1 within the theoretical framework, the ALE approach uses two calculation steps per time step. The first step is a classical Lagrangian step, while during the second step (advection step) a rezone of the computational mesh is performed and the transport of mass, internal energy and momentum across element boundaries is calculated. In LS-DYNA the number of cycles or time steps between two advection steps can be set inside the card `*CONTROL_ALE` with the option `NADV`.

The characteristic time step of the simulation-based approach using FSI is defined by the FEM model of the SPV. For the combined FEM model of the SPV Δt_e is equal to $2.33 \cdot 10^{-6}$s. This order of magnitude is a lot smaller as the physical phenomena, which are relevant for the advection step (free water surface and contact surface between the hull of the SPV and water). As the parametric study of the relevant FSI settings in section 6.2 suggests, a value of `NADV`=50 is a good compromise between computational effort and stability of the simulation using the ALE approach. A higher value for `NADV` can lead to numerical instabilities (divergence or even abort of the simulation). By setting `NADV`=50, the advection step is done only every 50^{th} time step. As Figure 6.6 shows, the computational effort is reduced by 24% compared to the baseline of `NADV`=1 as used in [98].

Parallelization using MPP version of LS-DYNA

For the FEM software LS-DYNA two different versions are available: symmetric multiprocessing (SMP) and massively parallel processing (MPP). The difference between SMP and MPP lies within the parallelization of the simulation. The MPP version of LS-DYNA is developed to run on a number of computers connected in a network in the form of a computational cluster [60]. An overview of the differences between the architecture of the SMP and MPP version of LS-DYNA can be found in [60] as well as [74].

MPP allows for better scalability of larger models with several million elements, as the model is split and distributed into smaller parts on more processors enabling a more efficient computation per processor. For most models a benefit regarding the use of MPP is reached after using more than eight cores [60]. Nowadays, MPP is state of the art for the simulation of big and complex models on a cluster environment. Examples are crash simulations in

the automotive sector as presented by Kondo and Makino [48] or Makino [65].

For the sideways launching process MPP is well suited choice for the simulation-based approach using FSI. One one hand the simulation model is big. For comparison: with roughly 10.1 million elements the model size is comparable to crash simulations in the automotive sector [48], [65]. On the other hand the computational costs per time step are high due to the advection step necessary for the ALE approach as well as the FSI algorithm. With MPP computational resources are used more efficiently due to a better distribution of the work load on each of the different cores of the cluster.

Before starting a simulation with the MPP version of LS-DYNA, the FEM model is divided into several parts, which are then assigned to each of the cores. This process is called decomposition. In general, the position of the cutting planes is based on the recursive coordinate bisection (RCB) method in LS-DYNA [60], [74]. The RCB method divides the model in such a way, that the the estimated computational costs per core are distributed evenly based upon the computational costs per element. The use of the RCB method for the FEM model of the sideways launching process is shown in Figure A.33. Using MPP together with the RCB method for the decomposition instead of the SMP version of LS-DYNA, the computational effort can be reduced by 13%.

However, as careful monitoring of the work load on each core shows, with the RCB method for decomposition the work load is not distributed evenly across all cores. The local refinement of the ALE domain using `*CONTROL_REFINE_ALE` is not accounted for. Due the finer mesh size (ALE as well as Lagrangian elements) the computational costs are way higher amidships compared to the fore and aft of the SPV. This is due to higher number of elements to be considered by the FSI algorithm. Lastly, the elements of the SPV and ALE elements are distributed arbitrary on the different cores and are not grouped together (compare Figure A.33). This results in high communication effort between the different cores due to the FSI algorithm.

In LS-DYNA different methods for controlling the decomposition of a model can be used depending on the problem to be solved within the simulation. The method of decomposition will effect the computational performance with the MPP implementation. Examples for the influence of different decompositions are discussed in [48], [60], [74]. For the sideways launching process the approach for decomposition used for crash simulations is adapted. For crash simulations, the FEM model of the car is often split perpendicular to the direction of motion as shown in [48], [60], [74]. By doing so, the computationally expensive crash area of the car is distributed more evenly among all computational cores. For the sideways launching process the FEM model is split along the x-axis of the ship perpendicular to its mean direction of motion (y-axis).

One example for such a decomposition is given in the Appendix A.10. The resulting decomposition can be seen in Figure A.34. A manual decomposition is chosen, where the cutting planes are set along the x-axis. The border are chosen, so that each of the cores has an almost similar working load. Furthermore, the Lagrangian elements of the SPV and corresponding ALE elements for the FSI algorithm are grouped together on the different cores (compare Figure A.34). This reduces communication costs between the cores during the simulations.

As Figure 6.6 shows, the computational effort is reduced by additional 30%, if the optimized decomposition is used instead of the RCB method. In total, with the optimized decomposition the computational effort is reduced by approx. 39% compared to the SMP version of LS-DYNA.

6.5. Results

Within the following section, the results of the simulation-based approach using FSI are discussed. The ship motion as well as the resulting hull structural loads during the sideways launching process are assessed for both loading conditions LC LAUNCH and LC LSW. A comparison with the results obtained from the simulation-based approach without FSI is given. Additionally, the influence of the same parameters as investigated within the experimental approach on the resulting hull structural loads are assessed.

6.5.1. Ship motion

Based on the simulation-based approach using FSI it is possible to asses the motion of the SPV on a very detailed level. Besides the roll angle and velocity ($\rightarrow$ height of waterline on side of SPV sides), the trajectory at the COG ($\rightarrow$ clearance between SPV and launch basin) was investigated. These results are plotted in Figure 6.8. In addition, a picture series of the ship motion obtained with the ALE approach for LC LAUNCH is provided in Appendix A.11.

The simulations were carried out up to the point, where a complete roll period of the SPV is captured. That includes the tipping around the edge of the pier, the maximal roll angle on PS $|\varphi_{min}|$, up-righting of the vessel, the first zero crossing, the maximal roll angle on STB φ_{max} and up-righting of the vessel to the second zero crossing (compare Figure 6.8a). One complete roll period is simulated due to two reasons. Firstly, by capturing both maximal roll angles (PS as well as STB) the height of the waterline on each side of the vessel can be assessed. This information can be used for planning which openings are to be closed during the sideways launching process to prevent uncontrolled flooding of the SPV. Secondly, by simulating such a long time period it can be checked how the SPV is decelerated during the sideways launching process and if additional measures are necessary, to control the ship motion after the sideways launching of the SPV (e.g. use of trusses / counter weights for stopping).

Both loading conditions of the SPV are safe to use regarding the resulting ship motion. The maximal roll angle on PS $|\varphi_{min}|$ is moderate. In the case of LC LAUNCH $|\varphi_{min}| = 35.9°$ and for LC LSW $|\varphi_{min}| = 39.9°$ can be observed (compare Figure 6.8a). For LC LAUNCH the main deck is not immersed into the water, as shown in the picture series in Appendix A.11. In the case of LC LSW minor green water can be observed on the main deck, as the maximal roll angle is slightly higher. Sufficient clearances between the SPV including palls and appendages and the launch basin are given (compare Figure 6.8c). Similar to the model tests the trajectory of the SPV is more or less stopped directly at the centre of the launch basin (compare Figure 6.8c and picture series in Appendix A.11). The greatest part of the speed at the COG in the yz-plane is lost during the first two seconds after the first contact with the water surface (compare Figure 6.8d).

The ship motion observed for both loading conditions is quite similar. No significant differences regarding the trajectory or velocity at the COG are given. The major difference is the roll motion of the SPV. As the position of the COG in z-direction COG_z is 3.5% higher for LC LSW compared to LC LAUNCH, the maximal resulting roll angle on PS $|\varphi_{min}|$ is increased by roughly 4.0°. This is an increase of 11.1%, which emphasizes the non-linear dependency between COG_z and $|\varphi_{min}|$ as observed during the model tests (compare Figure 4.10c). As the moment of inertia around the x-axis is 11.7% higher for LC LSW compared

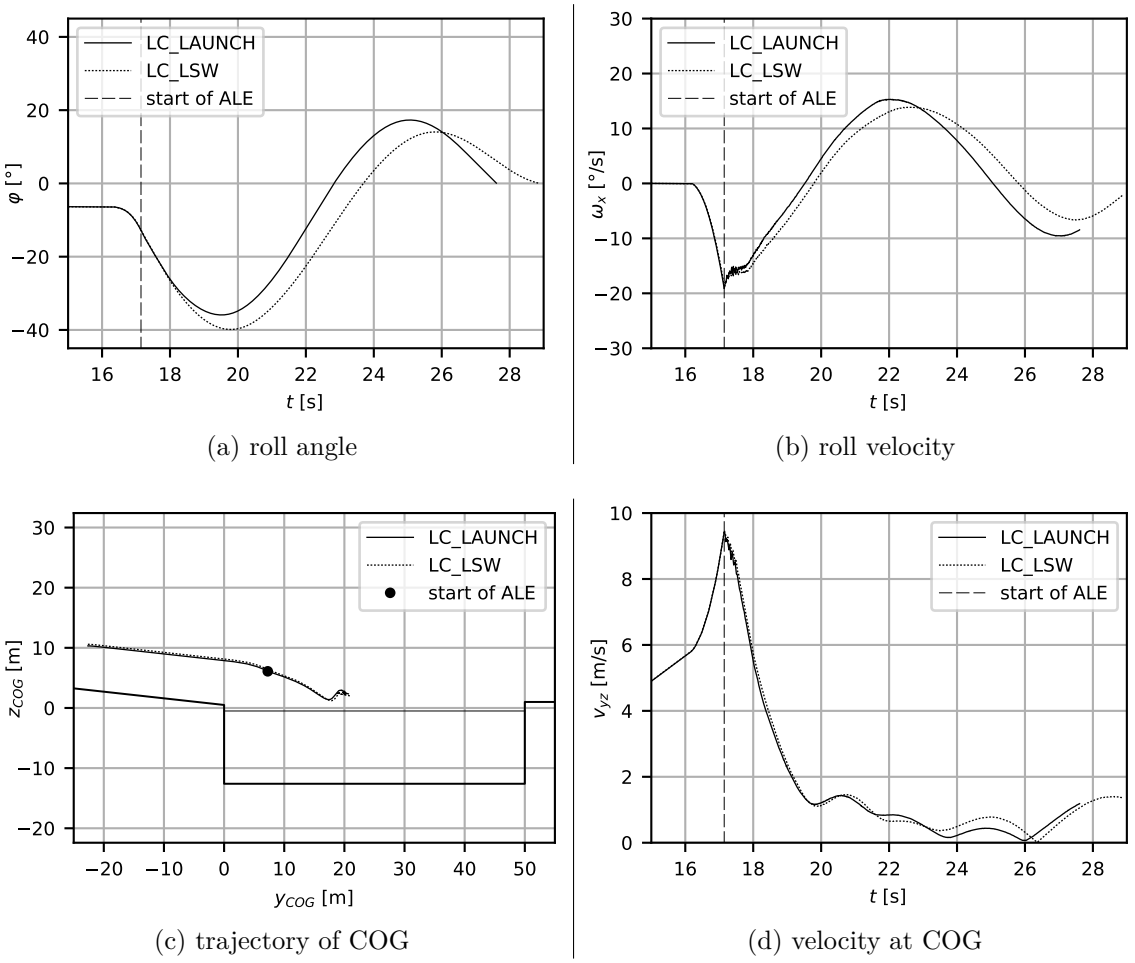

(a) roll angle

(b) roll velocity

(c) trajectory of COG

(d) velocity at COG

Figure 6.8.: results of ALE approach — ship motion

to LC LAUNCH, the roll motion of the SPV is more inert in the case of LC LSW. The SPV needs more time to completely upright itself (difference of about 0.9s). The roll period is increased by approx. 1.3s.

All in all the, the motion of the SPV during the sideways launching process obtained with the simulation-based approach using FSI is in good accordance with the behavior observed during model tests as discussed in section 4.3.2. One of the effects observed during the verification of the ALE approach based on the model tests is not present during the full-scale simulation. As discussed in section 6.3, a slight discontinuity in the roll velocity can be observed for the ALE approach right after the spray root is braking and a lot of fine spray was forming during model tests. This effect is not present in the full scale simulation, as Figure 6.8b shows. The simulations in full scale back up the hypothesis in section 6.3, that this effect is dominated by the the model scale (very fine spray during model tests; see picture series in Appendix A.4). As shown in Figure 6.9, the spray root forming in full scale is much more homogeneous / continuous compared to the model tests. The mesh size chosen for the ALE elements allows for a clear location and identification of the forming spray root during the immersion of the SPV.

In addition, an area of ventilation / flow separation can be observed on the bottom

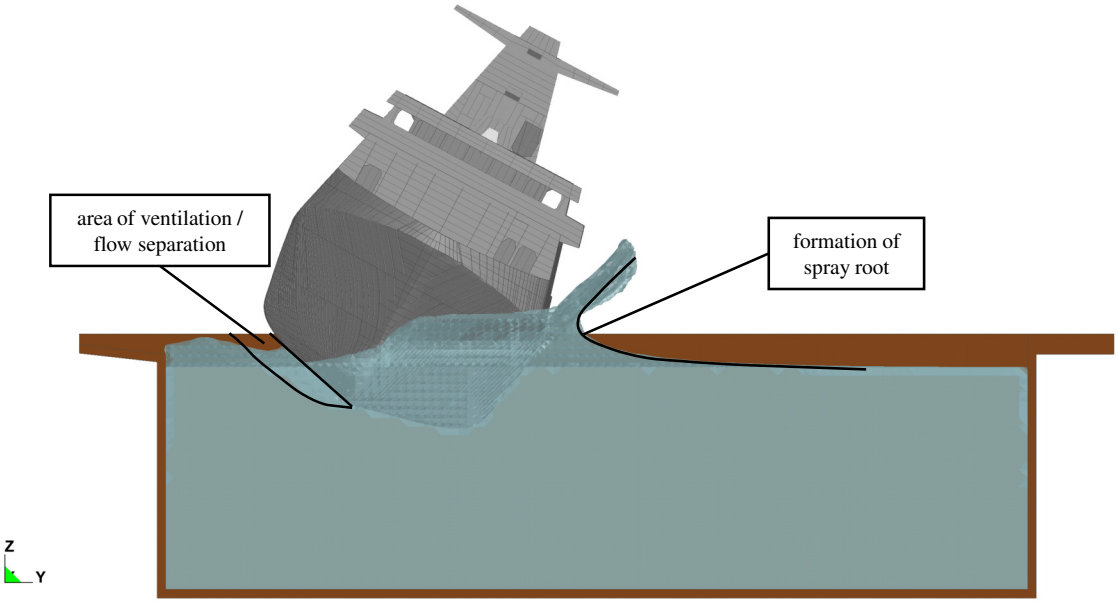

Figure 6.9.: results of ALE approach — interaction between ship hull and water surface

structure (STB) in Figure 6.9. This configuration is similar to type B flow (flow separation and ventilation) as observed in the slamming experiments conducted in [44]. Type B flow was observed for configurations with higher degree of asymmetry and small deadrise angles [44], which is true for the sideways launching process of the SPV as well.

6.5.2. Hull structural loads

Resulting load mechanism

The load mechanism as seen with the simulations without FSI (load mechanism 01 → impact with water surface) can be observed based on the simulation-based approach using FSI as well. However, a second load mechanism can be observed using the simulations with FSI. The hull structural loads resulting from this load mechanism are caused by transversal forces due to the deceleration of the hull structure of the SPV after immersing into the water. The principle of this second load mechanism is illustrated in Figure 6.10.

While immersing into the water the transverse / sway motion of the SPV from sliding down the slipway is stopped rather abruptly. As illustrated in Figure 6.10, especially the bottom structure of the vessel is decelerated, while the upper part wants to remain its transversal motion due to the inertia of the hull structure. This behavior results in high shear stresses inside transversal members of the hull structure. For the SPV this is especially true for the bulkhead plating at engine rooms between the bottom structure and the next higher, continuous deck. The resulting hull structural loads are shown in Figure 6.11.

As Figure 6.11a and 6.11b show, the shell of the hull structure and its supporting members like the web frames are highly loaded right after the impact with the water surface (→ load mechanism 01). However, at the web frames a switch of the loading direction is given due to the deceleration of the hull structure of the SPV (compare Figure 6.11b). In addition, inside the plating of the bulkhead high membrane and shear stresses are present due to this

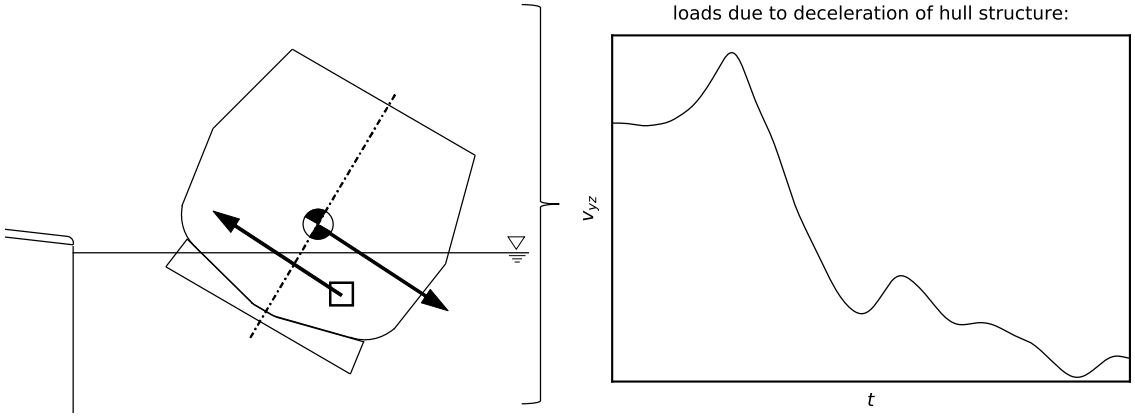

Figure 6.10.: load mechanism 2 — deceleration of hull structure

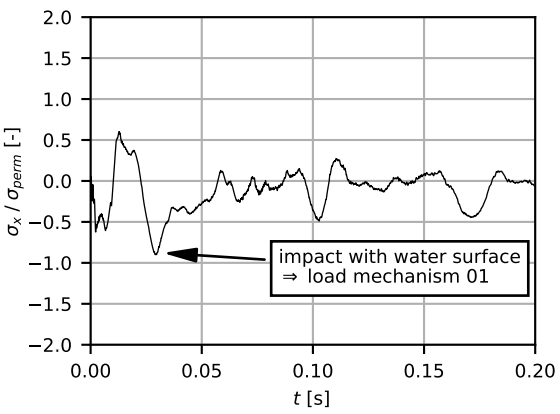

(a) shell plating (outer surface)

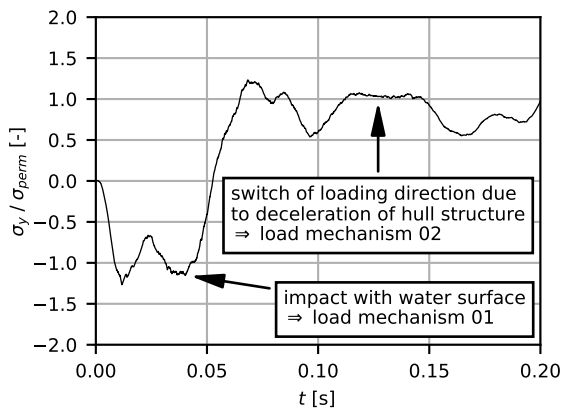

(b) corner of web frame (middle surface)

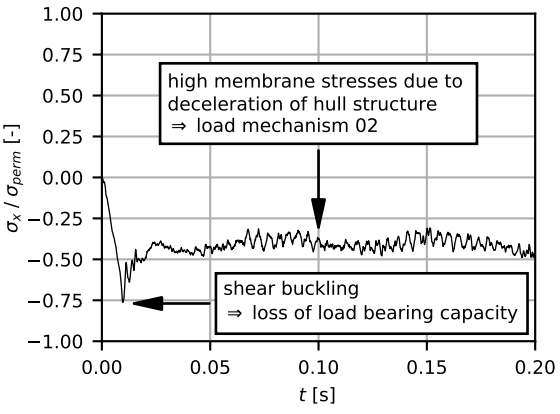

(c) bulkhead plating (middle surface)

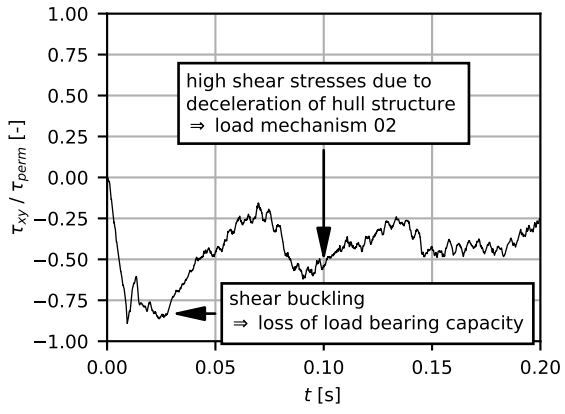

(d) bulkhead plating (middle surface)

Figure 6.11.: resulting hull structural loads — load mechanism 02 (combined FEM model of SPV + LC LSW)

load mechanism. These are shown in Figure 6.11c and 6.11d.

Right after the impact with the water surface, the greatest deceleration of the SPV can be observed during the first second (compare Figure 6.8d). This results in high membrane and shear stresses inside the bulkhead plating while immersing into the water. Shear buckling of parts of the bulkhead plating as marked in Figure 6.11c and 6.11d are the result of these high loads. This shear buckling is combined with out-of-plane plastic deformation of the affected bulkhead plating. The resulting stresses inside the affected parts drop suddenly (loss of load bearing capacity). After the first second, where the spray root starts to form as illustrated in Figure 6.9, the SPV is decelerated more steadily (compare Figure 6.8d). The resulting hull structural loads start to plateau around a certain level as Figure 6.11c and 6.11d show.

Such damages / this failure mode could only be observed within the simulation-based approach using FSI. As the bulkheads are the main load bearing components for the second load mechanism, this failure mode could potentially result in progressive collapse behavior if bigger parts of the bulkhead plating undergo shear buckling. A loss of shear stiffness of the bulkheads could result in great deformations of the shell and its supporting members equalling a total loss of the affected part of the hull structure in a worst case scenario. The resulting hull structural loads inside the bulkheads are to be assessed very carefully to ensure a safe sideways launching process of the SPV.

Parametric study

As the simulations with FSI allow for a detailed assessment and understanding of the resulting hull structural loads during the sideways launching process of the SPV, a parametric study was carried out. The same parameters as during the model tests were investigated regarding their influence on the resulting hull structural loads. This includes different loading conditions, the height of drop around the pier h_{drop} (change of height of palls h_p or water level h_{wl}) and the coefficient of friction μ_{sw}. An overview of the investigated parameters is given in Table 6.3. In Table 6.3 the conditions at the moment of impact with the water surface are provided as well. This includes the speed of the sway motion $v_{sway\ impact}$ (speed of SPV at COG in y_s direction in local ship coordinate system → see Figure A.1) and speed of impact at the ship hull v_{slam}. An overview of the resulting hull structural loads is given in Appendix A.12 (Figure A.39 to A.41).

The experimental approach showed, that v_{slam} is the main influence regarding the resulting loads on the hull structure in the form of the impulse $J_{i\ 50ms}$ (see Figure 4.14). The height of the drop was the most relevant parameter regarding v_{slam}. For the parametric study an increase of h_p by 0.50m was used (see Table 6.3). This results in an increase of v_{slam} by 15.3%. Based on the load model proposed in 5.3.2 used within the simulation-based approach without FSI, this is equal to an increase of the impulse resulting on the ship hull by approx. 16.1%.

As discussed in section 5.4.2, the loads right after impact of the ship hull with the water surface are responsible for load mechanism 01 as illustrated in Figure 5.5. The resulting hull structural loads are acting upon the shell plating and it's supporting members like web frames or the floor plating. However, the increase of the impulse by approx. 16.1% does not correlate directly with a corresponding increase of the resulting hull structural loads as shown in Figure 6.13. The resulting hull structural loads at the corner of the web frame right after the impact with the water surface are very similar. As the corner of the

Table 6.3.: parametric study of hull structural loads based on simulations with FSI

conditions as planned for sideways launching process (baseline):

LC	μ_{sw} [-]	h_{wl} [m]	h_p [m]	$v_{sway\ impact}$ [m/s]	v_{slam} [m/s]
LAUNCH	$\mu_{sw\,0}$	$h_{wl\,0}$	$h_{p\,0}$	9.42	5.48

variation of loading condition:

LC	μ_{sw} [-]	h_{wl} [m]	h_p [m]	$v_{sway\ impact}$ [m/s]	v_{slam} [m/s]
LSW	$\mu_{sw\,0}$	$h_{wl\,0}$	$h_{p\,0}$	9.55	5.51

variation of height of drop:

LC	μ_{sw} [-]	h_{wl} [m]	h_p [m]	$v_{sway\ impact}$ [m/s]	v_{slam} [m/s]
LAUNCH	$\mu_{sw\,0}$	$h_{wl\,0}$	$h_{p\,0} + 0.50$	9.94	6.32

variation of coefficient of friction:

LC	μ_{sw} [-]	h_{wl} [m]	h_p [m]	$v_{sway\ impact}$ [m/s]	v_{slam} [m/s]
LAUNCH	$0.50 \cdot \mu_{sw\,0}$	$h_{wl\,0}$	$h_{p\,0}$	10.00	5.57

web frame is highly loaded during the sideways launching process, local plastic deformation combined with out-of-plane buckling can be observed. The higher loads by an increased height of the drop result in higher plastic deformations, while the resulting hull structural loads as shown in the form of stresses remain on a similar level (compare Figure 6.13a).

Besides a higher v_{slam}, the increase of the height of drop is joined by an increase of $v_{sway\ impact}$. Table 6.3 shows, that the increase of h_p by 0.50m is corresponding to an increase of $v_{sway\ impact}$ of approx. 5.5%. Based upon Figure 6.13b, the increase of $v_{sway\ impact}$ correlates directly with an increase of the hull structural load inside the bulkhead plating resulting from load mechanism 02. The resulting membrane stresses are offset by nearly $0.25 \cdot \sigma_{perm}$ if compared to $h_{p\,0}$ (compare Figure 6.13b), while the offset of the resulting shear stresses oscillates between $0.10 \cdot \tau_{perm}$ and $0.20 \cdot \tau_{perm}$ (compare Figure A.40f).

The same effect is given, if the coefficient of friction μ_{sw} was decreased. As Table 6.3 suggests, a decrease of the coefficient of friction to $0.50 \cdot \mu_{sw\,0}$ does result in approx. the same $v_{sway\ impact}$ as in increase of h_p by 0.50m. A similar offset of the resulting hull structural loads due to the deceleration of the ship's hull structure can be observed. The resulting membrane stresses are offset by roughly $0.20 \cdot \sigma_{perm}$ if compared to $\mu_{sw\,0}$ (compare Figure 6.14b), while the offset of the resulting shear stresses is corresponding to approx. $0.25 \cdot \tau_{perm}$ (compare Figure A.41f).

Only the distribution of the resulting hull structural loads due to load mechanism 02 differs slightly (membrane $\leftrightarrow$ shear stresses). This is due to different angle between the ship and the water surface at the moment of impact ($\varphi_{x\ impact} = 14.1°$ for $h_p = h_{p\,0} + 0.50$m vs $\varphi_{x\ impact} = 12.5°$ for $\mu_{sw} = 0.50 \cdot \mu_{sw\,0}$) combined with a slightly different trajectory of the ship. A decrease of the coefficient of friction results in higher shear stresses inside the bulkhead plating. Due to the observed failure mode of shear buckling, higher shear stresses are more critical regarding the design of the hull structure of the SPV. That means, that the coefficient of friction μ_{sw} between the slipway and palls has to be known very precisely

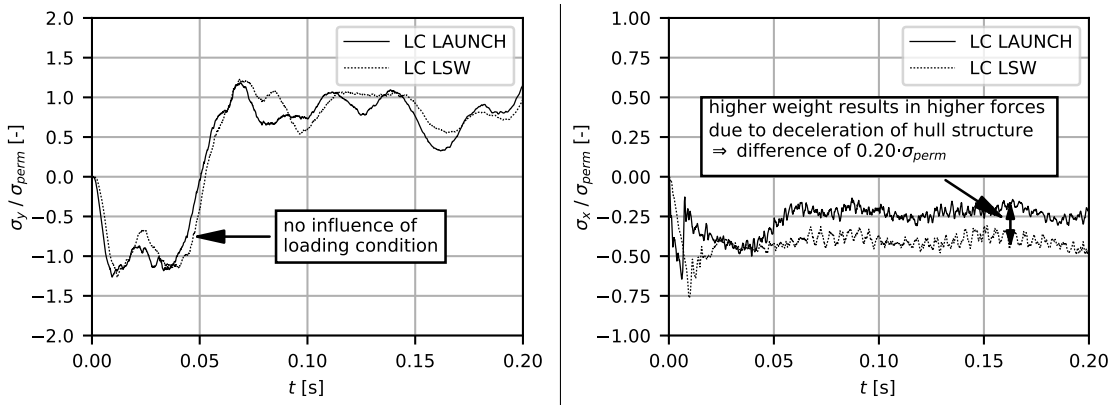

(a) corner of web frame (middle surface) (b) bulkhead plating (middle surface)

Figure 6.12.: resulting hull structural loads — influence of different loading conditions (combined FEM model of SPV)

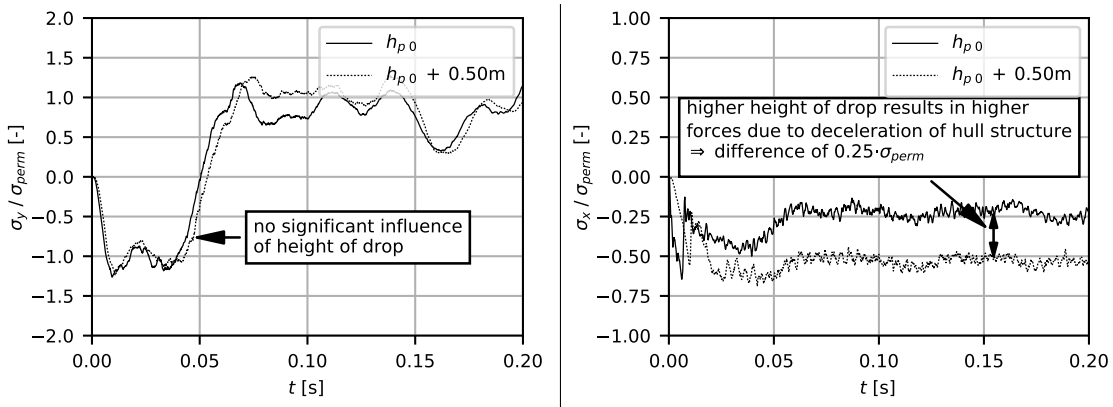

(a) corner of web frame (middle surface) (b) bulkhead plating (middle surface)

Figure 6.13.: resulting hull structural loads — influence of drop height (combined FEM model of SPV + LC LAUNCH)

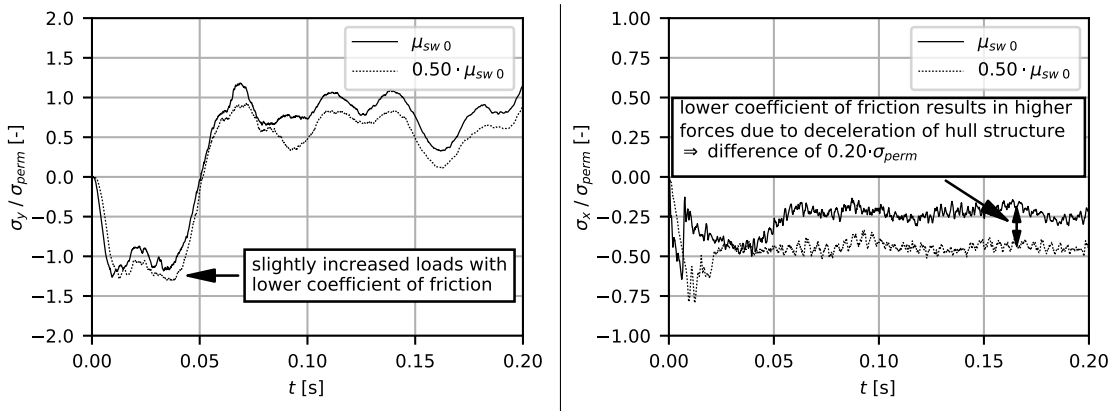

(a) corner of web frame (middle surface) (b) bulkhead plating (middle surface)

Figure 6.14.: resulting hull structural loads — influence of friction (combined FEM model of SPV + LC LAUNCH)

before the sideways launching process, to avoid potential damages due to load mechanism 02.

For investigating the influence of different loading conditions, the resulting hull structural loads of both LC LAUNCH and LC LSW were assessed and compared. Especially the difference of the weight of the SPV is of interest. The SPV is nearly 11.2% heavier based on LC LSW compared to LC LAUNCH (compare Table A.5). As Figure 6.12a indicates, the resulting hull structural loads due to the impact with the water surface (load mechanism 01) are virtually identical between both loading conditions. No significant difference of the resulting hull structural loads inside the corner of the web frame can be observed. This is to be expected, as the conditions at impact with the water surface were very similar (compare Table 6.3).

In contrast to load mechanism 01, the resulting hull structural loads due load mechanism 02 are influenced noticeable by the loading condition. Based on Figure 6.12b an offset of around $0.20 \cdot \sigma_{perm}$ of the membrane stresses inside the bulkhead plating is given by the higher weight of the SPV at LC LSW compared to LC LAUNCH. The resulting offset of the shear stresses is even higher with up to $0.40 \cdot \tau_{perm}$ (compare Figure A.39f). The influence of the loading condition on the resulting shear stresses inside the bulkhead plating is the highest of all three parameters investigated.

The loading condition used for the sideways launching process is to be monitored very carefully during the design as well as construction phase of the SPV. Not only is the ship motion — especially the maximal resulting roll angle — very sensitive regarding the position of the COG, but also are the resulting hull structural significantly influenced by the weight of the SPV. This is especially true load mechanism 02 (deceleration of the hull structure of the SPV).

Comparison to simulations without FSI

A comparison of the resulting hull structural loads with both simulation-based approaches for the highly loaded areas of the SPV is given in Appendix A.12 (see Figure A.36). This comparison is based upon the combined FEM model of the SPV and load model based on the model tests as proposed in section 5.3.2.

The loads after impact with the water surface acting upon the shell plating and its supporting structural members (load mechanism 01) show good agreement between the simulation-based approach without FSI and using FSI. As Figure 6.15a demonstrates, the hull structural loads resulting within the web frame due to load mechanism 01 are very similar. The same is true for the shell plating. The resulting plastic bending deformation is almost identical for the investigated panel of the shell plating, as Figure A.36b shows. In general, the hull structural loads resulting from load mechanism 01 are slightly higher using the simulations with FSI. Based on Figure A.36 the difference for the investigated shell plating as well as web frame are approx. 10%.

The main difference between the simulation-based approaches without FSI and using FSI is, that the simulations without FSI are not able to account for hull structural loads resulting from the deceleration of hull structure of the SPV (load mechanism 02). The simulations without FSI showed no switch of the loading direction inside the corner of the web frame. No significant membrane or shear stresses inside the bulkhead plating can be observed (see Figure 6.15b). In addition, no shear buckling of the bulkhead was induced during simulations without FSI (compare Figure 6.15b).

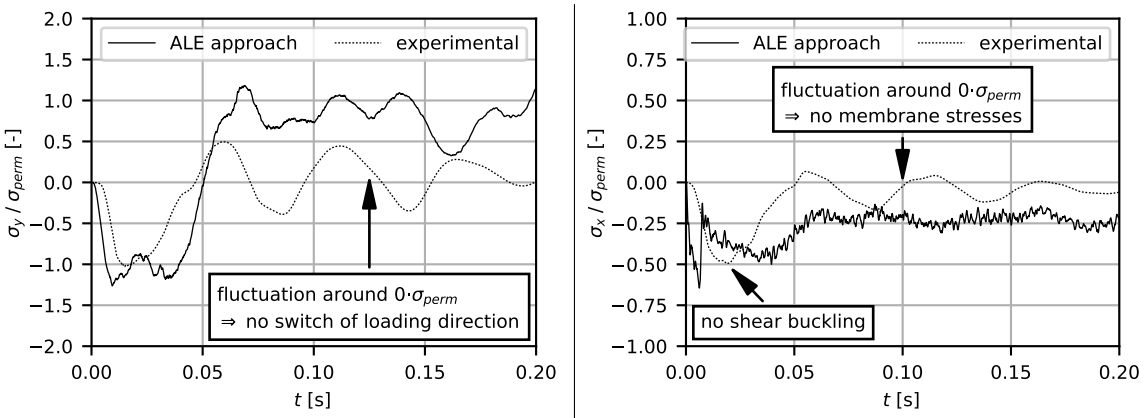

(a) corner of web frame (middle surface)

(b) bulkhead plating (middle surface)

Figure 6.15.: resulting hull structural loads — comparison between simulations without and with FSI (combined FEM model of SPV + LC LAUNCH)

Therefore, corresponding damages / failure modes linked to load mechanism 02 cannot be assessed using the simulation-based approach without FSI. As explained above, the potential damages due to this load mechanism could be severe if progressive collapse behavior would be induced into the hull structure of the SPV. The resulting hull structural loads inside the highly loaded bulkheads are to be assessed ideally with the proposed simulation-based approach using FSI to ensure a safe sideways launching process of the SPV.

Influence of FEM models of hull structure

Two different FEM models of the SPV were used within the simulation-based approach using FSI: the detailed FEM model of the highly loaded area as well the combined FEM model of the SPV (see section 5.2 regarding details for FEM models). A comparison of the resulting hull structural loads for both FEM models of the SPV is provided in Appendix A.12 (see Figure A.38). As the simulation-based approach without FSI showed, the global FEM model of the SPV is not able to asses the resulting hull structural loads sufficiently and is therefore not considered for the simulation-based approach using FSI.

One major drawback of the detailed FEM model of the SPV for the use with the simulation-based approach using FSI is, that not the complete hull structure of the SPV is modelled. The mass and moments of inertia of the complete hull structure is not accounted for. In an attempt to account for the missing hull structure, two different BC are investigated for the detailed FEM model of the SPV, which are provided in Appendix A.5 (compare Figure A.16 for BC_03 and Figure A.17 for BC_04). While using BC_03, the FEM model is just dropped onto the water surface and is allowed to move freely. This setup is comparable to the one described in section 6.1. For BC_04 the detailed FEM model is forced onto a given trajectory to overcome the missing weight / inertia of the missing hull structure. The trajectory is estimated based on the analytical approach.

Both BC_03 and BC_04 are able to account for the resulting hull structural loads right after impact with the water surface (load mechanism 01). This can be seen in Figure A.38a and A.38c. However, using BC_03 the inertia of the missing of the hull structure is not accounted for. The detailed FEM model is not able to immerse properly into the

water. The process can be compared to skipping a stone above a water surface. Due to this behavior, only BC_04 is able to account for the forces due to the deceleration of the hull structure of the SPV (load mechanism 02). However, deviations from the combined FEM model regarding the hull structural loads resulting in the bulkhead plating can be observed. Near the constrained equations on top of the bulkheads (compare Figure A.17), the stresses inside the bulkhead plating are higher compared to the combined FEM model. Farther away from the constrained equations (near the bottom structure) the resulting stresses are lower compared to the combined FEM model. This can be seen in Figure A.38e. As explained above, due to the potential failure mode of load mechanism 02, the resulting hull structural loads inside the bulkhead plating are to be assessed very carefully.

Therefore, the use of the detailed FEM model within the simulation-based approach using FSI cannot be recommended, as the necessary BC are joined by deviations of the hull structural loads compared to the combined FEM model. As the simulations with combined FEM model are set up as described in section 6.1, no additional BC are necessary, which could potentially alter or falsify the resulting hull structural loads. In addition, the combined FEM model allows for the assessment of the ship motion. All relevant aspects (ship motion as well as resulting hull structural loads) can be assessed using just one simulation with one FEM model of the SPV.

6.6. Benefits and limitations

One of the most important aspects of the proposed simulation-based approach using FSI is the identification of a second load mechanism ($\rightarrow$ deceleration of hull structure) as illustrated in Figure 6.10. Especially regarding the design of the hull structure of the SPV this second load mechanism is of relevance. As discussed above, the second load mechanism could potentially result in progressive collapse behavior, if bigger parts of the bulkhead plating undergo shear buckling. In a worst case scenario this could result in local failure of the hull structure at the affected area. As the simulation-based approach without FSI did not show this second load mechanism, the resulting hull structural loads would not have been accounted for during the design of the SPV. Damages to the hull structure of the SPV would have been possible in that case.

The biggest benefit of the simulation-based using FSI is, that all physical phenomena relevant during the sideways launching process of the SPV — such as added masses around the ship hull, loads at impact with the water surface (slamming events), interaction between the ship's hull structure and the free water surface (elevation of water surface / formation of spray root as well as effects of hydro-elasticity), loads due the declaration of the ship's hull structure among others — can be assessed simultaneously using just one simulation model. The simulation-based approach using FSI allows for a holistic investigation considering all those effects as closely to the conditions present at a full scale sideways launching process as possible. Both the ship motion as well as the resulting hull structural loads during a sideways launching process can be assessed using only one simulation model.

As only one FEM model of the SPV is needed, quick changes of the model considering updates of the ship design like an updated weight distribution or changes made to the design of the hull structure (e.g. weight optimizations) can be considered quickly. Combined with a modular approach for the setup of the ALE approach, the modelling effort is reduced to a point, that allows for parametric studies regarding the resulting hull structural loads

during the ongoing ship design process. This is true, even though the simulation models are big (10+ millions elements). The simulation-based approach using FSI was successfully deployed during the ship design process of the SPV, in order to derive measures for reinforcing the hull structure regarding the hull structural loads resulting during the sideways launching process. Even weight optimizations of these measures were possible within a limited time frame due to the start of the construction of the SPV.

In order to exploit the full potential of the ALE approach, a FEM model of a complete hull structure is necessary. A partial FEM model of the SPV (e.g. the detailed FEM model of the highly loaded areas) was not capable to consider all effects accordingly, as the stiffness and inertia of the complete hull structure were missing. This results in a higher modelling effort compared to the simulation-based approach without FSI, where the results of a partial FEM and complete FEM model showed reasonable agreement regarding the resulting hull structural loads in the case of the SPV. However, for modelling the complete hull structure the ship design has to be at a certain point ($\rightarrow$ basic design).

One of the biggest limitations and drawbacks of the proposed simulation-based approach using FSI is the necessary computational effort of the ALE approach. By considering optimization of the FSI settings as well as the general setup of the ALE approach inside LS-DYNA, the computational effort could be reduced by a significant factor of approx. 70% compared to the baseline used within [98]. However, the computational effort is still about two times higher compared to the simulation-based approach without FSI. Especially for the assessment of the ship motion a lot of computational time is necessary. Roughly 16 days were required for determining the maximum roll angle of the SPV.

Besides the computational effort, another drawback is the complexity of the ALE approach itself and the FSI algorithm based on the penalty method. A lot of specialized knowledge and experience are necessary, as settings for the FSI algorithm are specific for each use case [59]. Parametric studies of the setup of the ALE approach (e.g. the mesh density ratio between ALE and Lagrangian elements) as well as different FSI settings (e.g. scale factors for stiffness and damping of penalty method) are highly recommended [9], [10], [107]. Additionally, verification based on experiments or model tests are advisable [117], [118]. These two aspects raise the initial costs for the the successful setup of the proposed simulation-based approach using FSI. But overall, the benefits of the ALE approach (all physical phenomena relevant during the sideways launching process of the SPV covered with just one simulation model) did pay off these initial costs during the design process / different design phases of the SPV.

7. Discussion of results

After investigating the sideways launching process of the SPV with different approaches, the obtained results are discussed within this chapter. Firstly, newfound insights regarding the mechanics of sideways launching of ships are summarized. Afterwards the results and applicability of the different approaches regarding the sideways launching process of the SPV are compared and evaluated. Before the research questions are outlined and an evaluation of the research hypothesis is given in chapter 8, the consequences of the obtained results regarding the design of the SPV are presented briefly.

7.1. Newfound insights regarding the mechanics of sideways launching

Within this work parametric studies of the sideways launching process of a SPV were conducted. Different loading conditions (position of COG and weight of SPV), height of palls / change of water level inside launch basin (= height of drop of SPV around edge of pier) as well as coefficient of friction between palls and slipway were considered. The influence of these parameters on the resulting ship motion as well as the resulting loads was investigated.

Regarding the ship motion the maximal roll angle is one of the most important parameters (range of stability / prevention of further flooding). As discussed in detail in section 4.3.2, the position of the COG in z-direction has the most significant influence on the maximal roll angle. A non-linear dependency between the position of the COG and the maximal roll angle was observed, meaning that even a small shift of the COG can result in a significant increase of the resulting maximal roll angle. This dependency in case of the SPV is visualized in Figure 4.10c based upon the results obtained with the experimental approach (model tests). As Figure 4.10 illustrates, the influence of the other two parameters (coefficient of friction between palls and slipway and height of drop around edge of pier) on the maximum roll angle is negligible compared to the influence of the position of the COG.

Based on the proposed simulation-based approach using FSI two distinct load mechanisms acting upon the hull structure could be observed. The first load mechanism is the impact of the SPV with the water surface comparable to slamming events (asymmetrical slamming event with oblique speed). The loads resulting from this load mechanism are acting upon the shell of the hull structure and are transferred into its supporting structure (web frames and bottom structure). The second load mechanism is caused by transversal forces due to the deceleration of the hull structure of the SPV after immersing into the water. The bottom structure of the SPV is decelerated, while the upper part wants to remain its transversal motion due to the inertia of the hull structure. This behavior results in high shear stresses inside transversal members of the hull structure, especially inside bulkhead platings of the SPV.

As the deadrise angle of the SPV is approx. zero degree for all investigated configurations of the sideways launching process, the speed of the ship hull relative to the water surface at the moment of impact is the most relevant parameter regarding the first load mechanism (impact with water surface). The speed at impact is influenced by the height of the drop around the edge of pier, which is given defined by the height of palls and water level inside

launch basin. The influence of this parameter on the resulting hull structural loads is discussed in detail in section 6.5.2. Based on the model tests as discussed in section 4.3.2, an increase of the drop height of around 1m results in an increase of the loads on the ship hull of approx. 18%.

The hull structural loads resulting from the second load mechanism (deceleration of hull structure) are influenced by two distinct parameters, as discussed in detail in section 6.5.2. The first parameter is the speed in transversal direction (sway motion) of the SPV at the moment of impact with the water surface, which is defined by the coefficient of friction between the palls and slipway. As Figure 6.14b shows, the resulting stresses inside the bulkhead plating are significantly increased with an decreased coefficient of friction: halving the coefficient of friction did result in nearly a doubling of the stresses resulting inside the bulkhead plating. The second important parameter is the weight of the SPV (loading condition). An increase of the weight of the SPV of nearly 12% (loading condition as planned for launching → fully equipped SPV) did correspond to a doubling of the stresses resulting inside the bulkhead plating as well, as Figure 6.12b illustrates.

For the design of a hull structure against the hull structural loads resulting during a sideways launching process, both load mechanisms are to be accounted for accordingly. In case of the SPV, the second load mechanism (deceleration of hull structure) is more critical regarding the safety of the hull structure. This is discussed in detail in section 6.5.2.

7.2. Comparison and evaluation of different approaches

In order to evaluate the research hypothesis postulated within this work, the sideways launching process of SPV was investigated using different approaches. This allows for a comparison of the different approaches with the proposed simulation-based approach using FSI based on an ALE approach. Besides the ALE approach, conventional approaches — including a rule-based approach, analytical formulations as well as the use of model tests — and simulations without FSI were applied to the sideways launching process of the SPV. An in-depth discussion of benefits and limitations associated with each of these approaches is provided at the end of the corresponding sections / chapters.

According rules and regulations of the most common classification societies of IACS do not provide any approaches to assess a sideways launching process itself or the resulting hull structural loads. Most applicable would be design loads for the event of bottom slamming. However, as discussed in section 5.4.2, applicable design loads for bottom slamming were almost a factor of two lower compared to the results obtained from model tests of the sideways launching process of the SPV. Using solely a rule-based approach would result in an underestimation of the resulting hull structural loads.

Within the context of the investigated analytical approaches, the proposed ODE of motion were only able to assess the ship motion up to the point of the first contact of the SPV with the water surface. As the proposed ODE of motion are not able to account for the interaction of the water surface with the ship hull, the hydrodyanmic forces and resulting moments acting upon the hull of the SPV are estimated wrongly. Even a combination of the corresponding ODE of motion with a hydrodynamic code to predict the hydrodyanmic forces on a more detailed level as proposed in [38], [54], shows discrepancies between the obtained results and their respective reference cases.

Commonly used analytical models (e.g. OLM, GWM or MLM), that are able to account

for interaction of a ship hull and the water surface as well as the impact loads due to slamming, are not applicable for the conditions as given during the sideways launching process of the SPV. At the moment of impact of the SPV a three DOF motion is given with a high degree of asymmetry (high ratio of horizontal to vertical velocity combined with a deadrise angle of approx. zero degree), for which the best-suited model proposed in [44] did show bigger differences between experimental data and the proposed model.

The experimental approach based on model tests of the sideways launching process is an excellent choice for conducting parametric studies (see above for details regarding the investigated parameters). With a sufficient test matrix a wide design space and limits for a safe sideways launching process could be assessed quickly. This is true for the ship motion (e.g. maximal roll angle) as well as the resulting loads on the ship hull. In addition, model tests are an excellent choice regarding a verification of other approaches including the proposed simulation-based approach using FSI.

However, as the experimental approach did not allow for a direct assessment of the resulting hull structural loads, the combination of the experimental approach with a simulation-based approach without FSI is necessary. During model tests the pressure-time-signals at different points of the hull of the SPV were measured, which allowed for the derivation of a load model based upon the obtained experimental results as proposed in [100]. Compared to the proposed simulation-based approach using FSI a combination of these two approaches is more expensive to obtain both the ship motion ($\rightarrow$ experimental approach) and the resulting hull structural loads ($\rightarrow$ simulation-based approach without FSI). The planning, setup and conduction of model tests, derivation of a suitable load model, setup and conduction of simulations without FSI with according FEM models of the hull structure of the SPV are necessary. This sequential workflow does not allow for any too drastic changes during the planning of a sideways launching process or of the ship design (e.g. changes of the shape of the hull).

This is one of the biggest advantages of the simulation-based approach using FSI. With the ALE approach both the ship motion as well as the resulting hull structural loads inside the SPV can be assessed simultaneously. Only one approach and simulation model of the SPV was necessary. As shown within this work, the proposed simulation-based approach using FSI allows assessing the relevant aspects and physical phenomena of a sideways launching process on a very detailed level. A verification of the ALE approach showed very good agreement between the results obtained from the experimental approach and simulations using FSI. The ship motion can be captured very well with ALE approach. The same is true for the loads resulting on the ship hull. As the ALE approach enables a detailed assessment of the resulting hull structural loads including the localization of areas above permissible stress levels, each of the different measures for reinforcing the hull structure were limited to the smallest extent possible. All measures were optimized regarding their weight using the ALE approach.

One important aspect to mention is, that the second load mechanism (deceleration of hull structure) could only be observed based on the simulation-based approach using FSI [101]. If only common approaches were used for assessing the sideways launching process of the SPV, no measures for reinforcing the hull structure against the second load mechanism would be considered.

All investigations with the ALE approach were made during the ongoing design process of the SPV. This proves that simulations using FSI can be utilized as an active design tool. The necessary computational resources and time frames of the ALE approach, which

are usually considered as one of the biggest drawbacks, are nowadays on an acceptable level. The influence of different measures to reduce the necessary computational effort of the ALE approach is discussed in section 6.4 of this work. In total, about three days of computational time are necessary for the assessment of the resulting hull structural loads. However, the necessary computational effort of the ALE approach is still two times higher compared to the simulation-based approach without FSI.

7.3. Consequences regarding the design of the special purpose vessel

The results of the simulation-based approach were used as the basis for the planning of the sideways launching process of the SPV. As discussed in section 6.5.1, both loading conditions investigated are safe to use with regards to the ship motion. With a maximal roll angle below 40°, only minor green water can be observed on the main deck. The ship motion obtained with the ALE approach was further used to determine the height of the waterline on each side of the SPV. This allowed for a check, which openings inside the shell of the SPV will come into contact with the water and are to be closed to prevent further flooding of the SPV during the sideways launching process.

The design of the hull structure of the SPV against the loads resulting during the sideways launching process was done based on the results with the ALE approach as well. As investigated in section 6.5.2, the loading condition of the SPV ($\rightarrow$ weight) has a significant influence on the resulting hull structural loads. This is especially true for the second load mechanism (deceleration of hull structure) and the resulting hull structural loads inside the bulkhead plating. Therefore, LC LSW (light ship weight / fully equipped SPV) was used as the basis for the design of the hull structure of the SPV. By doing so, a safety margin for the progression of the construction progress / level of outfitting is accounted for. An example could be an incorrect weight calculation or a delay of the sideways launching process ($\rightarrow$ higher level of outfitting as initially planned).

As shown in section 6.5.2, the resulting hull structural loads at highly loaded areas of the SPV as illustrated in Figure 5.1 are above permissible limits for the initial design of the hull structure. Local plastic bending deformation of the shell plating and out-of plane buckling of supporting web frames could be observed (second load mechanism $\rightarrow$ impact with water surface). Additionally, shear buckling including plastic out-of-plane deformation could be observed for specific parts of the bulkhead plating (second load mechanism $\rightarrow$ deceleration of hull structure). Using the ALE approach, different measures for reinforcing the hull structure of the SPV at these highly loaded areas were investigated. As the ALE approach allows for a very detailed assessment of the resulting hull structural loads and localization of areas above permissible limits, each of the different measures were limited to these exact parts of the hull structure. Furthermore, all measures for reinforcing the hull structure against the loads during the sideways launching process were optimized regarding their weight using the ALE approach.

In total, about 40 iterations of the hull structure were investigated with the simulation-based approach using FSI. The additional weight of all measures could be reduced to approx. 1.5t of additional steel weight. These investigation as well as the measures for reinforcing the hull structure were obtained within a limited time frame of approx. 30 days, which was given by the start of the construction of the SPV.

8. Conclusion

Although a sideways launching process is a common way to launch different type of ships, its assessment is complex. Different physical phenomena are to be covered by an approach of choice. This includes the ship motion (six DOF motion with according equation of motions including added masses and hydrodynamic damping). The free water surface and its interaction with the ship hull plays an important role (formation of spray root and waves around the ship hull). Dynamic loads at the impact of the ship hull with the water surface comparable to slamming events can be observed, for which the resulting hull structural loads are to be assessed. Depending on the configuration given at the moment of impact of a ship with the water surface, effects of hydro-elasticity can be relevant as well.

Based on the current state of the art different research questions joined by an according research hypothesis are formulated in section 2.4.1 of this work. To answer the different research questions, the sideways launching process of a SPV is investigated using different approaches. A simulation-based approach using FSI based on an ALE approach is proposed within this work. The results obtained with the proposed simulation-based approach using FSI are compared to common approaches, which include a rule-based approach, analytical formulations, the use of model tests as well as simulations without FSI.

Before evaluating the research hypothesis, the answers to the research questions are briefly summarized. A more detailed discussion of the obtained results and the comparison of the different approaches regarding their applicability for the sideways launching of ships can be found in chapter 7. Due to missing knowledge in the discussed state of the art, the first research question asked within this work is as follows:

> How do the loads on a ship hull during the different phases of a sideways launching process look like as a function of time?

During model test of the sideways launching process of the SPV pressure-time-signals were measured, that are typically observed during slamming events. A harsh peak pressure acting only for a few milliseconds joined by a quick decay of the pressure could be observed. Based on these results a load model for assessing the pressure on the ship hull in the case of simulations without FSI is proposed within this work, which considers the conditions of a ship at the moment of impact with the water surface (speed as well as deadrise angle).

Following the loads resulting on a ship hull, the next research questions are concerned with the resulting hull structural loads:

> Which hull structural loads can be observed during a sideways launching process at different parts of the hull structure? What are the main load mechanisms acting upon the hull structure?

Based on simulations without FSI a load mechanism comparable to slamming events was observed. The loads resulting from the impact of the ship hull with the water surface act upon the shell of the hull structure and are transferred into its supporting structure. Based on the proposed simulation-based approach using FSI a second load mechanism during the sideways launching process of the SPV could be observed. This second load mechanism is caused by transversal forces due to the deceleration of the hull structure after immersing into the water. The bottom structure is decelerated, while the upper part wants to remain

its transversal motion due to the inertia of the hull structure. This behavior results in high shear stresses inside transversal members of the hull structure.

From a design point of view it is important to know, which parameters of the sideways launching processes do influence the resulting hull structural loads / load mechanisms as well as the ship motion to ensure a safe sideways launching of a ship. This results in the following research questions:

> Which parameters of a sideways launching process are the most relevant ones regarding the ship motion as well as the resulting loads on the hull structure / hull structural loads? How big is the influence of each parameters on the different aspects of a sideways launching process?

As the model tests showed, the maximal roll angle as one of the most important parameters regarding the ship motion is very sensitive regarding the position of the COG in z-direction of a ship (non-linear dependency). The influence of the investigated parameters on the hull structural loads is different for both load mechanisms. The hull structural loads resulting from the first load mechanism (impact with water surface) are mainly influenced by the conditions given at the impact with the water surface (speed and deadrise angle). These conditions are defined to a great extent by the height of the palls and the water level inside the launch basin (increase of height of drop around the edge of pier of 1m $\rightarrow$ increase of 18% of loads on ship hull). The second load mechanism is influenced by two parameters: the weight of the ship and the coefficient of friction between the palls and slipway (halving of coefficient of friction / increase of weight of approx. 12% $\rightarrow$ doubling of the stresses inside bulkhead plating). Note, that these relationships were obtained for the investigated SPV and could differ for other ships / ship types.

Besides these insights regarding the mechanics of sideways launching of ships, from a methodical point of view a reliable tool for predicting and assessing all relevant phenomena during the ship design process is of importance. This yields in the last research question:

> How does a setup of a sufficient and reliable simulation-based approach look like, which is able to account for the relevant physical effects of asymmetrical slamming events as present during a sideways launching process?

A simulation-based approach using FSI based on an ALE approach is proposed and presented in detail within this work. The ALE approach allows assessing the relevant aspects and physical phenomena of a sideways launching process as given above. The verification of the ALE approach showed very good agreement with the results obtained from the model tests of the sideways launching process of the SPV. Furthermore, by optimizing the computational effort of the ALE approach, it is feasible to incorporate these simulations using FSI within the ongoing ship design process.

Based on these research questions, the following research hypothesis regarding the different approaches applicable to assess a sideways launching process is derived in section 2.4.1 of this work:

> A simulation-based approach using FSI is the best-suited choice for assessing water entry problems / slamming phenomena like a sideways launching process of a ship, as these are the only approaches able to consider all relevant physical aspects and phenomena accordingly allowing for a holistic assessment and optimization of a ship design.

The findings within this work confirm the research hypothesis. In contrast to the investigated common approaches, the proposed simulation-based approach using FSI is able to account for all relevant and physical phenomena during the sideways launching of a ship sufficiently. The ALE approach is the only approach allowing for a simultaneous assessment of the ship motion and resulting hull structural loads. New insights into the mechanics of sideways launching of ships could be obtained. Notably, only the proposed simulation-based approach using FSI was able to account for the second load mechanism (deceleration of hull structure). Therefore, only with the ALE approach the influence of different parameters of the sideways launching process on both load mechanisms could be assessed. For the investigated case study of the sideways launching process of a SPV, the planning was completely based upon the obtained simulation results. The ALE approach was used to reinforce the hull structure of the SPV against the resulting hull structural loads during the sideways launching process. These measures were limited precisely to the highly loaded areas of the hull structure and were optimized regarding the least additional weight.

However, the simulation-based approach using FSI proposed within this work is accompanied by one limitation regarding the postulated research hypothesis. The ALE approach with the FSI algorithm based on the penalty method is very complex compared to simulations without FSI or even other simulation-based approaches using FSI. A lot of experience and specialised knowledge is necessary to successfully apply this method, as settings for the FSI algorithm are specific for each use case [59]. Parametric studies of the setup of the ALE approach as well as of different FSI settings are highly recommended [9], [10], [107]. Additionally, verification based on experiments or model tests are advisable [117], [118].

For the sideways launching process of the SPV such parametric studies regarding the setup of the ALE approach and FSI settings as well as a verification based on model tests were conducted thoroughly. A very good agreement between the results obtained from the model tests and the ALE approach could be observed. However, the parametric study and verification rose the initial costs for the the successful setup of the proposed simulation-based approach using FSI. But overall the above mentioned benefits of the ALE approach did pay off these initial costs during the design process / different design phases of the SPV. This is still true, even if the costs of the model tests for the verification of the ALE approach are accounted for. The costs of the conducted model tests combined with the initial costs of the simulation-based approach using FSI are low compared to the total budget involved for the design and construction of the investigated SPV and the risks associated with an insufficiently planned sideways launching process of the SPV.

In order to reduce the initial costs with such a simulation-based approach using FSI for other, similar applications, all necessary information for a setup of the ALE approach are provided in this work. This includes the material models and general setup of the ALE approach within the main part of this work. In addition, all findings regarding different settings of the FSI algorithm are provided within Appendix A.10. Besides the investigated use case of a sideways launching process, these results are a sound basis for the assessment of other slamming phenomena or water entry problems. Due to the investigated configuration of the sideways launching process of the SPV, these settings are a very good starting point for other asymmetric slamming / water entry problems with oblique speed. E.g. the provided setup and settings of the ALE approach within this work can be used to extend the current research / state of the art such as [64], [112] regarding asymmetric slamming events of ship hull structures using a two-way FSI considering the effects of hydro-elasticity.

Bibliography

[1] S. Abrate, "Hull Slamming," *Applied Mechanics Reviews*, vol. 64, no. 6, pp. 60 803–1–60803–35, 2011. DOI: 10.1115/1.4023571.

[2] M. Adoum and V. Lapoujade, "Examples' manual for *USER_LOADING option," in *Proceedings of 4th European LS-DYNA® Users Conference*, Ulm, Germany, 2003, G–I–29–G–I–38.

[3] American Bureau of Shipping, *Guide for Slamming Loads and Strength Assessment for Vessels* (Edition December 2021). Houston, USA, 2021.

[4] American Bureau of Shipping, *Rules for Building and Classing High Speed Craft* (Edition January 2022). Houston, USA, 2022.

[5] American Bureau of Shipping, *Rules for Building and Classing Light Warships, Patrol and High-Speed Naval Vessels* (Edition January 2022). Houston, USA, 2022.

[6] American Bureau of Shipping, *Rules for Building and Classing Marine Vessels* (Edition January 2022). Houston, USA, 2022.

[7] N. Aquelet, M. Souli, and L. Olovsson, "Euler–Lagrange coupling with damping effects: Application to slamming problems," *Computer Methods in Applied Mechanics and Engineering*, vol. 195, no. 1, pp. 110–132, 2006. DOI: 10.1016/j.cma.2005.01.010.

[8] N. Aquelet, "ALE Adaptive Mesh Refinement in LS-DYNA®," in *Proceedings of 12th International LS-DYNA® Users Conference*, Detroit, USA, 2012, pp. 1–20.

[9] D.-M. Bae and A. F. Zakki, "Comparisons of multi material ALE and single material ALE in LS-DYNA for estimation of acceleration response of free-fall lifeboat," *Journal of the Society of Naval Architects of Korea*, vol. 48, no. 6, pp. 552–559, 2011. DOI: 10.3744/SNAK.2011.48.6.552.

[10] D.-M. Bae, A. F. Zakki, H.-S. Kim, and J.-G. Kim, "Estimation of acceleration response of freefall lifeboat using FSI analysis technique of LS-DYNA code," *Journal of the Society of Naval Architects of Korea*, vol. 47, no. 5, pp. 681–688, 2010. DOI: 10.3744/SNAK.2010.47.5.681.

[11] A. Bayatfar, A. Amrane, and P. Rigo, "Towards a Ship Structural Optimisation Methodology at Early Design Stage," *International Journal of Engineering Research and Development*, vol. 9, no. 6, pp. 76–90, 2013.

[12] W. J. C. Boef, "Launch and impact of free-fall lifeboats. Part I. Impact theory," *Ocean Engineering*, vol. 19, no. 2, pp. 119–138, 1992. DOI: 10.1016/0029-8018(92)90011-R.

[13] W. J. C. Boef, "Launch and impact of free-fall lifeboats. Part II. Implementation and applications," *Ocean Engineering*, vol. 19, no. 2, pp. 139–159, 1992. DOI: 10.1016/0029-8018(92)90012-S.

[14] M. Bohm, O. Heine, T. Arndt, and R. Moritz, "Best Practice Application between AVEVA Hull Finite Element Modeler and ANSYS Workbench for Detailed Design Phase in Shipbuilding Industry," in *Proceedings of ANSYS Conference & 32nd CADFEM Users' Meeting*, Nuremberg, Germany, 2014.

[15] P. Bourke, "Calculating the area and centroid of a polygon," *Swinburne University of Technology*, vol. 7, 1988.

[16] K. S. Burchard, "Einfluss von Massen im Rahmen dynamischer Finite-Elemente Analysen von Überwasserschiffen," M.S. thesis, Technische Universität Hamburg-Harburg, Hamburg, Germany, 2017.

[17] Bureau Veritas, *Rules for the Classification of Naval Ships (NR 483)* (Edition October 2020). Paris, France, 2020.

[18] Bureau Veritas, *Environmental Conditions Loads and Induced Responses of Marine Units (NI691)* (Edition December 2022). Paris, France, 2022.

[19] Bureau Veritas, *Rules for the Classification of Steel Ships (NR 467)* (Edition January 2022). Paris, France, 2022.

[20] A. Califano and K. Brinchmann, "Evaluation of Loads During a Free-Fall Lifeboat Drop," in *32nd International Conference on Offshore Mechanics and Arctic Engineering*, Nantes, France, 2013. DOI: 10.1115/OMAE2013-11350.

[21] China Classification Society, *Rules for Classification of Sea-Going Steel Ships* (Edition July 2022). Beijing, China, 2022.

[22] China Classification Society, *Rules for Construction and Classification of Sea-Going High Speed Craft* (Edition July 2022). Beijing, China, 2022.

[23] S.-L. Chuang, "Experiments on Slamming of Wedge-Shaped Bodies," *Journal of Ship Research*, vol. 11, no. 03, pp. 190–198, 1967. DOI: 10.5957/jsr.1967.11.3.190.

[24] G. R. Cowper and P. S. Symonds, "Strain-hardening and strain-rate effects in the impact loading of cantilever beams," Division of Applied Mathematics, Brown University, Tech. Rep. no. 28, 1957.

[25] DNV, *Recommended Practice: Environmental Conditions and Environmental Loads (DNV-RP-205)* (Edition October 2010). Høvik, Norway, 2010.

[26] DNV, *Class Guideline: Finite element analysis (DNV-CG-0127)* (Edition August 2021). Høvik, Norway, 2021.

[27] DNV, *Rules for classification: Ships (DNV-RU-SHIP)* (Edition July 2021). Høvik, Norway, 2021.

[28] DNV GL, *Rules for classification: Naval vessels (RU-NAVAL)* (Edition December 2015). Høvik, Norway, 2015.

[29] DNV GL, *Standard: Design of free-fall lifeboats (DNVGL-ST-E406)* (Edition January 2016). Høvik, Norway, 2016.

[30] J. Donea, A. Huerta, J.-P. Ponthot, and A. Rodríguez-Ferran, "Arbitrary Lagrangian-Eulerian Methods," in *Encyclopedia of Computational Mechanics*, E. Stein, R. de Borst, and T. J. R. Hughes, Eds., Hoboken, USA: John Wiley & Sons, 2004, pp. 413–437. DOI: 10.1002/0470091355.ecm009.

[31] S. Ehlers, J. Broekhuijsen, H. Alsos, F. Biehl, and K. Tabri, "Simulating the collision response of ship side structures: A failure criteria benchmark study," *International Shipbuilding Progress*, vol. 55, pp. 127–144, 2008. DOI: 10.3233/ISP-2008-0042.

[32] S. Ehlers and P. Varsta, "Strain and stress relation for non-linear finite element simulations," *Thin-Walled Structures*, vol. 47, no. 11, pp. 1203–1217, 2009. DOI: 10.1016/j.tws.2009.04.005.

[33] J. F. Epperson, *An Introduction to Numerical Methods and Analysis: Solutions Manual to Accompany*, Third Edition. Hoboken, USA: John Wiley & Sons, 2021. DOI: 10.1002/9781119604570.

[34] A. Fitriadhy and A. M. A. Malek, "Computational fluid dynamics analysis of a ship's side launching in restricted waters," *Journal of Mechanical Engineering and Sciences*, vol. 11, pp. 2993–3003, 2017. DOI: 10.15282/jmes.11.4.2017.3.0269.

[35] N. Fonseca, E. Antunes, and C. Guedes Soares, "Whipping Response of Vessels With Large Amplitude Motions," in *Proceedings of the 25th International Conference on Offshore Mechanics and Arctic Engineering*, vol. 2: Ocean Engineering and Polar and Arctic Sciences and Technology, Hamburg, Germany, 2006, pp. 433–442. DOI: 10.1115/OMAE2006-92412.

[36] D. F. Griffiths and D. J. Higham, *Numerical Methods for Ordinary Differential Equations: Initial Value Problems* (Springer Undergraduate Mathematics Series), ´. London, United Kingdom: Springer-Verlag London, 2010. DOI: 10.1007/978-0-85729-148-6.

[37] C. Guedes Soares, "Transient response of ship hulls to wave impact," *International Shipbuilding Progress*, vol. 36, no. 406, pp. 137–156, 1989.

[38] B. Hak, "Numerical simulation of the side launching of a ship," M.S. thesis, University of Groningen, Groningen, Netherlands, 2005.

[39] H. Hamashima, Y. Kato, and S. Itoh, "Determination of JWL Parameters for Non-Ideal Explosive," *AIP Conference Proceedings*, vol. 706, no. 1, pp. 331–334, 2004. DOI: 10.1063/1.1780246.

[40] S. Hiermaier, *Structures Under Crash and Impact: Continuum Mechanics, Discretization and Experimental Characterization*. New York, USA: Springer Science + Business Media, 2008. DOI: 10.1007/978-0-387-73863-5.

[41] J. H. Hollomon, "Tensile deformation," *Transactions of the American Institute of Mining, Metallurgical and Petroleum Engineers*, vol. 162, pp. 268–290, 1945.

[42] M. Izadi, P. Ghadimi, M. Fadavi, and S. Tavakoli, "Hydroelastic analysis of water impact of flexible asymmetric wedge with an oblique speed," *Meccanica*, vol. 53, no. 10, pp. 2585–2617, 2018. DOI: 10.1007/s11012-018-0846-y.

[43] M. J. Javaherian, Z. Ren, and C. Gilbert, "Flow Visualization, Hydrodynamics, and Structural Response of a Flexible Wedge in Water Entry Experiments," *Journal of Ship Research*, pp. 1–13, 2022. DOI: 10.5957/JOSR.12200060.

[44] C. Judge, A. Troesch, and M. Perlin, "Initial water impact of a wedge at vertical and oblique angles," *Journal of Engineering Mathematics*, vol. 48, no. 3, pp. 279–303, 2004. DOI: 10.1023/B:engi.0000018187.33001.e1.

[45] T. von Kármán, "The Impact on Seaplane Floats during Landing," National Advisory Committee for Aeronautics, Tech. Rep. no. 321, 1929.

[46] M. Kierstein, "144-Meter-Schiff rutscht bei Ferus Smit in den Hafen," *Ostfriesen Zeitung*, Published on November 18th, 2022.

[47] M. Kierstein, "Ferus-Smit-Werft: Neuer Tanker erfolgreich zu Wasser gelassen," *Ostfriesen Zeitung*, Published on January 8th, 2022.

[48] K. Kondo and M. Makino, "Crash Simulation of Large-Number-of-Elements Car Model by LS-DYNA on Highly Parallel Computers," *Fujitsu Scientific & Technical Journal*, vol. 44, no. 4, pp. 467–474, 2008.

[49] Korean Register of Shipping, *Rules and Guidance for the Classification of High Speed and Light Crafts (RB-11-E)* (Edition July 2022). Busan, Republic of Korea, 2022.

[50] Korean Register of Shipping, *Rules for the Classification of Steel Ships (RA-03-E)* (Edition July 2022). Busan, Republic of Korea, 2022.

[51] A. Korobkin and Š. Malenica, "Modified Logvinovich model for hydrodynamic loads on asymmetric contours entering water," in *20th International Workshop on Water Waves and Floating Bodies*, Oslo, Norway, 2005.

[52] A. Korobkin, "Analytical models of water impact," *European Journal of Applied Mathematics*, vol. 15, no. 6, pp. 821–838, 2004. DOI: 10.1017/S0956792504005765.

[53] A. Korotkin, *Added Masses of Ship Structures* (Fluid Mechanics and its Applications Vol. 88). New York, USA: Springer Science + Business Media, 2009. DOI: 10.1007/978-1-4020-9432-3.

[54] M. Krawskowski, "Simplified RANSE simulation of a side launching," *Archives of Civil and Mechanical Engineering*, vol. 7, no. 3, pp. 151–159, 2007. DOI: 10.1016/S1644-9665(12)60022-3.

[55] J. Kubiczek, K. Burchard, S. Ehlers, and M. Schöttelndreyer, "Material relationship identification for finite element analysis at intermediate strain rates using optical measurements," in *Progress in the Analysis and Design of Marine Structures*, C. G. Soares and Y. Garbatov, Eds., Leiden, Netherlands: CRC Press/Balkema, 2017, pp. 459–468. DOI: 10.1201/9781315157368-59.

[56] C. M. Leavitt, "Launching," in *Ship Design and Construction*, R. Taggart, Ed., New York, USA: Society of Naval Architects and Marine Engineers, 1980, pp. 657–698.

[57] F. M. Lewis, "The inertia of the water surrounding a vibrating ship," in *Meeting of The Society of Naval Architects and Marine Engineers (SNAME)*, vol. 37, 1929, pp. 1–20.

[58] S. G. Lewis, D. A. Hudson, S. R. Turnock, and D. J. Taunton, "Impact of a free-falling wedge with water: synchronized visualization, pressure and acceleration measurements," *Fluid Dynamics Research*, vol. 42, no. 3, 035509 (30pp), 2010. DOI: 10.1088/0169-5983/42/3/035509.

[59] Livermore Software Technology Cooperation, *LS-DYNA® Theory Manual*, r:10859 (February 20th, 2019). Livermore, USA, 2019.

[60] Livermore Software Technology Corporation, *Introduction to MPP version of LS-DYNA® (Webinar)*, https://ftp.lstc.com/anonymous/outgoing/support/PRESENTATIONS/mpp_201305.pdf, accessed: April 14th, 2024, 2013.

[61] Lloyd's Register, *Rules and Regulations for the Classification of Naval Ships* (Edition January 2021). London, United Kingdom, 2021.

[62] Lloyd's Register, *Rules and Regulations for the Classification of Ships* (Edition July 2021). London, United Kingdom, 2021.

[63] G. V. Logvinovich, *Hydrodynamics of Free-Boundary Flows*, Tranlasted from Russian by Israel Program for Scientific Translations. Springfield, USA: U.S. Department of Commerce, National Technical Information Service, 1972.

[64] L. Lu, H. Li, H. Ren, J. Zou, S. Chen, and R. Liu, "Numerical Method for Whipping Response of Ultra Large Container Ships Under Asymmetric Slamming," *Available at SSRN 4478205*, 2023. DOI: 10.2139/ssrn.4478205.

[65] M. Makino, "The Performance of 10-Million Element Car Model by MPP Version of LS-DYNA® on Fujitsu PRIMEPOWER," in *Proceedings of 10th International LS-DYNA® Users Conference*, Detroit, USA, 2008, pp. 5–7–5–10.

[66] K. Mielcarek, "Stapellauf in Leer: Schiff erobert sich mit Riesen-Fontäne sein Element," *Ostfriesen Zeitung*, Published on February 23th, 2021.

[67] C. Mittelstedt, *Structural Mechanics in Lightweight Engineering*. Cham, Switzerland: Springer Nature Switzerland, 2021. DOI: 10.1007/978-3-030-75193-7.

[68] O. Moctar, T. Schellin, and H. Söding, *Numerical Methods for Seakeeping Problems*. Cham, Switzerland: Springer Nature Switzerland, 2021. DOI: 10.1007/978-3-030-62561-0.

[69] M. R. Moore, S. D. Howison, J. R. Ockendon, and J. M. Oliver, "Three-dimensional oblique water-entry problems at small deadrise angles," *Journal of Fluid Mechanics*, vol. 711, pp. 259–280, 2012. DOI: 10.1017/jfm.2012.391.

[70] M. Muzaffar, *US warship reportedly damaged in disastrous launch*, https://www.independent.co.uk/news/world/americas/uss-cleveland-launch-tugboat-collision-footage-b2322306.html, accessed: April 14th, 2024, 2023.

[71] Nippon Kaiji Kyōkai, *Rules for High Speed Craft* (Edition January 2022). Chiyoda, Japan, 2022.

[72] Nippon Kaiji Kyōkai, *Rules for the Survey and Construction of Governmental and Naval Ships* (Edition January 2022). Chiyoda, Japan, 2022.

[73] Nippon Kaiji Kyōkai, *Rules for the Survey and Construction of Steel Ships* (Edition January 2022). Chiyoda, Japan, 2022.

[74] Oasys, *Introduction to MPP LS-DYNA (Webinar)*, https://www.oasys-software.com/dyna/wp-content/uploads/2019/01/Webinar_MPP-LS-DYNA.pdf, accessed: April 14th, 2024, 2018.

[75] J. K. Paik, *Ultimate Limit State Analysis and Design of Plated Structures*, Second Edition. Hoboken, USA: John Wiley & Sons, 2018. DOI: 10.1002/9781119367758.

[76] J. K. Paik and J. Y. Chung, "A basic study on static and dynamic crushing behavior of a stiffened tube," *Transactions of the Korean Society of Automotive Engineers*, vol. 7, no. 1, pp. 219–238, 1999.

[77] A. Papanikolaou, *Ship Design: Methodologies of Preliminary Design*. Dordrecht, Netherlands: Springer Science + Business Media, 2014. DOI: 10.1007/978-94-017-8751-2.

[78] J. Peschmann, "Berechnung der Energieabsorption der Stahlstruktur von Schiffen bei Kollisionen und Grundberührungen," Ph.D. dissertation, Technische Universität Hamburg-Harburg, Hamburg, Germany, 2001.

[79] S. Qiu, H. Ren, and H. Li, "Computational Model for Simulation of Lifeboat Free-Fall during Its Launching from Ship in Rough Seas," *Journal of Marine Science and Engineering*, vol. 8, p. 631, 2020. DOI: 10.3390/jmse8090631.

[80] S. Qiu, H. Ren, N. Wang, and H. Liu, "3D motion model for the freefall lifeboat during its launching from a moving ship," *Ocean Engineering*, vol. 278, p. 114 363, 2023. DOI: 10.1016/j.oceaneng.2023.114363.

[81] M. Ramzi and F. Pacuraru, "Automatic procedure of side ship launching calculation," *Annals of "Dunarea de Jos" University of Galati. Fascicle XI Shipbuilding*, vol. 41, pp. 133–138, 2018. DOI: 10.35219/AnnUGalShipBuilding.2018.41.20.

[82] K. J. Rawson and E. C. Tupper, *Basic Ship Theory*, Fifth Edition. Oxford, United Kingdowm: Butterworth-Heinemann, 2001. DOI: 10.1016/B978-0-7506-5398-5.X5000-6.

[83] Registro Italiano Navale, *Rules for the Classification of Fast Patrol Vessels,* (Edition January 2007). Genova, Italy, 2007.

[84] Registro Italiano Navale, *Rules for the Classification of High-Speed Craft* (Edition January 2015). Genova, Italy, 2015.

[85] Registro Italiano Navale, *Rules for the Classification of Naval Ships* (Edition July 2017). Genova, Italy, 2017.

[86] Registro Italiano Navale, *Rules for the Classification of Ships* (Edition January 2022). Genova, Italy, 2022.

[87] P. Rigo, J.-D. Caprace, Z. Sekulski, A. Bayatfar, and S. Echeverry, "Structural Design Optimization — Tools and Methodologies," in *A Holistic Approach to Ship Design: Volume 1: Optimisation of Ship Design and Operation for Life Cycle*, A. Papanikolaou, Ed., Cham, Switzerland: Springer Nature Switzerland, 2019, pp. 295–327. DOI: 10.1007/978-3-030-02810-7_9.

[88] J. W. Ringsberg, S. E. Heggelund, P. Lara, B.-S. Jang, and S. E. Hirdaris, "Structural response analysis of slamming impact on free fall lifeboats," *Marine Structures*, vol. 54, pp. 112–126, 2017. DOI: 10.1016/j.marstruc.2017.03.004.

[89] M. Schöttelndreyer, "Füllstoffe in der Konstruktion: Ein Konzept zur Verstärkung von Schiffsseitenhüllen," Ph.D. dissertation, Technische Universität Hamburg-Harburg, Hamburg, Germany, 2015.

[90] H. Schürmann, *Konstruieren mit Faser-Kunststoff-Verbunden*, 2., bearbeitete und erweiterte Auflage. Berlin / Heidelberg, Germany: Springer-Verlag Berlin Heidelberg, 2007. DOI: 10.1007/978-3-540-72190-1.

[91] Y. S. Shin, M. Lee, K. Y. Lam, and K. S. Yeo, "Modeling Mitigation Effects of Watershield on Shock Waves," *Shock and Vibration*, vol. 5, pp. 225–234, 1998. DOI: 10.1155/1998/782032.

[92] M. Souli, A. Ouahsine, and L. Lewin, "ALE formulation for fluid–structure interaction problems," *Computer Methods in Applied Mechanics and Engineering*, vol. 190, no. 5, pp. 659–675, 2000. DOI: 10.1016/S0045-7825(99)00432-6.

[93] D. J. Steinberg, "Spherical Explosions and the Equation of State of Water," Lawrence Livermore National Laboratory, University of California, research rep. UCID-20974, 1987. DOI: 10.2172/6766676.

[94] S. Tödter, O. el Moctar, J. Neugebauer, and T. E. Schellin, "Experimentally Measured Hydroelastic Effects on Impact-Induced Loads During Flat Water Entry and Related Uncertainties," *Journal of Offshore Mechanics and Arctic Engineering*, vol. 142, no. 1, pp. 011 604–1–011604–9, 2020. DOI: 10.1115/1.4044632.

[95] V. Tredge, T. E. Halvorsen, and K. O. Underhaug, "Simulation of Free Fall Lifeboats – Impact Forces, Slamming and Accelerations," in *11th International Conference on Fast Sea Transportation (FAST 2011)*, Honolulu, USA, 2011, pp. 669–674.

[96] D. D. Truong, B.-S. Jang, C.-E. Janson, *et al.*, "Benchmark study on slamming response of flat-stiffened plates considering fluid-structure interaction," *Marine Structures*, vol. 79, p. 103 040, 2021. DOI: 10.1016/j.marstruc.2021.103040.

[97] D. D. Truong, B.-S. Jang, H.-B. Ju, and S. W. Han, "Prediction of slamming pressure considering fluid-structure interaction. Part I: numerical simulations," *Ships and Offshore Structures*, vol. 17, no. 1, pp. 7–28, 2022. DOI: 10.1080/17445302.2020.1816732.

[98] A. Ulbertus and M. Schöttelndreyer, "Das verborgene Potential globaler Festigkeitsberechnungen in der Konstruktionsphase," in *Jahrbuch der Schiffbautechnischen Gesellschaft*, vol. 110, Hamburg, Germany: Schifffahrts-Verlag "Hansa", 2016, pp. 160–174.

[99] A. Ulbertus, M. Schöttelndreyer, and S. Ehlers, "Sideways launching process of a ship using the Arbitrary-Lagrangian-Eulerian approach," in *Proceedings of 13th European LS-DYNA® Users Conference*, Ulm, Germany, 2021.

[100] A. Ulbertus, M. Schöttelndreyer, and S. Ehlers, "Assessment of loads on a ship hull during a sideways launching process based on model tests," in *Advances in the Analysis and Design of Marine Structures*, C. G. Soares and J. W. Ringsberg, Eds., Leiden, Netherlands: CRC Press/Balkema, 2023, pp. 13–21.

[101] A. Ulbertus, M. Schöttelndreyer, and S. Ehlers, "Hull structural loads during a sideways launching process using fluid-structure interaction," in *Advances in the Analysis and Design of Marine Structures*, C. G. Soares and J. W. Ringsberg, Eds., Leiden, Netherlands: CRC Press/Balkema, 2023, pp. 23–32.

[102] W. S. Vorus, "A Flat Cylinder Theory for Vessel Impact and Steady Planing Resistance," *Journal of Ship Research*, vol. 40, no. 2, pp. 89–106, 1996. DOI: 10.5957/jsr.1996.40.2.89.

[103] H. Wagner, "Über Stoß- und Gleitvorgänge an der Oberfläche von Flüssigkeiten," *Zeitschrift für Angewandte Mathematik und Mechanik*, vol. 12, no. 4, pp. 193–215, 1932. DOI: 10.1002/zamm.19320120402.

[104] S. Wang and C. Guedes Soares, "Review of ship slamming loads and responses," *Journal of Marine Science and Application*, vol. 16, no. 4, pp. 427–445, 2017. DOI: 10.1007/s11804-017-1437-3.

[105] S. Wang and C. Guedes Soares, "Asymmetrical Water Impact of Two-Dimensional Wedges with Roll Angle with Multi-Material Eulerian Formulation," *The International Journal of Maritime Engineering*, vol. 156, no. A2, A115–A130, 2014. DOI: 10.3940/rina.ijme.2014.a2.280.

[106] S. Wang, H. Islam, and C. Guedes Soares, "Uncertainty due to discretization on the ALE algorithm for predicting water slamming loads," *Marine Structures*, vol. 80, p. 103 086, 2021. DOI: 10.1016/j.marstruc.2021.103086.

[107] Y. Wang, D. Shu, Y. Fujii, A. Takita, T. Ishima, and R. Araki, "Comparison between numerical analysis and the levitation mass method measurement test of a spherical structure early impacting water," *Advances in Mechanical Engineering*, vol. 10, no. 1, p. 1 687 814 017 748 076, 2018. DOI: 10.1177/1687814017748076.

[108] A. M. Winslow, "Equipotential zoning of the interior of a three-dimensional mesh," Lawrence Radiation Laboratory, University of California, research rep. UCRL-7312, 1990.

[109] B. Wolters, "Stapellauf in Leer," *Ostfriesen Zeitung*, Published on April 4th, 2019.

[110] B. Wolters, "„Arklow Willow" in Leer vom Stapel gelaufen," *Ostfriesen Zeitung*, Published on September 6th, 2019.

[111] P. Wriggers, *Computational Contact Mechanics*, Second Edition. Berlin / Heidelberg, Germany: Springer-Verlag Berlin Heidelberg, 2006. DOI: 10.1007/978-3-540-32609-0.

[112] H. Xie, F. Liu, H. Tang, and X. Liu, "Numerical study on the dynamic response of a truncated ship-hull structure under asymmetrical slamming," *Marine Structures*, vol. 72, p. 102 767, 2020. DOI: 10.1016/j.marstruc.2020.102767.

[113] G. D. Xu, W. Y. Duan, and G. X. Wu, "Numerical simulation of oblique water entry of an asymmetrical wedge," *Ocean Engineering*, vol. 35, no. 16, pp. 1597–1603, 2008. DOI: 10.1016/j.oceaneng.2008.08.002.

[114] G. D. Xu, W. Y. Duan, and G. X. Wu, "Wedge impact on liquid surface through free fall motion in three degrees of freedom," in *25th International Workshop on Water Waves and Floating Bodies*, Harbin, China, 2010, pp. 177–180.

[115] Z. Ye, "Dynamics of ships side launching," *Computers & Structures*, vol. 53, no. 4, pp. 861–865, 1994. DOI: 10.1016/0045-7949(94)90374-3.

[116] Z. Yu, J. Amdahl, M. Greco, and H. Xu, "Hydro-plastic response of beams and stiffened panels subjected to extreme water slamming at small impact angles, part II: Numerical verification and analysis," *Marine Structures*, vol. 65, pp. 114–133, 2019. DOI: 10.1016/j.marstruc.2019.01.003.

[117] A. F. Zakki, A. Windyandari, and D. M. Bae, "The Investigation of Launching Parameters on the Motion Pattern of Freefall Lifeboat Using FSI Analysis," *Procedia Earth and Planetary Science*, vol. 14, pp. 110–117, 2015. DOI: 10.1016/j.proeps.2015.07.091.

[118] A. F. Zakki, A. Windyandari, and D. M. Bae, "The development of new type free-fall lifeboat using Fluid Structure Interaction analysis," *Journal of Marine Science and Technology*, vol. 24, pp. 575–580, 2016. DOI: 10.6119/JMST-015-1126-1.

[119] G. Zaraphonitis, T. Plessas, A. Kraus, H. Gudenschwager, and G. Schellenberger, "Parametric Optimisation in Concept and Pre-contract Ship Design Stage," in *A Holistic Approach to Ship Design: Volume 1: Optimisation of Ship Design and Operation for Life Cycle*, A. Papanikolaou, Ed., Cham, Switzerland: Springer Nature Switzerland, 2019, pp. 209–245. DOI: 10.1007/978-3-030-02810-7_7.

[120] R. Zhao, O. Faltinsen, and J. Aarsnes, "Water entry of arbitrary two-dimensional sections with and without flow separation," in *Proceedings of the 21st Symposium on Naval Hydrodynamics*, Trondheim, Norway, 1996, pp. 408–423.

A. Appendix

A.1. Different phases of sideways launching process

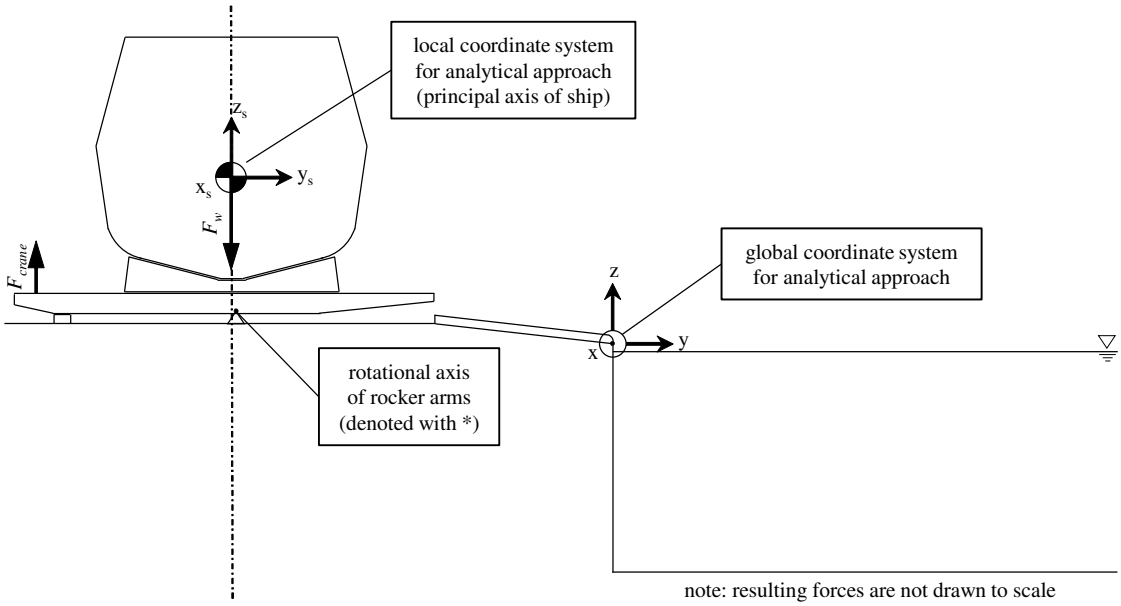

Figure A.1.: start of phase 0 — rotation

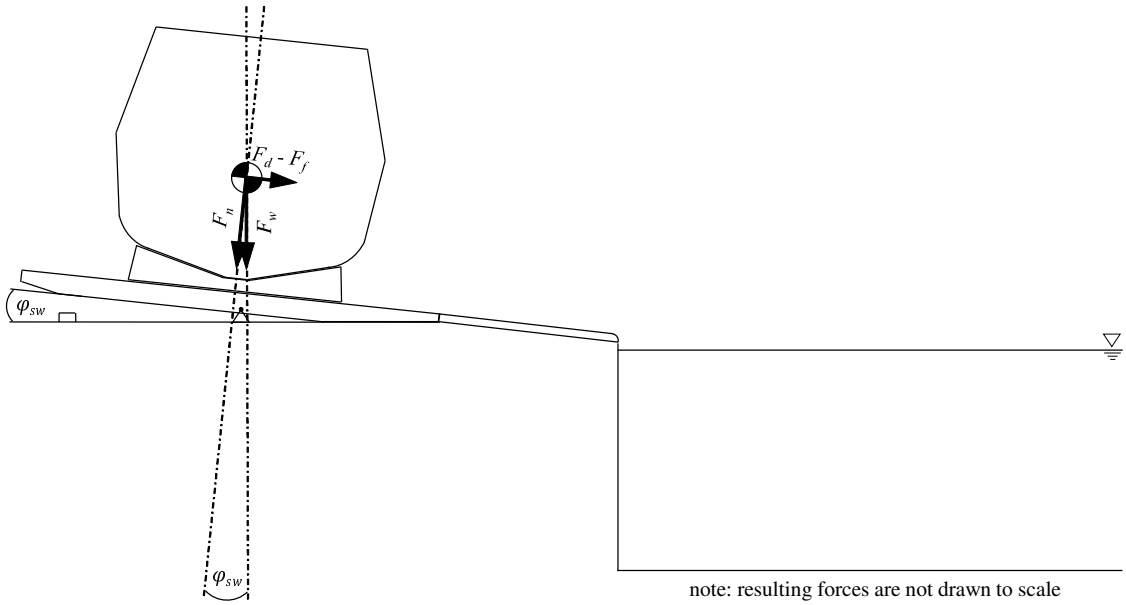

Figure A.2.: end of phase 0 — rotation | start of phase 1 — sliding

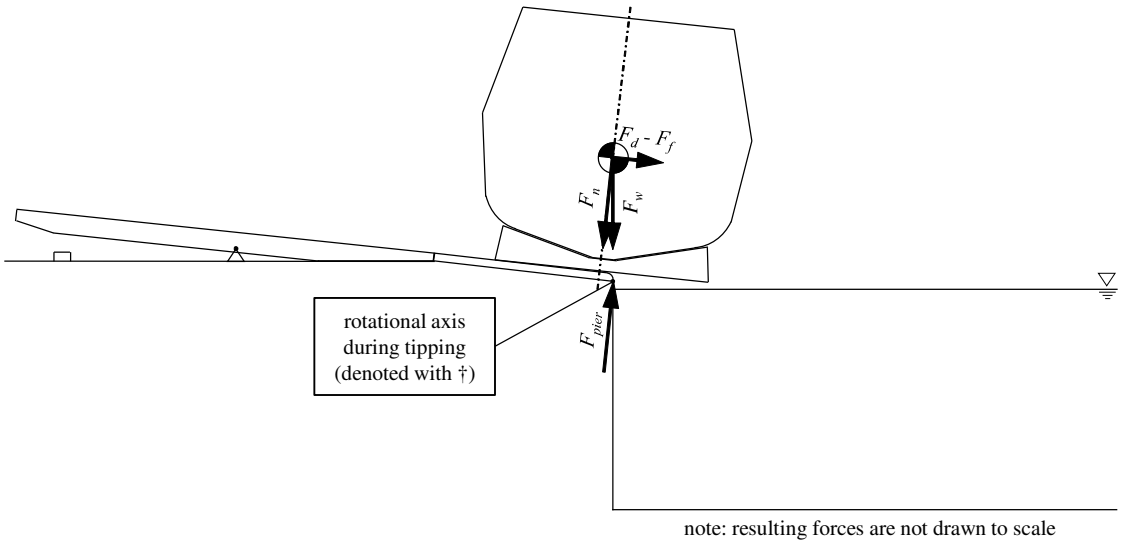

Figure A.3.: end of phase 1 — sliding | start of phase 2 — tipping

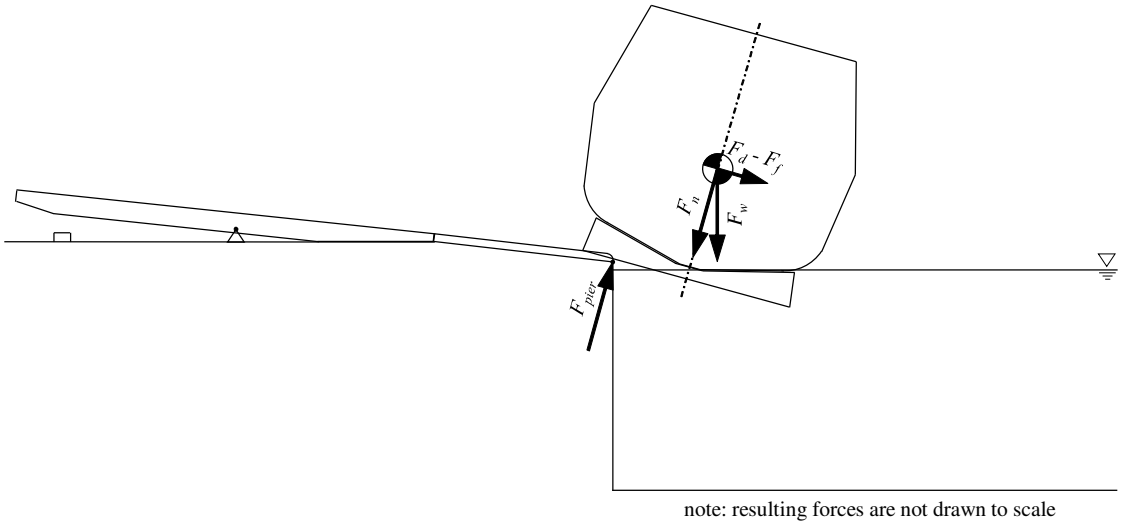

Figure A.4.: end of phase 2 — tipping | start of phase 3 — tipping and immersion

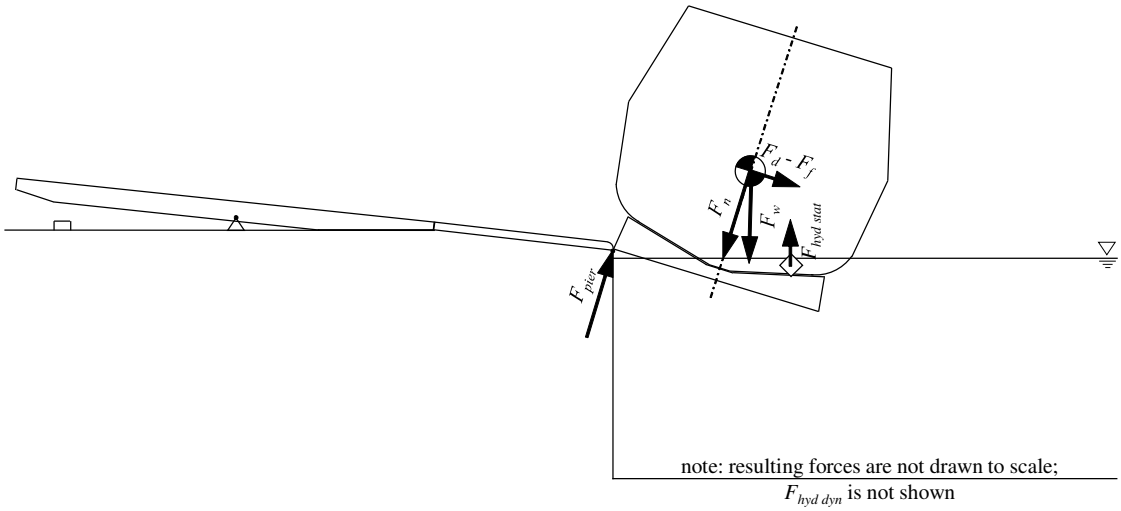

Figure A.5.: end of phase 3 — tipping and immersion | start of phase 4 — dropping and raise

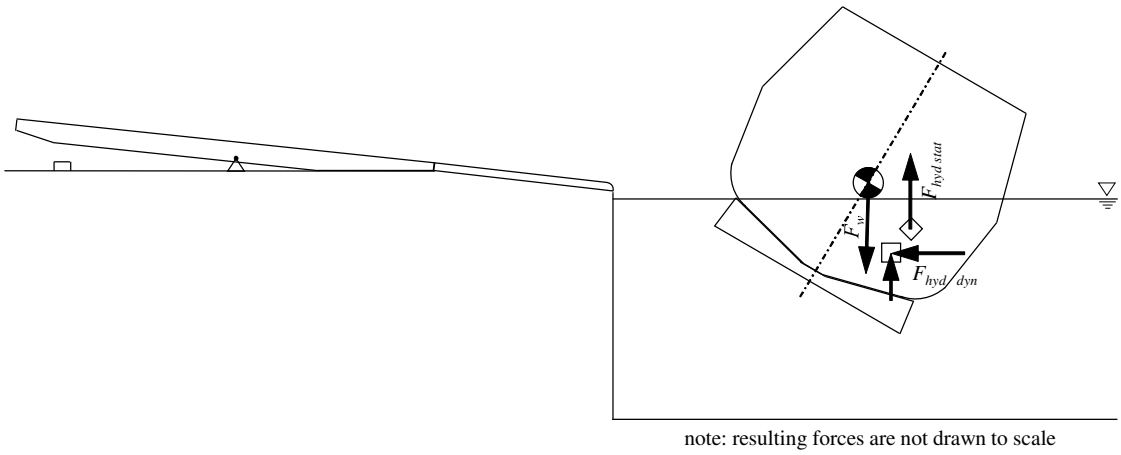

Figure A.6.: phase 4 — dropping and raise (free ship motion)

A.2. Regulations of classification societies: launching and bottom slamming

On the next two pages an overview of rules and regulations of different classification societies regarding the loads during the launching of a ship as well as design loads for bottom slamming is provided.

Only in *Rules and Regulations for the Classification of Naval Ships* [61] the launching process of a vessel is mentioned. In [61] (Volume 1, Part 3, Chapter 5, Section 11.5) the following remarks regarding the consideration of loads during launching of a ship are made:

> 11.5.1 The launching loads are to be checked by the shipbuilder using conventional analytical methods appropriate to the method of launch. If via a slipway, the structure in way of the fore poppet should be suitable for the high loads that will be transmitted in this area. If adequate structure is not available, temporary stiffening is to be arranged.
> 11.5.2 The global strength of the hull girder is to be adequate under the loads imposed by launching, in particular for NS1 ships.

class	regulation	source	loads during launching	bottom slamming loads
ABS	Marine Vessels	[6]	—	no load model provided (only empirical approach for plate thickness)
	Naval Vessels	[5]	—	empirical approach for design loads considering velocity and deadrise angle (only valid for planning vessels) (Part 3, Chapter 2, Section 2.1.3.1)
	High Speed Craft	[4]	—	identical approach as in [5]
	Slamming Guide	[3]	—	general guidance for deriving slamming loads (see text in section 4.1 for details)
BV	Steel Ships	[19]	—	purely empirical approach for design loads (Part B, Chapter 8, Section 1.3.2)
	Naval Vessels	[17]	—	purely empirical approach for design loads (Part B, Chapter 8, Section 1.3.2)
	Environmental Loads	[18]	—	general guidance for deriving slamming loads (see text in section 4.1 for details)
CCS	Steel Ships	[21]	—	approach based on Ochi-Mottor theory (Part 2, Chapter 2, Appendix 4, Section 2.1.1)
	High Speed Craft	[22]	—	empirical approach for design loads considering acceleration and deadrise angle (Chapter 4, Section 4.2.2)
DNV	Ships	[27]	—	purely empirical approach for design loads (Part 3, Chapter 10, Section 2.2.1)
	Naval Vessels	[28]	—	purely empirical approach for design loads (Part 3, Chapter 1, Section 5.3.2)
	Environmental Loads	[25]	—	general guidance for deriving slamming loads (see text in section 4.1 for details)
KR	Steel Ships	[50]	—	empirical approach for design loads considering deadrise angle (Part 3, Chapter 7, Section 804.1)

class	regulation	source	loads during launching	bottom slamming loads
KR	High Speed / Light Crafts	[49]	—	empirical approach for design loads considering acceleration and deadrise angle (only valid for planning vessels) (Part 3, Chapter 2, Section 301.1)
LR	Ships	[62]	—	purely empirical approach for design loads (Part 3, Chapter 5, Section 1.6.4)
	Naval Vessels	[61]	to be considered (Volume 1, Part 3, Chapter 5, Section 11.5)	empirical approach for design loads considering velocity and deadrise angle + approach for dynamic load model provided (Volume 1, Part 5, Chapter 3, Section 4.2)
NK	Steel Ships	[73]	—	different empirical approaches for design loads depending on length and speed of ship (Part C, Chapter 4, Section 4.8.2.2)
	High Speed Craft	[71]	—	empirical approach for design loads considering velocity and deadrise angle (Part 5, Chapter 2, Section 2.2.1)
	Governmental / Naval Vessels	[72]	—	design loads according to [73] or [71] (Part 5, Chapter 2, Section 2.3.5)
RINA	Ships	[86]	—	no approach provided
	Naval Vessels	[85]	—	purely empirical approach for design loads (Part B, Chapter 8, Section 1.3.2.1)
	Fast Patrol Vessels	[83]	—	empirical approach for design loads considering acceleration and deadrise angle (Part B, Chapter 5, Section 2.3.3.1)
	High-Speed Craft	[84]	—	identical approach as in [83]

A.3. Results of analytical approach

Table A.1.: proposed modifications to analytical approach

original term	modified term	used in equation
$c_{w\,xz} = 1.00$	$c_{w\,xz} = 5.00$	4.20
$c_{w\,xy} = 1.00$	$c_{w\,xy} = 2.75$	4.21
$F_{hyd\,dyn\,y} \cdot [z_{A\,xz} - z_{COG\,tot}]$	$0.15 \cdot F_{hyd\,dyn\,y} \cdot [z_{wl} - z_{COG\,tot}]$	4.22
λ_{44}	$3.33 \cdot \lambda_{44}$	4.23, 4.24

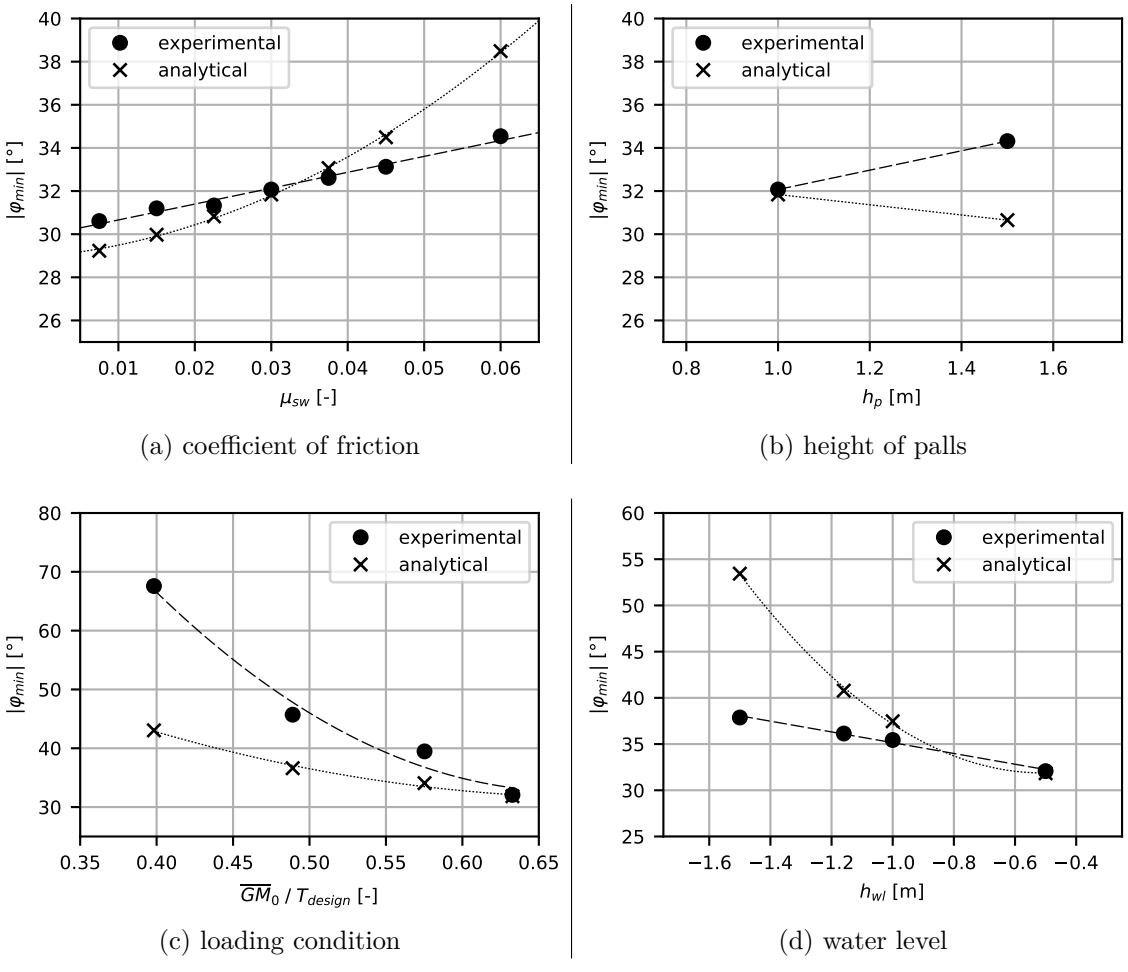

(a) coefficient of friction

(b) height of palls

(c) loading condition

(d) water level

Figure A.7.: comparison of results of analytical approach (with modifications as given in Table A.1) to experimental approach — maximal roll angle

A.4. Results of experimental approach

Table A.2.: measured variables and measurement devices used for model tests

sampling rate = 35.4Hz (200Hz in model scale):

measured value	unit	measuring device	scale
speed at COG in yz-plane	[m/s]	derived based on optical tracking system	$\lambda_{sm}{}^{0.5}$
longitudinal motion at COG	[m]	optical tracking system	λ_{sm}
lateral motion at COG	[m]		λ_{sm}
vertical motion at COG	[m]		λ_{sm}
roll motion	[°]		1
pitch motion	[°]		1
yaw motion	[°]		1
roll velocity	[°/s]	inertial measurement unit	$\lambda_{sm}{}^{-0.5}$

sampling rate = 848.5Hz (4,800Hz in model scale):

measured value	unit	measuring device	scale
pressure on ship hull	[kPa]	pressure transducer	$\rho_{w\,fs}/\rho_{w\,ms} \cdot \lambda_{sm}{}^{3}$

Table A.3.: results of model tests — uncertainties regarding measurement of ship motion

LC_01:

	φ_i in [°] @ run				$\bar{X}_i$	SD_i	CV_i
	No. 1	No. 2	No. 3	No. 4	in [°]	in [°]	in [%]
φ_{impact}	-14.59	-14.21	-14.56	-13.87	-14.31	0.15	1.03
φ_{min}	-32.09	-32.07	-31.66	-33.07	-32.22	0.26	0.81
calm water	✓	✓	X	X	-	-	-

LC_02:

	φ_i in [°] @ run				$\bar{X}_i$	SD_i	CV_i
	No. 1	No. 2	No. 3	No. 4	in [°]	in [°]	in [%]
φ_{impact}	-14.14	-15.10	-14.19	-15.52	-14.74	0.30	2.01
φ_{min}	-39.47	-39.12	-39.18	-39.43	-39.30	0.08	0.19
calm water	✓	X	✓	X	-	-	-

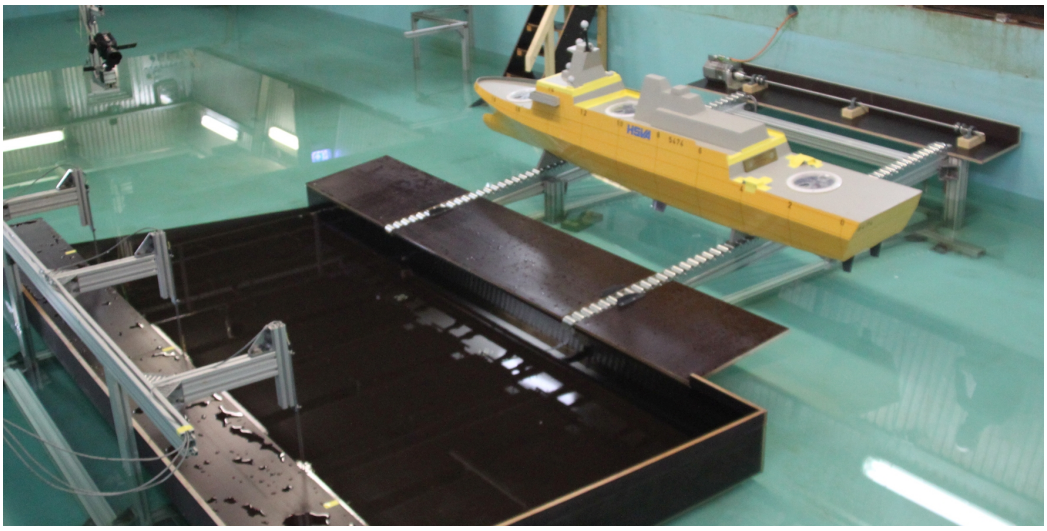

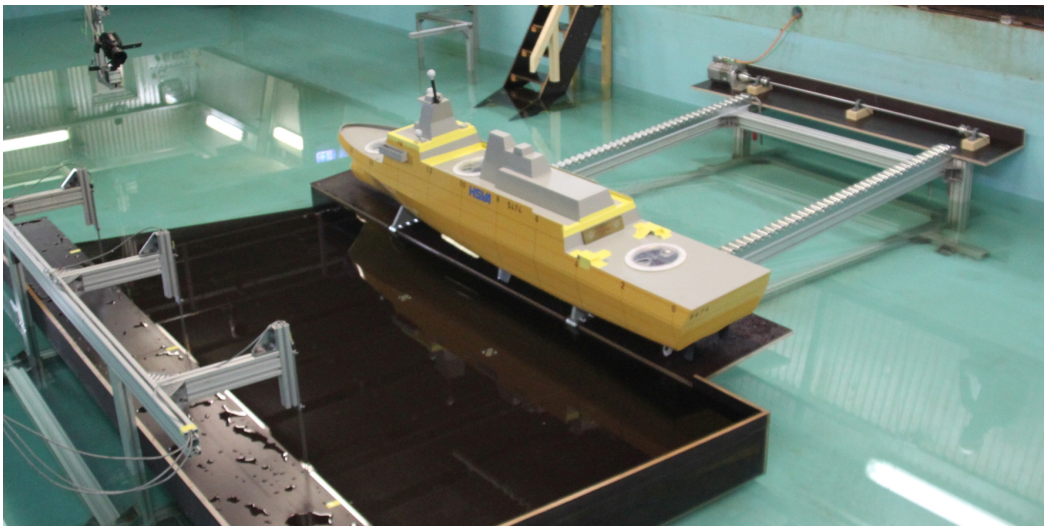

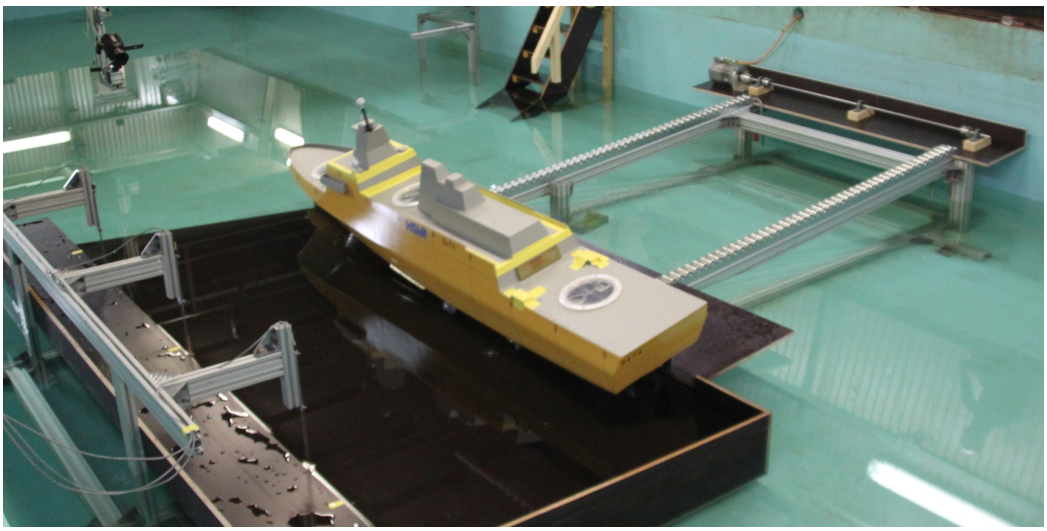

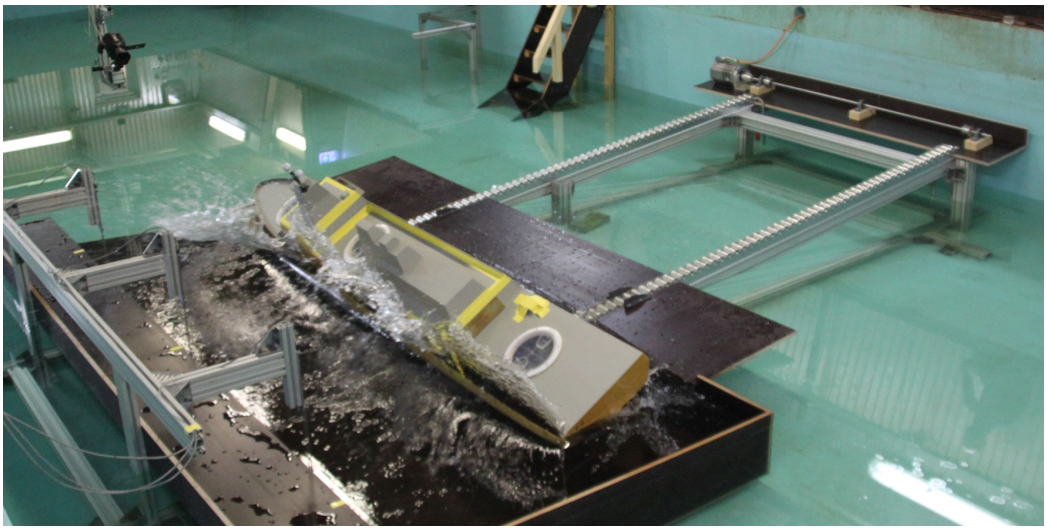

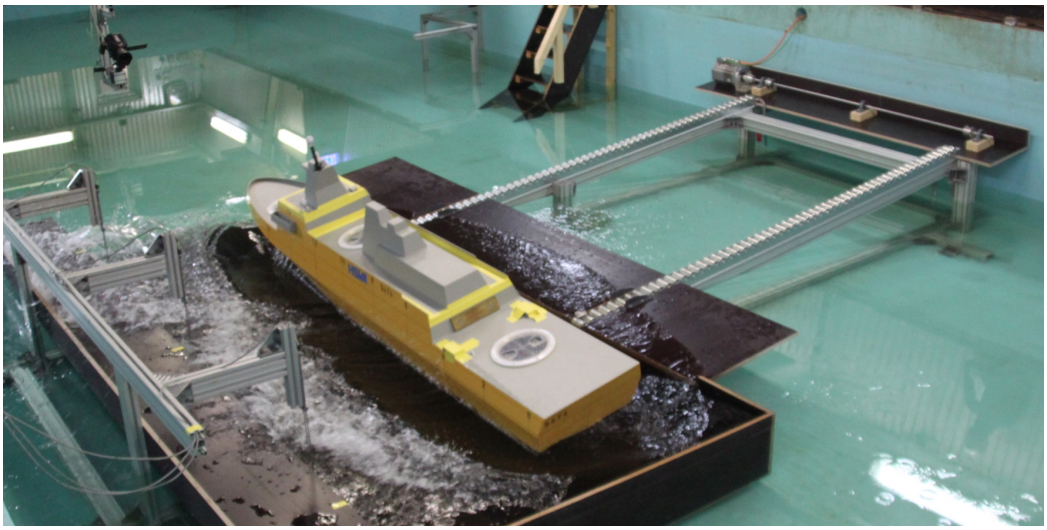

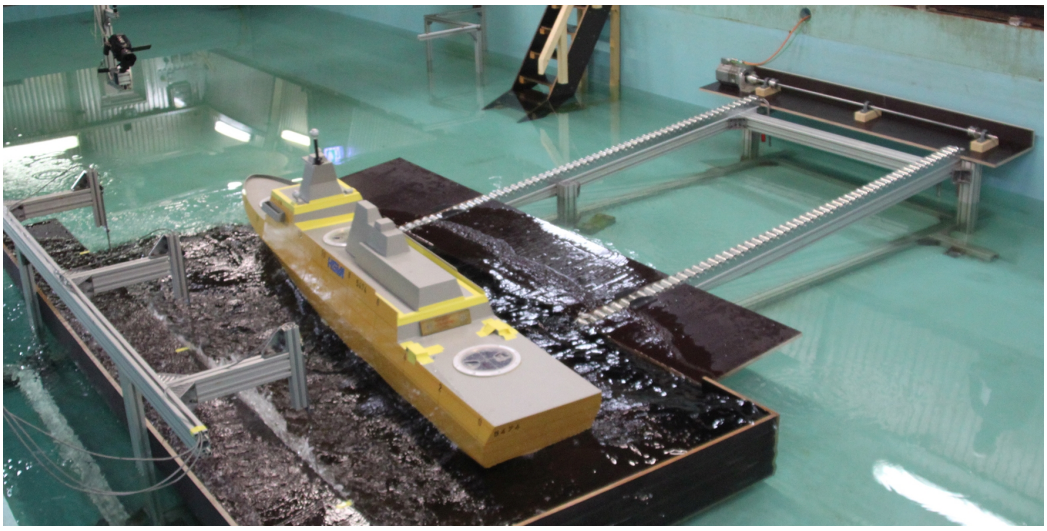

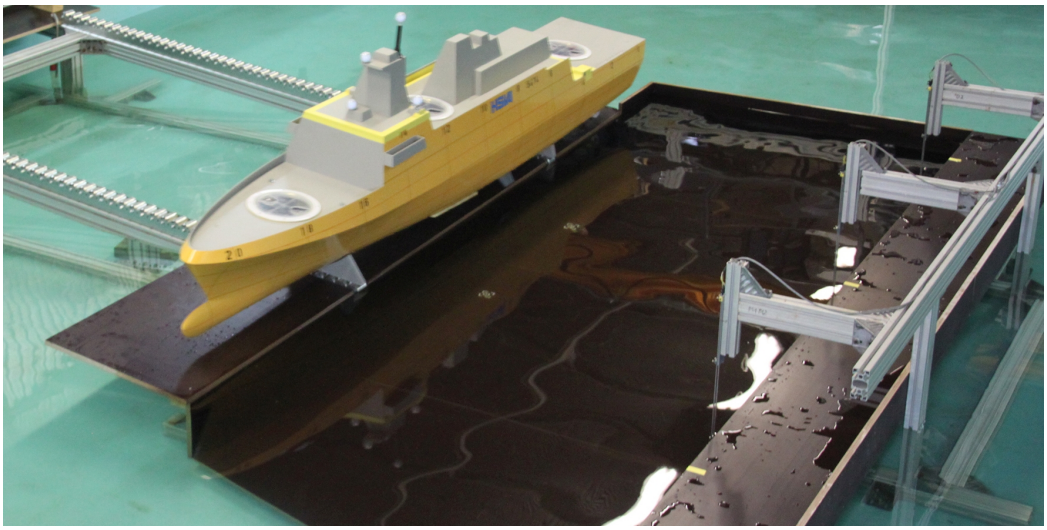

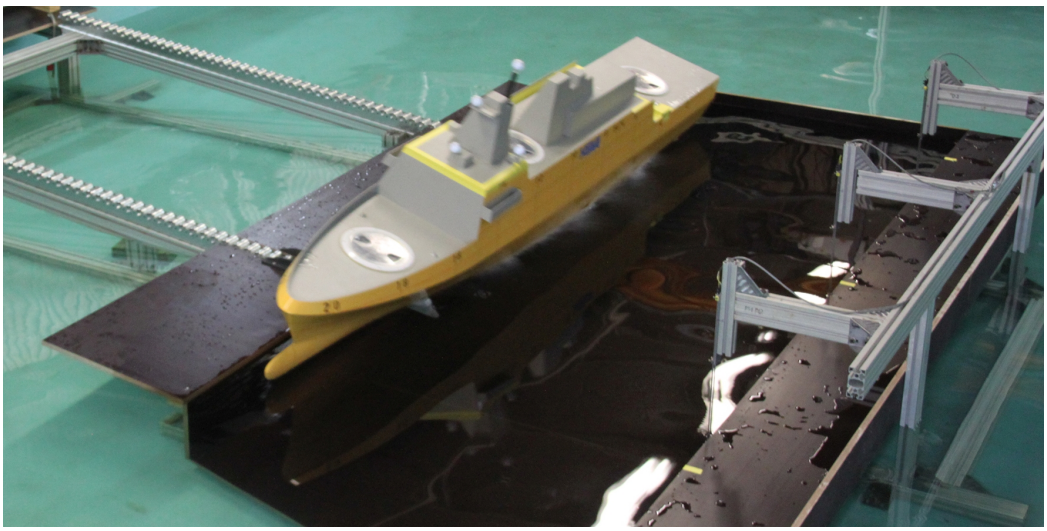

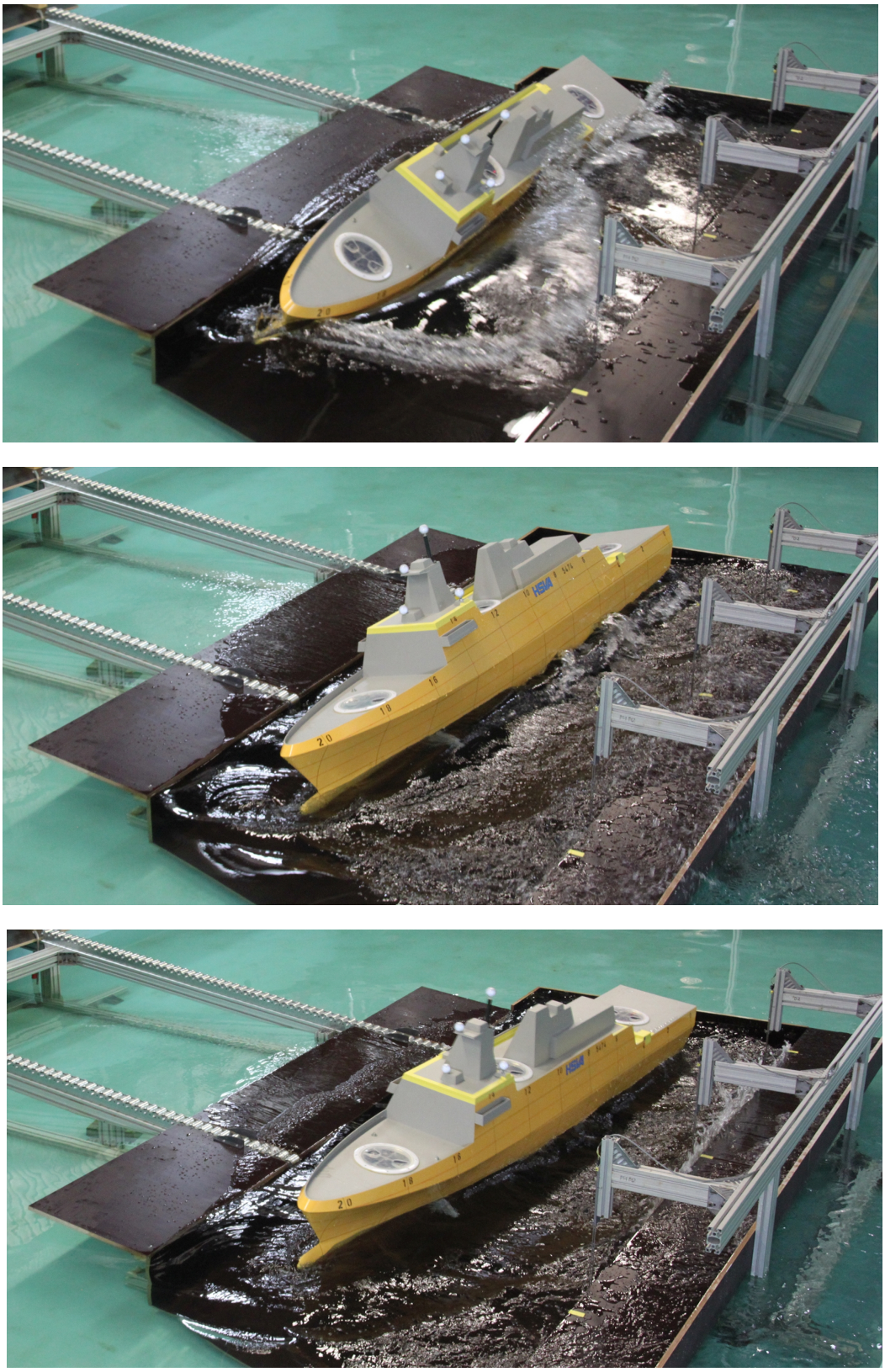

Figure A.8.: picture series of model tests (LC_01 is shown)

A.5. Modelling of hull structure of the special purpose vessel

Table A.4.: element formulations used for FEM models

element type	ELFORM in LS-DYNA	element formulation	reference for details
beam	1	Hughes-Liu with cross section integration	[59, Ch. 7]
shell	2	Belytschko-Lin-Tsay	[59, Ch. 9]
solid	1	constant stress solid element	[59, Ch. 4]
ALE	11	1 point ALE multi-material element	[59, Ch. 20]

Table A.5.: loading conditions used for FEM models of SPV

parameter	unit	LC LAUNCH	LC LSW	model test (LC02)
Δ	[t]	$0.813 \cdot \Delta_{design}$	$0.903 \cdot \Delta_{design}$	$0.837 \cdot \Delta_{design}$
COG_x^*	[m]	$0.460 \cdot L_{pp}$	$0.466 \cdot L_{pp}$	$0.458 \cdot L_{pp}$
COG_y	[m]	$0.000 \cdot B_{wl}$	$0.000 \cdot B_{wl}$	$0.000 \cdot B_{wl}$
COG_z	[m]	$0.500 \cdot D_{main}$	$0.518 \cdot D_{main}$	$0.507 \cdot D_{main}$
$\overline{GM}_0$	[m]	$0.623 \cdot T_{design}$	$0.470 \cdot T_{design}$	$0.580 \cdot T_{design}$
i_{xx}	[m]	$0.394 \cdot B_{wl}$	$0.395 \cdot B_{wl}$	$0.417 \cdot B_{wl}$
i_{yy}	[m]	$0.257 \cdot L_{pp}$	$0.256 \cdot L_{pp}$	$0.258 \cdot L_{pp}$
i_{zz}	[m]	$0.257 \cdot L_{pp}$	$0.256 \cdot L_{pp}$	$0.257 \cdot L_{pp}$

*: referred to aft perpendicular

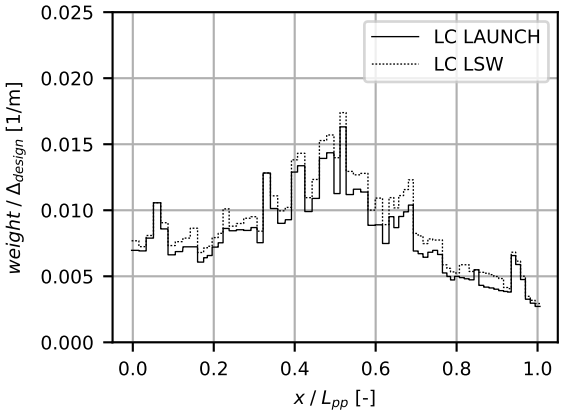

Figure A.9.: weight distribution used for FEM models of SPV

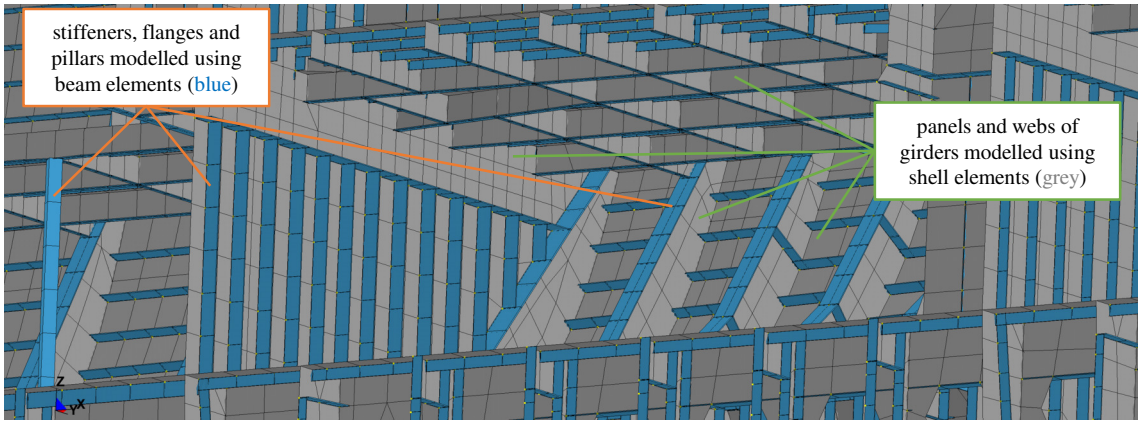

Figure A.10.: view inside global FEM model of the hull structure of the SPV

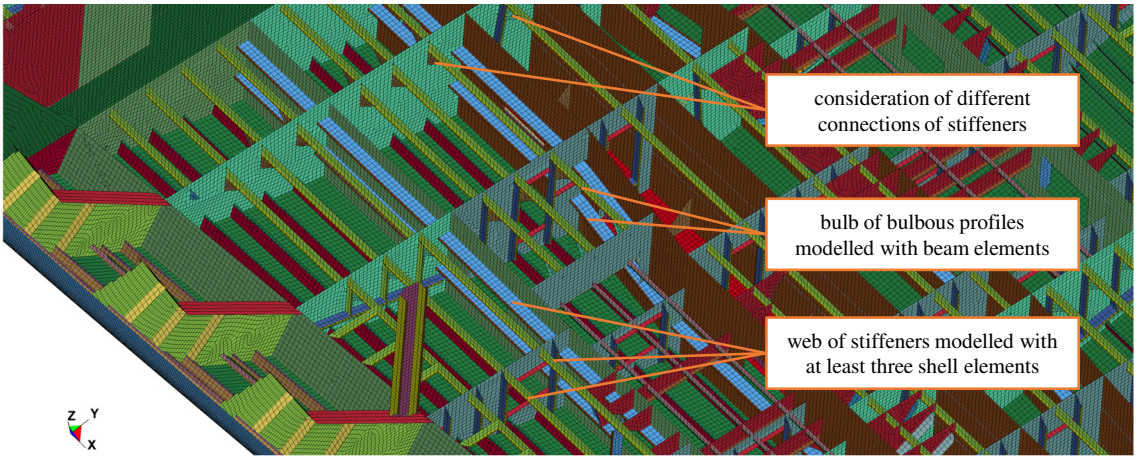

Figure A.11.: view inside detailed FEM model of the SPV

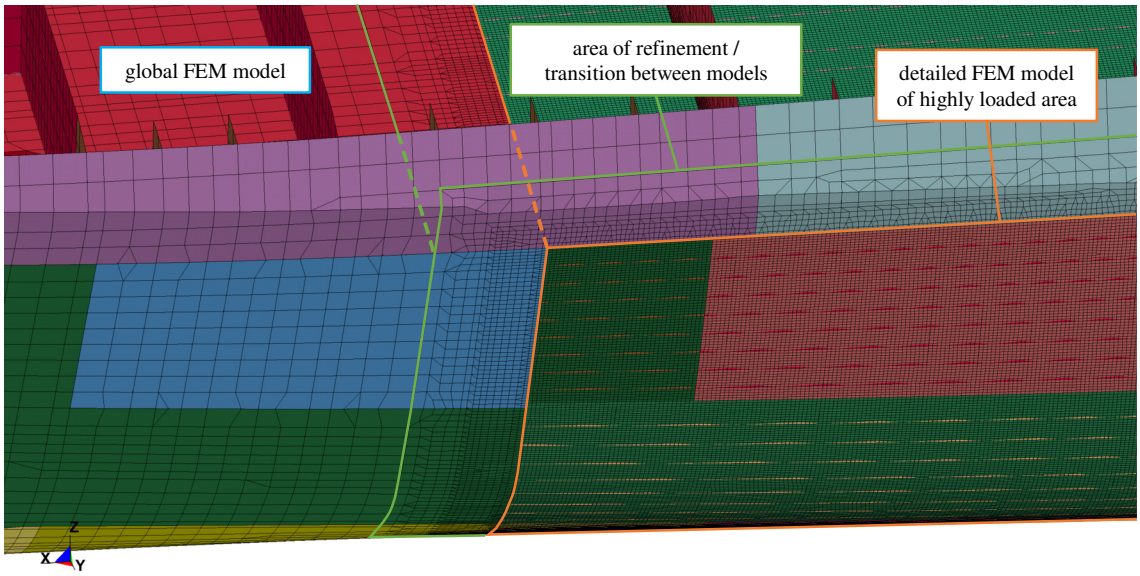

Figure A.12.: area of transition of combined FEM model of the SPV

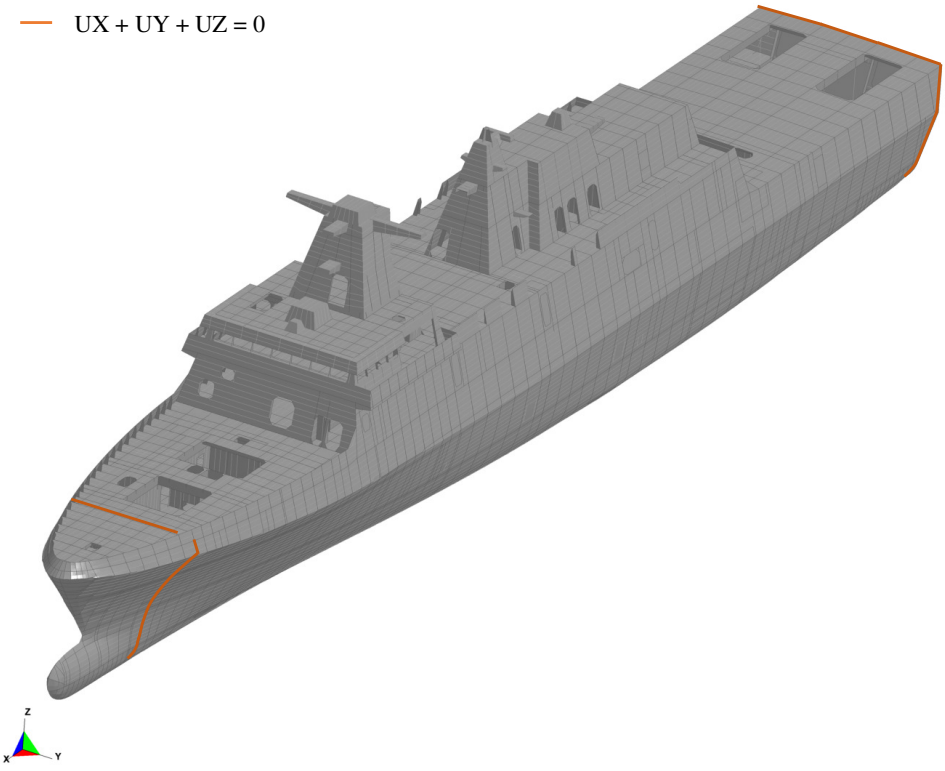

Figure A.13.: BC used for global FEM model of SPV

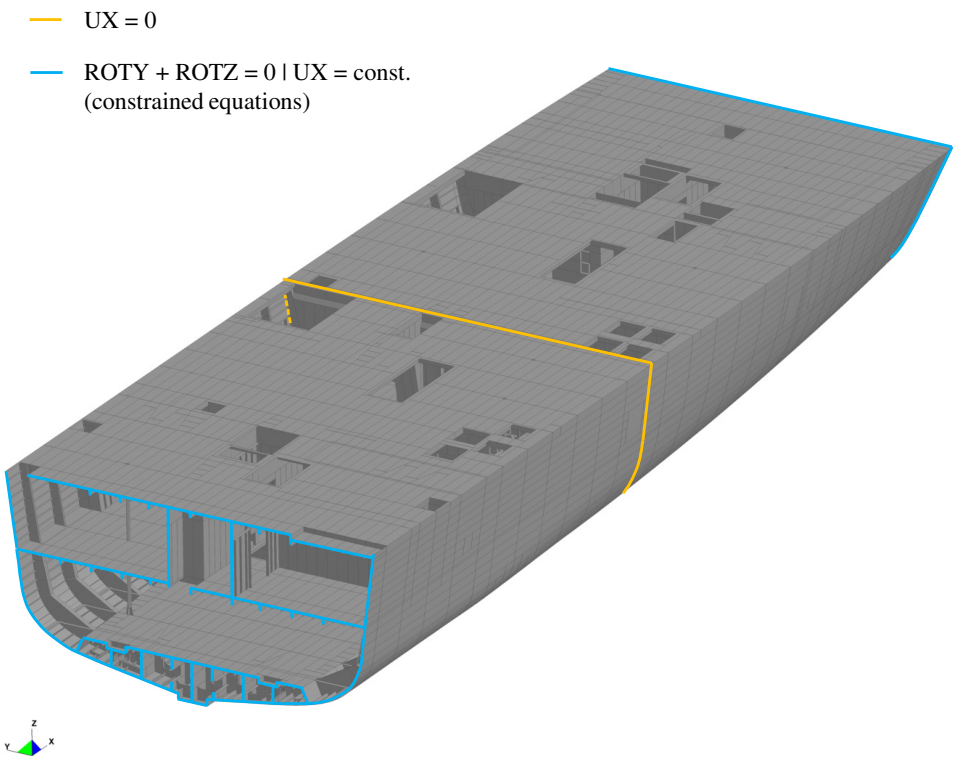

Figure A.14.: BC used for detailed FEM model of SPV (BC_01)

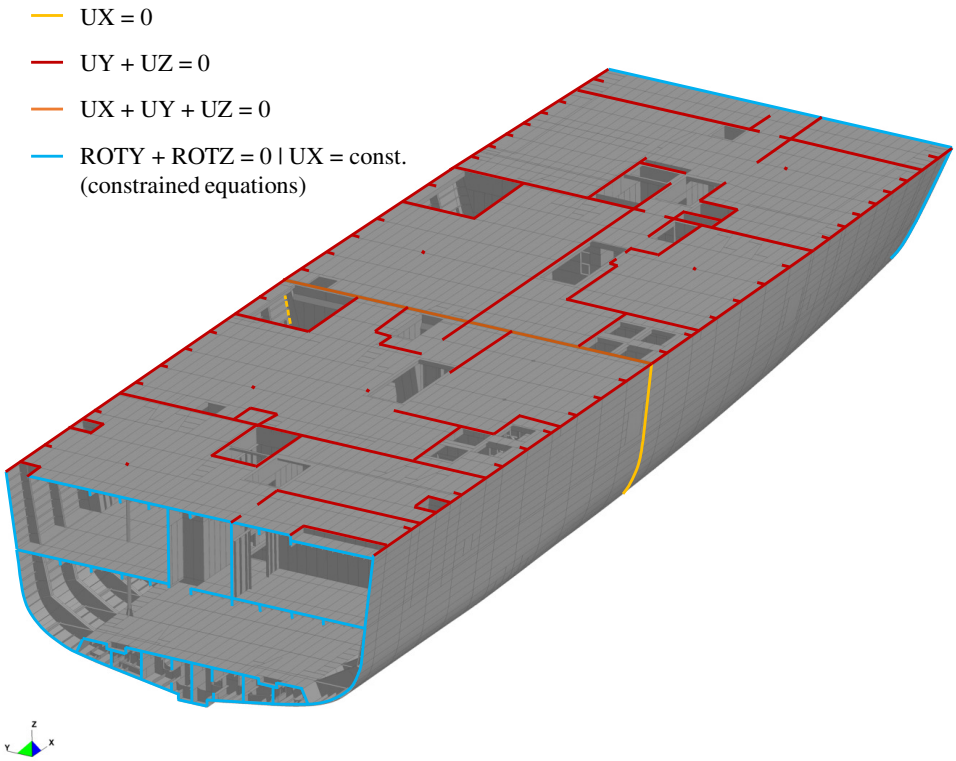

Figure A.15.: BC used for detailed FEM model of SPV (BC_02)

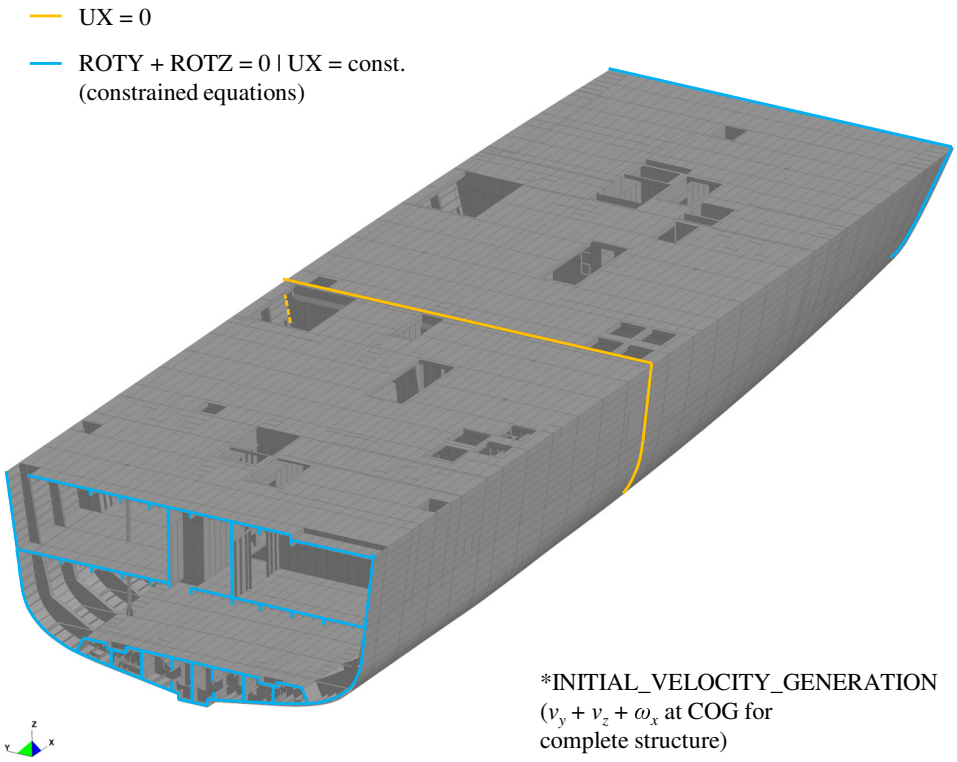

Figure A.16.: BC used for detailed FEM model of SPV (BC_03)

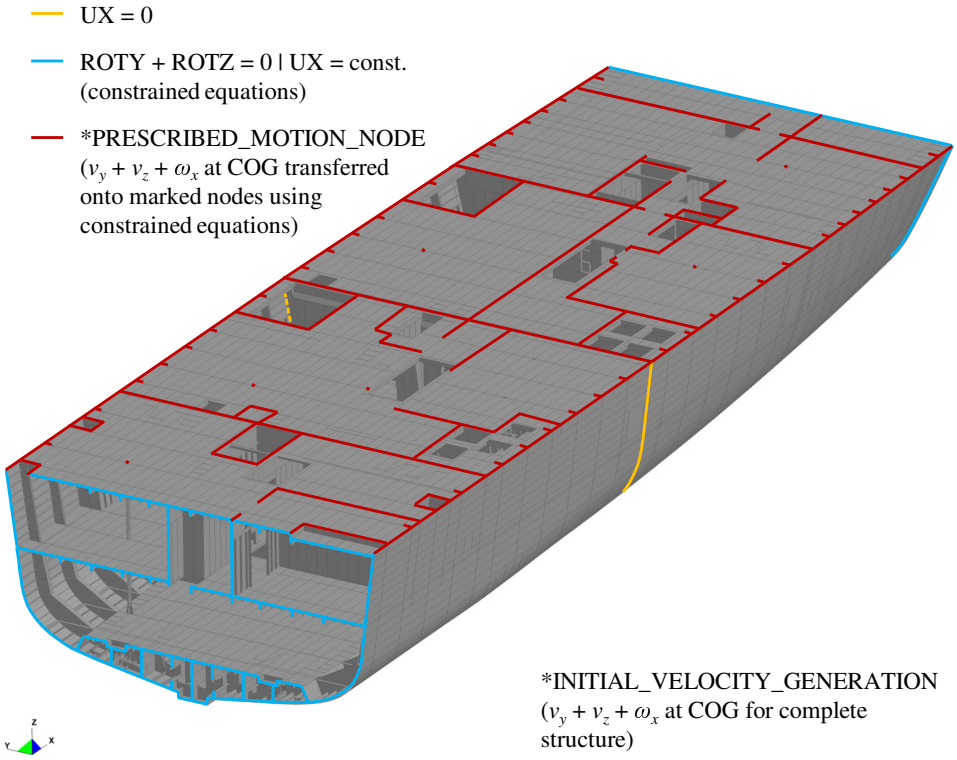

Figure A.17.: BC used for detailed FEM model of SPV (BC_04)

A.6. User defined load model in LS-DYNA - rule-based approach

```
*DEFINE_FUNCTION
$#      fidheading
      10509Load_Model_Rule_Based_10509
$# function
float p_rb_10509(float t)
{
float t_impact, v_impact, deadrise;
t_impact=0.000185;
v_impact=-4.745;
deadrise=-0.417;
float p_bi, p_dyn, t_r;
p_bi=310684.92;
p_dyn=11259.77;
t_r=0.014183;
float t1, t2, t3;
t1=t_impact;
t2=t_impact+t_r;
t3=t_impact+2*t_r;
float p_act;
if(t<t1){
p_act=0;
}
else if((t>=t1) & (t<t2)){
p_act=p_bi*((t-t_impact)/t_r);
}
else if((t>=t2) & (t<t3)){
p_act=p_bi-(p_bi-p_dyn)*((t-(t_impact+t_r))/t_r);
}
else{
p_act=p_dyn;
}
return p_act;
}
*LOAD_SEGMENT_SET_ID
$#       idheading
      10509Load_Model_Rule_Based_10509
$       SSID        LCID          SF          AT
      10509       10509         1.0         0.0
```

A.7. User defined load model in LS-DYNA - experimental approach

```
*DEFINE_FUNCTION
$#      fidheading
     10609Load_Model_Model_Test_10609
$# function
float p_mt_10609(float t)
{
float t_impact, v_impact, deadrise;
t_impact=0.000185;
v_impact=-4.745;
deadrise=-0.417;
float k_v, k_beta;
k_v=0.903;
k_beta=0.985;
p_mt_max, p_mt_scaled, p_dyn, p_act;
p_mt_max=915000.00;
p_mt_scaled=k_v*k_beta*p_mt_max;
p_dyn=11259.77;
float k_mt, t_r_mt;
k_mt=89.274500;
t_r_mt=0.046260;
float t1, t2;
t1=t_impact;
t2=t_impact+t_r_mt;
if(t<t1){
p_act=0;
}
else if((t>=t1) & (t<t2)){
p_act=p_mt_scaled*exp(-k_mt*(t-t1));
}
else{
p_act=p_dyn;
}
return p_act;
}
*LOAD_SEGMENT_SET_ID
$#       idheading
     10609Load_Model_Model_Test_10609
$      SSID       LCID         SF         AT
     10509      10609        1.0        0.0
```

A.8. Parametric study of settings used for fluid-structure interaction

The following aspects of the used FSI algorithm inside `*CONSTRAINED_LAGRANGE_IN_SOLID` in LS-DYNA were varied:

- direction of coupling
  - `DIREC`=1: tension and compression
  - `DIREC`=2: compression only
- scaling factor of stiffness for coupling algorithm (`PFAC`)
- scaling factor for damping forces of coupling algorithm (`DAMP`)
- number of coupling points across each coupled Lagrangian element (`NQUAD`)

The following general settings for the ALE approach in `*CONTROL_ALE` were varied:

- ALE advection method
  - `METH`=1: Donor cell with half index shift (first order accurate)
  - `METH`=2: Van Leer with half index shift (second order accurate)
- number of cycles between ALE advection (`NADV`)

The following aspects of the general setup of the ALE approach were investigated:

- size of ALE-elements / element density ratio DR between ALE and Lagrangian elements
  - controlled by `NLVL` inside `*CONTROL_REFINE_ALE`
- influence of additional damping inside fluids / ALE elements
  - damping added by using `*DAMPING_PART_MASS` for ALE domain

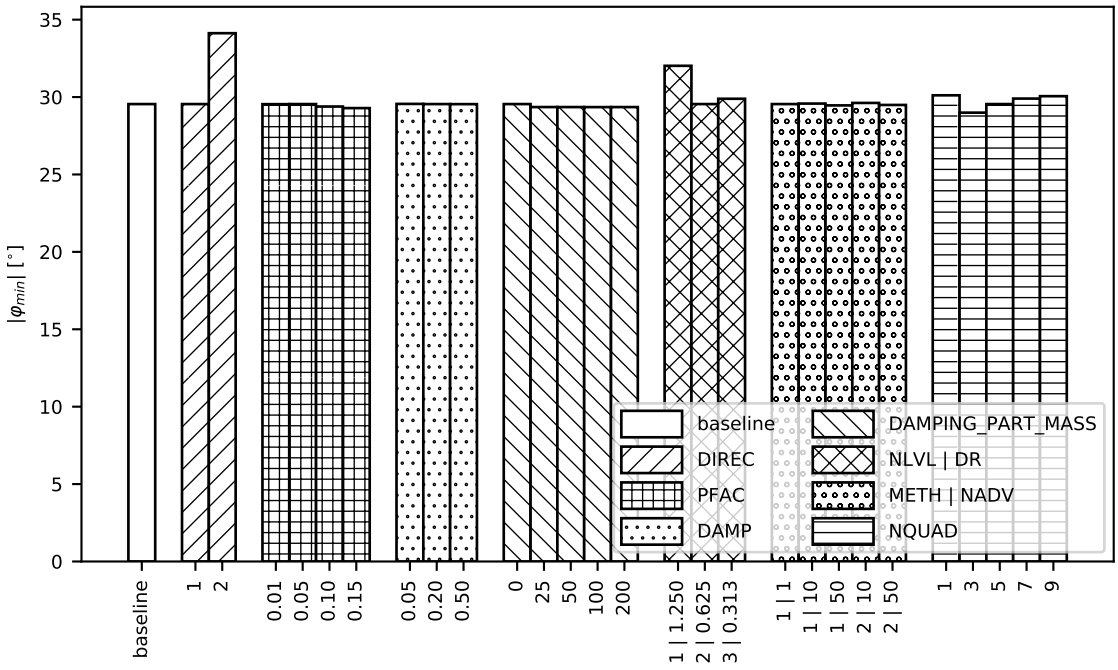

Figure A.18.: results of parametric study of FSI settings — maximal roll angle

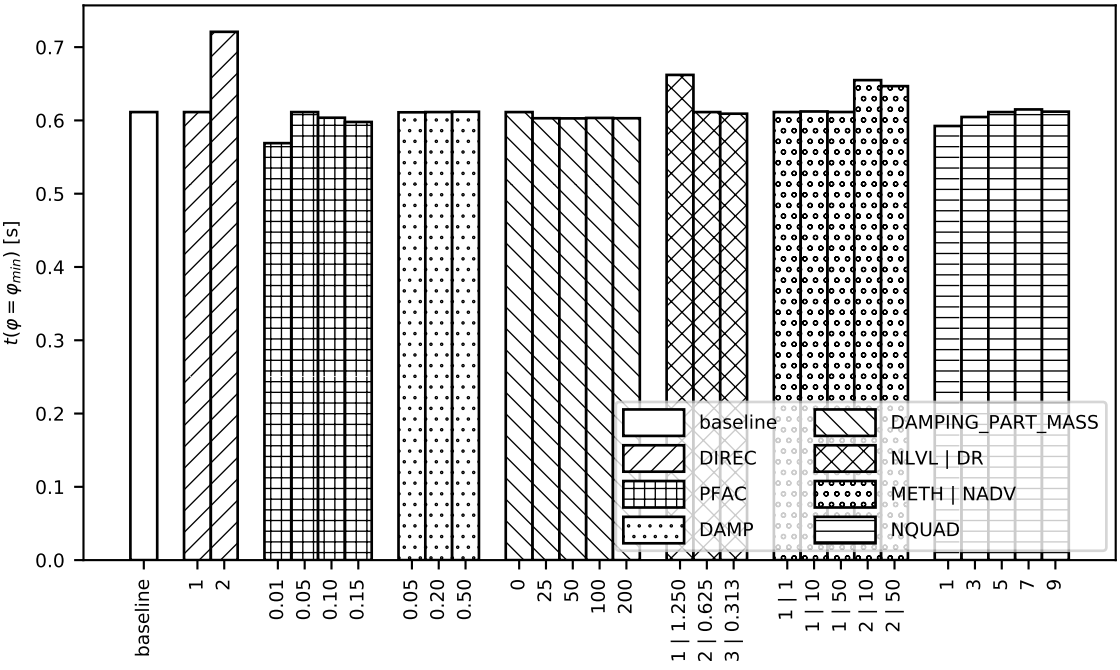

Figure A.19.: results of parametric study of FSI settings — time at maximal roll angle

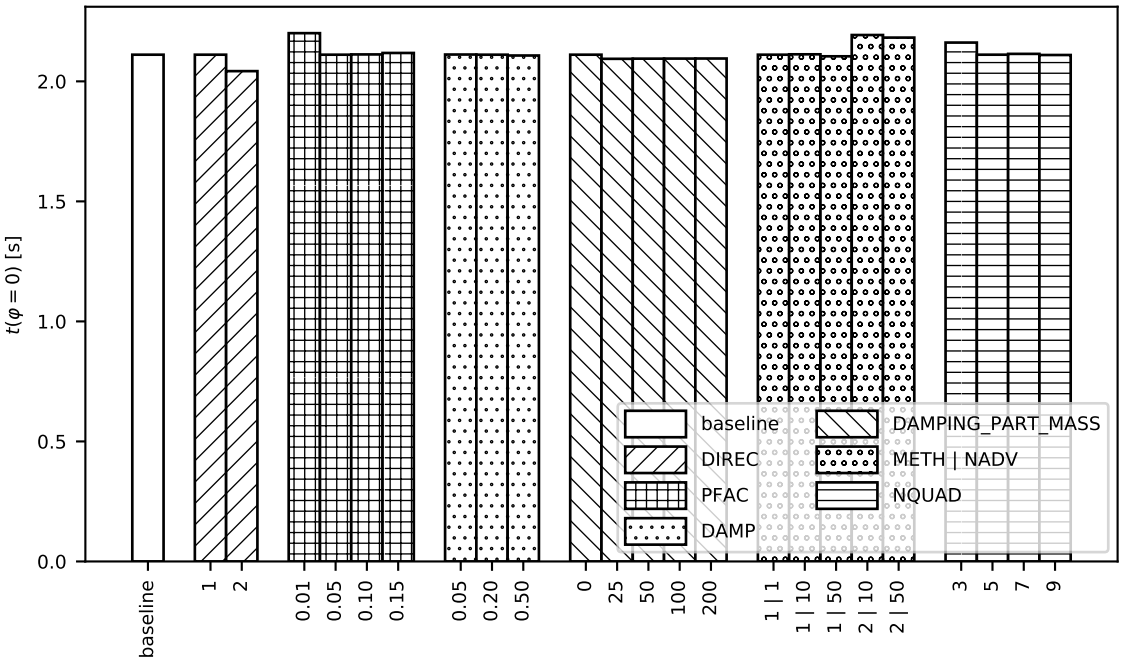

Figure A.20.: results of parametric study of FSI settings — time at roll angle equals zero

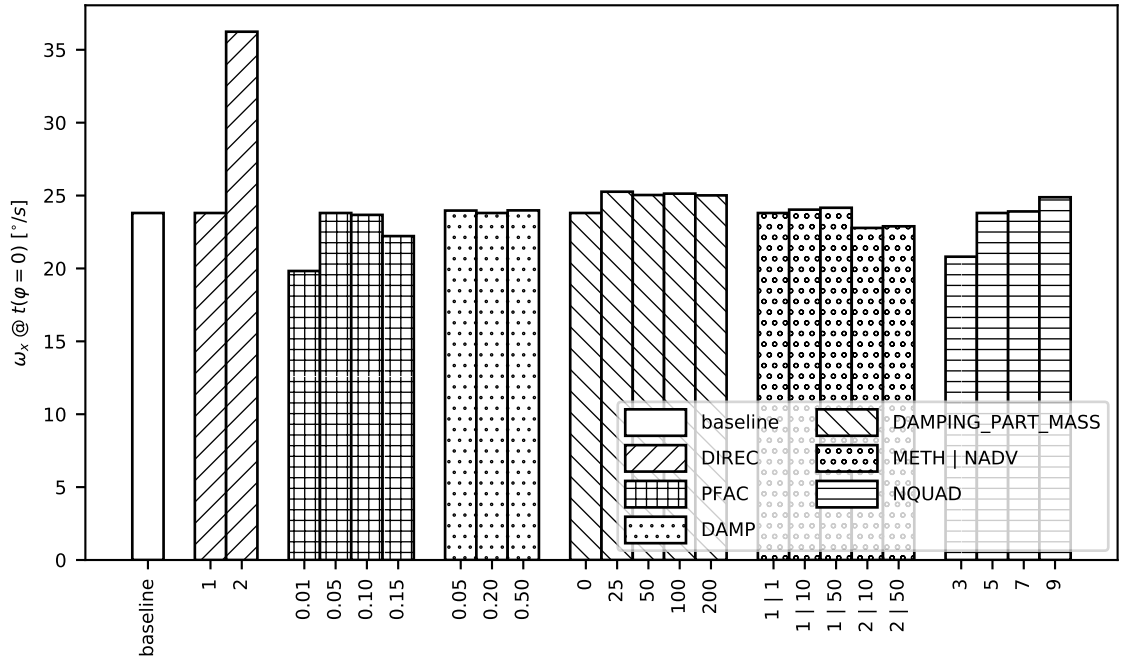

Figure A.21.: results of parametric study of FSI settings — roll velocity while roll angle equals zero

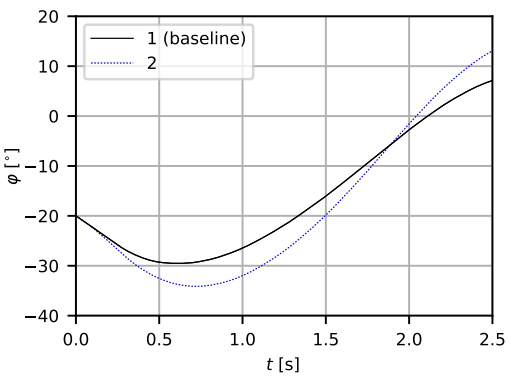

(a) DIREC

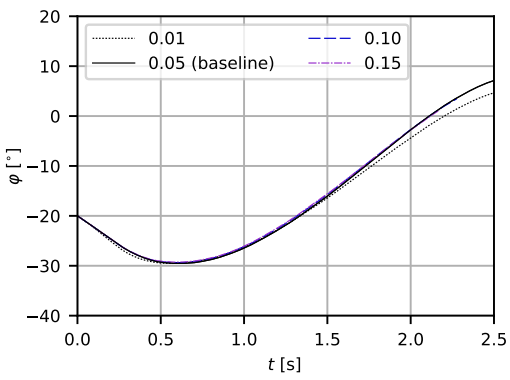

(b) PFAC

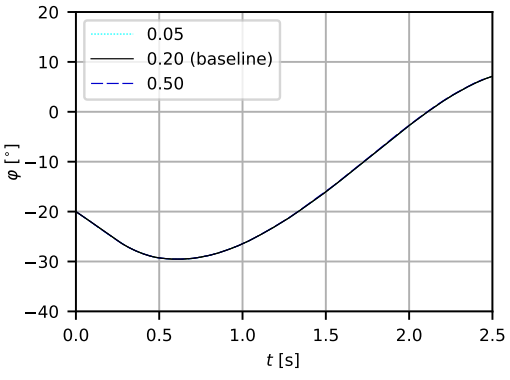

(c) DAMP

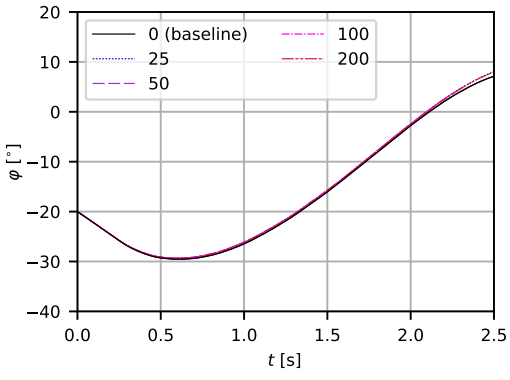

(d) DAMPING_PART_MASS

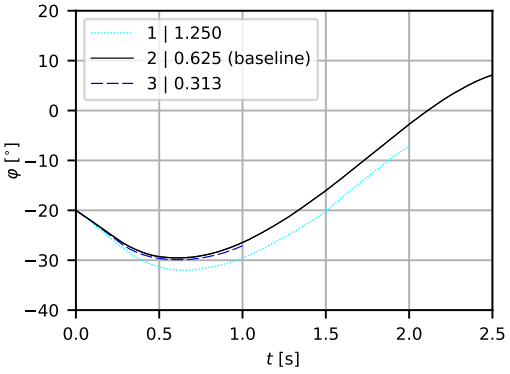

(e) NLVL | mesh density ratio

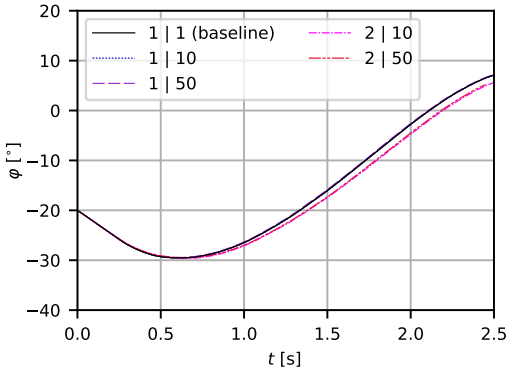

(f) advection method (METH | NADV)

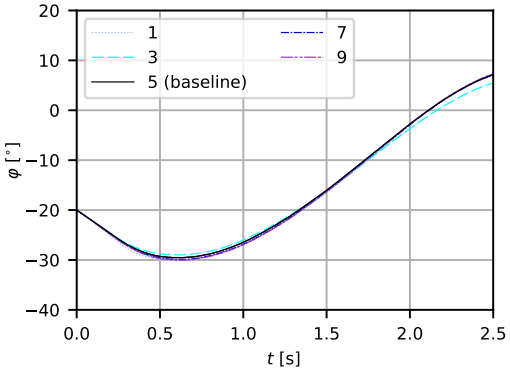

(g) NQUAD

Figure A.22.: results of parametric study of FSI settings — roll angle

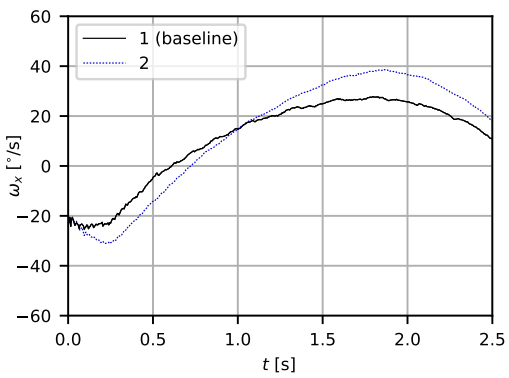

(a) DIREC

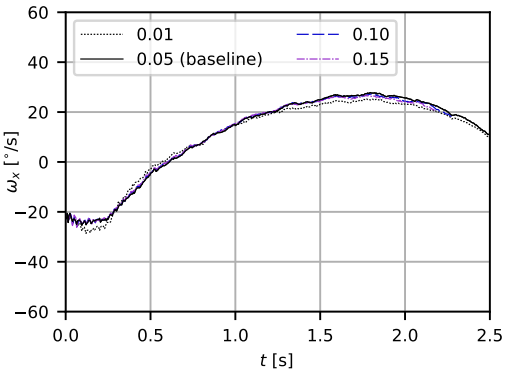

(b) PFAC

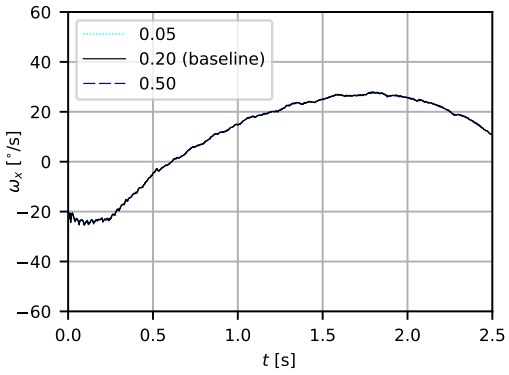

(c) DAMP

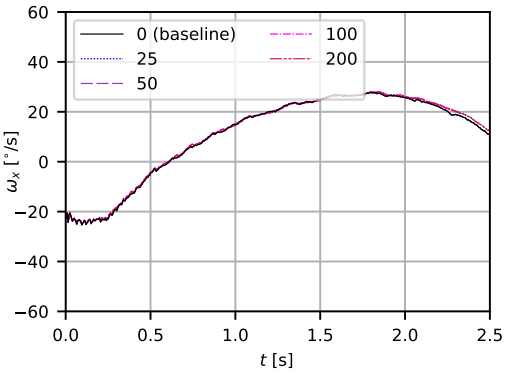

(d) DAMPING_PART_MASS

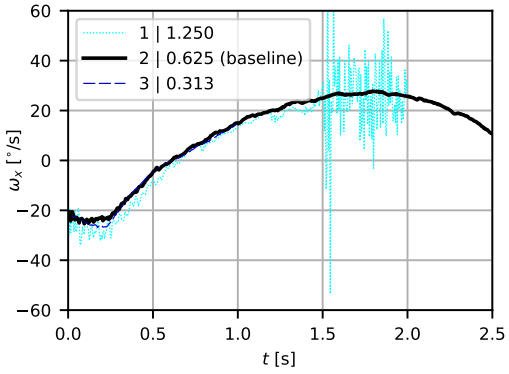

(e) NLVL | mesh density ratio

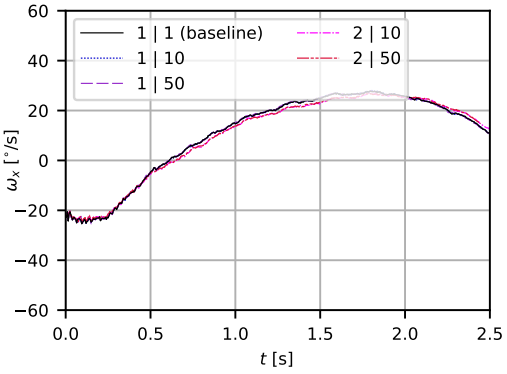

(f) advection method (METH | NADV)

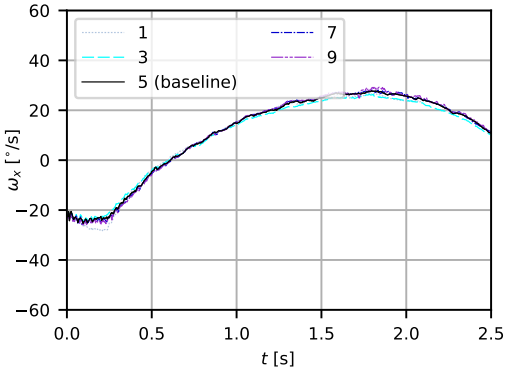

(g) NQUAD

Figure A.23.: results of parametric study of FSI settings — roll velocity

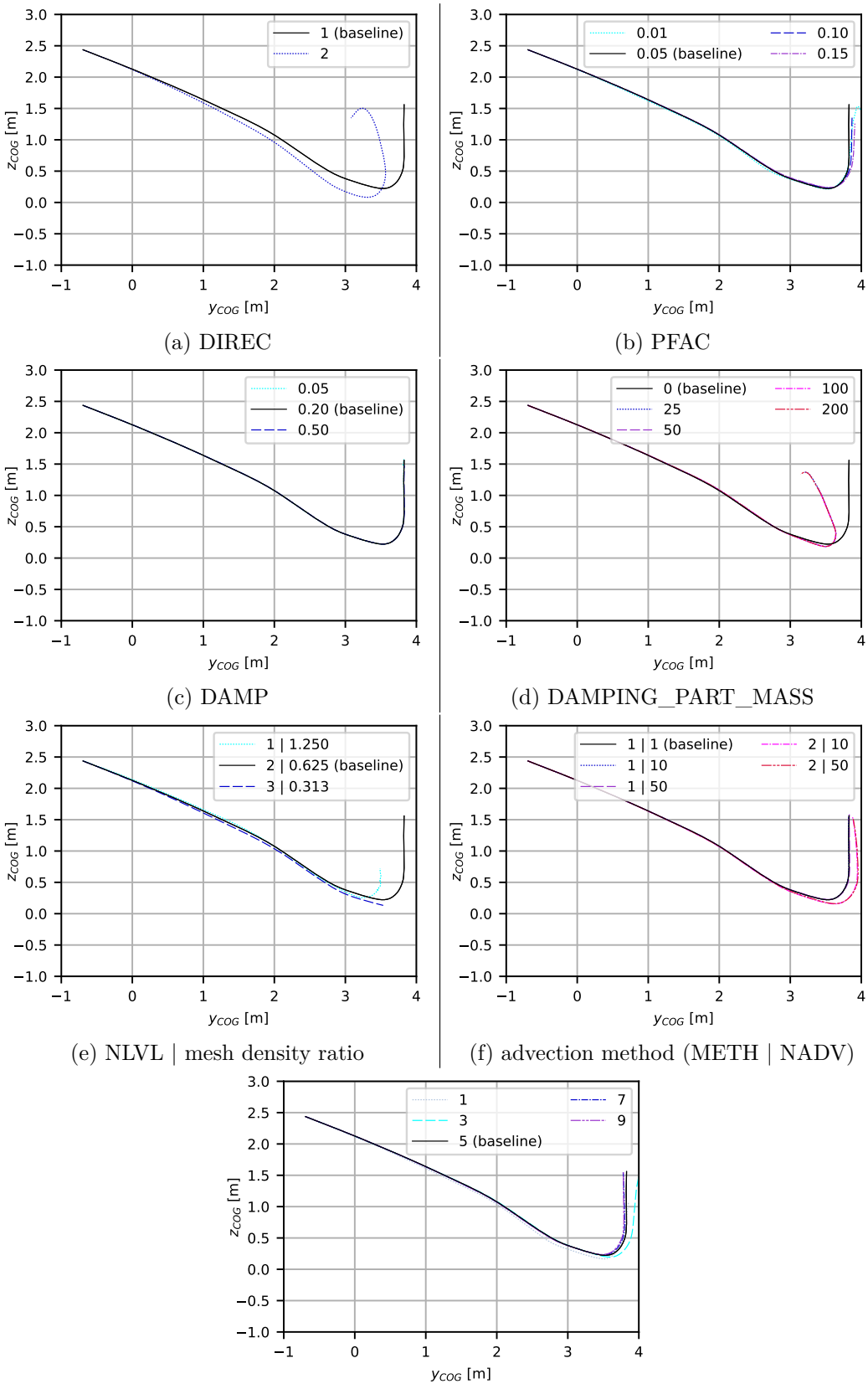

(a) DIREC

(b) PFAC

(c) DAMP

(d) DAMPING_PART_MASS

(e) NLVL | mesh density ratio

(f) advection method (METH | NADV)

(g) NQUAD

Figure A.24.: results of parametric study of FSI settings — trajectory of COG

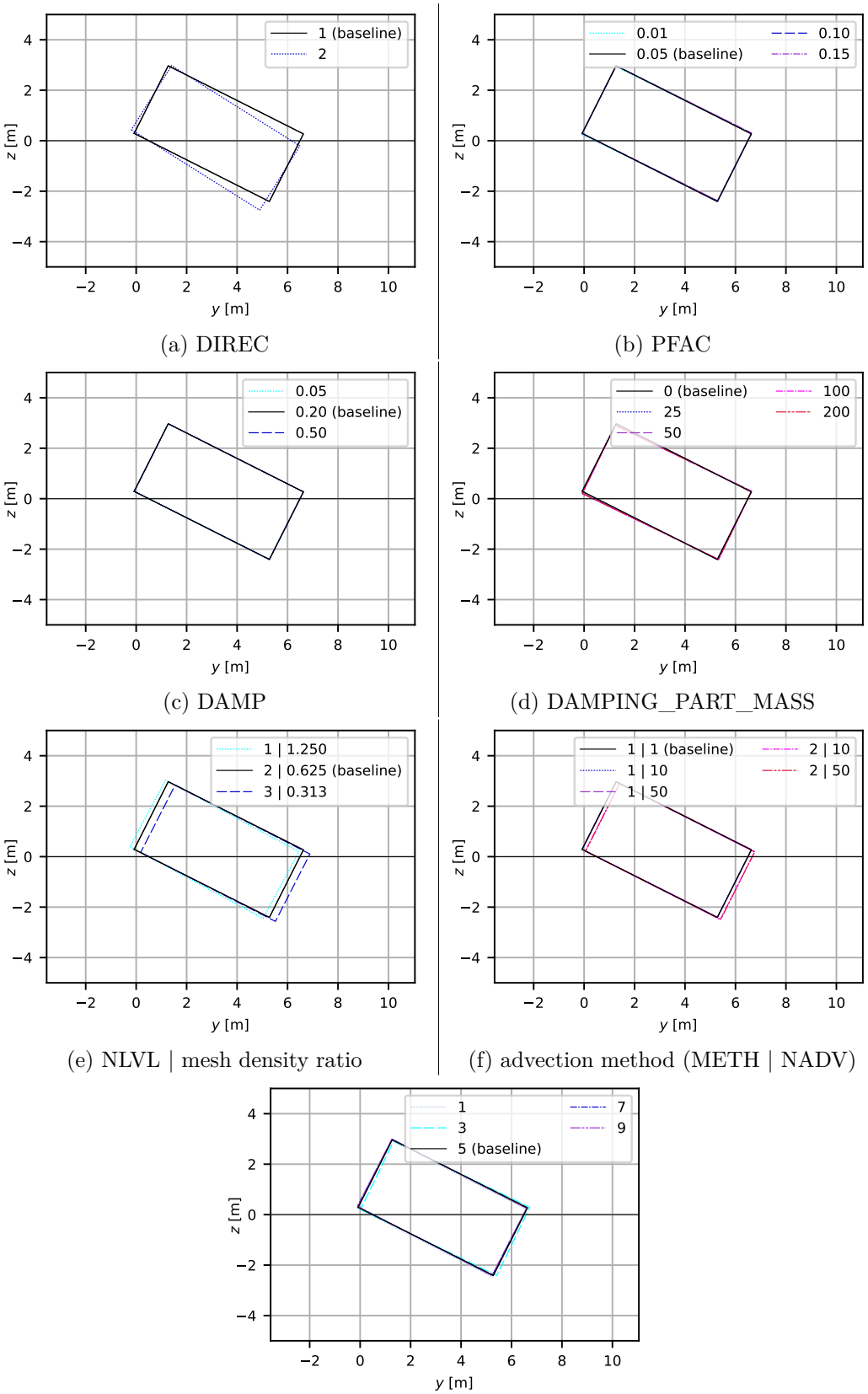

(a) DIREC

(b) PFAC

(c) DAMP

(d) DAMPING_PART_MASS

(e) NLVL | mesh density ratio

(f) advection method (METH | NADV)

(g) NQUAD

Figure A.25.: results of parametric study of FSI settings — point of deepest immersion

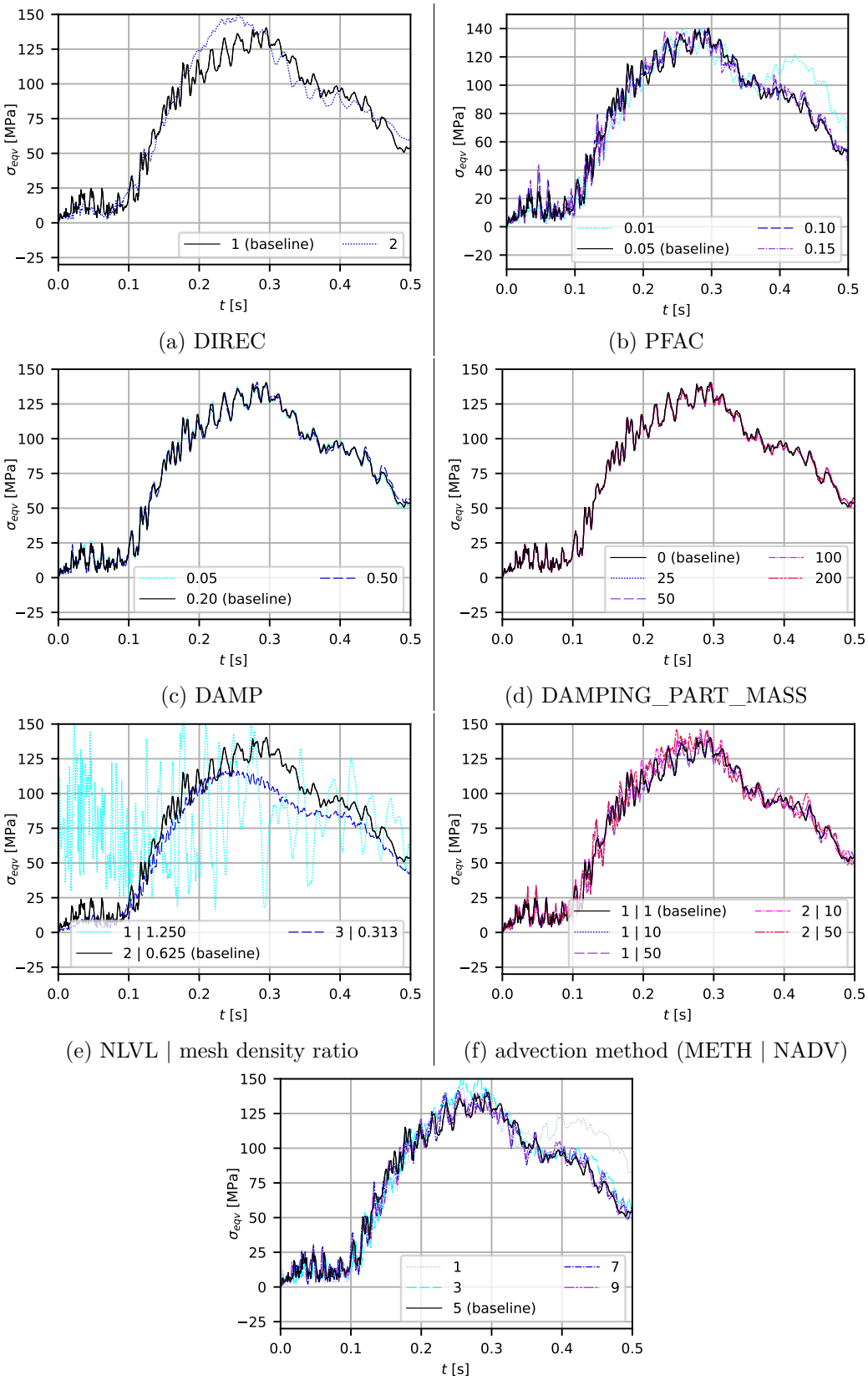

(a) DIREC

(b) PFAC

(c) DAMP

(d) DAMPING_PART_MASS

(e) NLVL | mesh density ratio

(f) advection method (METH | NADV)

(g) NQUAD

Figure A.26.: results of parametric study of FSI settings — stresses (side plating)

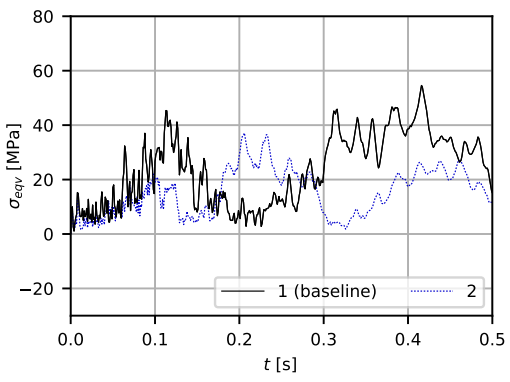

(a) DIREC

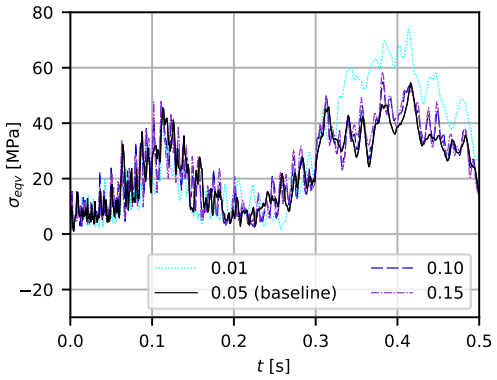

(b) PFAC

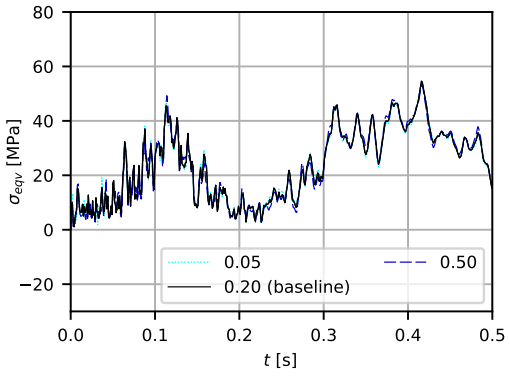

(c) DAMP

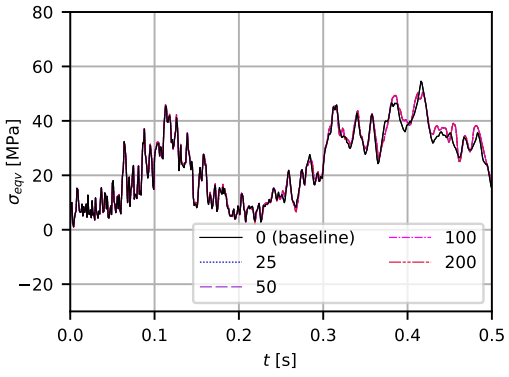

(d) DAMPING_PART_MASS

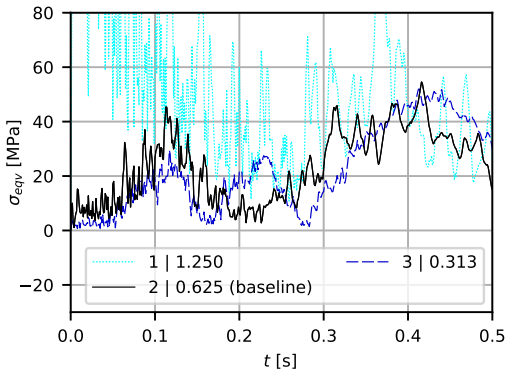

(e) NLVL | mesh density ratio

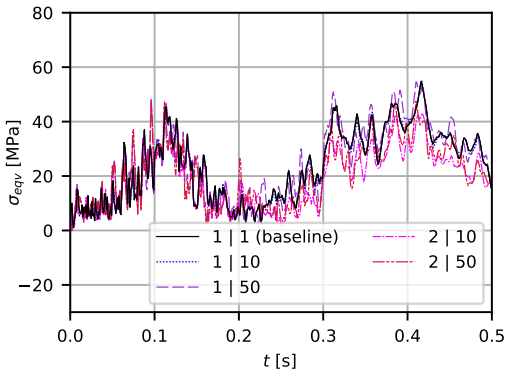

(f) advection method (METH | NADV)

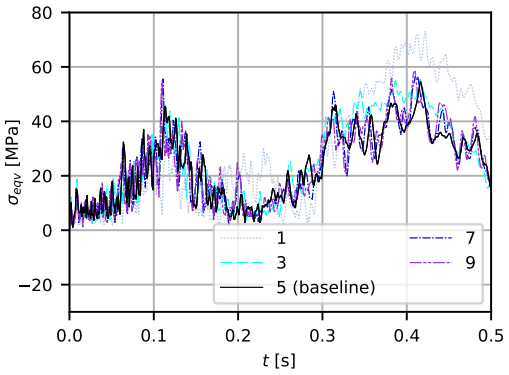

(g) NQUAD

Figure A.27.: results of parametric study of FSI settings — stresses (bottom plating)

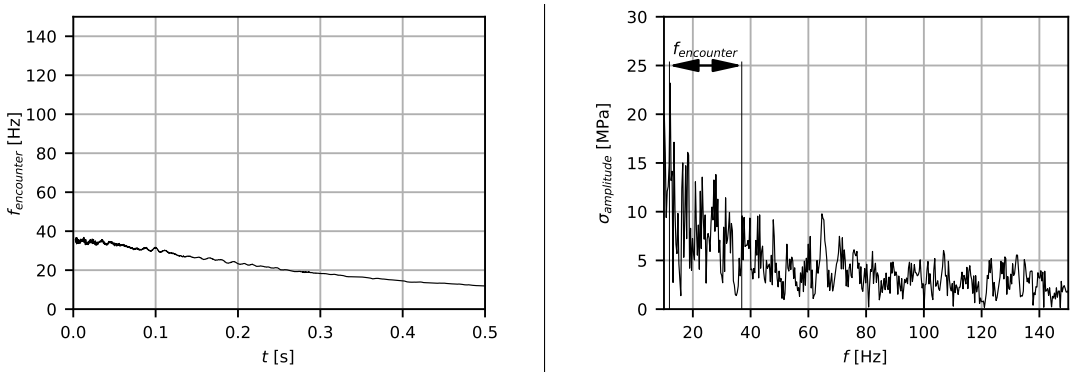

(a) encounter frequency (b) FFT

Figure A.28.: results of parametric study of FSI settings — fluctuations of stresses (NLVL=1 | DR = 1.250)

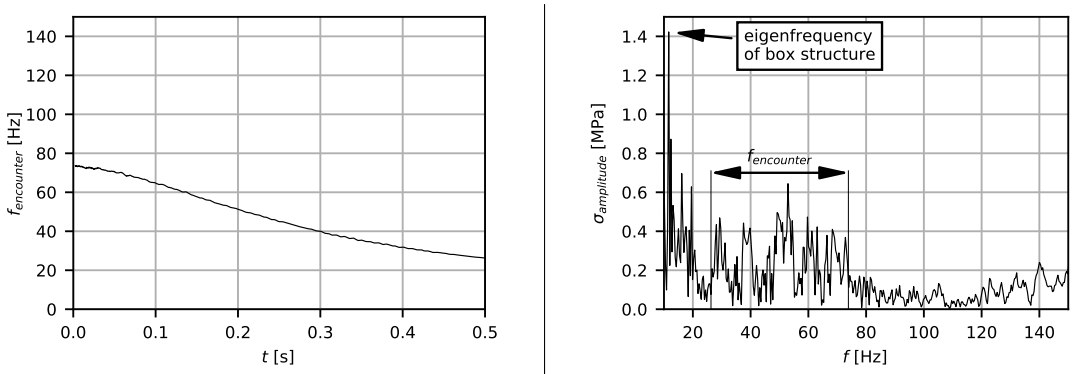

(a) encounter frequency (b) FFT

Figure A.29.: results of parametric study of FSI settings — fluctuations of stresses (NLVL=2 | DR = 0.625 | baseline)

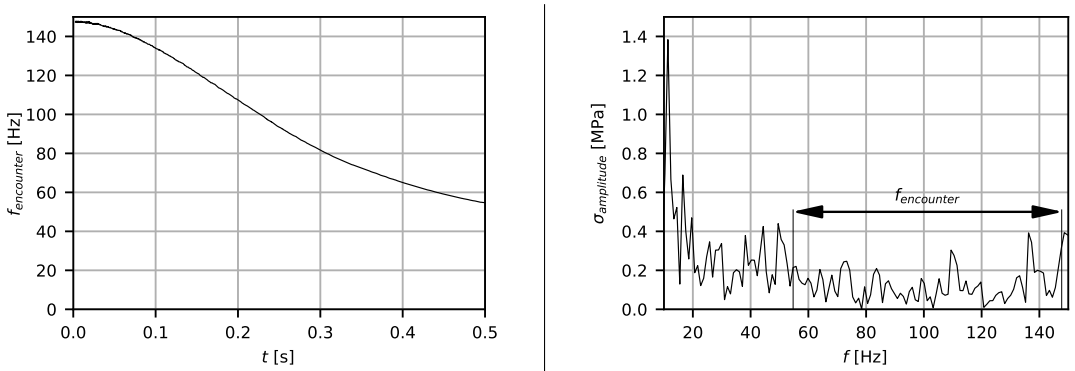

(a) encounter frequency (b) FFT

Figure A.30.: results of parametric study of FSI settings — fluctuations of stresses (NLVL=3 | DR = 0.313)

A.9. Verification of Arbitrary-Lagrangian-Eulerian approach

Table A.6.: verification of ALE approach — material models used for ship model

NFRPC:

parameter	unit	value
E_Y	[GPa]	35.00
ν	[-]	0.30
ρ	[kg/m^3]	1310

ABS plastis:

parameter	unit	value
E_Y	[GPa]	1.90
ν	[-]	0.30
ρ	[kg/m^3]	1030

wood (beech):

parameter	unit	value
E_Y	[GPa]	16.00
ν	[-]	0.30
ρ	[kg/m^3]	720

Table A.7.: verification of ALE approach — properties of FEM model of ship model

parameter	unit	value
shell elements	[-]	45,100
nodal rigid bodies	[-]	28
nodes	[-]	44,600

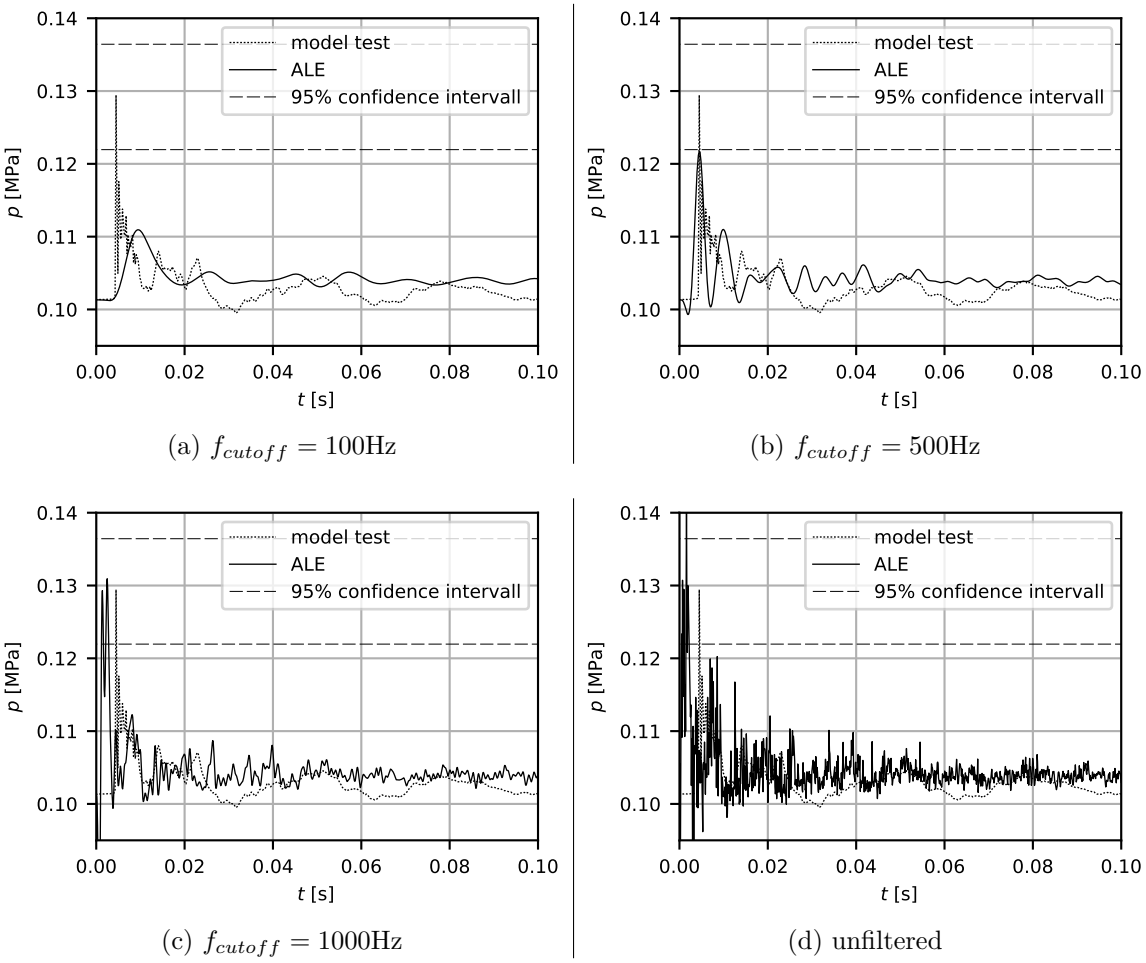

(a) $f_{cutoff} = 100\text{Hz}$ (b) $f_{cutoff} = 500\text{Hz}$

(c) $f_{cutoff} = 1000\text{Hz}$ (d) unfiltered

Figure A.31.: verification of ALE-approach — influence of filter settings on pressure-time-signals (P2 @ LC_01)

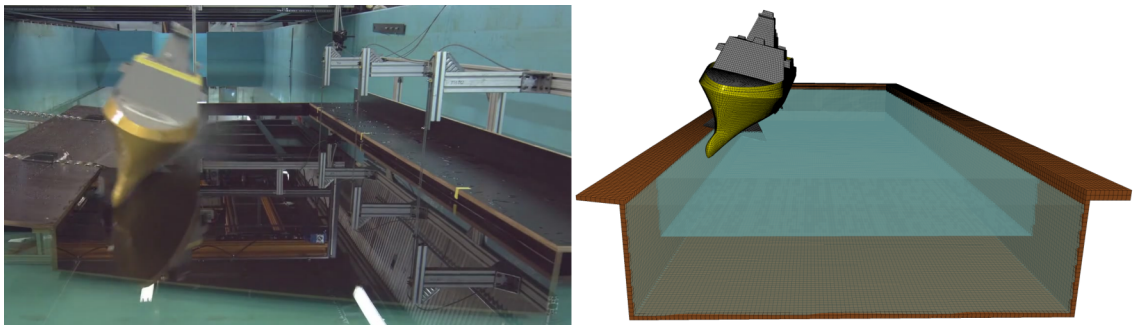

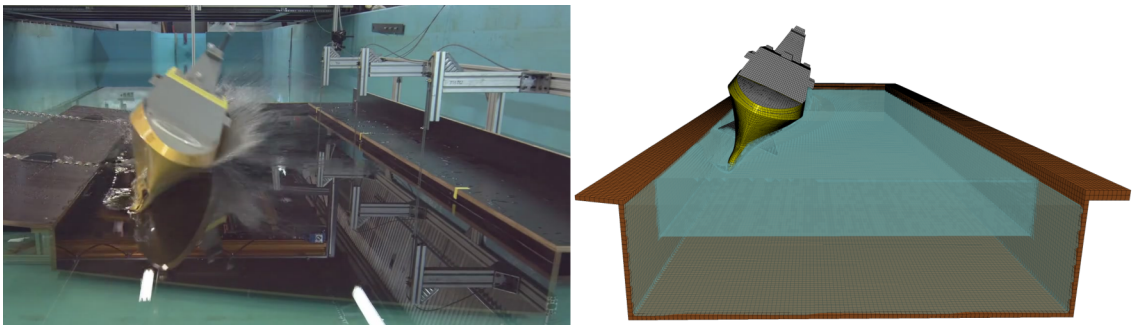

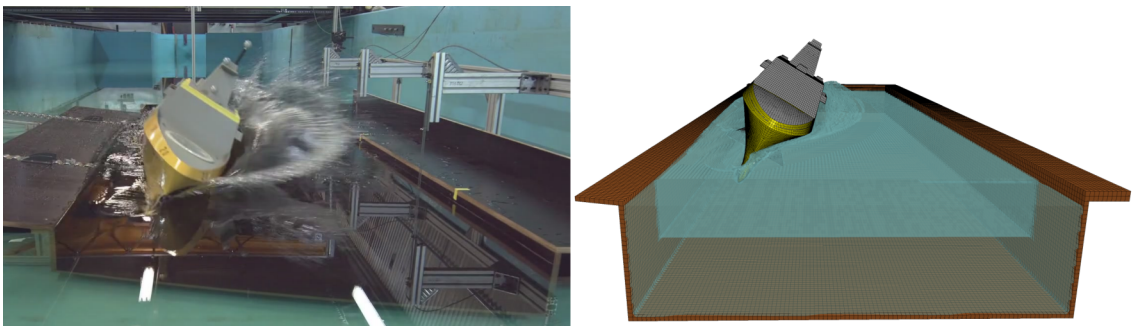

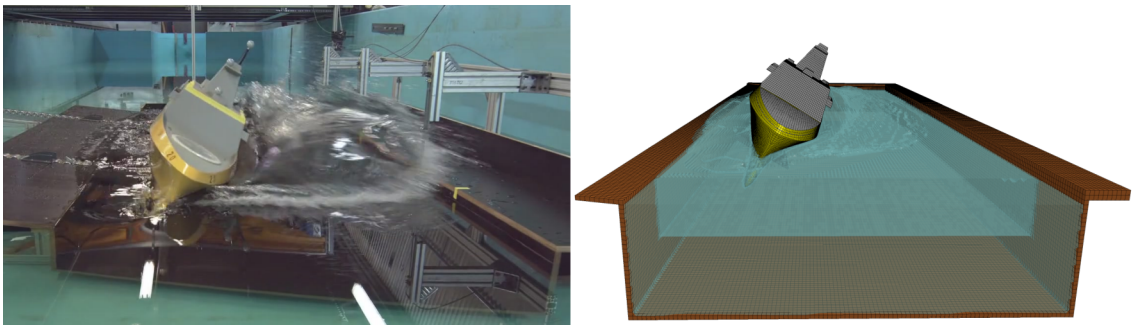

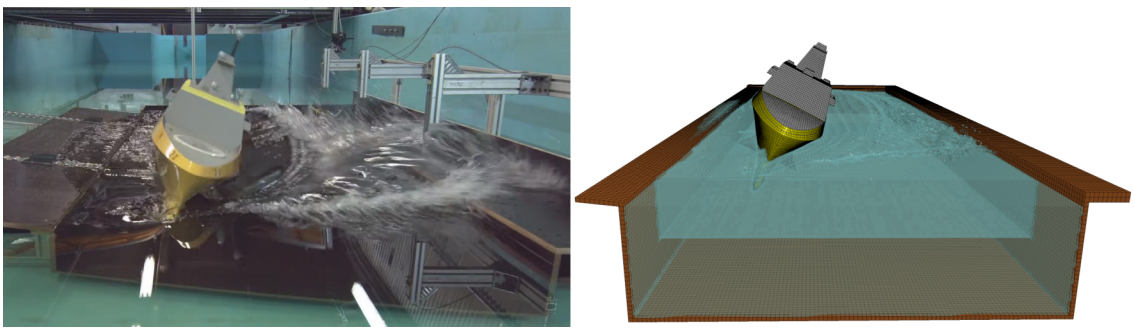

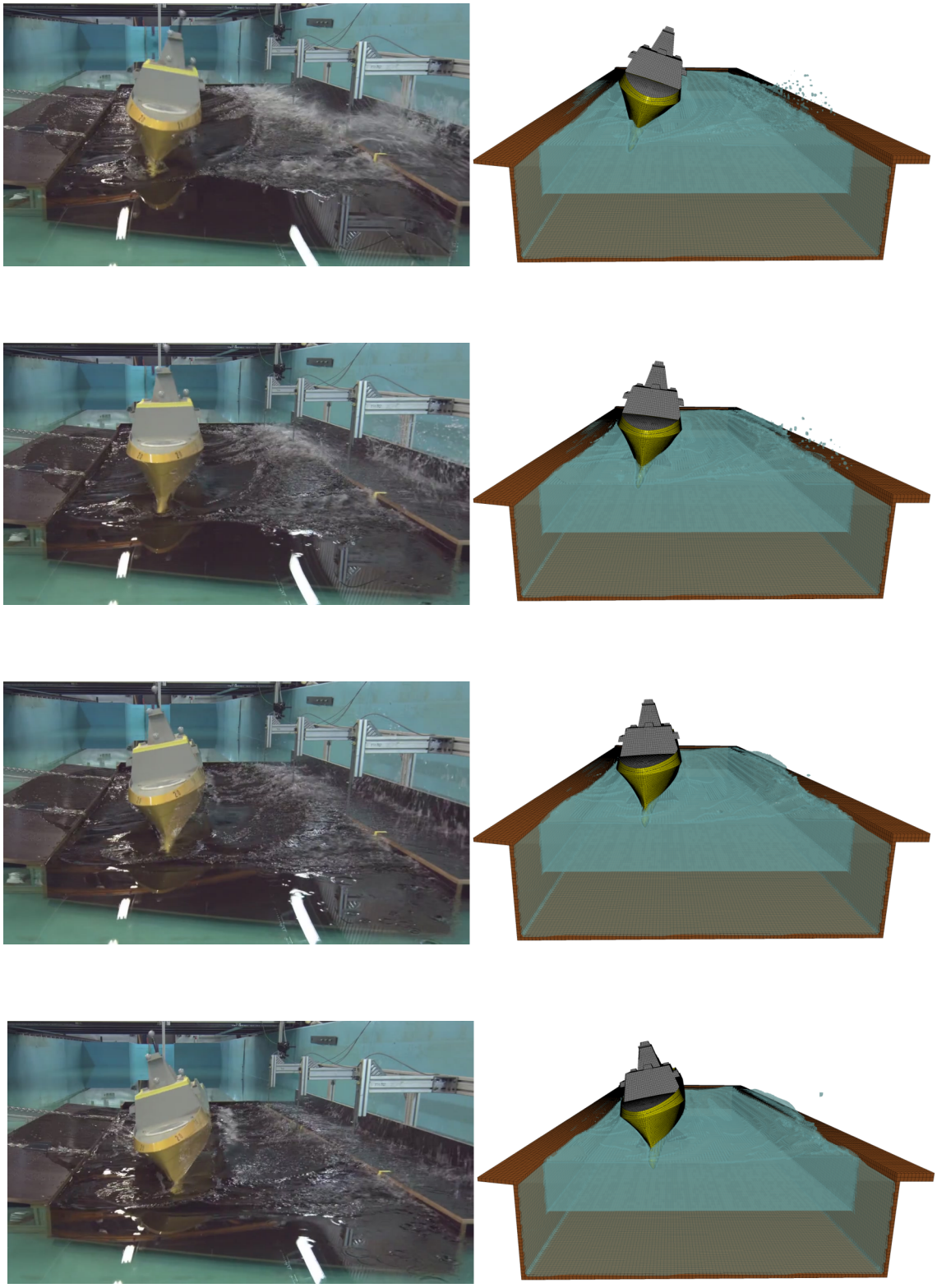

Figure A.32.: verification of ALE approach — comparison with model tests (LC_01)

A.10. Settings used for Arbitrary-Lagrangian-Eulerian approach

Within this section of the Appendix all settings specific to simulations using FSI based on the ALE approach are provided. The following settings are used within the k-File of LS-DYNA for the setup of the ALE approach / FSI algorithm:

```
*CONTROL_ALE
$#      DCT      NADV      METH      AFAC      BFAC      CFAC      DFAC      EFAC
        -1        50         2      -1.0       0.0       0.0       0.0       0.0
$#    START       END     AAFAC     VFACT      PRIT       EBC      PREF  NSIDEBC
        0.0   1.0E20       1.0   1.0E-6         0         0  1.013E5         0
$#     NCPL      NBKT    IMASCL    CHECKR   BEAMIN  MMGPREF   PDIFMX  DTMUFAC
        1         50         0       0.0       0.0         0       0.0       0.0

*CONTROL_REFINE_ALE
$#       ID      TYPE       NLVL     MMSID      IBOX
        46         0          1        47         1
$#   NTOTRF    NCYCRF    CRITRF    VALRF     BEGRF     ENDRF     LAYRF
   1000000     100.0         0       0.0       0.0       0.0         2
$#    MAXRM    NCYCRM    CRITRM    VALRM     BEGRM     ENDRM    MMSRM
        0       0.0         0       0.0       0.0       0.0         0

*CONSTRAINED_LAGRANGE_IN_SOLID_TITLE
Lagrange_in_Solid_Hull_Structure
$#    SLAVE    MASTER     SSTYP     MSTYP     NQUAD     CTYPE     DIREC     MCOUP
      10002        41         0         0         1         4         2       -42
$#    START       END      PFAC      FRIC    FRCMIN      NORM   NORMTYP      DAMP
        0.0   1.0E20      0.05      0.10      0.30         0         1      0.20
$#       CQ      HMIN      HMAX     ILEAK     PLEAK   LCIDPOR     NVENT  BLOCKAGE
        0.0       0.0       0.0         0     1E-4         0         0         0
$#   IBOXID   IPENCHK    INTFORC   IALESOF    LAGMUL    PFACMM      THKF
        0         0         1         0       0.0         0       0.0

*DAMPING_PART_MASS_SET
$#      PSID      LCID        SF      FLAG
        44         1      10.0         0

*DEFINE_CURVE_TITLE
Unit Curve
$#      LCID      SIDR       SFA       SFO      OFFA      OFFO    DATTYP     LCINT
        1         0         1.0       1.0       0.0       0.0         0         0
$#                  A1                  O1
                   0.0                 1.0
                1.0E20                 1.0
```

The following two pfile are used for the decomposition of the FEM model for the ALE approach as necessary for the MPP version of LS-DYNA.

This pfile divides the model for a simulation with 16 cores using the RCB method (decomposition with RCB method — default):

```
decomposition {
    file decomposition
    numproc 16
}
```

The resulting decomposition is shown in Figure A.33. The values for `x_min`, `x_max`, `y_min`, `y_max`, `z_min` and `z_max` are the border of the FEM model. Corresponding values are to be inserted into the pfile. The colours in Figure A.33 represent the distribution of the FEM model on the different cores used for the simulation.

The following pfile divides the model for a simulation with 16 cores along the x-axis of the model based on 16 manually defined regions (decomposition along x-axis — optimized settings):

```
decomposition {
    file decomposition
    numproc 16
    region { box x_min x_1 y_min y_max z_min z_max sx 5000}
    region { box x_1 x_2 y_min y_max z_min z_max sx 5000}
    region { box x_2 x_3 y_min y_max z_min z_max sx 5000}
    region { box x_3 x_4 y_min y_max z_min z_max sx 5000}
    region { box x_4 x_5 y_min y_max z_min z_max sx 5000}
    region { box x_5 x_6 y_min y_max z_min z_max sx 5000}
    region { box x_6 x_7 y_min y_max z_min z_max sx 5000}
    region { box x_7 x_8 y_min y_max z_min z_max sx 5000}
    region { box x_8 x_9 y_min y_max z_min z_max sx 5000}
    region { box x_9 x_10 y_min y_max z_min z_max sx 5000}
    region { box x_10 x_11 y_min y_max z_min z_max sx 5000}
    region { box x_11 x_12 y_min y_max z_min z_max sx 5000}
    region { box x_12 x_13 y_min y_max z_min z_max sx 5000}
    region { box x_13 x_14 y_min y_max z_min z_max sx 5000}
    region { box x_14 x_15 y_min y_max z_min z_max sx 5000}
    region { box x_15 x_max y_min y_max z_min z_max sx 5000}
}
```

The resulting decomposition is shown in Figure A.34. The values for `x_min`, `x_max`, `y_min`, `y_max`, `z_min` and `z_max` are the border of the FEM model. The different values for `x_i` are the manually derived borders of the FEM model, at where an optimal distribution of work load on all 16 cores is given. Corresponding values are to be inserted into the pfile. The colours in Figure A.34 represent the distribution of the FEM model on the different cores used for the simulation.

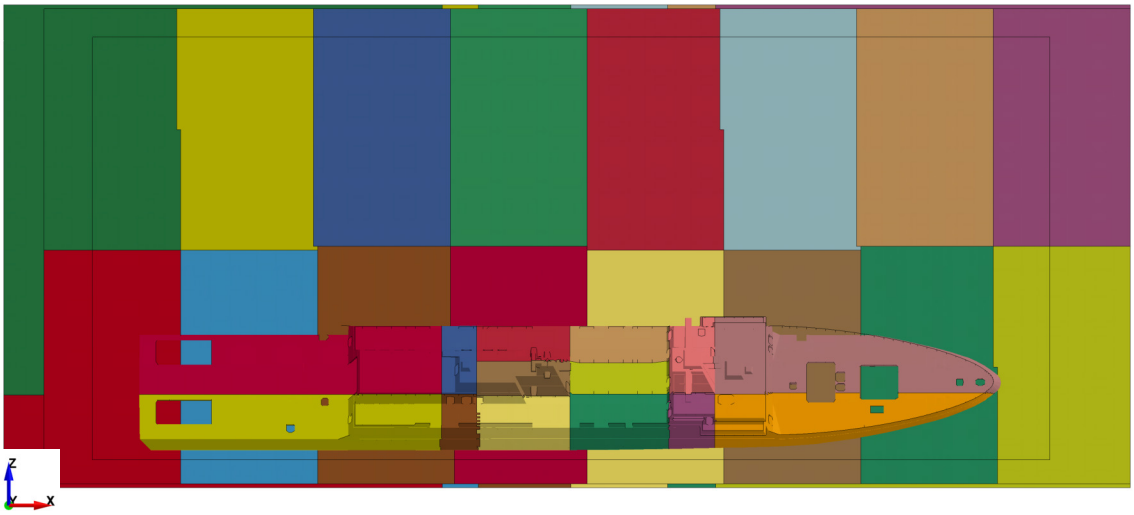

Figure A.33.: settings for simulation-based approach using FSI — decomposition of combined FEM model of SPV with RCB method (default settings)

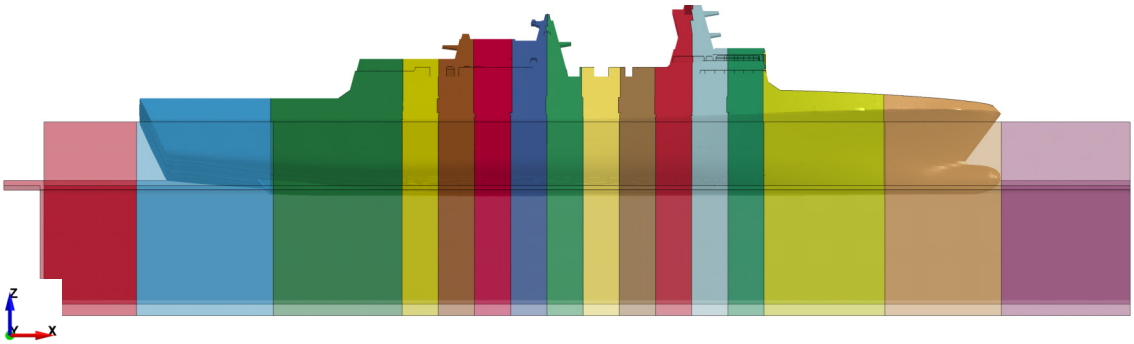

Figure A.34.: settings for simulation-based approach using FSI — decomposition of combined FEM model of SPV along x-axis (optimized settings)

A.11. Ship motion obtained with Arbitrary-Lagrangian-Eulerian approach

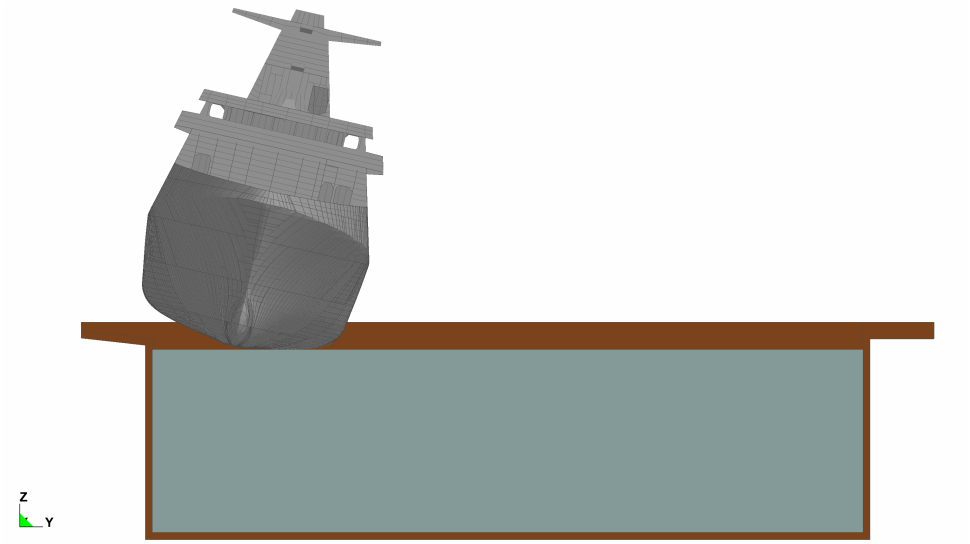

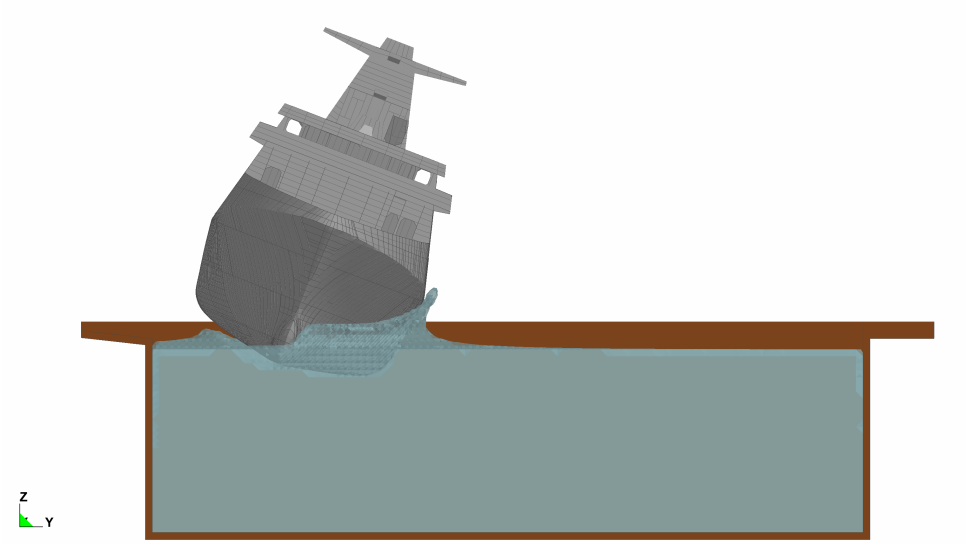

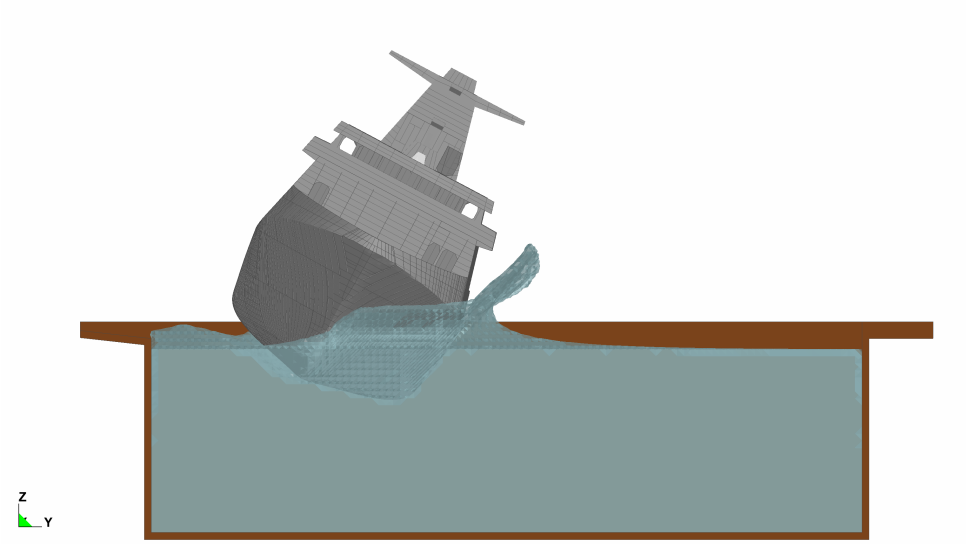
Z
Y

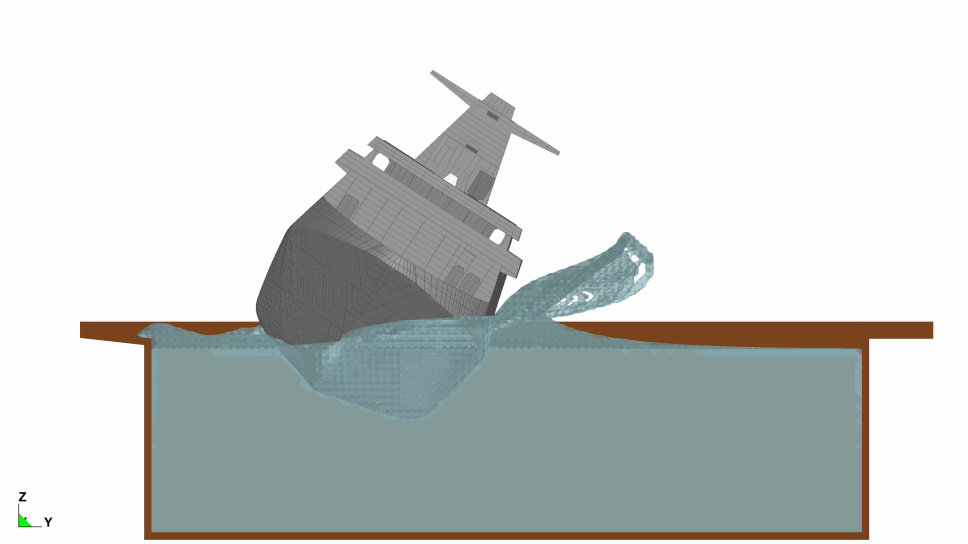
Z
Y

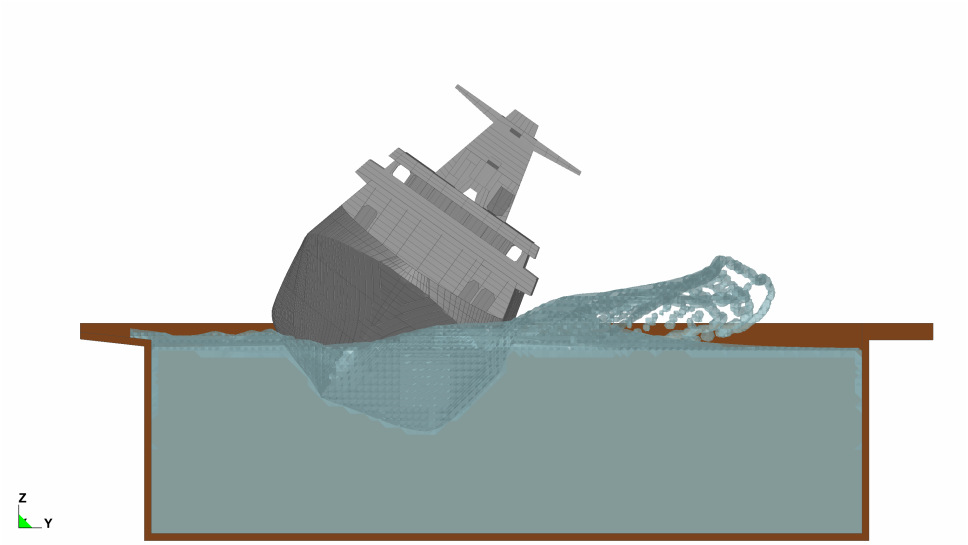
Z
Y

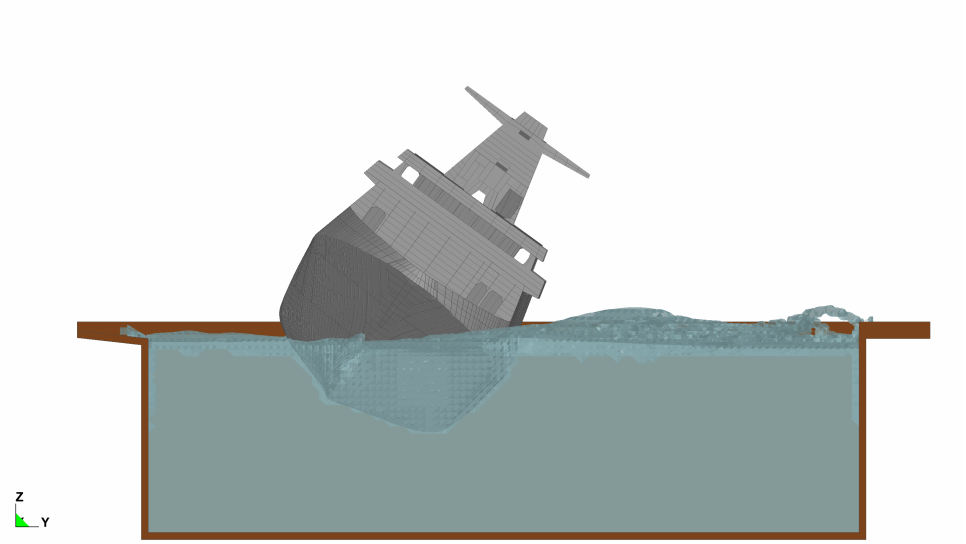
Z
Y

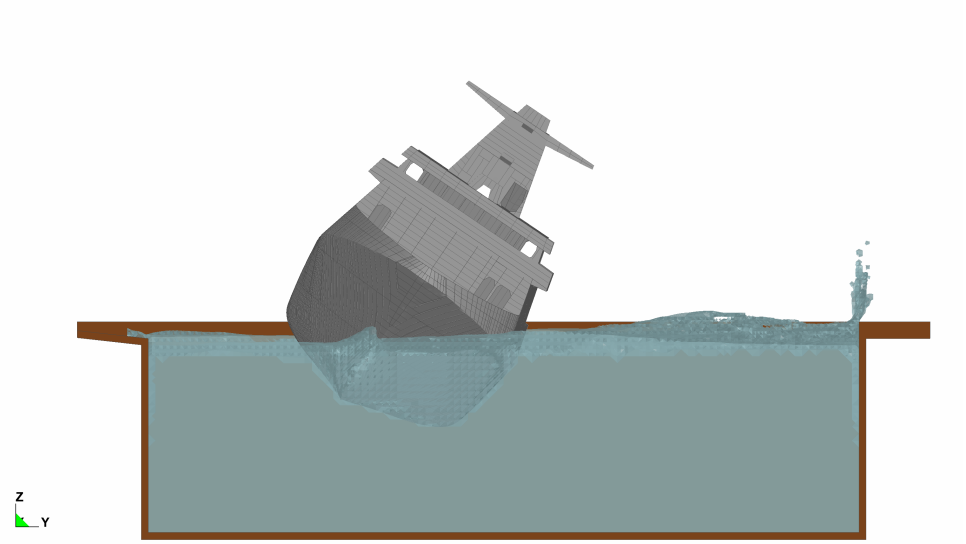
Z
Y

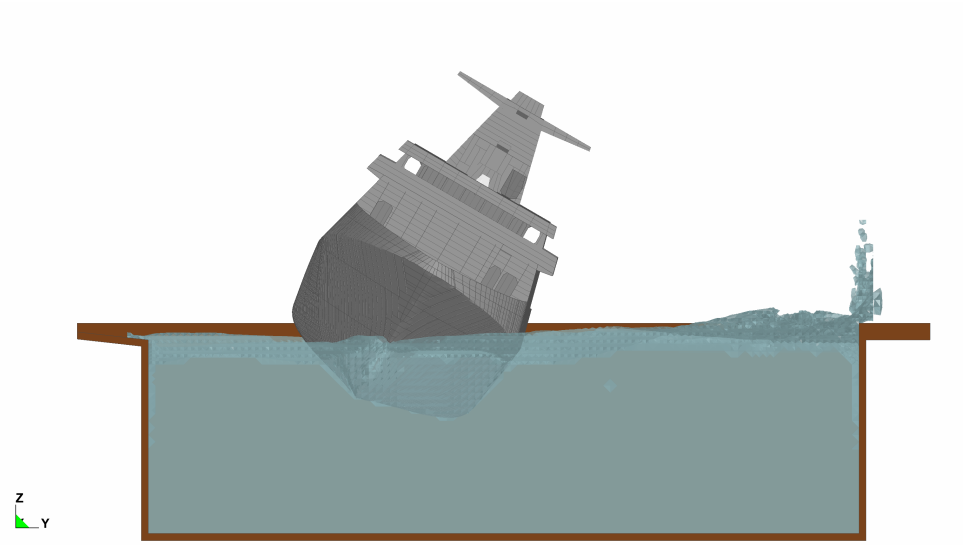
Z
Y

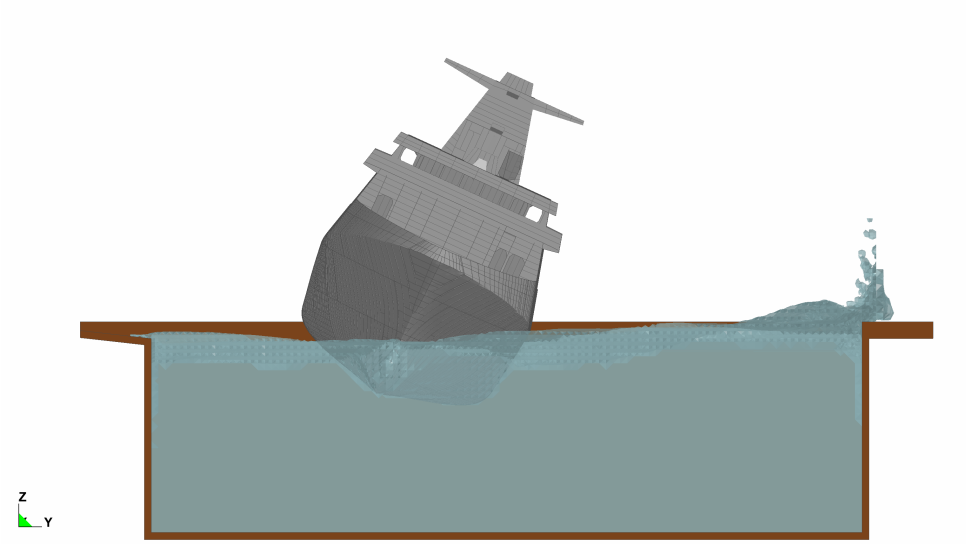
Z
Y

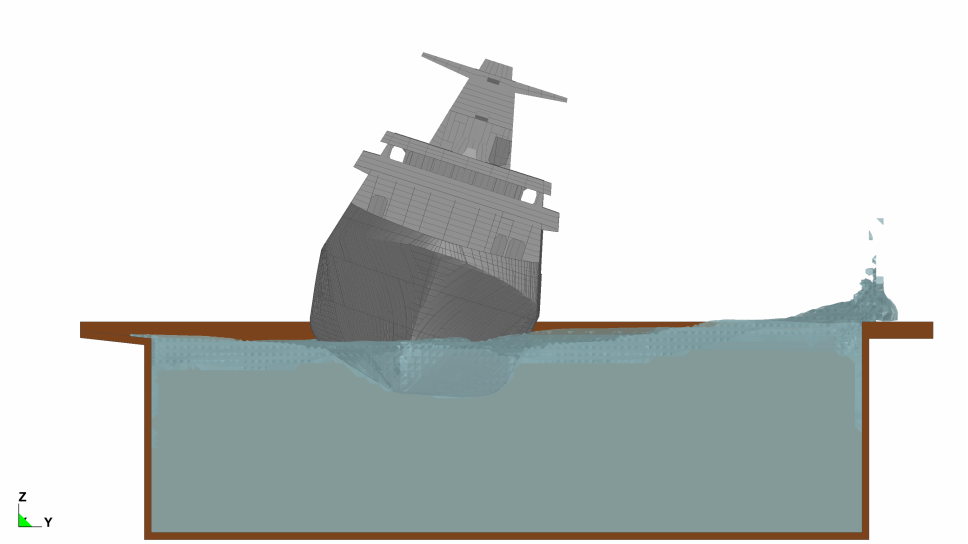
Z
Y

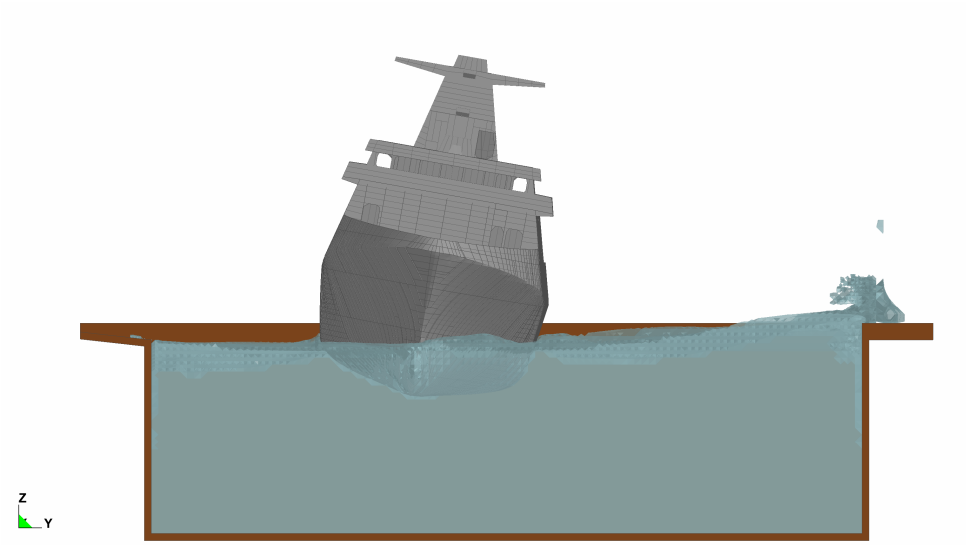
Z
Y

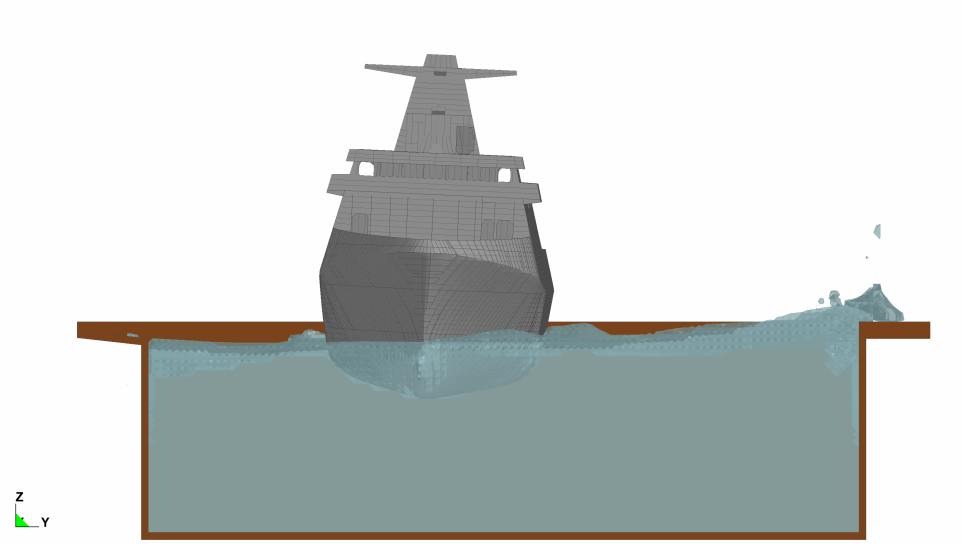
Z
Y

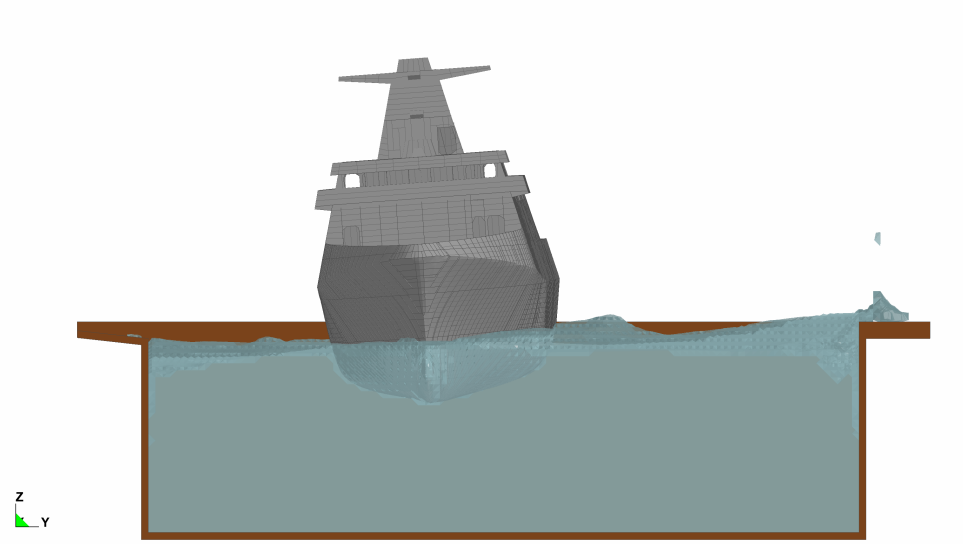
Z
Y

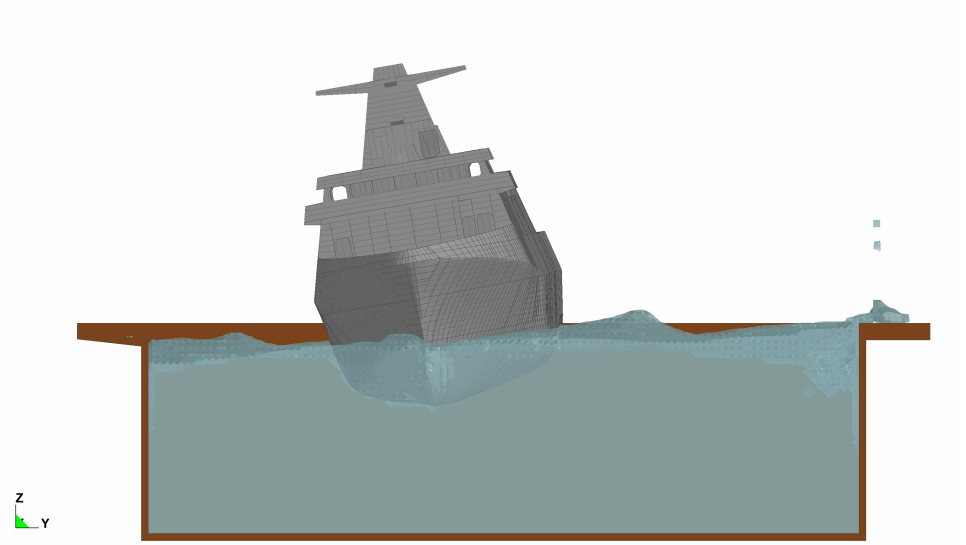
Z
Y

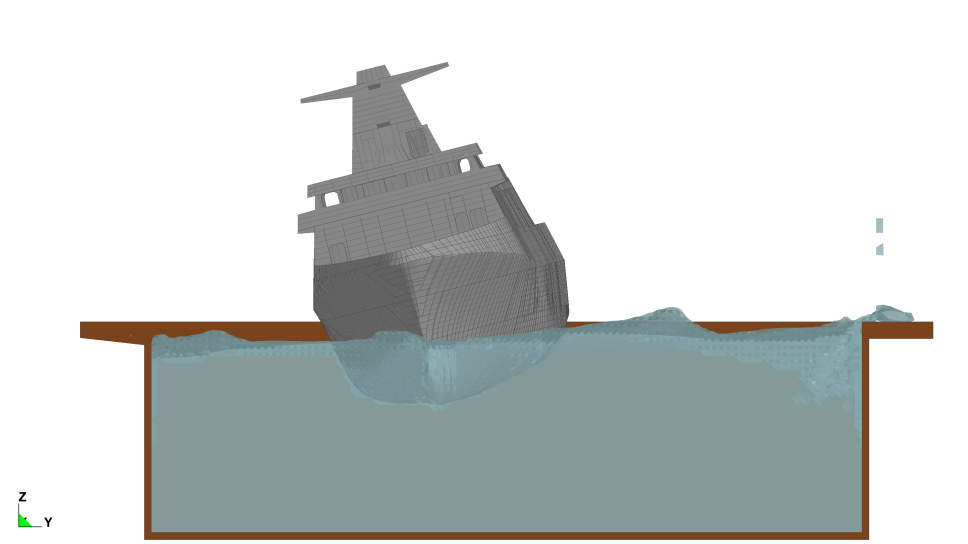
Z
Y

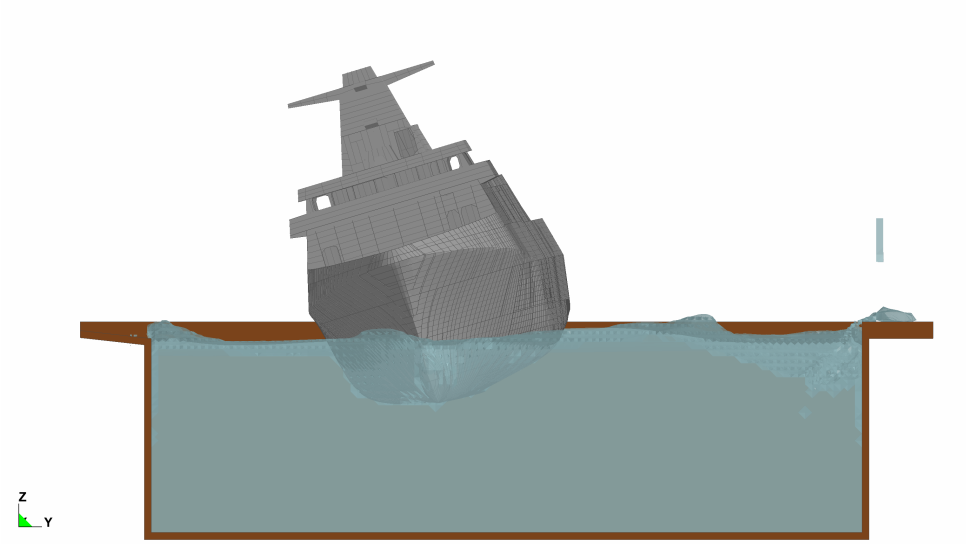
Z
Y

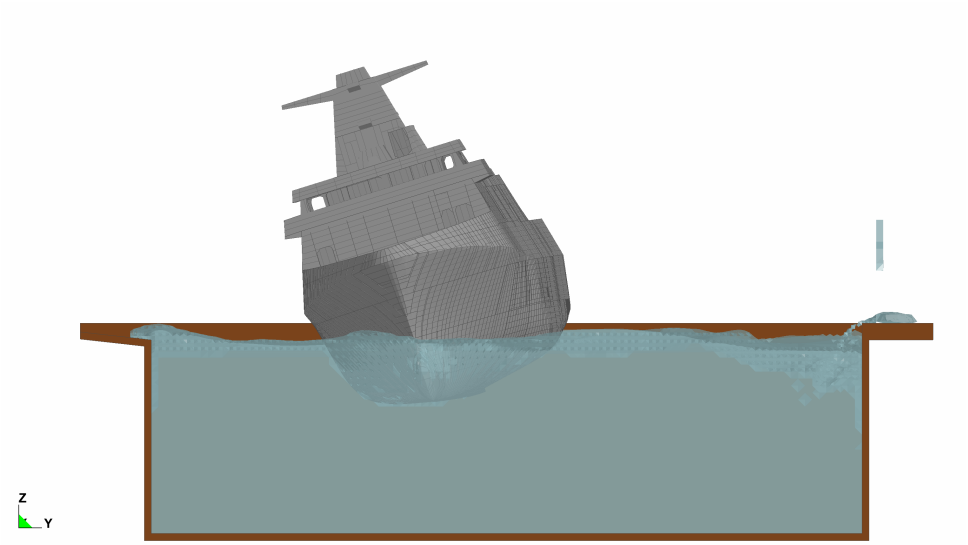
Z
Y

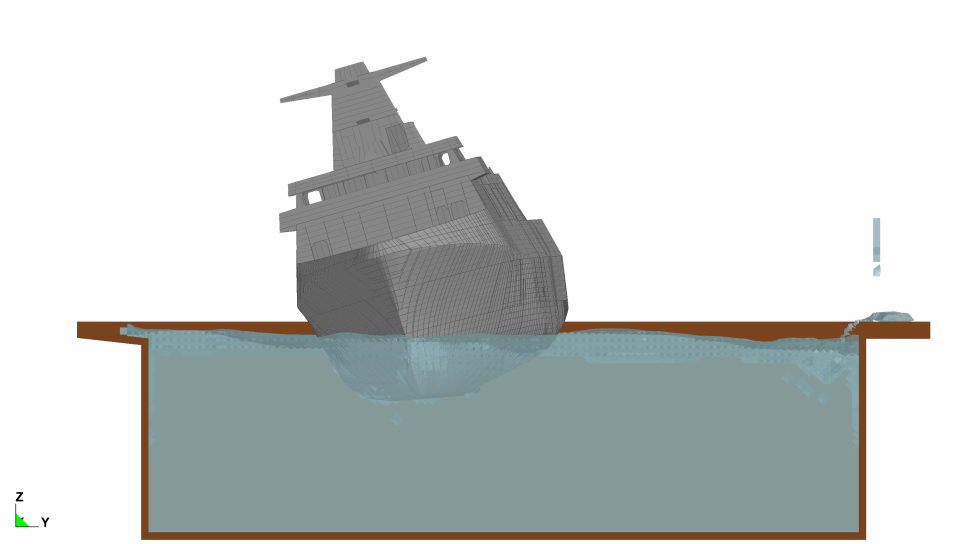
Z
Y

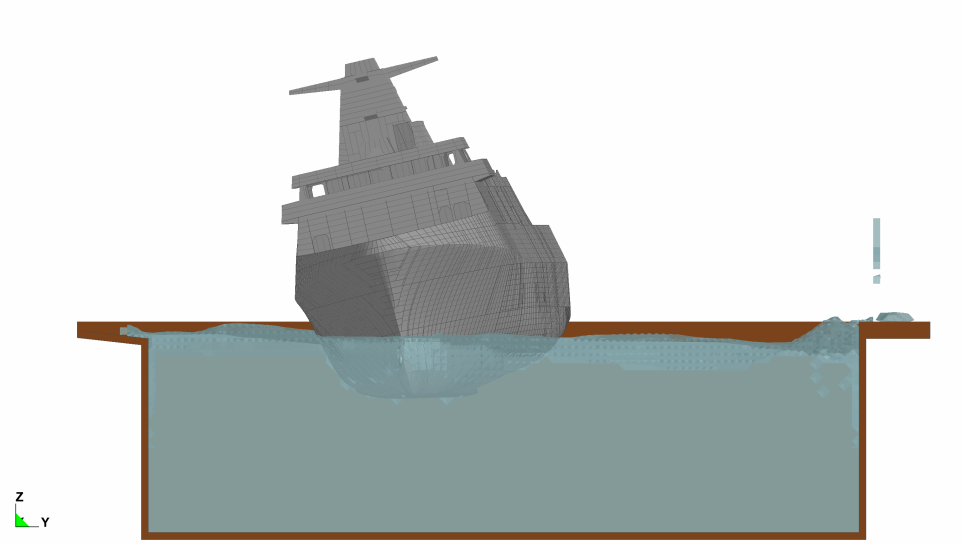
Z
Y

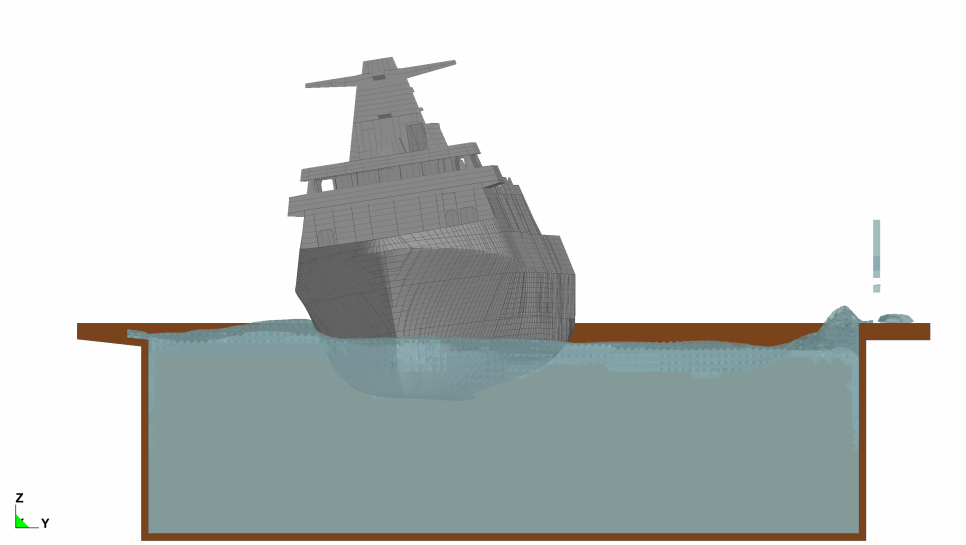
Z
Y

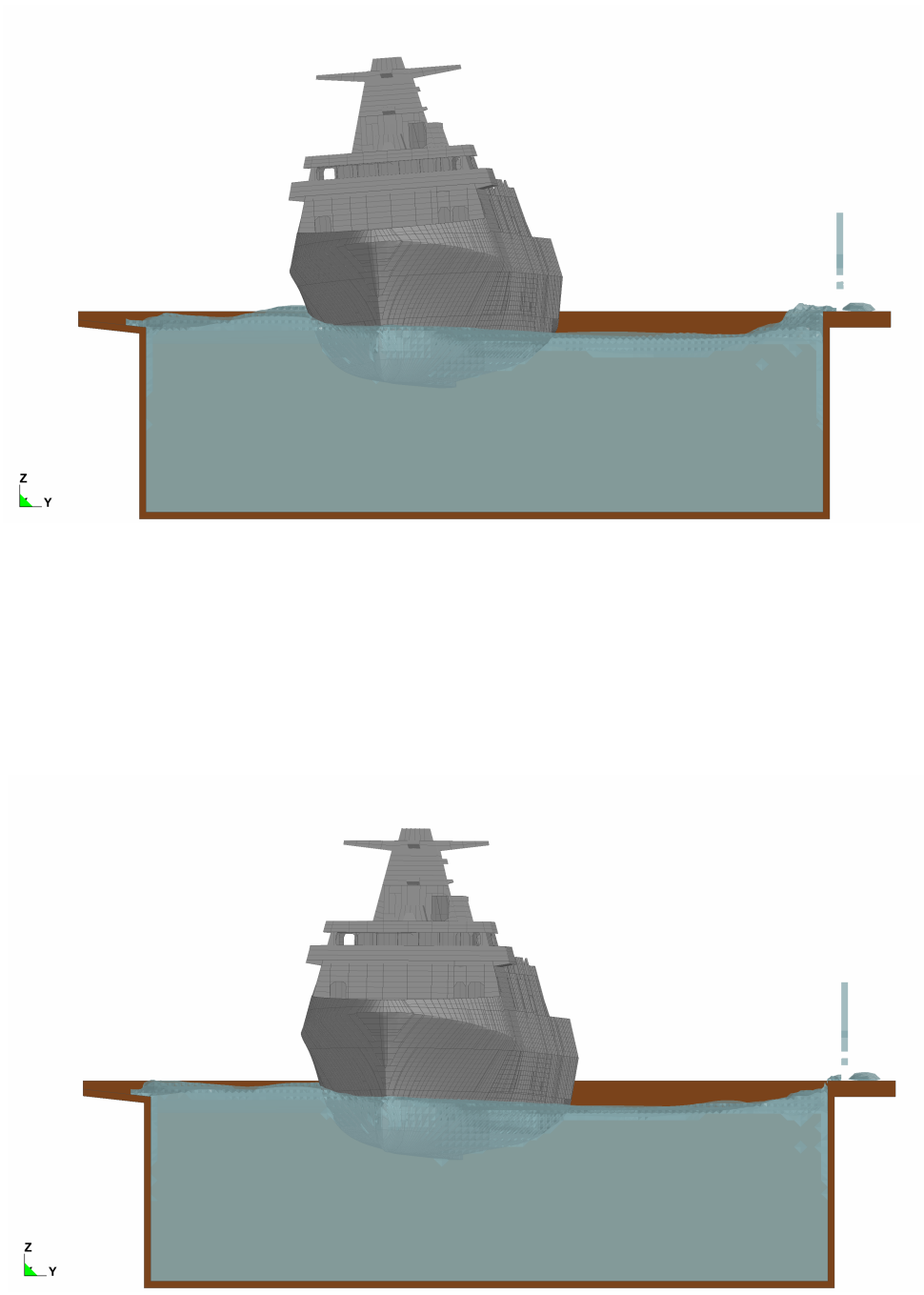

Figure A.35.: pictures series of ship motion obtained with ALE approach (LC LAUNCH is shown in 0.50s intervals)

A.12. Resulting hull structural loads

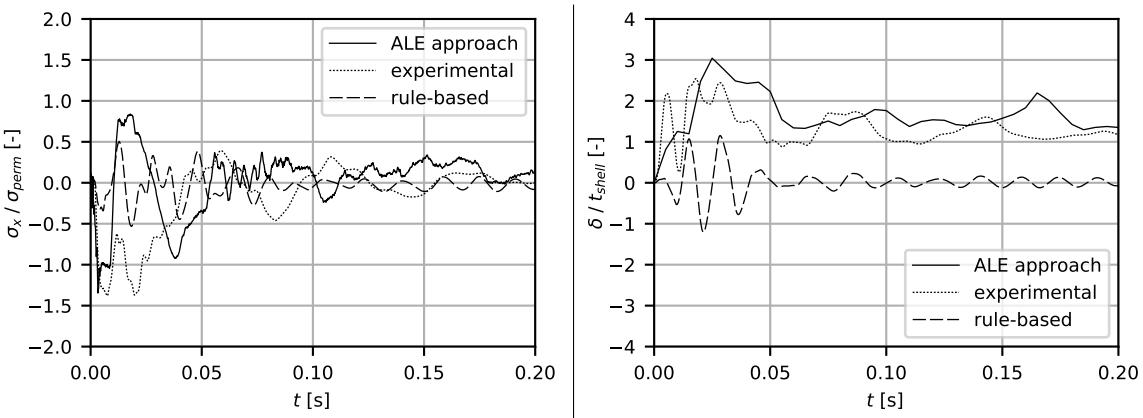

(a) shell plating (outer surface)

(b) bending deformation of shell plating

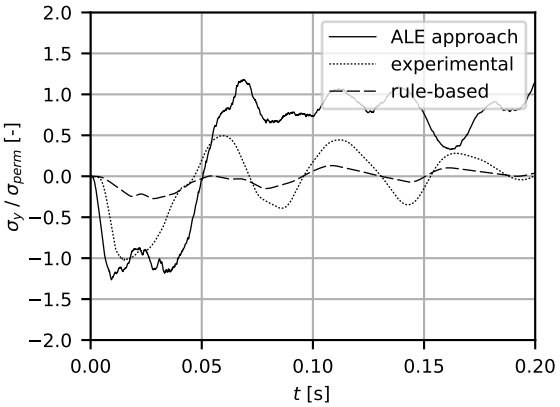

(c) corner of web frame (middle surface)

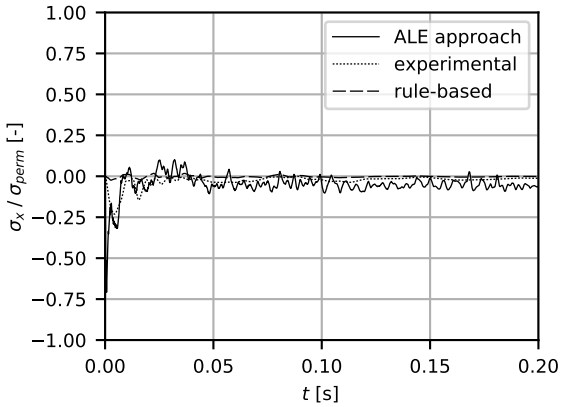

(d) floor plating (middle surface)

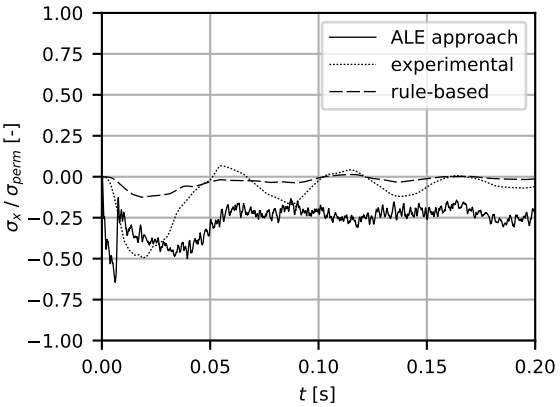

(e) bulkhead plating (middle surface)

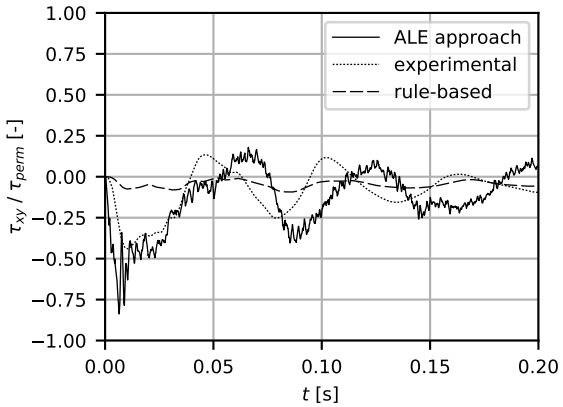

(f) bulkhead plating (middle surface)

Figure A.36.: resulting hull structural loads — influence of different load models (combined FEM model of SPV + LC LAUNCH)

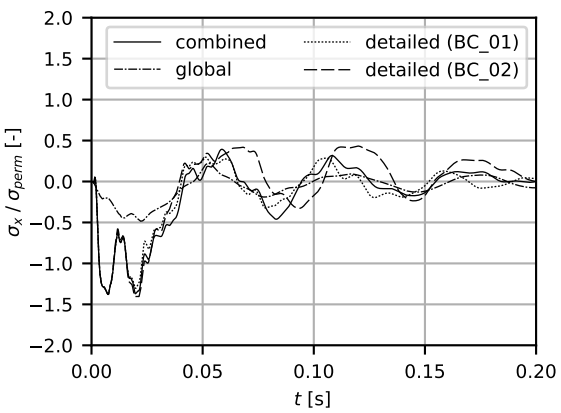

(a) shell plating (outer surface)

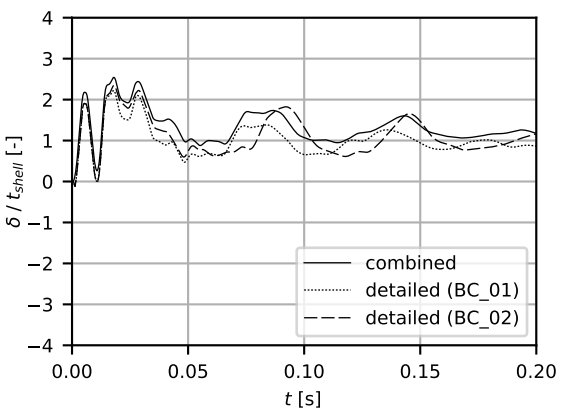

(b) bending deformation of shell plating

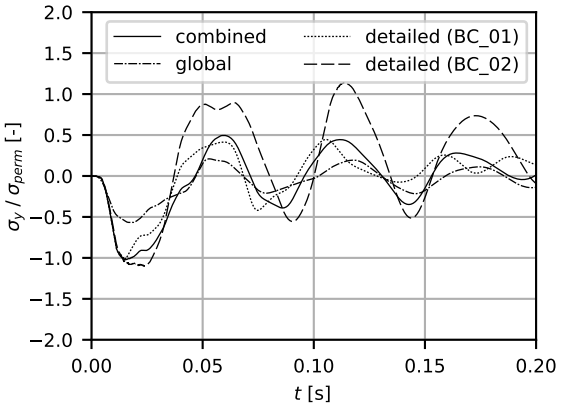

(c) corner of web frame (middle surface)

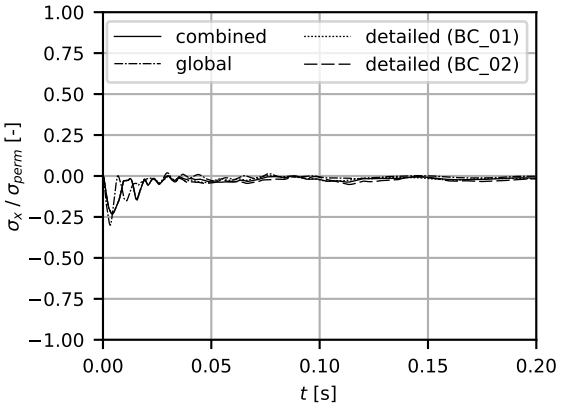

(d) floor plating (middle surface)

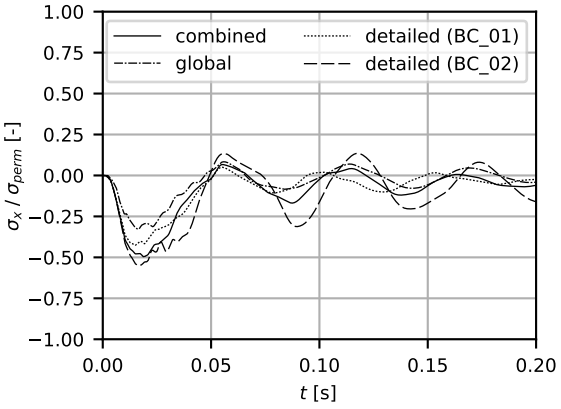

(e) bulkhead plating (middle surface)

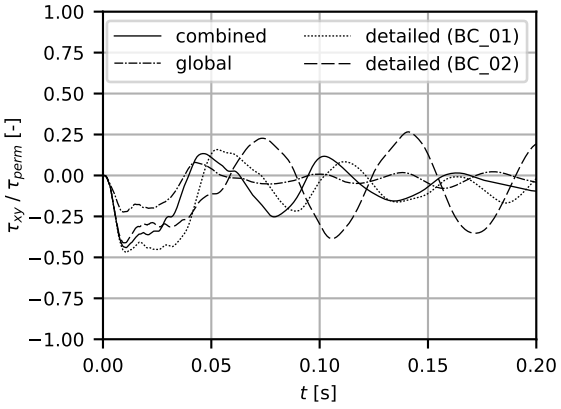

(f) bulkhead plating (middle surface)

Figure A.37.: resulting hull structural loads — influence of different FEM models of SPV (load model based on model tests + LC LAUNCH)

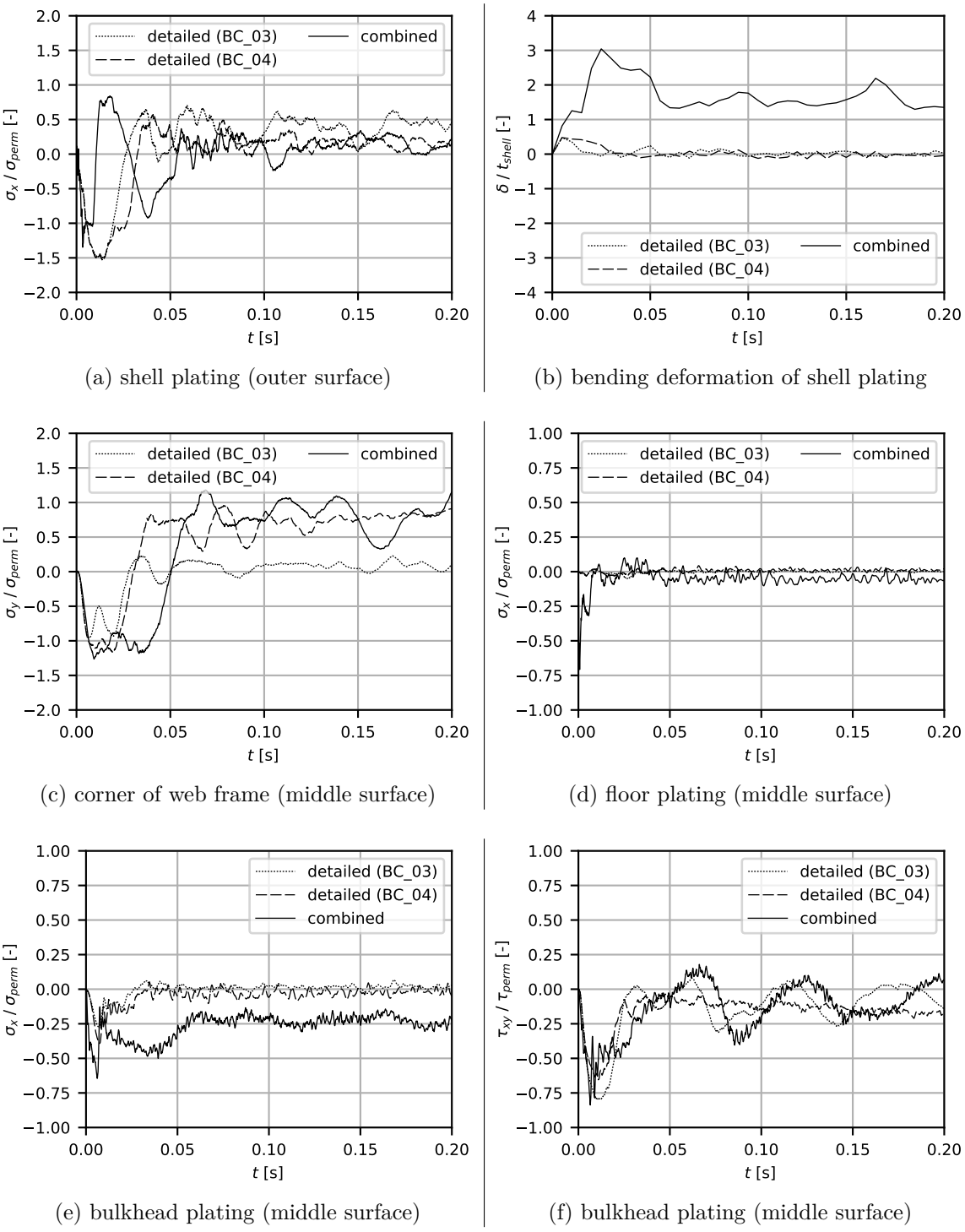

(a) shell plating (outer surface)

(b) bending deformation of shell plating

(c) corner of web frame (middle surface)

(d) floor plating (middle surface)

(e) bulkhead plating (middle surface)

(f) bulkhead plating (middle surface)

Figure A.38.: resulting hull structural loads — influence of different FEM models of SPV (ALE approach + LC LAUNCH)

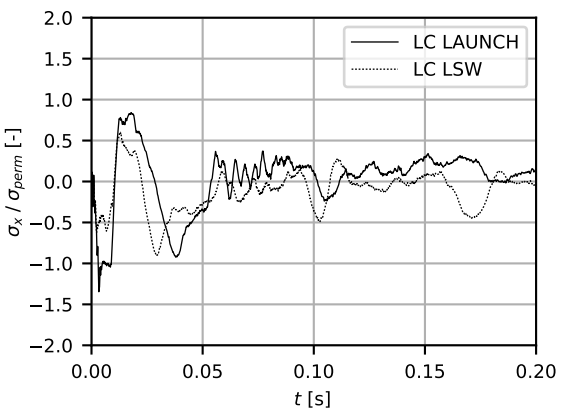

(a) shell plating (outer surface)

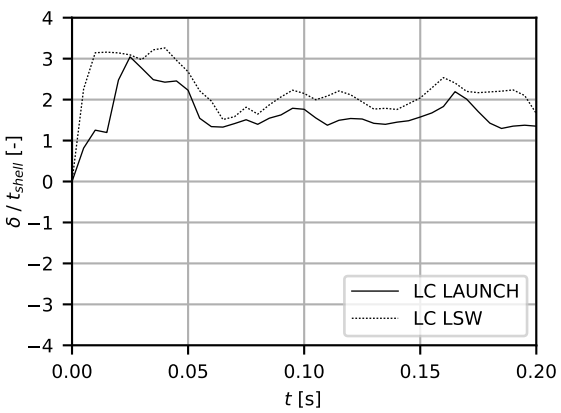

(b) bending deformation of shell plating

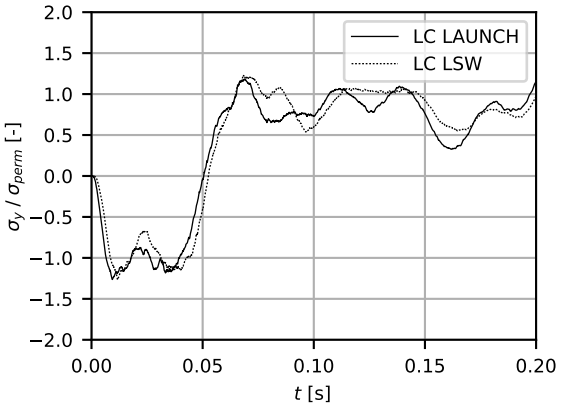

(c) corner of web frame (middle surface)

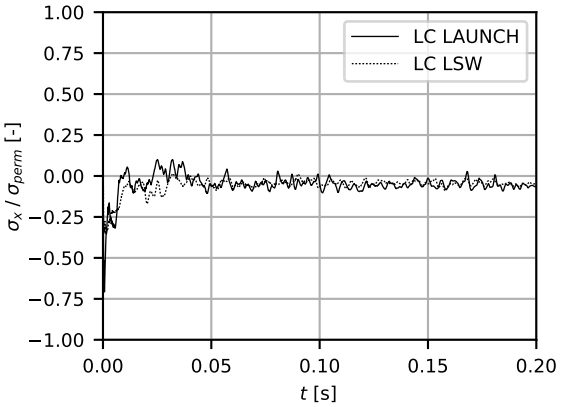

(d) floor plating (middle surface)

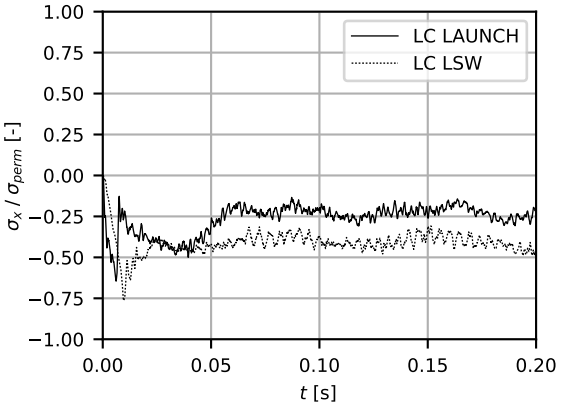

(e) bulkhead plating (middle surface)

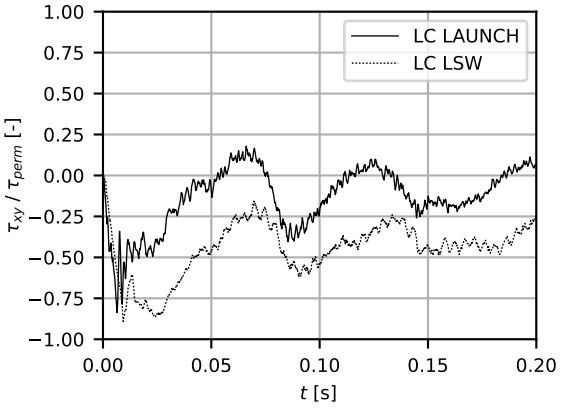

(f) bulkhead plating (middle surface)

Figure A.39.: resulting hull structural loads — influence of different loading conditions (ALE approach + combined FEM model of SPV)

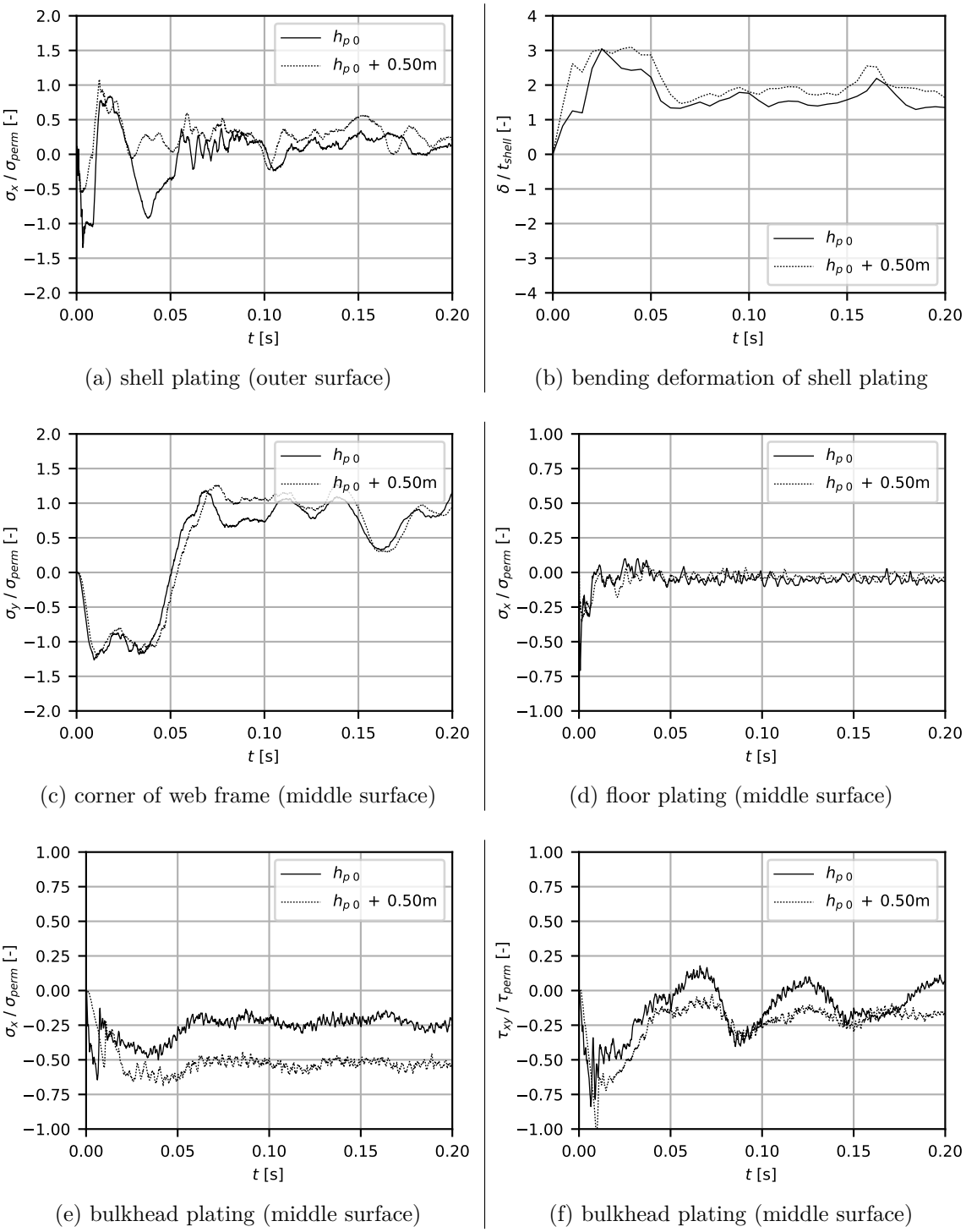

(a) shell plating (outer surface)

(b) bending deformation of shell plating

(c) corner of web frame (middle surface)

(d) floor plating (middle surface)

(e) bulkhead plating (middle surface)

(f) bulkhead plating (middle surface)

Figure A.40.: resulting hull structural loads — influence of height of drop (ALE approach + combined FEM model of SPV + LC LAUNCH)

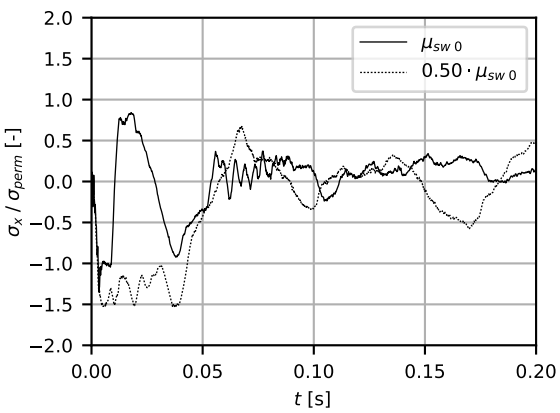

(a) shell plating (outer surface)

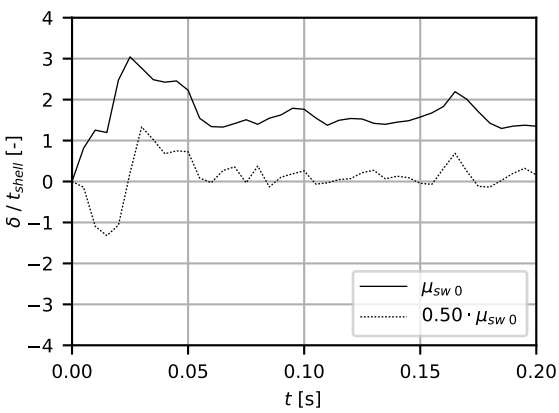

(b) bending deformation of shell plating

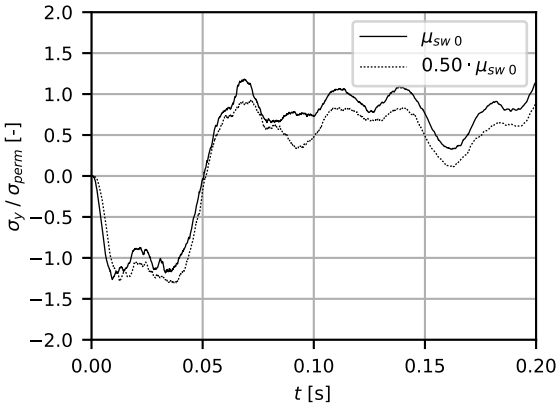

(c) corner of web frame (middle surface)

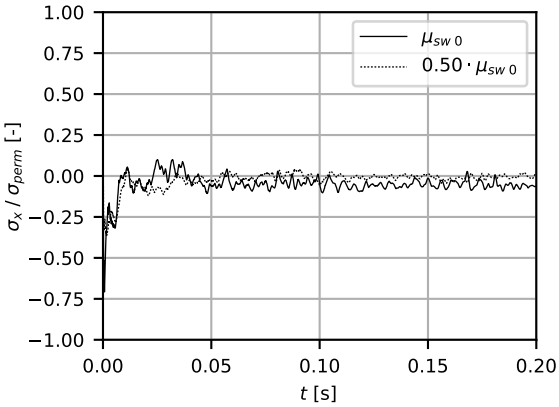

(d) floor plating (middle surface)

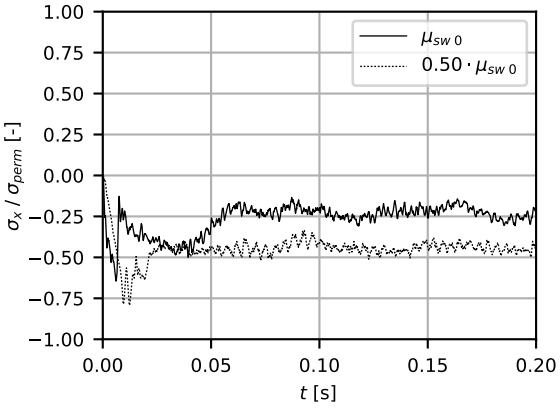

(e) bulkhead plating (middle surface)

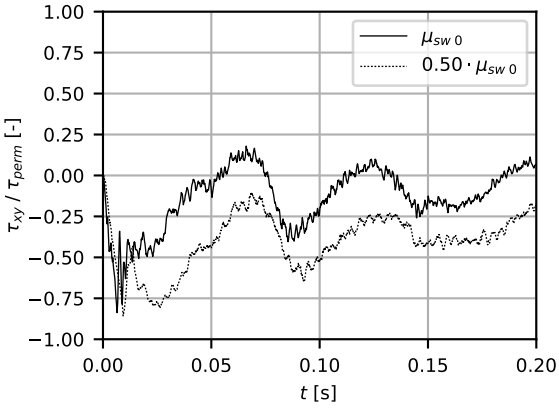

(f) bulkhead plating (middle surface)

Figure A.41.: resulting hull structural loads — influence of coefficient of friction (ALE approach + combined FEM model of SPV + LC LAUNCH)